Flow and sedimentation of pyroclastic density currents. From large scale to boundary layer processes

Guilhem Amin Douillet

München 2014

This page was intentionally left blank.

Flow and sedimentation of pyroclastic density currents. From large scale to boundary layer processes

Guilhem Amin Douillet

Dissertation
an der Fakultät für Geowissenschaften,
Sektion für Mineralogie, Petrologie, und Geochemie
der Ludwig–Maximilians–Universität
München

vorgelegt von
Guilhem Amin Douillet
aus Saint Louis (Frankreich)

München, den 7. Oktober 2014

Erstgutachter: Professor Donald Bruce Dingwell
Zweitgutachter: Professor Shane Cronin
Tag der mündlichen Prüfung: 05. Februar 2015

Contents

This page was intentionally left blank.

Zusammenfassung

Unsere Erde ist ein lebendiger Planet. Plattentektonische Prozesse bringen Gesteinsserien an die Erdoberfläche, wo sie Erosion, Transport und Ablagerung ausgesetzt sind. Pyroklastische Dichteströme (PDCs, englisch für *pyroclastic density currents*) vereinen alle diese Prozesse in einem einzigen Phänomen. Während explosiver Vulkanausbrüche wird pyroklastisches Material, d.h. Bruchstücke des aufsteigenden Magmas bzw. des Nebengesteins, ausgeworfen. Diese Pyroklasten können als eine Mischung aus Gas und Partikeln als PDC weitertransportiert werden. PDCs können Umgebungsluft aufnehmen, Partikel ablagern oder von der Oberfläche erodieren bis sie schlussendlich ihre kinetische Energie verbraucht haben und sich als Sediment ablagern.

Dadurch sind PDCs ein Transport Prozess der zur Klasse der partikel-geführten Dichteströme gehört. Dies sind 1) Mischungen von Partikeln und Umgebungsmedium (gasförmig oder flüssig), die sich 2) als Gesamtkörper wie eine Flüssigkeit verhalten, 3) deren Momentum in ihrer höheren Dichte im Vergleich zum Umgebungsmedium begründet ist, und 4) wo die höhere Dichte von der Partikelfracht herrührt. Darüber hinaus haben die Partikel, die kombinierte Rolle von Momentumlieferand während des Transports und sind auch die Ablagerung, wenn das Momentum abnimmt.

Mit zunehmenden technologischen Entwicklungen werden Experimente und Modelle zunehmend realitätstreu. Numerische Simulationen können auf immer grössere Rechenkapazitäten zurückgreifen. Analog-Modelle und -Experimente können mit sehr hoher zeitlicher und räumlicher Auflösung in 3D aufgezeichnet werden. Diese sind grundlegend für ein besseres Verständnis der dynamischen Prozesse im Inneren von PDCs. Eine Frage bleibt aber: Was soll man modellieren oder experimentell nachstellen? Wie weiß man, welcher physikalische Prozess am wichtigsten ist, welche Werte man als Input-Parameter verwenden soll und ob ein Modell überhaupt realitätsnah ist. Die Antworten auf diese Fragen müssen auf Beobachtungen der Natur beruhen und verlangen nach detaillierten Studien natürlicher Ablagerungen durch Geländesedimentologen.

Die vorliegende Arbeit hat PDC-Ablagerungen detailliert untersucht mit dem Ziel, die Fließprozesse zu bestimmen. Im Gegensatz zu früheren Arbeiten, die den Bezug zwischen Vulkanausbruch und Partikeltransport untersucht haben, wurde in dieser Arbeit analysiert,

welche Aussagen über den Partikeltransport man auf der Basis von Ablagerungen treffen kann. Der Großteil der Geländearbeiten betrifft die Ablagerungen des Ausbruchs des Vulkans Tungurahua (Ecuador) vom 17. August 2006. Die Ablagerungen dieses verhältnismäßig kleinen Ausbruchs sind sehr gut erhalten und zeigen eine große Bandbreite an sedimentären Strukturen und Erhebungen in Dünenform (english *dune bedforms*) an der Oberfläche. Es wurden unterschiedliche Kombinationen von Methoden verwendet: 1) Geländeuntersuchungen in-situ gepaart mit Labor Messungen und Sedimentimpregnation (*sediment peels*). 2) Georadar (*Ground Penetrating Radar*) und *Terrestrial Laser Scanning* der Erdoberfläche zur Darstellung der Dünenformen in 3D. Letztere Ergebnisse wurden finanziert durch die LMU und durchgeführt in enger Zusammenarbeit mit der *Ecole et Observatoire des Sciences de la Terre* (EOST, Strasburg, Frankreich), können hier jedoch nicht dargelegt werden, da sie bereits in der Doktorarbeit von Jean Remi Dujardin (EOST) aufgeführt sind.

Diese Arbeit ist aufgebaut nach dem Prinzip "Reise vom Großen ins Kleine". Die Kartierung und Beschreibung der Ablagerungen zeigt das großmaßstäbliche Verhalten von pyroklastischen Dichteströmen im ganzen. Bildung und Ablagerung von PDCs mit geringem Partikelfracht werden stark von der Geländetopographie beeinflusst. *Flow stripping* Prozesse sind häufig an Klippen oder Kurven gebunden, wo der Hauptstrom weiter im Tal fließt und PDCs mit geringerer Partikelfracht gebildet werden. Aufgrund ihrer geringeren Dichte können die letzteren Täler verlassen. Sie verlieren nach ihrer Abspaltung häufig sehr schnell an Momentum und sind charakterisiert durch hohe Sedimentationsraten auf angrenzenden Talrücken. Auf der Oberfläche befinden sich Hunderte von mehreren Metern großen Dünenformen. Ihre komplexen internen Strukturen wurden in der Literatur häufig als Antidünen interpretiert. Im Zuge dieser Arbeit wurde diese Interpretation in Frage gestellt, da Antidünen durch transkritische und stationäre Gravitätswellen produziert werden, die sich an Dichtegrenzflächen entwickeln. Diese Arbeit zeigt alternative Bildungsbedingungen auf. Schlussendlich wurden die Bedingungen an der Grenzfläche zwischen PDC und Substratum untersucht. Messungen in einem Windkanal erlaubten die Bestimmungen des Grenzwertes für Saltation und damit die quantitative Beschreibung der Fließbedingungen auf der Basis der Analyse von Transportbedingungen und verwendeter Korngröße. Die Bedingungen an der basalen Grenzfläche sowie der Ablagerung kann man durch die Untersuchung von sogenannten *soft sediment deformation* Strukturen ermitteln. Sediment-Lackfilmen (english *sedimentary/lacquer peel*) von unveränderten Ablagerungen in situ sind eine hochauflösende Methode zur Untersuchung von sedimentologischen Details, die bis dato nur von Analogexperimenten bekannt waren. Auf dieser Basis kann man Korngrößenwechsel zwischen mehreren laminae (jede nur weniger als 1 mm dick) feststellen, mit den Ergebnissen der Windkanal Messungen kombinieren und somit unterschiedlich starke Turbulenzen in PDCs mit geringem Partikelfracht bestimmen.

All diese Ergebnisse sind aber nur die Basis für weitere Untersuchungen in vulkanischer Sedimentologie. Während ein besseres Verständnis von Ausbruchsmechanismen dazu dient, explosive Vulkanausbrüche vorherzusagen, erlaubt eine detaillierte Analyse der Ablagerun-

gen Aussagen über deren räumliche Verbreitung und die Bandbreite der Erscheinungsform. Da PDCs partikel-geführte Dichteströme sind, lassen sich die ermittelten Ergebnisse auch auf andere, möglicherweise ökonomisch interessante Sedimentarten übertragen, wie zum Beispiel glaziale Schwereströme oder Trübeströme.

This page was intentionally left blank.

Summary

Our Earth is a living Planet in which rocks are exhumed at the surface, and subjected to erosion, transport and deposition. Pyroclastic density currents (PDCs) concentrate all these steps in a single phenomenon. During explosive volcanic eruptions, rock fragments known as pyroclasts are ejected from the inside of the Earth to the surface. They can then be transported as a mixture of gas and particles, the PDC, possibly entraining air and eroding their bed until they lack kinetic energy and dissipate as sediment.

PDCs are thus a fundamental transport mode associated with explosive eruptions, and belong to the class of particulate density currents. Those are mixtures of particles and ambient fluid, which behave, as a whole, as a fluid, and where the agent of excess density driving the momentum is the particles. Particles forming PDCs thus combine the roles of driving the momentum and be the resulting deposit when momentum comes to lack.

With the improvements of technology, models and experiments become more and more sophisticated. Numerical simulations benefit from greater calculation capacities, whereas analogue models and experiments can be recorded at high speed and resolution in 4D. These tools are fundamental to the understanding of the otherwise inaccessible internal dynamics of PDCs. Yet the question remains, what to model? How to know which effects are acting, if a model is accurate, and what should be the input parameters? The answers must be entirely based on observations of the natural phenomenon, and the field sedimentologist has the role to answer these questions.

This study investigates deposited PDCs, with the goal of understanding their former flow dynamics. Whereas others have made the link between the eruption and the particle transport, the present target is to understand the particle transport from the study of the sediment. The field examples are predominantly based on the deposits of the August 17. 2006 eruption of Tungurahua volcano (Ecuador). This small volume eruption deposited sediments that present a great variety of sedimentary characteristics including dune bedforms in an well-preserved state. A combination of methods are used: direct field observation benefit from laboratory instruments and sedimentary peel techniques. Ground Penetrating Radar and Terrestrial Laser Scanner record the 3D architecture of bedforms. Unfortunately, the latter results, acquired in collaboration with the *Ecole et Observatoire*

des Sciences de la Terre -EOST, Strasbourg, France- (and financed by THESIS and LMU for this PhD), cannot be detailed in this work since they are present in the PhD dissertation from Jean Remi Dujardin (2014, EOST).

The structure of the dissertation is a a voyage through the scales, from the eruption scale to the particle scale. The mapping of the deposits highlights the large-scale behavior driven by the whole flow. The formation of dilute PDCs is linked to flow stripping processes at cliffs and curves of valleys confining the main flows.The lower density of dilute PDCs permitted them to overflow valley-walles on outer overbanks of curves and rapidly deposit. At the meter scale, pristine dune bedforms shape the surface of these deposits, and show an evolution in their dimension, form as well as internal patterns. Beyond the usual interpretation as antidunes, those bedforms are found to contain a great richness of information. Antidunes are indeed almost systematically evoked for the formation of PDC bedforms. However, this type of structures represents anecdotic phenomena related to transcritical, stationary gravity waves developing at density interfaces. Several alternatives to the antidune interpretation are presented throughout the dissertation. Finally, the scale of the basal boundary interaction between the flow and substrate is scoped. Wind tunnel measurements of the saltation threshold permit to derive quantitative flow parameters from the recognition of the transport mechanism and grain size of involved particles. The basal flow processes and sediment state are approached from the study of soft sediment deformation. Sedimentary peels (lacquer peels of undisturbed deposits) enlighten levels of details that permit to recognize features previously only suspected from analogue experiments. The variation of deposit grain size between laminae with sub-mm thickness can be linked with the wind tunnel measurements and tell about levels of turbulence in dilute PDCs. The answer is blowing in the wind.

All these results represent but a prime in volcanic sedimentology. Whereas understanding eruption mechanisms helps to forecast these events in time, the study of the deposit permit to constrain their dispersion in space. As particulate density currents, many of the mechanisms evidenced from PDCs are also valid for economically relevant sedimentary targets such as glacial hyperpycnal flows or turbidity currents.

List of Figures

List of Tables

This page was intentionally left blank.

Part I

Large scale features

Chapter 1

Sedimentology and geomorphology of the deposits from the August 2006 pyroclastic density currents at Tungurahua volcano, Ecuador

This chapter was published in the Journal "Bulletin of Volcanology" in 2013 together with chapter 3. It describes the large scale sedimentary characteristics of the August 2006 eruption of Tungurahua volcano.

This page was intentionally left blank.

Bull Volcanol (2013) 75:765
DOI 10.1007/s00445-013-0765-7

RESEARCH ARTICLE

Sedimentology and geomorphology of the deposits from the August 2006 pyroclastic density currents at Tungurahua volcano, Ecuador

Guilhem Amin Douillet · Ève Tsang-Hin-Sun · Ulrich Kueppers · Jean Letort · Daniel Alejandro Pacheco · Fabian Goldstein · Felix Von Aulock · Yan Lavallée · Jonathan Bruce Hanson · Jorge Bustillos · Claude Robin · Patricio Ramón · Minard Hall · Donald B. Dingwell

Received: 21 January 2013 / Accepted: 20 September 2013 / Published online: 24 October 2013

Abstract The deposits of the pyroclastic density currents from the August 2006 eruption of Tungurahua show three facies associations depending on the topographic setting: the massive, proximal cross-stratified, and distal cross-stratified facies. (1) The massive facies is confined to valleys on the slopes of the volcano. It contains clasts of >1 m diameter to fine ash material, is massive, and interpreted as deposited from dense pyroclastic flows. Its surface can exhibit lobes and levees covered with disk-shaped and vesicular large clasts. These fragile large clasts must have rafted at the surface of the flows all along the path in order to be preserved, and thus imply a sharp density boundary near the surface of these flows. (2) The proximal cross-stratified facies is exposed on valley overbanks on the upper part of the volcano and contains both massive coarse-grained layers and cross-stratified ash and lapilli bedsets. It is interpreted as deposited from (a) dense pyroclastic flows that overflowed the gentle ridges of valleys of the upper part of the volcano and (b) dilute pyroclastic density currents created from the dense flows by the entrainment of air on the steep upper flanks. (3) The distal cross-stratified facies outcrops as spatially limited, isolated, and wedge-shaped bodies of cross-stratified ash deposits located downstream of cliffs on valleys overbanks. It contains numerous aggrading dune bedforms, whose crest orientations reveal parental flow directions. A downstream decrease in the size of the dune bedforms, together with a downstream fining trend in the grain size distribution are observed on a 100-m scale. This facies is interpreted to have been deposited from dilute pyroclastic density currents with basal tractional boundary layers. We suggest that the parental flows were produced from the dense flows by entrainment of air at cliffs, and that these *diluted* currents might rapidly deposit through "pneumatic jumps". Three modes are present in the grain size distribution of all samples independently of the facies, which further supports the interpretation that all three facies derive from the same initial flows. This study emphasizes the influence of topography on small volume pyroclastic density currents, and the importance of flow transformation and flow-stripping processes.

Keywords Tungurahua · Pyroclastic density currents · Flow stripping · Sedimentary wedge · Hydraulic jump

Editorial responsibility: V. Manville

G. A. Douillet (✉) · U. Kueppers · F. Goldstein · F. Von Aulock · Y. Lavallée · J. B. Hanson · D. B. Dingwell
Earth & Environmental Sciences, Ludwig-Maximilians-Universität, Munich, Germany
e-mail: g.douillet@min.uni-muenchen.de

G. A. Douillet · È. Tsang-Hin-Sun · J. Letort · J. Bustillos
Ecole et Observatoire des Sciences de la Terre, Université de Strasbourg, Strasbourg, France

G. A. Douillet · D. A. Pacheco · C. Robin · P. Ramón · M. Hall
Instituto Geofísico, Escuela Politécnica Nacional, Quito, Ecuador

G. A. Douillet · C. Robin
Institut de Recherche pour le Développement, UMR volcan, Quito, Ecuador

È. Tsang-Hin-Sun
Laboratoire de Géosciences Marines, Université de Brest, Plouzané, France

J. Letort
Laboratoire de Géophysique Interne et Techtonophysique (LGIT), Grenoble, France

Introduction

During explosive eruptions or upon catastrophic collapse of lava domes, density currents composed of clasts and gas flow down the volcanic edifice at hundreds of kilometers per hour, threatening the surrounding populations (Druitt 1996). Since direct observation is problematic, the understanding of such pyroclastic density currents (PDCs) represents a challenge whose solution is mainly based on analysis of deposit characteristics. Given the wide range of sedimentological patterns in PDC deposits, the parent flows are interpreted to have had a large range of solids concentrations (e.g., Sparks 1976), combined with different transport mechanisms (e.g., Burgisser and Bergantz 2002) evolving both spatially and temporally (Fisher 1983; Calder et al. 1997; Gardner et al. 2007). Here, we analyze the deposits of the pyroclastic density currents from the August 2006 eruption of Tungurahua volcano (Ecuador) in order to understand the origin and emplacement dynamics of the parental flows.

Conceptual models

Historically, pyroclastic deposits have been classified into three conceptual parental transport end-members: flow, fall, and surge (Sparks 1976; Wohletz and Sheridan 1979). Field observations however have revealed gradational deposit types (Valentine and Giannetti 1995; Wilson and Hildreth 1998; Sulpizio et al. 2008; 2010), which are thought to reflect different and transitional transport mechanisms (Burgisser and Bergantz 2002). Recent studies emphasize that deposits reflect only boundary layer processes during sedimentation and suggest a classification into "granular flow-", "tractional flow-" and "direct fallout-" dominated flow boundary end members (reviewed and conceptualized in Branney and Kokelaar (2002, p. 37–49)). For simplification, we use a threefold definition below: (1) massive, unsorted, and coarse-grained deposits are thought to reflect the absence of a basal tractional flow boundary during deposition, plus high particle concentration, and dominant particle–particle interactions in the parental flow (Brissette and Lajoie 1990; Boudon et al. 1993; Branney and Kokelaar 2002; Sarocchi et al. 2011). Where deposits are confined to topographic lows, the density (and solids concentration) of the entire parental flow is believed to have been high (Cole et al. 1998). We term this conceptual PDC-type "dense pyroclastic flow" in this study. (2) Cross-stratified and relatively finer-grained deposits are thought to form from turbulent flows with a basal tractional boundary layer and an important interparticle fluid presence with gas support (Crowe and Fisher 1973; Brissette and Lajoie 1990; Branney and Kokelaar 2002; Dellino et al. 2004). Such deposits are often found on interfluves and a lower density of the parental flows is inferred. Previously known as "pyroclastic surges" (Sparks 1976; Wohletz and Sheridan 1979), we term this conceptual PDC-type "dilute PDC" in this study. (3) We use the term "co-ignimbrite ash clouds" for dilute parts of the PDCs that are dominated by buoyancy. In such cases, even though the particles are gas supported during transport, no tractional flow-boundary zone is present because most momentum is transferred vertically and no consequent lateral currents are present (Talbot et al. 1994; Dellino et al. 2004). Thus, particles deposit by direct fallout and the associated sediment can be stratified, but not cross-stratified (Talbot et al. 1994).

The different PDC end-members can be present within the same flow as a basal dense pyroclastic flow and upper dilute PDC (Fisher 1995), vertically grading within a continuously density stratified current (Valentine 1987; Burgisser and Bergantz 2002), or evolve from one type to the other downflow (Gardner et al. 2007; Sulpizio et al. 2008; Andrews and Manga 2012).

Interaction with topography

Topography affects segregation mechanisms within granular flows (Baines 1998; Waltham 2004), determining threat for local populations in the case of PDCs (Fisher 1995; Abdurachman et al. 2000; Lube et al. 2011). Topographic separation into an upper, overflowing, less dense part and basal concentrated part is known as "flow stripping" in the case of turbidity currents (Piper and Normark 1983; Fildani et al. 2006). Branney and Kokelaar (2002) emphasize that "flow stripping" is preferable to "flow separation" because it does not imply two initially separate flows. Legros and Kelfoun (2000) analyzed momentum dissipation and showed that dilute PDCs may overflow topographic barriers with more ease than do dense flows. This is especially so for small volume PDCs, where a sharp interface between a basal dense pyroclastic flow and overriding dilute PDC is inferred (Fisher 1995; Takahashi and Tsujimoto 2000; Abdurachman et al. 2000; Saucedo et al. 2002; Cole et al. 2002; Charbonnier and Gertisser 2008). Takahashi and Tsujimoto (2000) showed that such dilute PDCs can travel independently of the main body, but their growth or waning depends on the supply of particles and gas from the main body, so they are no longer sustained and come to a stop after diverging from the course of the main body. Obstacles in a PDCs pathway also lead to partial diversion of dense flows in secondary "passes of saddles" (Branney and Kokelaar 2002). Lube et al. (2011) showed that the overflow of dense basal parts of the PDCs on interfluves at Merapi (Indonesia) was mainly controlled by three channel parameters: the cross-sectional area, confinement, and sinuosity.

Hydraulic jumps

A hydraulic jump is a sudden thickening and deceleration of a flow at the transition from supercritical to subcritical regime (Drazin 2002). Experiments on subaqueous, particle-driven, density currents showed that the coarse bedload deposits with the shape of a wedge at a break in slope due to a sudden decrease in shear velocity, possibly related to development of a hydraulic jump (García and Parker 1989; García 1993; Mulder and

Alexander 2001; Macías et al. 1998). Such "sedimentary wedges" (as defined in Sequeiros et al. 2009) are also observed in deep-sea turbidite fans (Prather 2003; Fildani et al. 2006). Within PDC deposits, lithic breccias emplaced at the base of a break in slope (Freundt and Schmincke 1985; Macías et al. 1998) or upstream obstacles (Freundt and Schmincke 1985) were interpreted to be the sedimentary signature of "pneumatic jumps" (the gaseous equivalent of a hydraulic jump, Branney and Kokelaar 2002, p. 18). At a metric scale, massive and unsorted stoss-depositional layers lying against the upstream face of buried buildings (Gurioli et al. 2002, 2007), or steep-sided truncations of pre-existing deposits (Schmincke et al. 1973; Freundt and Schmincke 1985; Giannetti and Luongo 1994) were interpreted as resulting from internal "pneumatic jumps" in density-stratified dilute PDCs. "Pneumatic jumps" triggered by cliffs are also supposed to be at the origin of co-ignimbrite plumes (Hoblitt 1986; Calder et al. 1997). These authors also noted that at a bend in the containing valley, an "ash cloud surge" overrode the channel and shortly after generating a buoyant plume.

Dune bedforms in PDCs

Dilute PDCs frequently deposit dune bedforms (DBs). Aggrading cross-stratified bedsets with up- or downstream migration of the crests are the most widespread internal structures observed (see Douillet et al. 2013 and references therein). However, controversies still exist on the interpretation of their fluid dynamical significance (Walker 1984; Sulpizio et al. 2008; Douillet et al. 2013). The size of DBs is usually observed to decrease with distance from the crater (Fig. 4 of Wohletz and Sheridan (1979); Fig. 8 of Druitt (1992)). In the 1965 Taal deposits, Moore (1967) reported DB wavelengths (length in our nomenclature) decreasing from 19 m in proximal areas to 4 m at 2.5 km from the volcano, the evolution occurring over the shortest distance where slope was acting against flow direction. Crests were aligned perpendicular to the flow direction. These size trends are sometimes related to an evolution of the outer bedform shapes and internal stratification patterns (Douillet et al. 2013 and references therein). Notably, dune-bedded deposits are also reported on levees and overbanks of turbidite-containing canyons (Normark et al. 2002; Fildani et al. 2006).

Tungurahua volcano and the August 2006 eruption

Tungurahua is an active andesitic stratovolcano (Hall et al. 1999) in the eastern Cordillera of the Northern Volcanic Zone in Ecuador (Hall et al. 2008). The present summit crater (5,023 m; base at 1,800 m above sea level (a.s.l.)) is breached to the northwest, directing lava flows and PDCs, together with the general westward wind direction for PDCs and ash clouds. In 1999, the volcano entered a period of activity with intermittent explosive phases and generation of PDCs. This activity poses a threat to many villages on the flanks, the city of Baños (25,000 inhabitants), the second largest hydroelectric dam in Ecuador and surrounding farmland (Samaniego et al. 2008). PDCs generated during a period of heightened activity in July and August 2006 reached populated areas, causing fatalities and severe damage to infrastructure and the agricultural sector (Barba et al. 2006; Kelfoun et al. 2009). The deposits of this eruptive episode are well studied. Kelfoun et al. (2009) mapped the deposits and numerically modeled the dense pyroclastic flows. Samaniego et al. (2011) presented a petrological description of the erupted products. Eychenne et al. (2012) analyzed the fall deposits associated with the August eruption, revealing a bimodal grain size distribution and suggesting that there was simultaneous deposition from the eruptive plume and co-ignimbrite ash clouds. Douillet et al. (2013) describe the dune bedforms deposited by dilute PDCs.

The August events began and ended with major fall events (Fide observatory-OVT staff). The eruptive column reached a height greater than 16 km, but did not collapse to form PDCs, which instead resulted from episodic destabilization of erupted material accumulated near the vent (Kelfoun et al. 2009). Several PDCs traveled down the northern, western, and southwestern flanks, controlled by the hydrological network to the base of the edifice (~1,800 m a.s.l.) where the deposits dammed the Chambo River for several hours (see map in Kelfoun et al. (2009)). The mean frontal velocity was estimated at 30 m/s using seismic data (Kelfoun et al. 2009) and the number of PDCs inferred to have passed through the study area (Fig. 1) was constrained to about five using monitoring data (e.g., Barba et al. 2006). The explosive event lasted for less than 8 h.

Kelfoun et al. (2009) mapped the deposits of the July and August eruptions and distinguished "dense flow deposits", mainly confined in the valleys, and "surge and fallout deposits" outcropping on the overbanks around dense flow deposits and on top of them (Fig. 1). In the lowermost zones of "los Pájaros" (Fig. 1), three depositional units were observed, the two basal units are coarse-grained and massive, and capped with a centimetric thick ash cover, the uppermost unit lacks any ash cover. Here, we present a sedimentological and geomorphological analysis of the deposits that reveals the transport and emplacement mechanisms of the August 2006 PDCs.

Facies associations

Nomenclature

In our field survey, we recognized three facies associations: "massive facies" (equivalent to "dense flow deposits" in Kelfoun et al. 2009), "proximal cross-stratified facies" and "distal cross-stratified facies" (later on, *Ma*, *P-Xst* and *D-Xst*, respectively).

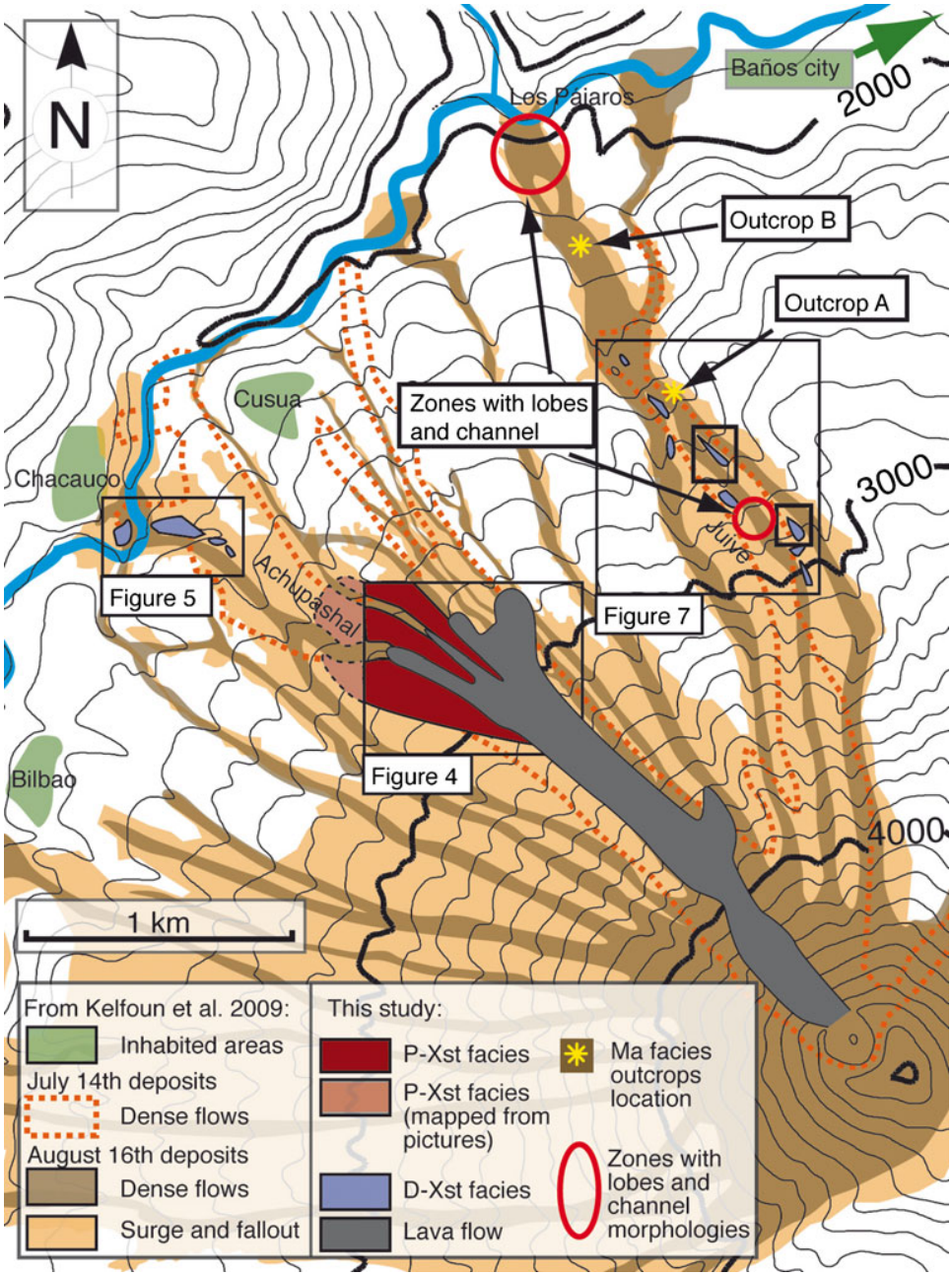

Fig. 1 General map of the deposits from the July and August 2006 eruptions of Tungurahua with "dense flows" and "surge and fallout" deposits modified from Kelfoun et al. (2009), "lava flow" modified from Samaniego et al. (2011) and Goldstein (2011), "*P-Xst*" and "*D-Xst*" facies from this study. Location of key features and outcrops are indicated

Planar stratified deposits identified as co-ignimbrite ash cloud deposits are not dealt with here. The *P-Xst*, *D-Xst* facies and co-ignimbrite ash cloud deposits of this study are all subdivisions of the "surge and fallout deposits" in Kelfoun et al. (2009). We use the term "facies" for deposits with common characteristic patterns. Facies includes lithofacies, spatial location, and geomorphic surface information. We term a millimeter-scale stratum a "lamina"; a "bedset" is a decimeter-scale group of laminae with similar structural characteristics. We use "layer" in order to avoid any genetic implication (such as implied in "unit") and it merely refers to an internally massive and thick (greater than centimeter-scale) stratum.

Fall deposits

The August eruptive period started and ceased with major ash and scoria fall. Field observations confirmed the presence of two thin, ashy layers at the base and top of the August deposits (outcrop A). The lower layer is approximately 1 cm thick and consists of fine ash with very porous clasts (up to 1 cm). The top August fall deposit is *ca*. 2 cm thick and made up of coarse ash and fine lapilli. The quasi-undisturbed nature of this final layer proves the excellent preservation state of the surface. The reader is directed to Kelfoun et al. (2009) and Eychenne et al. (2012) for details on the fall deposits.

Massive facies

The *Ma* facies is organized into multidecimeter-scale layers of massive and unsorted deposits of ash, lapilli and clasts of up to a few meters in diameter. It is mainly found confined to valleys of the drainage network and was partially eroded by the time we undertook our fieldwork (2009 and 2010). *Ma* facies deposits outcrop continuously from an altitude of ca. 3,800 m a.s.l. down to the base of the volcano at 1, 800 m a.s.l., where they spread and dammed local rivers for several hours (Barba et al. 2006). The thickness can reach tens of meters. Kelfoun et al. (2009) have interpreted this facies as deposits from dense pyroclastic flow. A maximum of six units corresponding to different PDCs or to pulses in a single flow were identified, but more might have occurred (Kelfoun et al. 2009).

Stratigraphic units

Two outcrops of *Ma* facies (A and B) from the Juive valley are described (Goldstein 2011) and have been sampled for granulometry (Fig. 2). They are both located downstream of the main ash deposition zones (see below; location in Fig. 1) in low-slope areas.

Outcrop A Outcrop A (Fig. 2a, b) is located 2.8 km from the vent, just upstream of the mouth of a steep-sided valley that confined the parent PDCs and downstream of a break in slope from 25° to about 13°. The exposure is 6 m thick and can be followed laterally for about 100 m parallel to the inferred parent flow direction. The top part (1.5 m) consists of sediments identified as reworked debris (lahar deposits), while the base corresponds to pre-2006 material, leaving 3.7 m of pristine 2006 deposit. Six individual layers (L1 to L6) were identified, described, and the matrix (taken as the fraction <2 cm) sampled for grain size analysis (Table 1).

Visual observation show that lithics are prominent in L1 (ca. 60 vol.%) but never reach more than 40 vol.% in other layers. This correlates with a smaller percentage of coarse material in the sieving results (Fig. 2c). In contrast, L2 to L6 are all matrix-supported and show similar componentry and grain size. Additionally, outcrop A is located at the runout limit of the July 2006 PDCs and an ashy layer is visible between L1 and L2 interpreted as representing a time between the flows that permitted deposition of a fall deposit by settling. The L1–L2 contact is interpreted as the record of the fall deposition at the beginning of the August events and L1 related to the July eruption, though it is unclear whether L1 represents a primary deposit or secondary lahar deposit.

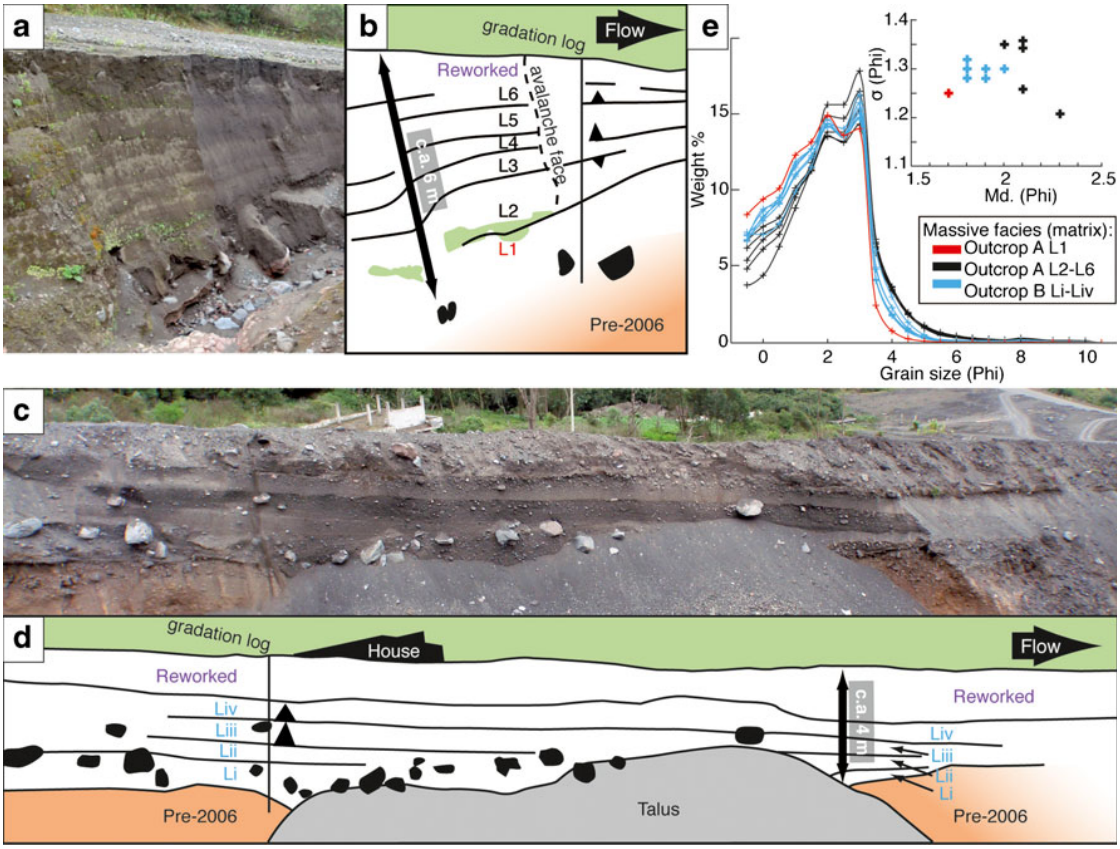

Fig. 2 Massive facies deposits ("Ma"). **a**, **b** Outcrop A; **c**, **d** ouutcrop B. The *sketches* emphasize layers and large clasts, and contain a scale, and *triangles* mark grading layers. **e** Grain size distribution of the different layers of outcrops A and B with median diameter versus sorting coefficient in *inset*

Table 1 Principal characteristics of the two massive facies outcrops

Layer	Organization	Thickness	Matrix (%)	Clast (%)	Clast size	Clast composition	Md (Φ)	Sorting (Φ)
Outcrop A								
TOP	Reworked debris (lahar deposits)							
L6–top	Inverse grading after 20 cm		60 %	40 %	Up to 20 cm			
L6–base	Normal grading in the basal 40 cm	L6 is >1.2 m	75 %	25 %	Average 4 cm		2.3	1.2
Border		*c.a.* 2 cm						
L5		40 cm	90 %	10 %	Up to 5 cm: matrix of ash and lapilli		2.1	1.35
Border		*c.a.* 1 cm						
L4	Quite homogenous	30 to 40 cm	90 %	10 %	Up to 7 cm; matrix of ash and small lapilli	Tabular clasts seem aligned with suspected flow direction	2.1	1.35
Border	Sudden decrease in clast >3 cm; possibly erosive, not planar							
L3–top	Upper 20 cm inversely graded	40 cm (could represent two independent layers)			1 to 8 cm	15 % red lithics; 35 % black porous scoria; 40 % black dense juveniles		
L3–base	Basal 15 cm similar to L2		75 %	20 %		<20 % lithics; mainly juvenile scoria	2.1	1.25
Border	Linear mossy vegetation growth on a competent protuding irregularity							
L2		50 cm	75	25	Up to 6 cm; mainly ranging 1–3 cm	<20 % lithics; mainly juvenile scoria	2	1.35
Border	Light gray ashy	*c.a.* 1 cm	-	-	<1 cm	Porous, fragile and not rounded		
L1	Border matrix/clast support	80 cm	40	60	Size up to 30 cm; 90 % between 1 and 10 cm	40–50 % colorful and dense (lithics)	1.7	1.25
BASE								
Outcrop B								
Top	Anthopogenic rubble material							
Liv–top			60 %	40 %	Up to 30 cm, average 8 cm		1.8	1.3
Liv–base	Coarsening up in clast concentration and size	>1 m	80 %	20 %	Up to 8 cm, average 4 cm		1.8	1.3
Border	Well defined ash layer							
Liii–top							1.9	1.3
Liii–base	Coarsening up by increase of clast concentration	90 cm			2 to 8 cm and some blocks		1.9	1.3
Border	Contact seems not erosive, following the top of Li							
Lii		80 cm	80 %	20 %	Lapilli range	Mainly angular juvenile clasts	1.9	1.3
Border	Contact seems not erosive, following the top of Li							
Li	Fills underlying depression. Presence of blocks up to 1.5 m diam.	>90 cm	60 %	40 %	4 to 7 cm		2	1.3
BASE	Soil with pre-existing depressions. The contact contains vegetation and is thus not erosive							

Outcrop B Outcrop B (Fig. 2d, e) lies ca. 1.1 km downstream of outcrop A, in an area where the parent PDCs were not confined by topography. The visible exposure has a total length of about 30 m in the downslope direction. Total thickness varies from 3 to 5 m where a depression is filled with deposits. The base is marked by sediments with a reddish color containing roots and is interpreted as the pre-2006 paleosol. The top is covered with anthropogenically reworked material. Four layers are recognized in the 2006 deposits. Large clasts are distributed throughout the outcrop (16 clasts >0.5 m; largest ca. 1.5 m). Layers 1 and 2 were sampled once; layers 3 and 4 were sampled at their base and top since they showed inverse grading.

"Pancake-lobes"

The surface of the *Ma* deposits locally exhibits a fingered lobe-and-channel morphology (Fig. 3a). The lobes strictly follow topographic lows on the surface of earlier deposits

and build up with a droplet-like morphology: a concave upper surface upstream, ending in a convex morphology, with steep fronts and sides. Upstream from the terminal lobes, only the side levees record the path of the flows (Fig. 3b). They have been observed on the steep slopes of the Chontal sector as well as on low slopes in the distal parts of the Juive valley (Fig. 3a).

The surface of the lobes and levees contains numerous large clasts (>6.4 cm diameter). We termed "pancakes" large clasts characteristically flat and disk-shaped (length and width are about five times the thickness) with a bread-crusted texture (Fig. 3c). The inner part of the pancakes is rich in spherical or elongate bubbles, whereas the rim is denser, sometimes glassy, and shows deep cracks (Fig. 3c). These oblate and fragile pancakes are sometimes intensely folded, but are found unbroken more than 6 km away from the vent, on the lobe and levee surfaces.

Measurements of the long, intermediate, and short axes were performed for all large clasts encountered on three parts of a lobe: on the side, upper surface, and at a depth of about 40 cm below the surface (Fig. 3d). The maximum projection sphericity (Sneed and Folk 1958) was calculated:

$$S = \left((dS\hat{}2)/\left(dL * dI\right)\right)\hat{}(1/3)$$

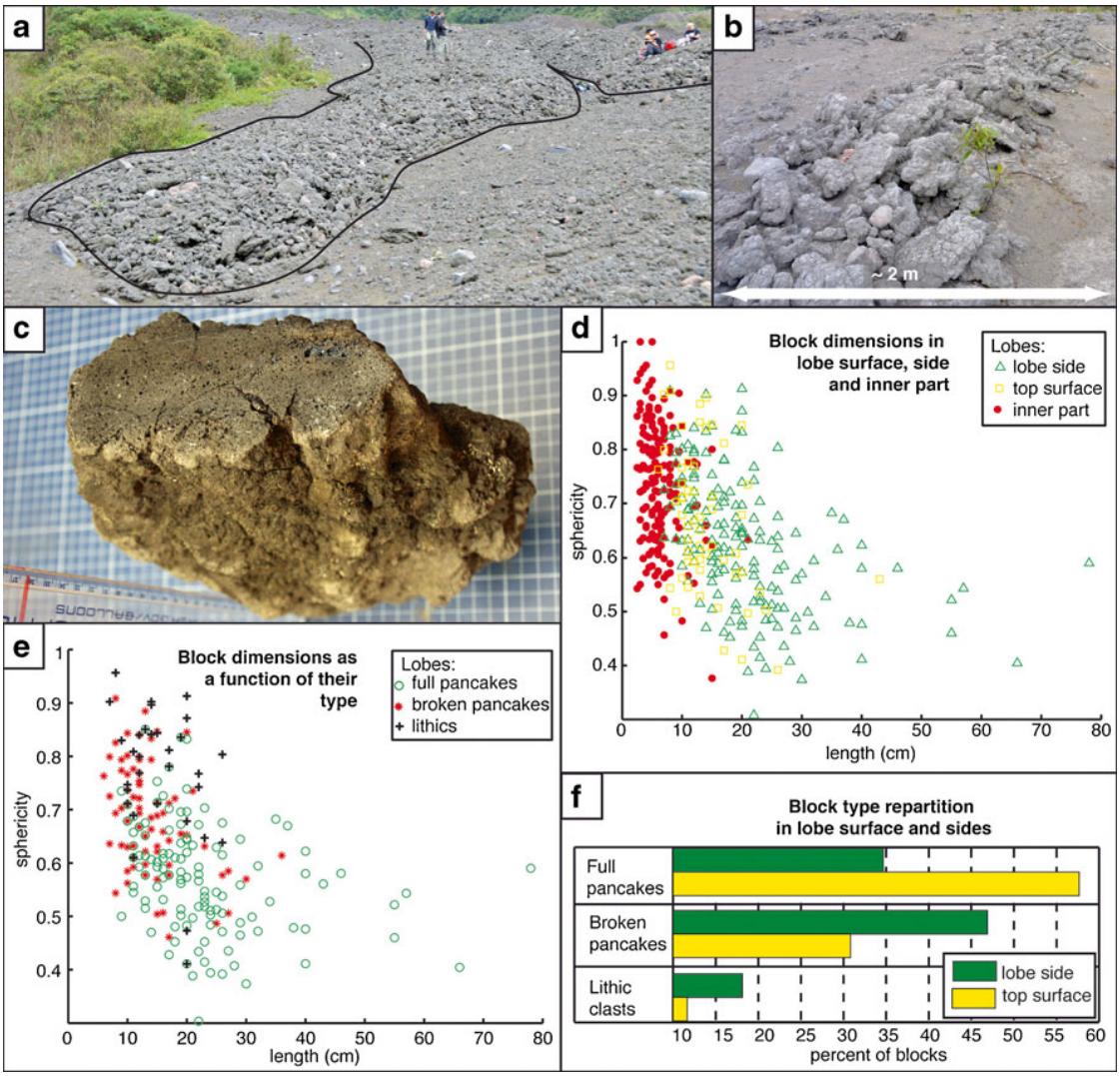

Fig. 3 Lobe and cleft morphologies at the surface of the massive facies. **a** A terminal lobe, geologists in the background for scale. **b** Marginal levée containing "pancakes". **a**, **b** Location in Fig. 7. **c** Cut though a "pancake", background scale and vertical scale marked in cm, the red line marks 26 cm height. **d** Length versus sphericity plot of clasts encountered on a lobe. **e** Length versus sphericity plot of clasts encountered at the surface and side of a lobe versus their type. **f** Relative proportions of full "pancakes", broken pieces of "pancakes" and lithic clasts on the side and top surface of a lobe

With dS the short axis; dI the intermediate axis and dL the long axis.

Large clasts on the lobe sides are the most flattened and longest, whereas the inner lobe contains the smallest and most spherical ones (Fig. 3d). Distinction between large clasts identified as full pancakes, broken pancakes, and lithics was made in the field on lobe upper surface and flanks (Fig. 3e, f). Both parts contain a majority of juvenile pancakes and few lithics, but the upper surface is made of a majority of full pancakes, whereas the flanks contain more broken pancakes. Full pancakes are flatter than the broken pieces, but lithics show the most spherical shapes (Fig. 3e).

Cross-stratified facies

Two types of "cross-stratified facies" (*Xst*) are recognized in the deposits: (1) the proximal facies (*P-Xst*) on the steep upper slopes, where the valleys of the drainage network are not sharply defined (Fig. 4) and (2) the distal facies (*D-Xst*) where valleys are deeply incised (Figs. 5, 6, 7, 8, and 9). Both are predominantly composed of ash and are well stratified with abundant cross-stratification, although massive, decimeter-thick lenses, sometimes with fining-upward trends are present (Figs. 4c and 8f). These massive layers in places grade into diffusely to crudely stratified laminae and vice versa. These deposits occur on the overbanks of the valleys containing the *Ma* facies. Their surfaces reveal well-developed, meter-scale dune bedforms (DBs; Figs. 4b, d and 8e), whose shapes and structures are detailed in a companion paper (Douillet et al. 2013). They vary from 1 to 20 m in length and 0.1 to 2 m in thickness. A 2 cm thick fall deposit was observed draping the DBs, testifying to their pristine shape. Internally, the DBs exhibit cross-stratification patterns typical of PDC deposits, mainly aggrading and stoss-depositional structures (e.g., Schmincke et al. 1973; Cole 1991). Cut-and-fill structures occur locally. No ripple beds, soft sediment deformation structures, or overturned beds have been observed. Partially carbonized wood fragments are present in places. Apart from these characteristics, the two types of *Xst* facies show different patterns in their overall architecture and types of sedimentary structures that justify their distinction.

Proximal cross-stratified facies

The *P-Xst* facies mainly exhibits long (3.2–17.5 m) but not very broad (2.4–12 m) elongate DBs with diffuse crests producing only a slight bulge on the surface (Fig. 4b). They have poorly defined transverse shapes and are widely separated (>20 m). Internally, DBs exhibit thick (up to 20 cm), stoss-constructional, lensoidal layers of a massive mixture of ash, lapilli, and isolated large clasts <10 cm diameter (Fig. 4d). These patterns alternate with thin (1–2 mm) and finer-grained (mainly ash) laminae forming aggrading bedsets with an upstream migration of the crests locally grading into massive ashy layers and vice versa (Fig. 4c). The DBs are interpreted to have formed from high capacity and competence currents and produced at the transition between granular- and tractional-dominated boundary zones by topographic blocking of the bedload (Douillet et al. 2013).

Adjacent eucalyptus trees (15–30 cm diameter) have lost their bark and exhibit 3-cm-deep dents (Fig. 4b). Only minor charring is visible above the deposits, but significantly carbonized parts are found buried in the deposit. In areas near the *Ma* facies, trees are broken, some above their roots (covered in the deposits), others above the surface of the deposits (Fig. 4a). Outside the area of highest impact, trees are still standing but dead.

Distal cross-stratified facies

In comparison with the *P-Xst* facies, the *D-Xst* facies is much poorer in coarse clasts and primarily composed of ash with a subordinate fine-lapilli component distributed throughout in the ash or grouped in decimetric-thick lenses (Fig. 8f). No agglomeration structures are observed and low moisture content of the fluid phase is inferred. Several isolated deposition zones of *D-Xst* facies were observed along a single valley but in restricted areas (Figs. 5, 6, 7, 8, and 9).

DBs are much steeper-sided than for the *P-Xst* facies and an evolution of their morphology is observed (Douillet et al. 2013). The largest ones have transverse shapes, reaching lengths of 17 m. Smaller DBs can show lunate shapes (crests concave upstream), as noted by Sigurdsson et al. (1987) at El Chichón (México). On outer edges of the deposition zones, DBs tend to be very short but wide, more symmetrical, and organized into trains, and are thus termed "two dimensional". Internally, and contrarily to the *P-Xst* facies, cross-stratification exclusively consists of crude millimeter-scale laminae organized in stoss-aggrading bedsets, locally grading into diffusely stratified to massive and vice versa. They are interpreted as having formed under the influence of both direct fallout and traction-dominated boundary layer flows (Douillet et al. 2013).

Spatial distribution

Mapping method

The *Xst* deposit distribution was mapped with a handheld GPS along the two valleys most affected by PDCs, the Juive and Achupashal valleys (Fig. 1). In areas containing abundant DBs, the orientation, and sometimes length, thickness, and width of several hundred DBs were measured (Figs. 4a, 5a, 6, and 8). The direction of the parent currents was inferred assuming that DB crests are oriented perpendicular to the flow direction (as observed by Moore (1967) at Taal). Although

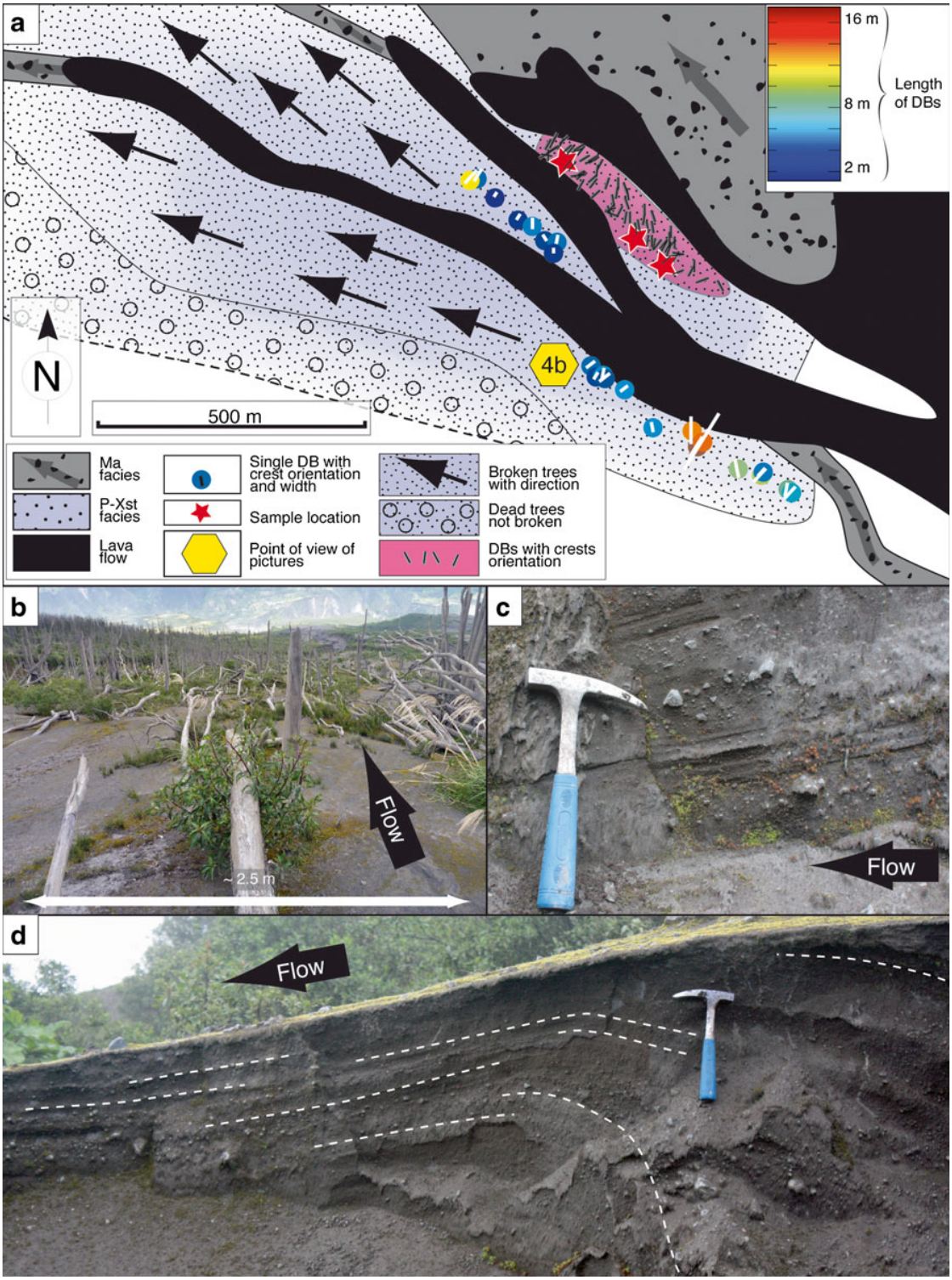

Fig. 4 Proximal cross-stratified facies in Achupashal valley. **a** Map of the deposits with DB orientation, length and width, direction of fallen trees, and extent of damaged trees. **b** Trees are broken and align in the downstream direction. **c** Variation in sedimentological patterns within a proximal DB. **d** Cross-section of a DB from proximal zone

outer shapes only reflect the final stages of a DB's formation, cross-sections show general stability of the DB crests throughout deposition.

Color-coded isopach maps of the dimensions of the DBs were produced using Matlab™. Linear interpolation was done by Delaunay triangulation, connecting each data point to its

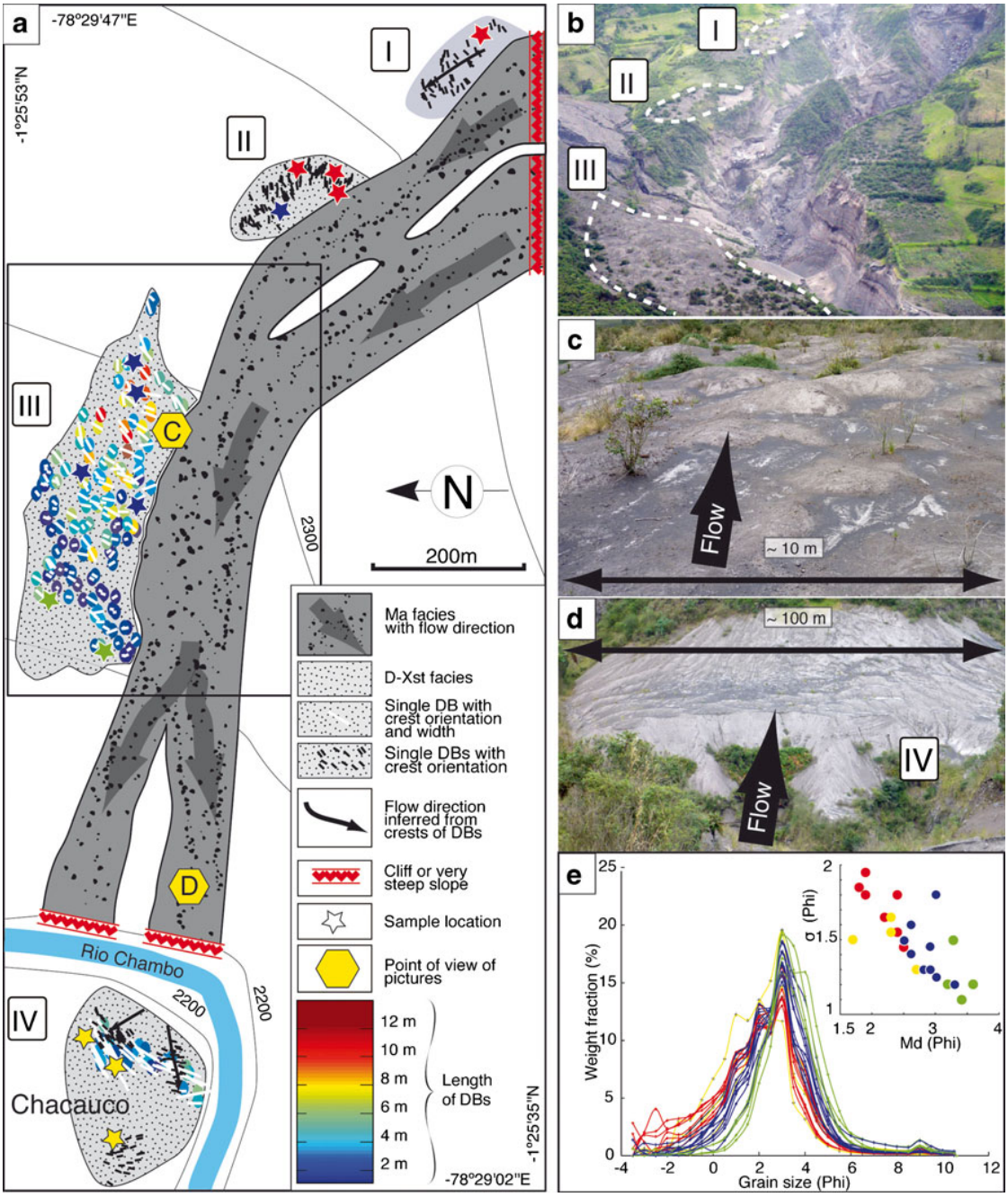

Fig. 5 Distal cross-stratified facies in Achupashal valley. **a** Map of the deposits with DB orientation, length and width. **b** Photograph showing ash bodies I, II, and III. **c** DBs at the surface of ash body III. **d** Ash body IV, note wide but short DBs on the surface. Points of view of pictures are marked on the map. **e** Grain size distribution of the distal Achupashal samples. *Inset* shows median diameter versus sorting coefficient. Sample location on map (*stars*). Note downstream fining

natural neighbor and the Voronoi polygon around each resulting point was plotted with color coding (Sandwell 1987; Barber et al. 1996). This method was preferred to a kriging because the variogram or expectation of the data is unknown but the data are reliable (Cressie 1993). The density of polygons reflects the density of data and the lines representing the crests of DBs have a width proportional to those of the DBs (Figs. 4a, 5a, 6, 7, and 8a, b).

Proximal cross-stratified deposits: the upper Achupashal valley

The *P-Xst* deposits in the Achupashal valley are found below 3,100 m a.s.l. (3.1 km from the crater rim) at a general decrease in slope angle (from 30° to 25°; Fig. 1), where the drainage network is not as sharply defined as lower down. The deposits outcrop on the overbanks of the valleys in a sheet-like

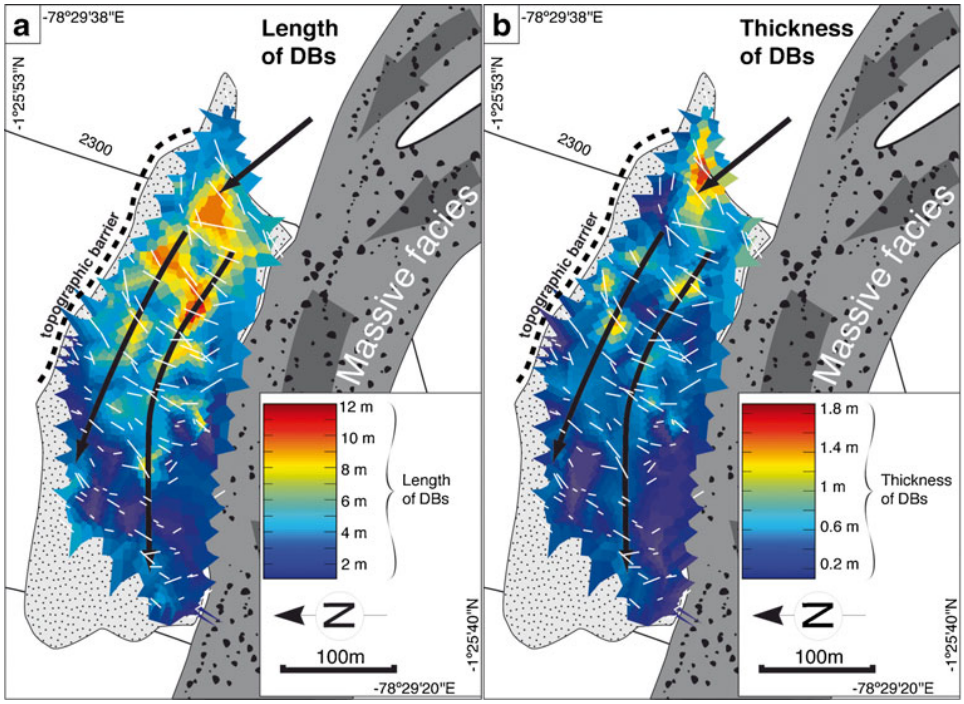

Fig. 6 DB dimensions on ash body III. *White lines* mark the crests of DBs with their orientation and the length is proportional to the width of the DBs. *Arrows* mark the inferred flow direction

fashion (c.a. 2×1 km^2; Fig. 4a), which gradually thins from a minimum of 5.5 m (base not observed) in central zones, until it eventually vanishes laterally.

Fallen tree tops align in a direction thought to reflect the parent flows' direction (Fig. 4b), but show less variation in orientation than the DBs. Crest orientation of DBs are subparallel to the valleys and follow the main gradient, though DBs closest to the *Ma* facies deposits are oriented perpendicular to the valleys.

Distal cross-stratified ash bodies

In distal zones, well-developed drainage channels directed PDCs. Whereas *Ma* facies deposits are confined to the valleys, the *D-Xst* facies is organized as several spatially isolated and disparate "ash bodies" (Figs. 5, 6, 7, and 8). By ash body, we mean a significant volume of *D-Xst* facies deposits distributed over a restricted area, regardless of its genesis. The main characteristics of each ash body are listed in Table 2 for the distal Achupashal valley and Table 3 for the Juive drainage network. They often show a sedimentary wedge shape, i.e., a sharp increase in thickness at the upstream end, and a gentle decrease downstream (Fig. 9a). This wedge shape onset is best shown by ash body C (Fig. 8), where it takes the shape of a quarter pipe, 82 m in width, that thickens from 0 to 5.5 m over less than 14 m in the flow direction (Fig. 8c, d). There, DBs' orientation radiate from the quarter pipe and have crests normal and in train with it near the onset (Fig. 8a–c). In sedimentary wedges, DBs decrease in size downstream.

Granulometry and componentry

Methods

Samples were collected in August 2009 for granulometry. For the *Ma* facies, the <2 cm fraction was sampled in each layer from outcrops A and B (10 samples; Fig. 2). Thirty-five samples were taken on the stoss and lee sides of DBs: 6 in the *P-Xst* facies, 26 in the lower Achupashal and 3 in the Juive valley (location Figs. 4a, 5a and 7, respectively). For those in DBs, the top 5 cm were removed prior to sampling in order to exclude the final fallout deposits and reduce weathering and modification effects from wind and precipitation.

Mechanical sieving (10 min, 0.5 Φ interval between −3.5 Φ and +3 Φ) was performed on dry aliquots of 250 and 75 g for the *Xst* and *Ma* facies samples, respectively. The fine fraction (+3.5 to +10.5 Φ) was measured by laser diffraction in a LS230 (Beckman-Coulter, 5×5 runs of 0.1 g averaged). The data were merged to produce a single continuous curve, with cumulative percent of material (<3.5 Φ) in the laser data corresponding with the mechanical one (Fig. 10a, c, e).

The results were interpolated ("interp1–pchip option" in Matlab™) and integrated to obtain cumulative curves, and compute the mean grain size (M_d) and sorting coefficient (σ) (Otto 1939; Fig. 10a, c, e):

$$M_d = \Phi_{50}; \sigma = (\Phi_{16} - \Phi_{84})/2;$$

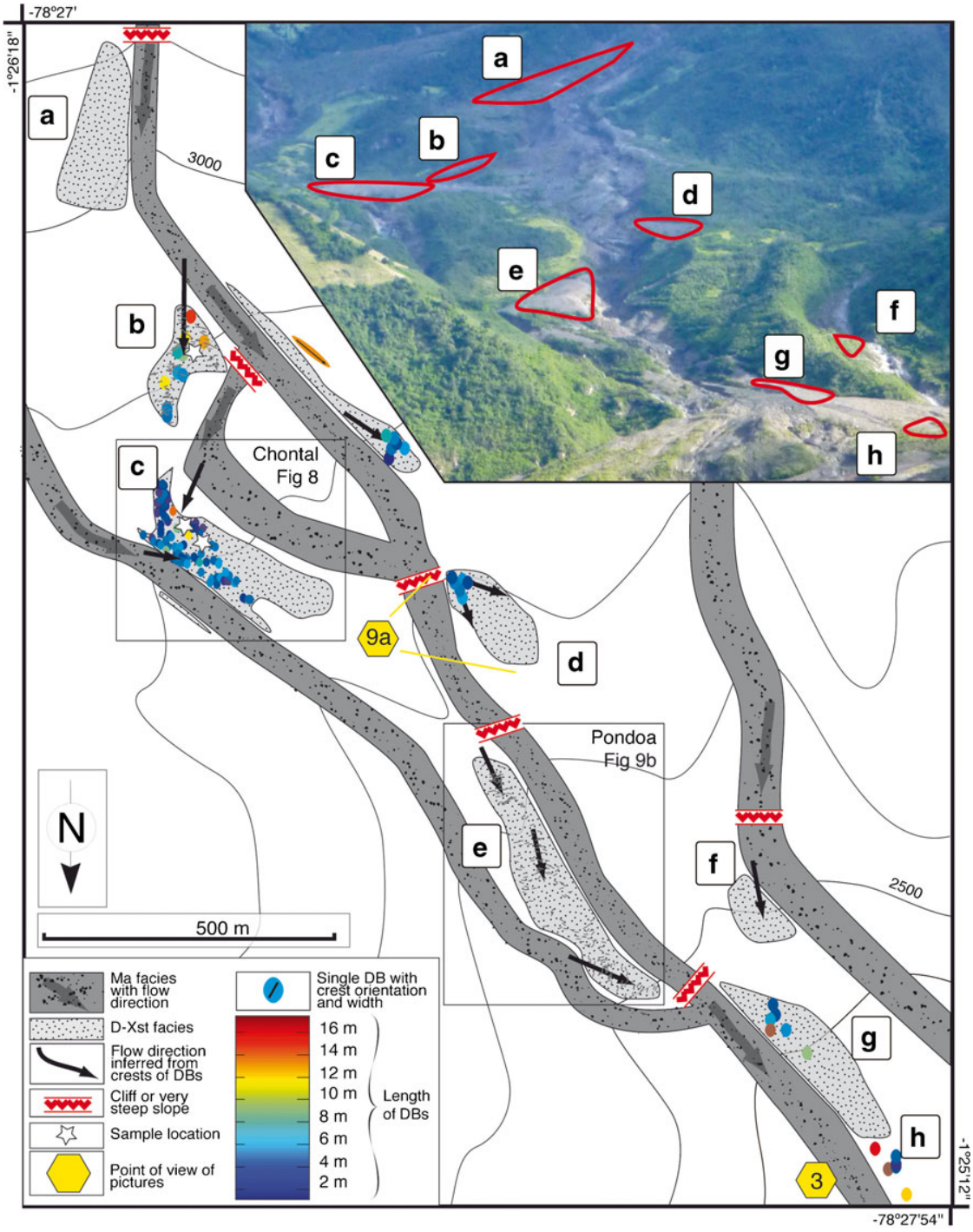

Fig. 7 Map of the Juive drainage with DB orientation, length, and width. In inlet is a photograph of the zone. *Rectangles* surround the map of Chontal (Fig. 8a, b) and Pondoa (Fig. 9b)

where Φ_i is the grain size for which i% of the total material is smaller than the given grain size.

Componentry analysis was performed on the 0 Φ (1 mm) fraction of c.a. 16,000 clasts from five samples with four groups defined: crystal fragments, altered, vesiculated, and dense clasts (Fig. 10f).

Results

The occurrence of three modes at 1, 2, and, the main one, at 3 Φ independently of the facies is striking in all samples (Fig. 10a, c, e). At outcrop A, the matrix of L1 was found to be coarser than in L2–L6, the latter being all very similar

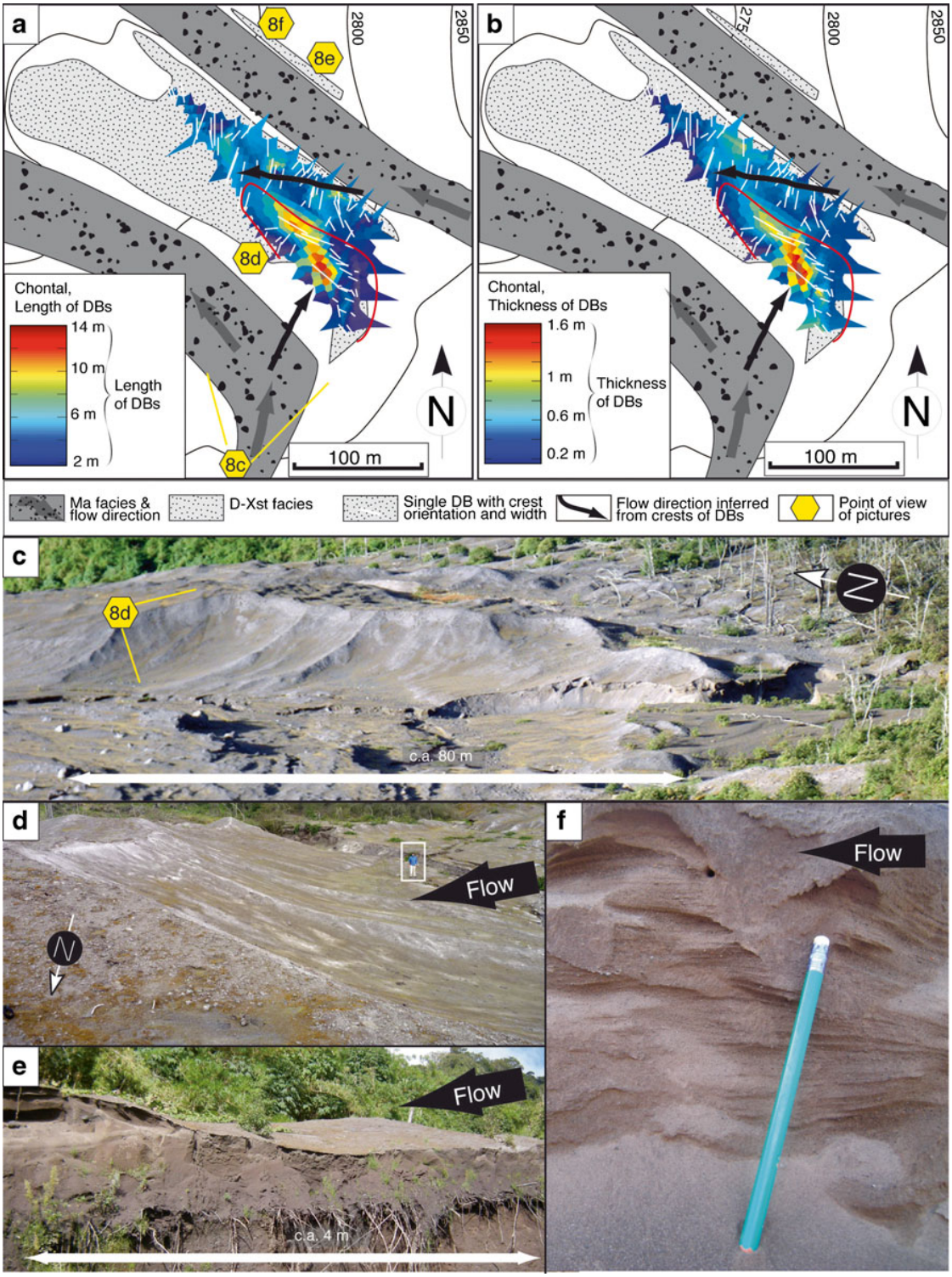

Fig. 8 Distal cross-stratified facies in Chontal sector. **a**, **b** DB dimensions; *white lines* mark the crests of DBs with their orientation and the length is proportional to the width of the DBs. *Arrows* mark the inferred flow direction. **c**, **d** the sudden quarter pipe shape of the western upstream side of the ash body. **e** DBs on the edge of the ash body. Note vegetation at the basal contact between the deposit and underlying soil. **f** Ash cross-stratifications in the Chontal sector

(Fig. 2c). This confirms the particularity of L1 from field observation (higher clast content and size; Fig. 2c). The matrix of the four layers from outcrop B exhibit very similar grain size distributions between each other and contain less material

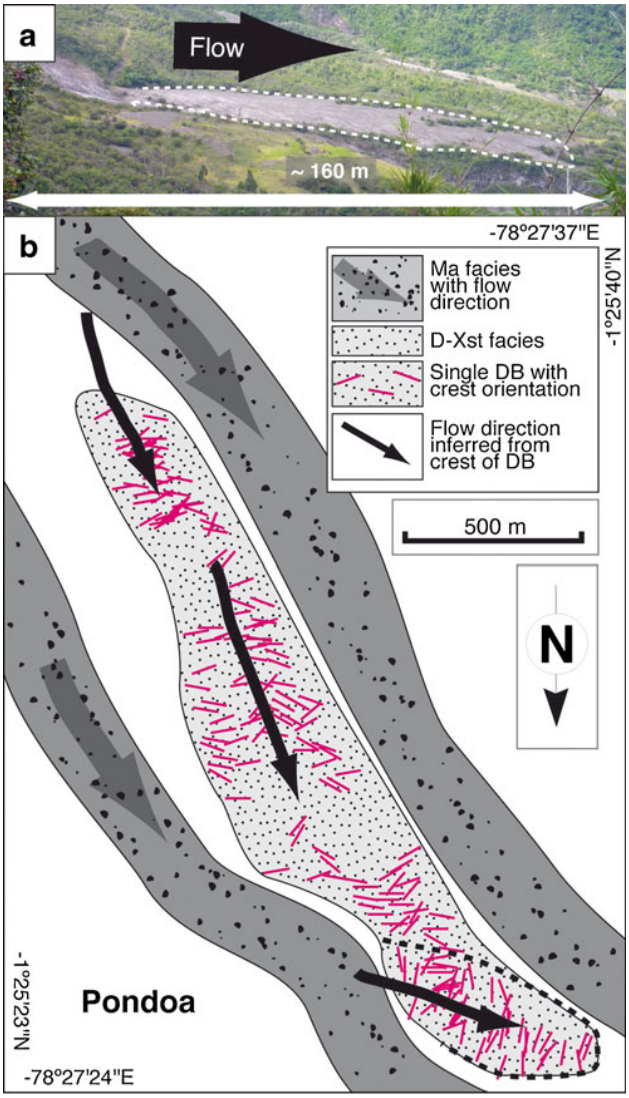

Fig. 9 Ash bodies within the Juive drainage. **a** Ash body D downstream of a cliff, picture location in Fig. 7, looking westward. **b** Map of ash body E with DB orientation. The influence of two currents is visible by the orientation of the dune bedforms and the eastern valley influence zone is underlined by dashed line

<1.5 Φ and finer M_d compared to outcrop A (Fig. 2c). No correlation between layers from the two outcrops could be done, but L1 from outcrop A seems absent in outcrop B. Samples from the matrix fraction of the *Ma* facies show better sorting (probably due to the cutoff at 2 cm) but a coarser content relative to the *Xst* samples.

Samples from *P-Xst* and *D-Xst* facies are similar, poorly sorted (following the verbal classification of Folks 1964, i.e., 1 Φ<σ<2 Φ) with M_ds between 1.8 Φ and 3.7 Φ (Fig. 10b). In a M_d vs σ graph, they plot within the flow field described by Walker (1971), but not in the most probable zone. They also partially overlap with the fall field (Fig. 10d) and fit very well with the "base-surge field" defined by Crowe and Fisher (1973; Fig. 10d), even if Walker (1984) showed that large variations in the grain size parameters of pyroclastic cross-bedding occur.

Samples from the lower Achupashal valley show a downstream fining between ash bodies I, II, and III (green, pink, and black, respectively, in Fig. 5e). Samples from ash body IV (the lowermost deposit) are rather similar to the *P-Xst* samples, as also observed in the field, and interestingly, ash body IV is located at the base of a cliff.

Componentry was performed on samples from the *P-Xst* zone, ash bodies II, III, and IV in the lower Achupashal and ash body B in the Juive drainage (Fig. 10f). Two samples differ significantly from the average results (57 wt.% vesiculated, 19.5 wt.% dense, 12.5 wt.% crystal, 11 wt.% altered): the *P-Xst* sample reveals less vesiculated (38.5 %) and more dense non-altered clasts (35.1 %) and crystal fragments (17.1 %). The sample from ash body B shows more vesiculated (69 %) and less dense clasts (7.9 %).

Dynamic repose angle (the slope of a heap constructed by falling material) and static repose angle (the slope of a heap under excavation) are 32° and 41°, respectively, for bulk *D-Xst* samples and 38° and 52°, respectively, for the fine fraction (<250 μm).

Interpretation

Facies

Massive facies

Ma facies is massive and unsorted, contains large clasts, is coarse grained, and deposits are confined by topography, respectively, indicating that there was no traction-dominated flow boundary zone and that the parent flows had a large transport capacity and were too dense or thin or slow to overflow topography. *Ma* facies is interpreted as the deposits of parental dense pyroclastic flows. The different layers, in places separated by thin strata of ash interpreted as fall deposits, are the results of different flows separated by pauses. The report from direct observation of three main flows in this valley contrasts with the six layers observed at outcrop A and four at outcrop B, and we infer that some flows did not reach the lowermost parts of the valley. Predominance of lithics, smaller percentage of coarse in the sieving results, together with the location of outcrop A at the runout limit of the July PDCs and the ashy layer between L1 and L2 (interpreted as a time break in the flow), suggest that L1 was formed during the July eruption, though it is unclear whether L1 represents a primary deposit or secondary lahar debris deposit. The L1–L2 contact is thus interpreted as a fall deposit formed at the beginning of the August events.

The lobes and levees formed during the last flows reported from direct observation. They indicate self-channelization of

Table 2 Principal characteristics of the distal ash bodies from the Juive valley

Ash body	Location	Shape	DBs dimensions (max, min, mean)	DB type (see Douillet et al. 2013)	DBs orientation	Notes
Juive drainage network						
A	3.6 km from the vent; downstream cliff; steep slope (25°)	Fan; The thickness of the body is maximal in the central part and decreases toward the edges		Mainly transverse	Subparallel to valley before the bent, some DBs close to the valley are perpendicular to it	
B	Outer overbank of valley curve (from N0 to N330); steep slope (22°); elevation: 2,900–2,870 m.a.s.l.	Downstream decrease in DBs' dimensions	Width: (41×4×13.34); length: (14.8×5.7×9.34); thickness: (20.2×0.94);	Transverse; 2D	Subparallel to valley before the bent	
C/Chontal	On the outer overbank of two bordering valleys that curve; elevation: 2,843–2,772 m.a.s.l.	Sedimentary wedge; quarter pipe onset from the West; downstream decrease in DBs' dimensions;	Width: (18.5×1.4×6.40); length: (14×1.5×4.9333); thickness: (1.6×0.1×0.57);	Transverse at onset; lunate; 2D on edges; found without DBs in lower part (in Nov. 2010)	Subparallel to valleys before the bent; radiating from western quarter pipe. Crest orientation and size decrease of DBs show that currents from both valleys influenced the morphology;	Main input of sediment seems to come from western valley. Basal and downstream parts contain an increased amount of coarse, and it seems that Ma facies is present, though clearly absent on the edges (Fig. 8e).
D	Downstream cliff	Sedimentary wedge		Transverse; lunate	Subparallel to valley and opening angle (N340 to N290–valley N340)	
E/Pondoa	Downstream cliff	Elongate			Their orientation shows that the ash body was emplaced by currents overflowing from a curve higher in the valley (Fig. 9b). Orientation of DBs in the lower part of this zone is also influenced by currents coming from the eastern valley	
F	Downstream steep slope outer overbank of valley curve	Fan				
G	Downstream steep slope; behind topographic shield;					
H	6 km from vent; elevation: 2,040–2,025 m.a.s.l.	Not an ash body form	Width: (14×6.2×10.26); length: (17.3×2.5×9.5); thickness: (1.5×0.3×0.78);	Numerous composite DBs (climbing on each other)		

the parental flows, implying an upper free boundary and a dense and steady-state frictional regime (Félix and Thomas 2004). The higher amount of large clasts on levees and lobes surface compared to the inner part is commonly observed (Cole et al. 2002; Félix and Thomas 2004; Lube et al. 2007) and interpreted as due to rafting of coarse clasts to the front and sides of the flow (Calder et al. 2000). Indeed, the disk-shaped "pancakes" cannot be preserved over 6 km of transport in the inner part of a flow: size measurements show an absence of full pancakes inside the lobes. This further indicates a sharp density interface at the upper boundary of the dense pyroclastic flows producing the lobes.

As commonly observed in other deposits of dense pyroclastic flows (e.g., Boudon et al. 1993), outcrop A deposits (more upstream) contain fewer large clasts as well as finer-grained matrix than outcrop B deposits, indicating a bypass at outcrop A before deposition of the large clasts at outcrop B, and a lower carrying capacity at outcrop B.

Proximal cross-stratified facies

The broken trees and flatness of bedforms indicate the high energy of the parental flows. This facies shares similarities in its architecture with the "veneer and surge overbank facies"

Table 3 Principal characteristics of the distal ash bodies from the Achupashal valley

Ash body	Location	Shape	DBs dimensions (max, min, mean)	DB type (see Douillet et al. 2013)	DBs orientation	Notes
Lower Achupashal valley						
I	6.4 km from vent; downstream major cliff; behind a topographic shield		Width: up to 15 m; length: up to 12 m; thickness: up to 1 m;	Mainly transverse	Subparallel to valley before the bent	
II	Very close to valley			Mainly transverse	Initially out of the valley but towards the valley downstream	Local topography strongly dips toward the thalweg
III/Cusua	Outer overbank of valley curve elevation: 2,325–2,187 m.a.s.l.	Sedimentary wedge; large DBs hilight the onset and decrease in dimensions downstream	Width: (17.5×1.4×4.75); length: (12×1.1×4.56); thickness: (1.9×0.1×0.51);	Transverse; lunate; 2D on edges	Concentrically to upstream onset; subparallel to valley before the bent on upstream half; following gradient on lower part with possible splitting of the current (from orientation and size)	An abandoned house 50 m away from the ash body was almost completely preserved and only a few centimeters of ash entered it
IV/Chacauco	Downstream cliff; base of the volcano; on the opposite side of Chambo river (western side), dip against flow dection (-10º); elevation: 2,166–2,156 m.a.s.l.	Fan (Fig. 5d)	broad but short (Fig. 5d) width: (38×5.2×13.06); length: (6.2×1.84); thickness: (1.1×0.3×0.53);	Only 2D	Concentric to the eastern valley branch from Achupashal before cliff (Fig. 5a)	Direct observations: PDCs crossed the Chambo river and most material landed into it; steam and ash clouds billowing from the river. Field observations show an increased amount of coarse, comparable to P-Xst facies

described by Lube et al. (2011) for Merapi volcano. However, cross-stratification is more abundant at Tungurahua. Moreover, the location of overbank deposits with orientation of DBs pointing away from valleys do not support interpretation as a veneer flow deposit in the sense of Walker et al. (1981) as "the record of the passage of a pyroclastic flow, where the flow itself has moved farther on", since no flow has moved farther on in the direction indicated by the orientation of the DBs.

The *P-Xst* facies contains features indicating deposition from two alternating processes. The ashy bedsets evolving from cross-stratified to massive relate to dilute PDCs with a basal boundary evolving from tractional to granular due to changes in deposition rate (see Douillet et al. 2013). The intercalated coarse and massive layers are related to granular-dominated boundary zones and their coarser grain size compared to the cross-stratified bedsets also suggests that also the transport system was different, not only the boundary processes. We thus interpret those layers as deposits from dense pyroclastic flows that overflowed the poorly defined valleys of the proximal zone (Fig. 11).

The source of momentum likely comes from acceleration on the steep slopes because "visual observation indicates that the PDCs were formed under conditions of zero, or small, initial velocities" (Kelfoun et al. 2009). Moreover, the wide extent of the sheet-like deposit suggests that momentum could be maintained by the steepness of the flanks close to the repose angles.

Distal cross-stratified facies

The grain size distribution and sedimentary structures of the *D-Xst* facies indicate deposition from turbulent flows with a tractional basal boundary. Moreover, the ash bodies are found on interfluves, commonly on the outer overbank of curves with orientation of DBs aligning with the direction of the thalweg upstream of the curve (zones B, C, E, F, and III). This indicates that inertial effects dominated over gravitational ones, making the flows less susceptible to redirection in response to topography, and suggesting *dilute* flows. DBs in ash body II, III, and C indicate currents initially traveling away from the valley but reorienting to the local topography gradient after a short distance. Thus, even if initially driven by their inertia when overflowing, the parental flows were gravity driven as *density currents* rather than driven by energy acquired from a blast or column collapse. Thus, the *D-Xst* facies was deposited from *turbulent*, *dilute* pyroclastic *density currents* with a basal *tractional boundary*. The occasional gradations into massive, ashy layers indicate that the tractional boundary was sometimes inhibited by high basal clast concentrations due to high deposition rates, but still with a surrounding dilute PDC.

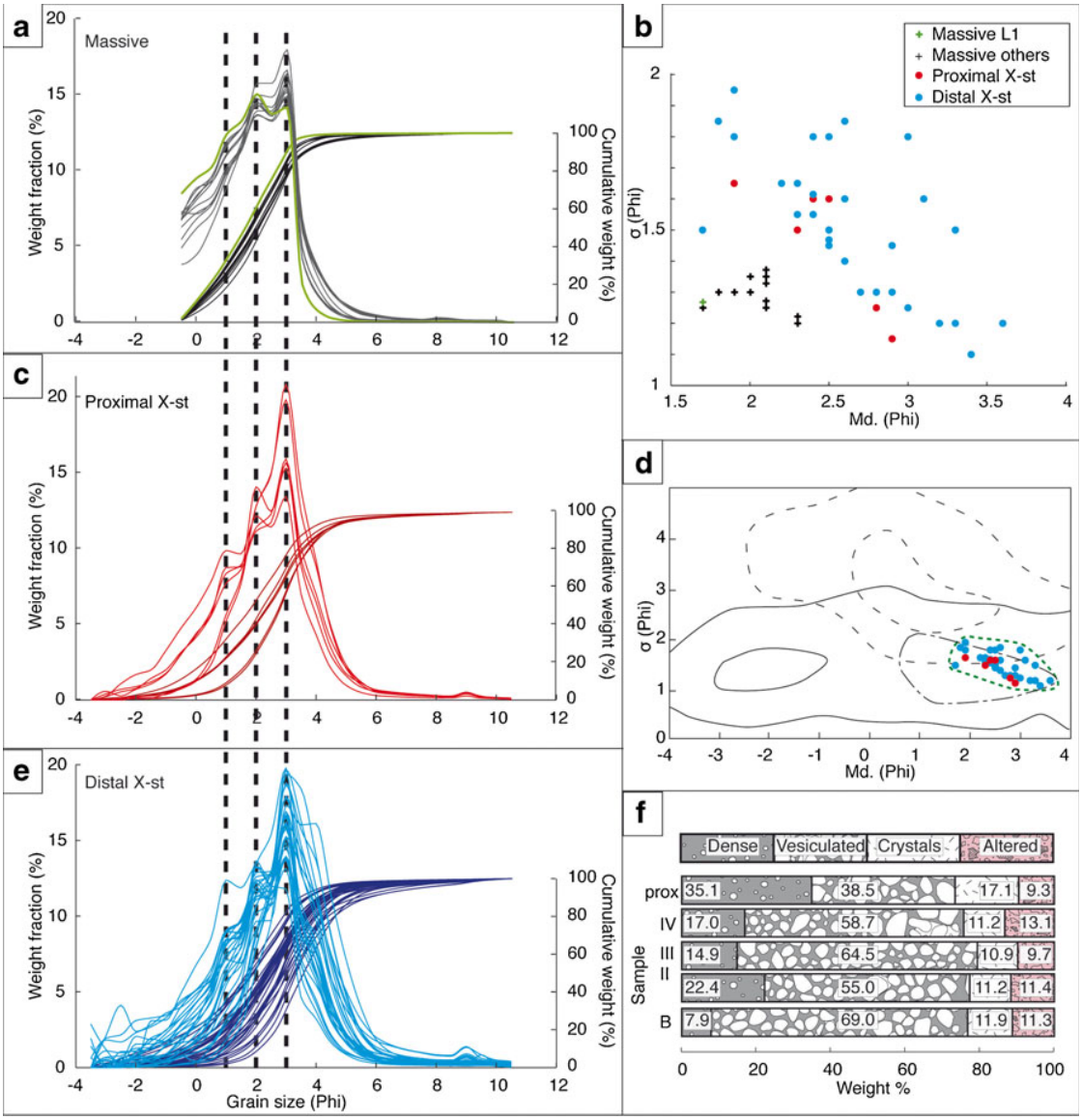

Fig. 10 Sample analysis. **a** Massive, **c** proximal, and **e** distal cross-stratified facies samples. The scale of the frequency curves on left axis, of cumulative weight on right axis. Note the three modes at 1, 2, and 3 phi present in most samples. **b** Median diameter versus sorting coefficient for all samples following the same color coding. **d** Cross-stratified samples plotted with flow (*full lines*) and fall (*dashed lines*) fields of Walker (1971) and "surge" field (*chain line*) of Crowe and Fisher (1973). **f** Componentry analysis within five cross-stratified samples

Origin and deposition of the dilute PDCs

Three main modes are present in the granulometry of most samples. Strikingly, three modes are also present in the fall deposits (though shifted to the fines compared to our dataset), which were interpreted as reflecting a mixed influence from the plume and very dilute and distal co-ignimbrite ash clouds (Eychenne et al. 2012). Within a single current, different modes can be related to different transport mechanisms (Branney and Kokelaar 2002, p. 25) or caused by particle aggregation within the suspended load. We favor an alternative explanation for the presence of the same modes in all facies at Tungurahua. The three modes might be a signature of the fragmentation process rather than the transport process, i.e., a single fragmentation phase was responsible for the flows producing the *Ma*, *P-Xst*, and *D-Xst* facies, implying that the differentiation between dense and dilute parts took place during flow. Otherwise, the fragmentation mechanisms and thus the grain size distributions should be different (Perugini and Kueppers 2012).

Co-ignimbrite plumes have been interpreted to be related to air entrainment at cliffs (Hoblitt 1986; Calder et al. 1997). Fisher (1983) postulated the existence of flow transformations in sediment gravity flows leading to the creation of dilute PDCs from dense flows. At Tungurahua, the steep upper slopes (30°, for dynamic repose angles of 32°) may have enhanced the entrainment of air, subsequently producing the

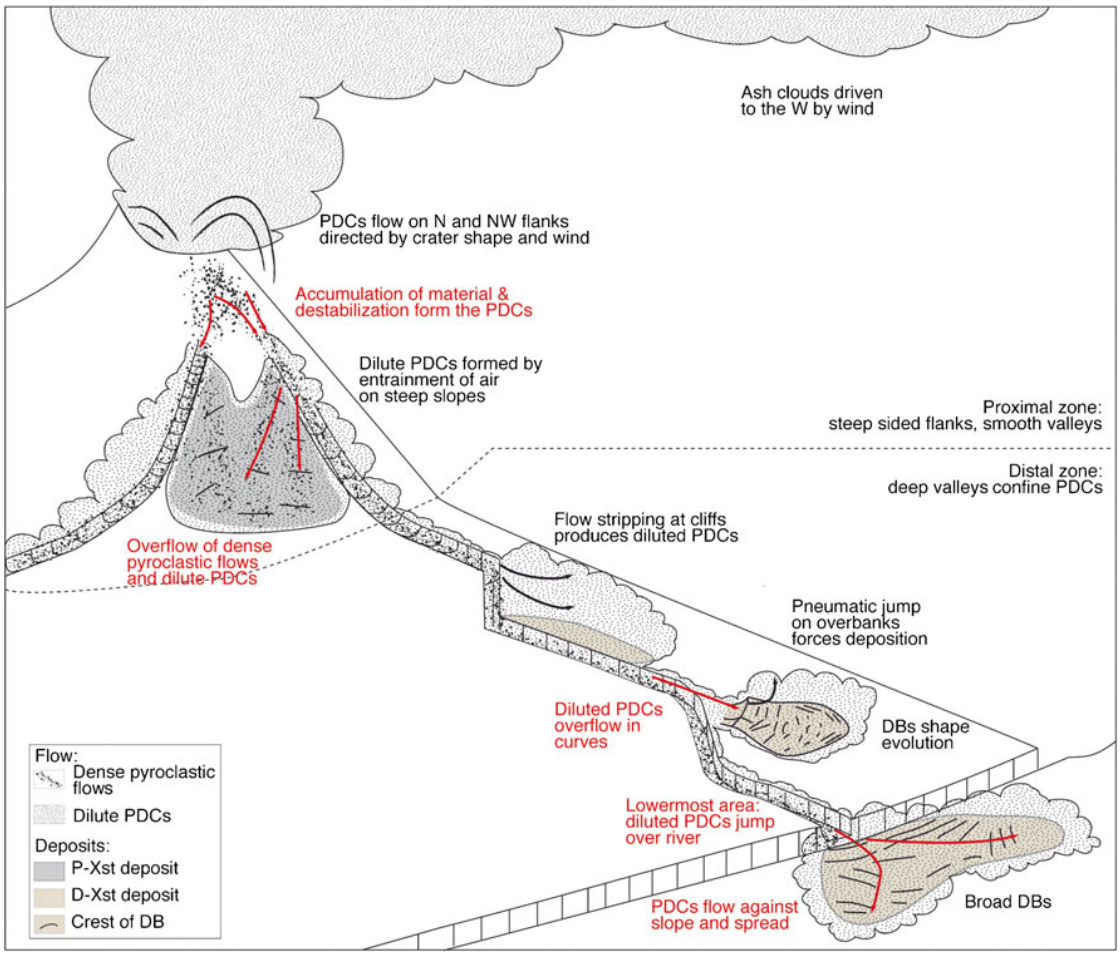

Fig. 11 Interpretative sketch for the formation and deposition of cross-stratified deposits from the August 2006 PDCs at Tungurahua

dilute PDCs responsible for the *P-Xst* facies (Fig. 11). In that case, the gas phase for the dilute PDCs would be mostly ambient air, explaining why trees were only burned when buried in the deposits.

If dilute PDCs had continuously and monotonically emplaced the distal ash bodies, one should observe a monotonic downstream fining trend in the grain size distributions and size decrease of the DBs. Instead, and contrary to most datasets on the size of DBs versus distance from the vent (Wohletz and Sheridan 1979; Sigurdsson et al. 1987; Druitt 1992), the decrease is local for each ash body from its upstream end point (Figs. 6 and 8), while no particular trend is observed with distance to the vent (zone H contains bigger DBs than A, though 2.5 km further away from the vent). Thus, local maximum of energy and/or particle concentration are acting individually for each ash body at their onset rather than a continuous flow. The location of the ash bodies downstream from cliffs further suggests that the latter triggered flow-stripping processes (Fig. 11).

Whether the dilute mode of PDCs existed prior to their encounters with the cliffs is not clear. We do not observe a general decrease of grain size with transport distance, but rather local fining trends depending on distance from the last cliff (Fig. 5e). The dilute PDCs depositing the *D-Xst* facies might thus be created from the dense pyroclastic flows at cliffs by air entrainment and mixing, and be very local features (Fig. 11). As such, they could be termed *diluted* PDCs, and not simply *dilute* PDCs. However, no continuous depositional units are observed and no correlation with the layers observed in the *Ma* outcrops can be done. Interestingly, Andrews and Manga (2012) suggested that the greatest extent of a lamina scales with turbulent eddy dimensions in a dilute PDC: which is 300 m for 125 μm particles and a 30 m/s current, comparable to the extent of the ash bodies.

A higher abundance of vesicular clasts is observed in the samples from the distal Achupashal compared with the proximal ones. This can result from preferential deposition of dense clasts leading to their depletion in distal parts, or can be a consequence of transport abrasion, a process often suggested in PDCs (Dufek and Manga 2008). Indeed, abrasion is more efficient on vesicular clasts (Kueppers et al. 2012). The large number of broken "pancakes" found inside the lobes must have produced vesicular ash by abrasion. These abrasion-induced vesicular ash particles are possibly the reason for the higher

amount of vesicular clasts in the ash fraction in distal zones, given that those dilute flows emanated from the dense.

Whether the dilute PDCs pre-date encounters with the cliffs or not, the local extent of the ash bodies shows that they lacked energy and sufficient particle load after flow stripping, and/or that they rapidly slowed and deposited (as suggested for Unzen by Takahashi and Tsujimoto (2000) and supporting Walker (1984) in his "overall impression that surges—i.e., dilute PDCs—are weak events"). Furthermore, the wedge shape of many ash bodies strikingly resembles sedimentary wedges deposited from experimental particulate density currents at breaks in slopes (Mulder and Alexander 2001) and hydraulic jumps (Sequeiros et al. 2009). The quarter pipe onsets best exemplified in ash body C recorded a strong transition from erosive to depositional currents. Douillet et al. (2013) interpret the associated sedimentary structures as formed by deposition along an intermediate tractional and direct fallout flow boundary. These wedge-shaped ash bodies are located at sharp breaks in slope of the underlying bed. We suggest that these sudden changes from erosive to depositional behavior might be produced by "pneumatic jumps" of the entire dilute PDCs, and the wedge-shaped ash bodies represent their sedimentary signature (Fig. 11). However, no data on the internal stratification of the entire bodies are so far available to settle this genetic question. "Pneumatic jumps" have been suggested for the generation of co-ignimbrite plumes at break in slope for "hot" PDCs (Hoblitt 1986; Calder et al. 1997). Hoblitt (1986) further describe an "ash cloud surge" that overrode the channel walls and shortly thereafter generated a buoyant plume, possibly linked to a "pneumatic jump". Such features might have forced deposition from dilute PDCs at Tungurahua by lowering lateral velocities.

While the long-lived *dilute* vs. local *diluted* nature of the PDCs and deposition through "pneumatic jumps" cannot be resolved, PDCs with a tractional basal boundary, low particle concentration, and very high deposition rates were the parent flows that deposited the distal cross-stratified facies. They were dependent upon the dense pyroclastic flows for provision of energy and supply of particles, and topography has had a significant role in their emplacement, triggering both their overflow and subsequent overbank deposition (Fig. 11).

Acknowledgments We thank our colleagues from Instituto Geofisico, Quito for their valuable information and discussion and Jackie Kendrick for editing the manuscript. The reviews by V Manville, R Cioni, L Guriol, and G Lube were very helpful. We are indebted to the following (partial) funding sources: Alsatian grant BOUSSOLE (GAD); the grant THESIS from the Elite Network of Bavaria (GAD); Deutsche Forschungsgemeinschaft grant KU2689/2-1 (GAD and UK), the Deutsche Forschungsgemeinschaft grant LA 2651/1-1 (FG, JBH, UK, YL); a Research Professorship (LMUexcellent) of the Bundesexzellenzinitiative (DBD); and an advanced grant from the European Research Council–EVOKES 247076 (DBD).

References

Abdurachman EK, Bourdier JL, Voight B (2000) Nuees ardentes of 22 November 1994 at Merapi volcano, Java, Indonesia. J Volc Geotherm Res 100(1–4):345–361

Andrews BJ, Manga M (2012) Experimental study of turbulence, sedimentation, and coignimbrite mass partitioning in dilute pyroclastic density currents. J Volc Geotherm Res 225:30–44

Baines PG (1998) Topographic effects in stratified flows. Cambridge University Press, Cambridge, p 500

Barba D, Arellano S, Ramón P, Mothes P, Alvarado A, Ruiz G, Troncoso L (2006) Cronología de los eventos eruptivos de Julio y agosto del 2006 del volcán Tungurahua. Resumen extendido de las 6tas. Jornadas en Ciencias de la Tierra. Ecuador, DG-EPN, 177–180

Barber CB, Dobkin DP, Huhdanpaa HT (1996) The quickhull algorithm for convex hulls. ACM Trans Math Softw 22(4):469–483

Boudon G, Camus G, Gourgaud A, Lajoie J (1993) The 1984 nuées-ardente deposits of Merapi volcano, Central Java, Indonesia: stratigraphy, textural characteristics and transport mechanisms. Bull Volcanol 55:327–342

Branney MJ, Kokelaar P (2002) Pyroclastic density currents and the sedimentation of ignimbrites. Geological Society Memoir no 27, London, p 143

Brissette FP, Lajoie J (1990) Depositional mechanics of turbulent nuées ardentes (surges) from their grain sizes. Bull Volcanol 53:60–66

Burgisser A, Bergantz GV (2002) Reconciling pyroclastic flow and surge: the multiphase physics of pyroclastic density currents. Earth Planet Sci Lett 202:405–418

Calder ES, Sparks RSJ, Woods AW (1997) Dynamics of co-ignimbrite plumes generated from pyroclastic flows of Mount St. Helens (7 August 1980). Bull Volcanol 58:432–440

Calder ES, Sparks RSJ, Gardeweg MC (2000) Erosion, transport and segregation of pumice and lithic clasts in pyroclastic flows inferred from ignimbrite at Lascar Volcano, Chile. J Volc Geotherm Res 104: 201–235

Charbonnier SJ, Gertisser R (2008) Field observations and surface characteristics of pristine block-and-ash flow deposits from the 2006 eruption of Merapi Volcano, Java, Indonesia. J Volc Geotherm Res 177:971–982

Cole PD (1991) Migration direction of sand wave structures in pyroclastic-surge deposits: implications for depositional processes. Geology 19:1108–1111

Cole PD, Calder ES, Druitt TH, Hoblitt R, Robertson R, Sparks RSJ, Young SR (1998) Pyroclastic flows generated by gravitational instability of the 1996–97 lava dome of Soufriere Hills Volcano, Montserrat. J Geophys Res Lett 25(18):3425–3428

Cole PD, Calder ES, Sparks RSJ, Clarke AB, Druitt TH, Young SR, Herd RA, Harford CL, Norton GE (2002) Deposits from dome-collapse and fountain-collapse pyroclastic flows at Soufriere Hills Volcano, Montserrat. In: Druitt TH, Kokelaar BP (eds) The eruption of Soufriere Hills Volcano, Montserrat, from 1995 to 1999, vol 21. Geological Society London, Memoir, pp 231–262

Crowe BM, Fisher RV (1973) Sedimentary structures in base-surge deposits with special reference to cross-bedding, Ubehebe Craters, Death Valley. California Geol Soc Amer Bull 84:663–682

Cressie N (1993) Statistics for spatial data Wiley series in probability and mathematical statistics: applied probability and statistics. Wiley, New York, Revised reprint of the 1991 edition

Dellino P, Isaia R, La Volpe L, Orsi G (2004) Interaction between particles transported by fallout and surge in the deposits of the Agnano-Monte Spina eruption (Campi Flegrei, Southern Italy). J Volc Geotherm Res 133:193–210

Douillet GA, Pacheco DA, Kueppers U, Letort J, Tsang-Hin-Sun È, Bustillos J, Hall M, Ramón P, Dingwell DB (2013) Dune bedforms produced by dilute pyroclastic density currents from the August

2006 eruption of Tungurahua volcano, Ecuador. Bull Volcanol 75:762. doi:10.1007/s00445-013-0762-x
Drazin PG (2002) Introduction to hydrodynamic stability. Cambridge texts in applied mathematics. Cambridge University Press, Cambridge, 258 pages
Druitt TH (1992) Emplacement of the 18 May 1980 lateral blast deposit ENE of Mount St. Helens, Washington. Bull Volcanol 54:554–572
Druitt TH (1996) Pyroclastic density currents. In: Gilbert JS, Sparks RSJ (eds) The physics of explosive volcanic eruptions, vol. 145. Geological Society, London, pp 145–182, Special Publications
Dufek J, Manga M (2008) In situ production of ash in pyroclastic flows. J Geophys Res 113, B09207
Eychenne J, Lepennec JL, Troncoso L, Gouhier M, Nedelec JM (2012) Causes and consequences of bimodal grain-size distribution of tephra fall deposited during the August 2006 Tungurahua eruption (Ecuador). Bull Volcanol 74(1):187–205
Félix G, Thomas N (2004) Relation between dry granular flow regimes and morphology of deposits: formation of levées in pyroclastic deposits. Earth Planet Sci Lett 221:197–213
Fildani A, Normark WR, Kostik S, Parker G (2006) Channel formation by flow stripping: large-scale scour features along the Monterey East Channel and their relation to sediment waves. Sedimentology 53: 1265–1287
Fisher RV (1983) Flow transformations in sediment gravity flows. Geology 11:273–274
Fisher RV (1995) Decoupling of pyroclastic currents: hazards assessments. J Volc Geotherm Res 66:257–263
Freundt A, Schmincke HU (1985) Lithic enriched segregation bodies in pyroclastic flow deposits of Laacher See volcano (East Eifel, Germany). J Volc Geotherm Res 25:193–224
Folk RL (1964) A review of grain size parameters. Sedimentology 6:73–93
García M, Parker G (1989) Experiments on hydraulic jumps in turbidity currents near a canyon-fan transition. Science 245:393–396
García MH (1993) Hydraulic jumps in sediment-driven bottom currents. J Hydraul Eng 119(10):1094–1117
Gardner JE, Burgisser A, Stelling P (2007) Eruption and deposition of the Fisher Tuff (Alaska): evidence for the evolution of pyroclastic flows. J Geology 115(4):417–435
Giannetti B, Luongo G (1994) Trachyandesite scoria-flow and associated trachyte pyroclastic flow and surge at Roccamonfina Volcano (Roman Region, Italy). J Volc Geotherm Res 59:313–334
Goldstein F (2011) Geological Mapping of the 2006 Pyroclastic Density Current Deposits on Tungurahua Volcano, Ecuador. Diplomkartierung ausgegeben und betreut von Prof. A. Altenbach München, 01. Januar 2011. Ludwig-Maximilians-Universität München. Department für Geo- und Umweltwissenschaften, Sektion Geologie/Paläontologie
Gurioli L, Cioni R, Sbrana A, Zanella E (2002) Transport and deposition of pyroclastic density currents over an inhabited area: the deposits of the AD 79 eruption of Vesuvius at Herculaneum, Italy. Sedimentology 49:929–953
Gurioli L, Zanella E, Pareschi MT, Lanza R (2007) Influences of urban fabric on pyroclastic density currents at Pompeii (Italy): flow direction and deposition (part I). J Geophys Res 112, B05213
Hall ML, Robin C, Beate B, Mothes P, Monzier M (1999) Tungurahua Volcano, Ecuador: structure, eruptive history and hazards. J Volc Geotherm Res 91:1–21
Hall ML, Samaniego P, Le Pennec JL, Johnson JB (2008) Ecuadorian Andes volcanism: a review of Late Pliocene to present activity. J Volc Geotherm Res 176(1):1–6
Hoblitt RP (1986) Observations of the eruptions of July 22 and August 7, 1980, at Mount St. Helens, Washington. U.S.A. Geological survey professional paper 1335
Kelfoun K, Samaniego P, Palacios P, Barba D (2009) Testing the suitability of frictional behaviour for pyroclastic flow simulation by comparison with a well-constrained eruption at Tungurahua volcano (Ecuador). Bull Volcanol 71(9):1057–1075
Kueppers U, Putz C, Spieler O, Dingwell DB (2012) Abrasion in pyroclastic density currents: insights from tumbling experiments. Phys Chem Earth 45–46:33–39
Legros F, Kelfoun K (2000) On the ability of pyroclastic flows to scale topographic obstacles. J Volc Geotherm Res 98:235–241
Lube G, Cronin SJ, Platz T, Freundt A, Procter JN, Henderson C, Sheridan MF (2007) Flow and deposition of pyroclastic granular flows: a type example from the 1975 Ngauruhoe eruption, New Zealand. J Volc Geotherm Res 161:165–186
Lube G, Cronin SJ, Thouret JC, Surono (2011) Kinematic characteristics of pyroclastic density currents at Merapi and controls on their avulsion from natural and engineered channels. Geol Soc Am Bulletin 123(5/6):1127–1140
Macías JL, Espíndola JM, Bursik M, Sheridan MF (1998) Development of lithic-breccias in the 1982 pyroclastic flow deposits of El Chichón Volcano, Mexico. J Volc Geotherm Res 83:173–196
Moore JG (1967) Base surge in recent volcanic eruptions. Bull Volcanol 30(1):337–363
Mulder T, Alexander J (2001) Abrupt change in slope causes variation in the deposit thickness of concentrated particle driven density currents. Mar Geol 175:221–235
Normark WR, Piper DJW, Posamentier H, Pirmez C, Migeon S (2002) Variability in form and growth of sediment waves on turbidite channel levees. Mar Geol 192:23–58
Otto GH (1939) A modified logarithmic probability graph for the interpretation of mechanical analysis of sediments. J Sed Petrol 9:62–76
Perugini D, Kueppers U (2012) Fractal analysis of experimentally generated pyroclasts: a tool for volcanic hazard assessment. Acta Geophysica 60(3):682–698
Piper DJW, Normark WR (1983) Turbidite depositional patterns and flow characteristics, Navy Submarine Fan, California Borderland. Sedimentology 30:681–694
Prather BE (2003) Controls on reservoir distribution, architecture and stratigraphic trapping in slope settings. Mar Pet Geol 20:529–545
Samaniego P, Le Pennec JL, Barba D, Hall M, Robin C, Mothes P, Yepes H, Troncoso L, Jaya D (2008) Mapa de los peligros potenciales del volcán Tungurahua. (Esc. 1/50.000), 3ra Edición, Edit. IGM-IG/EPN-IRD, Quito, Ecuador
Samaniego P, Le Pennec JL, Robin C, Hidalgo S (2011) Petrological analysis of the pre-eruptive magmatic process prior to the 2006 explosive eruptions at Tungurahua volcano (Ecuador). J Volc Geotherm Res 199(1–2):69–84
Sandwell DT (1987) Biharmonic spline interpolation of GEOS-3 and SEASAT Altimeter Data. Geophys Res Lett 14(2):139–142
Sarocchi D, Sulpizio R, Macías JL, Saucedo R (2011) The 17 July 1999 block-and-ash flow (BAF) at Colima Volcano: new insights on volcanic granular flows from textural analysis. J Volc Geotherm Res 204:40–56
Saucedo R, Macias JL, Bursik MI, Mora JC, Gavilanes JC, Cortes A (2002) Emplacement of pyroclastic flows during the 1998–1999 eruption of Volcan de Colima, Mexico. J Volc Geotherm Res 117: 129–153
Schmincke HU, Fisher RV, Waters AC (1973) Antidune and chute-and-pool structures in the base surge deposits of the Laacher See area, Germany. Sedimentology 20:553–574
Sequeiros OE, Spinewine B, García MH, Beaubouef RT, Sun T, Parker G (2009) Experiments on wedge-shaped deep sea sedimentary deposits in minibasins and/or on channel levees emplaced by turbidity currents. Part I: Documentation of the flow. J Sed Res 79: 593–607
Sigurdsson H, Carey SN, Fisher RV (1987) The 1982 eruption of E1 Chichón volcano, Mexico (3): physical properties of pyroclastic surges. Bull Volcanol 49:467–488

Sneed SD, Folk FL (1958) Pebbles in the lower Colorado River, Texas, a study of particle morphogenesis. J Geology 66(2):114–150

Sparks RSJ (1976) Grain size variations in ignimbrites and implications for the transport of pyroclastic flows. Sedimentology 23: 147–188

Sulpizio R, De Rosa R, Donato P (2008) The influence of variable topography on the depositional behaviour of pyroclastic density currents: the examples of the Upper Pollara eruption (Salina Island, southern Italy). J Volc Geotherm Res 175:367–385

Sulpizio R, Bonasia R, Dellino PF, Mele D, Di Vito MA, La Volpe L (2010) The Pomici di Avellino eruption of Somma–Vesuvius (3.9 ka BP). Part II: sedimentology and physical volcanology of pyroclastic density current deposits. Bull Volcanol 72:559–577

Takahashi T, Tsujimoto H (2000) A mechanical model for Merapi-type pyroclastic flow. J Volc Geotherm Res 98:91–115

Talbot JP, Self S, Wilson CJN (1994) Dilute gravity current and rain-flushed ash deposits in the 1.8 ka Hatepe Plinian deposit, Taupo, New Zealand. Bull VolcanoI 56:538–551

Valentine GA (1987) Stratified flow in pyroclastic surges. Bull Volcanol 49:616–630

Valentine GA, Giannetti B (1995) Single pyroclastic beds deposited by simultaneous fallout and surge processes: Roccamonfina volcano, Italy. J Volc Geotherm Res 64:129–137

Walker GPL (1971) Grain-size characteristics of pyroclastic deposits. J Geology 79:619–714

Walker GPL, Wilson CJN, Froggatt PC (1981) An ignimbrite veneer deposit: the trail-marker of a pyroclastic flow. J Volc Geotherm Res 9:409–421

Walker GPL (1984) Characteristics of dune-bedded pyroclastic surge bedsets. J Volc Geotherm Res 20:281–296

Waltham D (2004) Flow transformations in particulate gravity currents. J Sed Res 74(1):129–134

Wilson CNJ, Hildreth W (1998) Hybrid fall deposits in the Bishop Tuff, California: a novel pyroclastic depositional mechanism. Geology 26:7–10

Wohletz KH, Sheridan MF (1979) A model of pyroclastic surge. Geol Soc Am Special Paper 180:177–194

This page was intentionally left blank.

Figure 1.12: Interpretation of the August 2006 eruption of Tungurahua, seen from Cotaló. Note the confined nature of PDCs on the slopes (central part), stopping just above the soccer terrain in Bilbao village (lowermost part). The city of Baños to the left (yellow dots) is protected by a topographic barrier, though the swimming pools of the Vascún valley are threatened by small PDCs. Painting by Guillaume Herbertz and Jerôme Huss (2010, $38 * 46cm^2$).

This page was intentionally left blank.

Part II

Dune bedforms

Chapter 2

Supercritical bedforms unrelated to antidunes in deposits of pyroclastic density currents

This chapter presents some basic theoretical framework behind antidunes and supercritical bedforms. It helps for the interpretation of dune bedforms emplaced by dilute pyroclastic density currents presented in chapter 3. It is suggested that supercritical bedforms may occur unrelated to antidunes. This possibility was suggested in a poster at the European Geoscience Union general assembly 2014:

Douillet G.A., Kueppers U., Dingwell D.B. (2014). The antidune question for bedforms in deposits of dilute pyroclastic density currents. Geophysical Research Abstracts Vol.16, EGU2014-1520

This page was intentionally left blank.

Supercritical bedforms unrelated to antidunes in deposits of pyroclastic density currents

Abstract

In most textbooks and research papers, the term antidune is used for sedimentary bedforms that show backset lamination, are related to supercritical flows, and to stationary gravity waves. However, those three elements are not necessarily linked together. Misconception have arisen from loose nomenclature, especially for dune bedforms formed by dilute pyroclastic density currents. The exact same problem occurs with the term chute and pool.

A review of the evolution of the antidune history for pyroclastic deposits is presented here. The traditional linear problem that permits to link a gravity wave (and associated antidune) to the flow parameters is detailed in simple steps. The two flow behaviors in response to a bed morphology depending on the flow regime (supercritical and subcritical) are evidenced for simplistic conditions. From the latter result, it is suggested that bedforms with aggrading laminations can result from super critical flows not related to antidunes. In this case, the usual analysis that allows to link the deposits to quantitative flow parameters would not be applicable, and the interpretation of those bedforms should be refined. Through the energy-depth relationship for a simplified flow, the concepts around chute and pool are also evoked and misconceptions arisen in field studies are pointed.

1 Introduction

The term antidune was initially used for small-scale bedforms that were observed to migrate upstream in water tank experiments in order to emphasize this behavior (Gilbert 1914). This specificity was then understood to be due to upstream migrating gravity waves, whose shape was acting on the bed. At flow velocities close to the gravity wave velocity, the wave is almost stationary in regards to the ground, and shapes the bed surface with an antidune. The couple gravity wave-antidune can migrate together slightly up or downstream , following the dynamics of the gravity wave (Yokokawa et al. 2010, Alexander et al. 2001). Extensive studies were applied to antidunes (Kennedy 1961, 1963, Hand 1969) and the concept was rapidly adapted to density currents for turbidity currents (Hand 1974) and suggested as an analogue for pyroclastic density currents (PDCs) bedforms (Fisher and Waters 1969, Waters and Fisher 1971, Crowe and Fisher 1973). Indeed stoss-aggrading bedforms are found in the sedimentary record of both environments and can be used to derive quantitative flow parameters (Prave 1990, Brand and Clarke 2012). Nowadays, antidunes are evoked in many types of highly loaded geophysical flows such as lahars (Froude 2014), jokaulhaupt (Duller et al. 2008), sub- and pro-glacial outburst

deposits (Lang and Winsenman 2013), PDCs (Schmincke et al. 1973, Gencalioglu-Kuscu et al. 2007) and turbidity currents (Cartigny 2012, and references therein).

Whereas antidunes occur in the trans- to supercritical regime, hydraulic jumps are a sudden change in the flow regime from super- to sub-critical. Such sudden deceleration and increase in flow thickness may leave characteristic structures in the sedimentary record. Indeed, the main variables influencing the sedimentation rate are the flow velocity, particle concentration and turbulence level. All of them can be strongly affected by a hydraulic jump. Structures deposited by hydraulic jumps are called cyclic steps and chute and pool structures. Chute and pools represent the record of a single supercritical to subcritical transition, and cyclic steps are produced by stable trains of hydraulic jumps and re-accelerations. Whereas cyclic steps are the focus of extensive studies in turbidity current research (e.g. Cartigny 2012 and references therein), chute and pools are commonly evoked in PDC sedimentology. The term has undergone such misunderstandings and is so popular that a double use is not avoidable. The first sense is a descriptive term for the sedimentary structures initially associated to the physical phenomenon (Schmincke et al. 1973) whereas the hydrodynamic considerations of a hydraulic jump are automatically associated to the descriptive part (e.g. Kuscu et al. 2007, Brand et al. 2009). Here, the antidune history is reviewed for pyroclastic deposits, the theory of antidunes and hydraulic jumps is summarized, and suggestion is made for the genesis of supercritical dune bedforms unrelated to antidunes.

1.1 Terminology

Research on antidunes suffers from very loose nomenclature, both on descriptive and interpretative terms. Here the nomenclature of Douillet et al. (2013b) is used. A dune bedform (DBs) is an undulating sedimentary structure, independently of a genesis. Dune alone is reserved to DBs formed under subcritical flow conditions. The term sand or sediment wave is avoided because DBs are not waves, and sediment waves are related to large scale bedforms found in turbidites (Wynn and Stow, 2002). Backset laminations are laminations that dip against the flow direction, and are thus the preserved surface of stoss faces (upstream side) of bedforms. When laminations can be followed from the stoss to the lee side, they are called aggrading, stoss-aggradation implying more aggradation on the stoss than the lee.

1.2 DBs cross stratifications and the antidune interpretation

Cross-stratifications of decimeter to decameter scale in deposits of dilute PDCs (Figure 1) have been initially interpreted as secondary wind reworking (Frechen 1971). However, after observation of undulating bedforms in deposits of artificial explosions (e.g., Bikini test 1946 and Sedan test 1962, Carlson and Roberts 1963), or outcropping at the surface of historic eruptions (plate 24 in Richards 1959), their primary nature was recognized (Moore et al. 1966, Moore 1967). From the 1966 eruption at Taal volcano (Philippines), Moore described cross stratifications with both stoss and lee sides laminae, episodic scouring of the stoss side,

Figure 1: Steep-sided, stoss-aggrading laminasets of ash in a DB from the 2006 eruption of Tungurahua (Ecuador). Note episodic truncations on the stoss side and their absence on the lee. Douillet et al. 2013b

steeper stoss than lee angle, and a slight downstream migration of the crests (see also Fisher and Waters, 1970). Ancient cross-stratifications have initially been termed antidunes as a descriptive term for the constructional structures with low angle cross-laminations showing up- or down-stream migration of the crests and resembling "standing waves" (Fisher and waters 1969, Waters and Fisher 1971). Fisher and Waters (1970) "referred" to PDC DBs as antidunes because of the typical low angle laminations contrasting with the steep lee side angles which lie at or near the angle of repose of sub critical bedform evidenced by Simons and Richardsson (1966).

Waters and Fisher (1971) were the first to use antidune in its hydrodynamical meaning, i.e. as an interpretative term linked with the fluid dynamics definition. They interpreted DBs at Taal as antidunes formed under a standing wave at a relatively sharp density interface between the moving bed load and overriding cloud. Their argument was that the shape and internal cross stratifications resemble antidunes produced in aqueous analogue experiments by Middleton (1965), and turbidite outcrops interpreted as antidunes by Walker

(1967). They noted that only an important deposition rate would permit preservation of antidune cross stratifications, likely to occur in PDCs. Crowe and Fisher (1973) and Mattson and Alvarez (1973) followed Waters and Fisher for the antidune interpretation at several other sites. Schmincke et al. (1973) observed decametre scale cross-stratifications with back- and fore-set laminations (climbing-dunes) and sometimes with upstream migration of the crest, but with steep stoss and lee sides. Even if the primary argument (stoss and lee sides below the repose angle) was not observed, they interpreted these structures as antidunes. They thoroughly focused on more proximal structures made from stoss-aggrading lensoidal layers deposited on front of steep erosive surfaces that they interpreted as supposedly even higher energy structures, namely, chute and pools (Figure 2).

These interpretations were considered as "bolder" by Allen (1984). He stated that "the significance of these cross beddings remained obscure" and rather suggested that the up- or down-stream migration of the crests was related to the liquid water content in the PDCs. Upstream migration would be triggered by cohesion of the particles due to water, leading to a plastering effects on stoss sides. He suggested that upstream migrating structures would indicate "wet surges" while downstream migrating ones would be the product of "dry surges". However, Cole (1991) and Druitt (1992) showed that both up- and down-stream migrating bedforms could occur during the same eruptive event. Hence, they were not related to water content, but to local changes in the flow regime. Since this, many authors have followed pioneer interpretations as antidune and chute and pool structures (Rowley et al. 1985, Valentine 1987, Kuscu et al. 2007, Brand et al. 2009, Brand and Clarke 2012), even if a wide range of cross bedding patterns is observed (e.g. Douillet et al. 2013b).

Yet one statement must be done: grains can organize in only two ways when depositing: they either form a heap or an even surface. Thus before claiming on antidunes for bumpy deposits and upper plane beds for planar layers, one has to look further in details and decipher the processes involved. Careful observation reveals that there are in fact an infinity of depositional patterns. Details are thus key for interpretation, and several alternative explanations to the antidune genesis of PDC DBs exist. Nocita (1988) suggested that the stoss-depositional, over-steepened laminations often observed in PDC cross-bedding may be the result of underlying fluidization and diapirism. Sigurdsson (1987) noted a relative analogy between aeolian ripples and pyroclastic DBs, and related their formation to a combined effect of saltation-bedload transport, together with a suspension component. Conversely, Sulpizio et al. (2008) envisioned each laminaset as emplaced by *en masse* deposition. Andrews and Manga (2012) proposed that some regressive bedforms may be related to backflow by the uplift of pseudo-phoenix clouds that would suck back a PDC and produce a flow reversal. Douillet et al. (2013b) suggested differential draping in highly depositional environment for steep-sided stoss-aggrading DBS and a process of stoss-face blocking of granular-based flows to explain stoss-aggrading, lensoidal, massive layers. Douillet et al. (2014) further demonstrated with wind tunnel measurements that a saltating bed of pyroclasts is likely to deposit its load on the stoss of a bedform rather than on the lee. For chute and pools, Douillet et al. (submitted) provide an explanation for the formation of the characteristic steep basal erosive planes of these structures as related to

ballistic impacts. This discussion urges the need for a good theoretical understanding of the antidune phenomenon, which is intended here.

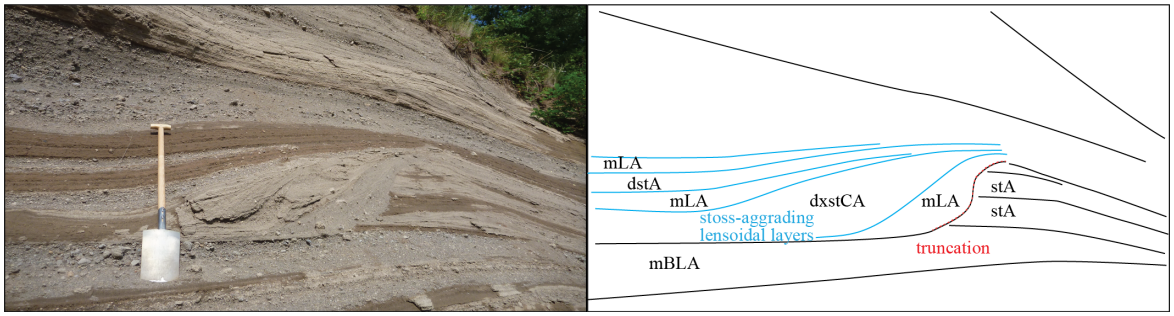

Figure 2: Typical patterns from type I "chute and pool" structures described in Schmincke et al. (1973) in the deposits of Laacher See (Germany). Abbreviations: mLA: massive lapilli and ash; dstA: diffusely stratified ash; dxstCA: diffusely cross-stratified coarse ash; mBLA: massive block lapilli and ash; stA: stratified ash

2 Physical formulations

Hereafter, the problem of the instability at the interface between two flows of different densities at the origin of antidune theory is detailed in easy steps in the first section. The second section presents the reaction of a supercritical and subcritical flow to a bed morphology. It is suggested that the supercritical response may be at the origin of steep-sided DBs found in PDC sediments. Finally, the third section introduces the energy-depth diagram to qualitatively explain the hydraulic jump phenomenon. These equations can be found in most fluid dynamics textbooks (e.g. Guyon et al. 2002, Drazin and Reid 2004, Vallis 2006). Although the assumptions on flows probably don't apply in the case of DBs produced by PDCs, they represent the simplest theoretical way to explain the difference between antidunes and dunes.

2.1 Antidunes and stationary gravity waves

When "antidunes" are recognized in the sedimentary record and used to derive quantitative flow parameters, the analysis intrinsically implies that the DB was produced by a stationary gravity wave. It supposes that the length and thickness of the bedform are a perfect mould of the overlying gravity wave, that is taken stationary over the bed. Then, the gravity wave wavelength and speed can be derived from the shape of the antidune using eq. (35). The formulation of the antidune problem is developed in many steps for the easy understanding of all in Annexe. It is based on the linear theory of stability for Kelvin-Helmholtz instabilities in Drazin and Reid (2004, p. 45-51) and Vallis (2006).

2.2 Supercritical DBs unrelated to antidunes

In this section, we show that backstep laminations, stoss aggradation or upstream migrating structures can exist in supercritical flows independently of a gravity wave. The problem is derived from the hydraulic jump problem from Guyon et al. (2002, p. 216-224). It is treated in two dimensions, in a reference $(\boldsymbol{e_x}, \boldsymbol{e_z})$ with $\boldsymbol{e_x}$ horizontal and positive in the direction of flow, and $\boldsymbol{e_z}$ vertical positive in the direction opposite to the gravity vector. Consider a flow with flux q, density ρ_f, thickness h, velocity $\boldsymbol{u(x,z)}$, and mean velocity $U(x)$ evolving on a bed with profile $z_0(x)$ (Figure 3). For simplifications, assumptions are made of incompressibility ($\rho = constant$), non-viscosity ($\mu = 0$), steadiness ($\frac{\partial}{\partial t} = 0$). For a constant flux, given incompressibility, one needs:

$$\int_{z=z_0}^{z_0+h} u(x,z)\rho_f dz = q = \rho_f \int_{z=z_0}^{z_0+h} u(x,z)dz = \rho_f U(x)h(x) \tag{1}$$

Newton's second law of momentum conservation yields to the conservation of energy (for a flow with constant mass i.e. no entrainment or deposition). In the absence of external forces, the conservation of energy simplifies in the Bernoulli equation:

$$P_{hstat} + \frac{1}{2}\rho_f U^2(x) + \rho_f g(h(x) + z_0(x)) = cste \tag{2}$$

P_{hstat} denotes the hydrostatic pressure, g is the gravity acceleration. The relation states that the total energy, i.e. the sum of the elastic (P_{hstat}), kinetic ($\frac{1}{2}\rho_f U^2(x)$), and potential -gravity- ($\rho_f gh$) energy is a constant of the flow in absence of external forces. Consider P_{hstat} resulting from a surrounding fluid of density ρ_s with a thickness Z_s large enough that its upper limit is not influenced by the change of thickness of the flow (Figure 3). Then:

$$P_hstat = \rho_s g Z_s \tag{3}$$

at elevation $z = 0$ in the absence of the flow. Thus, on top of the flow,

$$P_hstat = \rho_s g((Z_s - h(x) - z_0(x)) \tag{4}$$

And (2) can be rewritten as

$$\rho_s g Z_s + \frac{1}{2}\rho_f U^2(x) + g(\rho_f - \rho_s)(h(x) + z_0(x)) = cste \tag{5}$$

When the surrounding fluid's density is of the same order as the flow density, the hydrostatic pressure at the surface of a flow cannot be taken as constant. It can further be split into a constant term and a term with same dependence as the potential gravity energy. Derivation of (5) over x recalling that Z_s is constant:

$$\rho_f \frac{\partial U(x)}{\partial x} U(x) + g(\rho_f - \rho_s)(\frac{\partial h(x)}{\partial x} + (\frac{\partial z(x)}{\partial x}) = 0 \tag{6}$$

From the derivation of (1), recalling constant flux and density:

$$U(x)\frac{\partial h(x)}{\partial x} + \frac{\partial U(x)}{\partial x}h(x) = 0 \tag{7}$$

$\frac{\partial h(x)}{\partial x}$ expressed from (7) can be replaced in (6) to obtain, after rearrangement:

$$\frac{\partial U(x)}{\partial x}(U(x) - g\frac{\rho_f - \rho_s}{\rho_f}\frac{h(x)}{U(x)}) = -g\frac{\rho_f - \rho_s}{\rho_f}\frac{\partial z(x)}{\partial x} \tag{8}$$

The specific gravity $g' \equiv g\frac{\rho_f - \rho_s}{\rho_f}$ becomes apparent. Dividing (8) by g' and introducing the densiometric Froude number ($Fr_d \equiv \frac{U}{\sqrt{g'h}}$):

$$(1 - Fr_d^2)\frac{U(x)}{h(x)}\frac{\partial U(x)}{\partial x} = \frac{\partial z(x)}{\partial x} \tag{9}$$

Fr_d is an adapted version of the Froude number ($Fr = \frac{U}{\sqrt{gh}}$), for the case when hydrostatic pressure at the surface of a flow cannot be taken as constant (when the surrounding fluid's density is of the same order as the flow density). For open flows, ρ_s is negligible, and g' and Fr_d turn in g and Fr, respectively. Fr_d corresponds to the ratio of inertia forces to gravity forces and informs on flow regime: when $Fr_d > 1$, the flow is called super-critical or shooting, when $Fr_d < 1$, the flow is called sub-critical or tranquil (see hydraulic jump chapter).

In the frame of the problem, U and h are positive (the flow thickness is never negative, and the flow will not reverse). Then, the sign of the downstream variation in flow velocity ($\frac{\partial U(x)}{\partial x}$) is either correlated or inversely-correlated to the variation in bed thickness ($\frac{\partial z(x)}{\partial x}$), and depends on the value of Fr_d only.

When $Fr_d < 1$ (subcritical conditions), the velocity $U(x)$ increases with bed elevation $z(x)$. This means that the flow will accelerate while passing over an obstacle (Figure 3). If the obstacle is an erodible DB, the flow will possibly erode on the stoss side of the obstacle. Inversely, on the lee side, the obstacle height $z(x)$ decreases again, and the flow decelerates, possibly leading to deposition. Given the conservation of the flux (1), the thickness of the flow decreases when passing an obstacle. This is the fundamental mechanism for the formation of downstream migrating, subcritical dunes.

Inversely, when $Fr_d > 1$ (supercritical conditions), $U(x)$ decreases when $z(x)$ increases and the flow decelerates on the stoss side of an obstacle (Figure 3). If flow velocity is a proxy for deposition rate, this can lead to stoss side aggradation, backset lamina and upstream migration of a bedform. Inversely, on the lee side, $z(x)$ increases again, and the flow accelerates again until reaching the velocity before the obstacle.

The relation shows the fundamental role of the Froude number and the critical value of $Fr_d = 1$ for a conservative flow. The analysis should hold for density currents with low deposition rate compared to the whole charge. However, when deposition becomes significant, formulation becomes more complicated since Newton's second law is only valid for closed systems. Note that in the case of an infinitely thick flow (thickness of the current

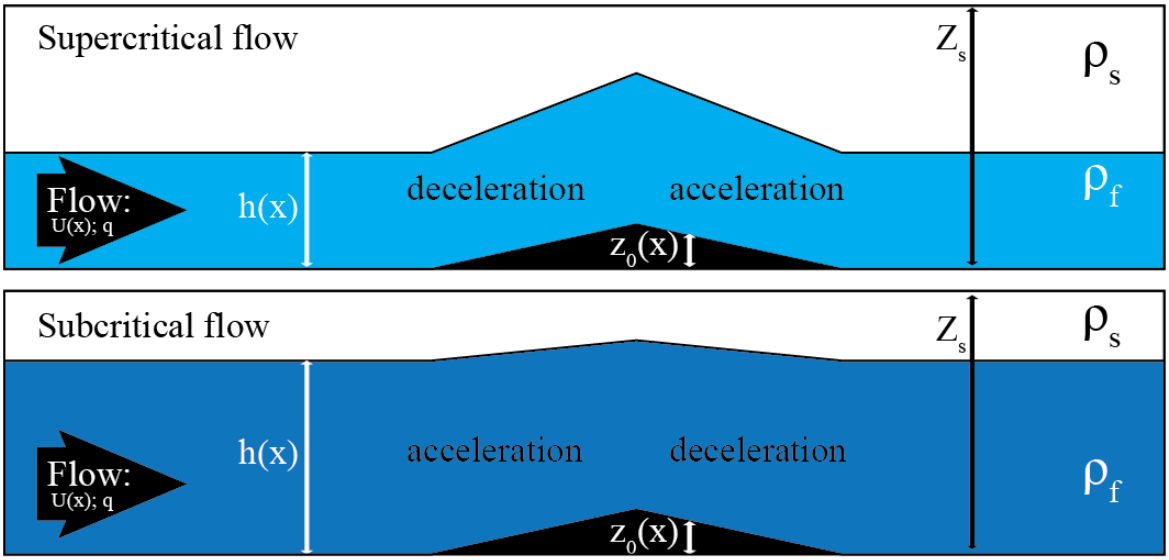

Figure 3: Simplistic flow over an obstacle and geometry of the problem.

much greater than scale of the bedform), subcritical dune patterns can still be produced, because the obstacle alone reduces the section of the flow and induces acceleration on the stoss side. In that case, the term mega-ripple is recommended, in order to emphasis that the DB is not produced by the interaction with a density interface. Conversely, it is not possible to produce a decrease in flow velocity at the front of an obstacle without a free flow surface.

2.3 Hydraulic jumps

A hydraulic jump is a fluid dynamics phenomenon that corresponds to the drastic increase of the thickness of a flow accompanied by a decrease of its velocity and/or density. A hydraulic jump is the expression of the transition of the flow from the supercritical to subcritical regime. This reflects a change in the energy balance between kinetic and gravity potential energy. A formulation of the energy-depth relationships is presented in order to understand hydraulic jumps. This part is based on the formulations for open water and hydraulic engineering classes.

Taking the conservation of energy (2) and conservation of flux (1) the relation between flow energy and thickness can be derived (Figure 4):

$$E_{tot} = \rho_s g Z_s + \frac{1}{2}\rho_f \frac{q^2}{h^2(x)} + g((\rho_f - \rho_s)(h(x)) \tag{10}$$

Bed surface changes are neglected for simplicity. This curve is entirely characterized by the discharge q, thus a conservative flow will remain on this curve at any time.

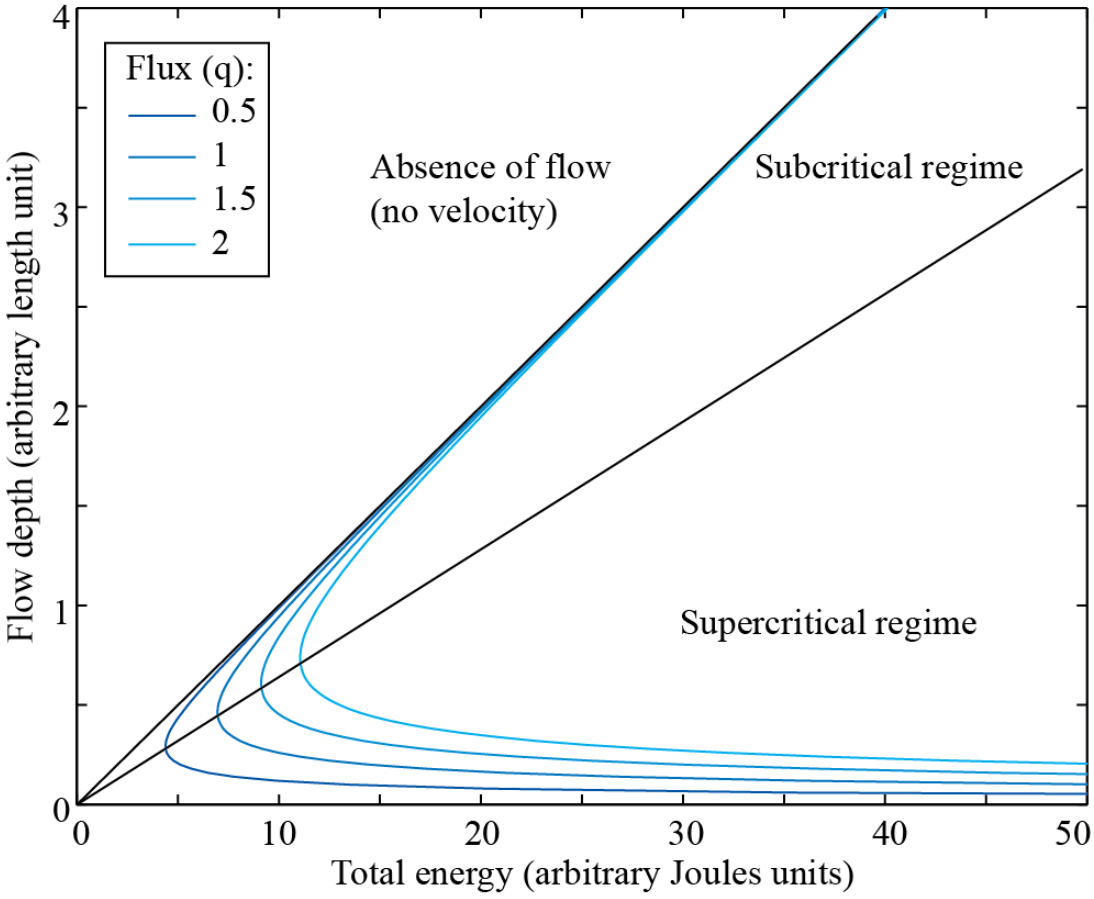

Figure 4: Curve of the Energy-Depth relationship for 4 different fluxes. Units are arbitrary.

The curve can be divided in two parts: the lower part of the curve corresponds to the supercritical regime, while the upper part corresponds to subcritical conditions. This is simply evidenced taking the derivative of energy over thickness:

$$\frac{\partial E_{tot}}{\partial h} = -\rho_f \frac{q^2}{h^3(x)} + g(\rho_f - \rho_s) \tag{11}$$

and equaling it to zero, to get the point separating the two parts of the curve, one finds

back the critical Froude number:

$$\begin{aligned} \frac{\partial E_{tot}}{\partial h} &= 0 \\ => \frac{1}{\frac{g(\rho_f - \rho_s)}{\rho_f}} \frac{Q^2}{h^3} &= 1 \\ => \frac{U^2}{g'h} &= 1 \\ => Fr_d^2 &= 1 \end{aligned} \tag{12}$$

Thus the upper and lower parts of the curve are separated by the critical Froude number. The associated flow thickness for which the energy is at its minimum is the critical depth. A flow at a given discharge can thus, without changing its total energy, always be in 2 and only 2 regimes with different flow thicknesses. The reason and exact position at which a flow will pass from one regime to the other is not easily predictable. It is related to turbulence forces that tend to transfer the flow-parallel motion in more vertical motions through eddies, decreasing kinetic energy and increasing flow thickness.

Without any external forcing, a flow will tend to minimize its energy, and be in the critical regime. Slope will bring him to the supercritical regime, and a dam or strong basal shearing forces the subcritical regime. The "smooth jumps" observed by many authors (Chanson 2009) are probably related to a flow simply evolving to the critical depth without external braking. For the case of a sedimentating particulate density current (such as a turbidity current or PDC), given that the agent of excess density is the future sediment, and sedimentation entrains consequent changes of discharge, the flow may evolve in the supercritical regime up to complete deposition. Kostic and Parker (2007) demonstrated by numerical modelling of particulate density currents that a hydraulic jump does not necessarily occurs until full dissipation. Huang et al. (2009) have shown similar results based on the specific energy equation. They enter two terms of discharge and concentration corrections into the criterion of hydraulic jump. However, these results might be biased by a misuse of Newton's second law of motion in the case of sedimentation (variable mass system), inducing a rocket effect (Plastino and Muzzio 1992).

3 Discussion

3.1 Supercritical dune bedforms vs. antidunes

Several authors noted that density currents are likely to be supercritical (Kostic 2011, Cartigny 2012), since the density difference with the ambient fluid or even within internally stratified flows is low. A flow overflowing a levee is likely critical at this point (Kostic submitted) and will further accelerate on outer slopes of the levee (changes of potential to kinetic energy), thus reaching a supercritical state. A flow tends toward reaching its minimal energy state (i.e. the critical state, Figure 4) in the absence of a dam or consequent

basal shear braking the flow. In the context of a sloping bed like the flank of a volcano, a PDC is thus likely to be supercritical. Moreover, given that a particulate density current may stay in a supercritical state over its whole existence (Kostic and Parker 2007, Huang et al. 2009), supercritical bedforms may occur even in very distal deposits.

Yet antidunes can only form at flow velocities very close to the gravity wave velocity (i.e. $Fr = 1$ in the non-dispersive case). Another statement rules out antidunes: pyroclastic DBs are found to migrate downstream, aggrade symmetrically, or show stoss-aggradation, but not a single outcrop exhibits lee-erosive patterns. If those DBs were linked to slightly up- and down-stream moving gravity waves, the absence of lee-erosive patterns would remain unexplained. Instead, steep-sided DBs are found to increase their dimensions, both in length and thickness over the whole construction phase. Moreover, if a flow-related gravity wave would be at the origin of these DBs, the mould they produce should keep stable dimensions, and only translate.

The simple analysis presented here (9) suggests that stoss-aggrading DBs may form at any supercritical Fr given a purely depositional context. This process would be in total agreement with field observations of continuous growth and absence of lee-erosion. This may especially be the case for some recent analogue models (Sequeiros et al. 2009, Spinewine et al. 2009), numerical models (Kostic submitted) and for steep-sided, stoss-aggrading bedforms. Many bedforms found in PDC deposits may in fact be supercritical bedform, but unrelated to antidunes.

3.2 Internal gravity waves

One redundant argument for explaining how PDCs observed to have flow thicknesses of several hundreds meters can form meter scale bedform is that PDCs are density stratified and that only the basal stratae of the flow are involved in the formation of antidunes. In that case, the antidune would lie at some hypothetic density interface close to the bed surface, or even be envisioned as an internal gravity wave (e.g. Schmincke et al. 1973, Valentine 1987, Brand and Clarke 2012). The Brunt-Väisälä frequency -nicely introduced in Vallis (2006, p. 92)- is then adopted in order to relate the wavelength of antidunes to flow parameters. It is to note however that internal gravity waves are singular phenomenon, which counter intuitively do not necessarily propagate parallel to the density gradient, but rather in an oblique flow-gravity direction (Vallis 2006). A formulation of internal gravity wave is above the scope of this chapter. Moreover, the interface hosting the gravity wave shall be close enough from the bed, so that both can interact. The analysis used to derive quantitative parameters suppose the bed to be infinitely far from the density interface, and be treated as a streamline. The interaction between bed and gravity wave deserves further attention, also above the scope of this chapter. Finally, the physical existence of an oscillating density interface can be questioned in the case of a particulate density current. The density interface in such flows is a limit between a level with a given concentration of particles, and overlying level with slightly lower concentration of particles. How stable is such an interface, and would it not be erased by turbulent mixing before undulating? A fluid dynamics specialist (such as a meteorologist) could answer these questions.

3.3 Misconceptions in the field

Misconceptions have arisen from the loose understanding by field geologists of the physical processes lying in the interpretation of antidunes and chute and pool structures. Prave (1990) described the problems related to loose analogies between open water and density stratified antidunes. In particular, he pointed that a difference exists in the equation leading to a flow's velocity: either the overlying fluid density is taken negligible (for open water flows), or the density contrast is negligible (for density currents). The two hypotheses lead a factor two difference in the velocity. Douillet et al. (2013b) have listed arguments against antidune interpretation for steep-sided aggrading bedforms and used geometrical considerations to show the very unlikely flow configuration that would result from such an interpretation.

Concerning chute and pool structures, it is unclear what part of structures should record a hydraulic jump (or pneumatic/granular jump). Indeed, a sudden, steep truncation further overlain by stoss-aggrading, lensoidal layers is visible in type I and II of Schmincke et al. (1973). If a hydraulic jump had produced the truncations, then this would be due to progressive erosion of the formerly deposited bed upstream from the structure, and thus likely to result in gentle dipping final truncations. Douillet et al. (submitted) have suggested that the steep truncation can be due to destabilization by impacts. If the stoss-aggrading, lensoidal layers are the record of the jump, then no arguments permit to settle on the supercritical nature upstream from the structure, and simple blocking of the bedload, as suggested in Douillet et al. (2013b) is sufficient. Moreover, the occurrence of these lensoidal layers in front of all surface disturbances (types III and IV of Schmincke et al. 1973) proves that these are only related to a basal obstacle. Thus it is unclear where a hydraulic/pneumatic/granular jump is recorded in those "chute and pool" structures. The answer is probably to search far upstream from the actual structure rather than at the truncation itself. Brand and Clarke (2012) interpreted chute and pools and use a difference in layer height to conclude on the supercritical to subcritical Fr_d ratio and derive flow velocities. However, if a ratio of flow thicknesses was present in the deposit, this should also include some timescale of the parent event and deposition rate, and be related to the deposit thickness rather than its elevation (figure 6 in Brand and Clarke 2012). Most outcrops are not parallel to the parent flow. Deriving a wavelength from such an outcrop automatically leads to a bias. Finally, if velocities are inferred, a simple check of their significance can be made by comparing the retrieved velocity to the grain size of the material deposited in the structure: at high velocities, flows do not deposit their load (Douillet et al. 2014).

4 Conclusion

Pyroclastic density currents, as a special type of particulate density currents, are likely to evolve, as a whole, in the supercritical regime. Antidunes and chute and pool structures have often been interpreted in their deposits. Those terms are however no sedimentological

descriptive terms but interpretation of the dynamics of the parent flows. In case of their occurrence, m-scale antidunes and chute and pools would be triggered as internal phenomenon in a density stratified flow. The geometry and fabric of those bedforms however leaves their interpretation under debate. An alternative interpretation to antidunes would be that steep sided, stoss-aggrading bedforms result from the supercritical nature of the parent flow reacting with the surface morphology, unrelated to gravity waves. This would explain most of the patterns observed in the field, including the steepness of bedforms, the absence of lee-erosive events, and the continuous growth in length and thickness over the whole construction phase.

A Appendix - Gravity waves

A.1 Initial flow

Consider two homogenous fluids F_1 and F_2, F_2 lying above F_1 and the interface an infinite horizontal plane (Figure 5). Suppose the fluids of densities ($\rho = \rho_1,\ \rho_2$) incompressible ($\frac{D\rho}{Dt} = 0$) and inviscid ($\nu = 0$). Vector are marked in ***bold*** and the problem is taken in an orthonormal reference frame ($\boldsymbol{e_x}$, $\boldsymbol{e_y}$, $\boldsymbol{e_z}$). The origin of the vertical axis is taken at the interface, and P_0 the pressure at this height, so that:

$$\begin{aligned} P(z) &= P_0 - \rho_2 g z \text{ for } z > 0, \\ P(z) &= P_0 - \rho_1 g z \text{ for } z > 0 \end{aligned} \tag{13}$$

Consider flows with constant horizontal velocity $u_{1,2}(z) = U_{1,2}\boldsymbol{e_x}$ and irrotational, so that the velocity can derive from a potential:

$$u_{1,2} = \boldsymbol{\nabla}\phi_{1,2} \tag{14}$$

A.2 Governing equations

The derivation of the Navier Stokes equations is extremely well presented in the online pdf by Kumar (2012). The continuity equation leads for each fluid:

$$\frac{\partial \rho_{1,2}}{\partial t} + \frac{\partial \rho u_{i1,2}}{\partial x_i} = 0 \text{ or } \frac{D\rho_{1,2}}{Dt} + \rho_{1,2}\boldsymbol{\nabla u_{1,2}} = 0$$

and given incompressibility, this simplifies into:

$$\boldsymbol{\nabla u_{1,2}} = 0$$

or

$$\triangle \phi_{1,2} = 0 \tag{15}$$

The momentum equation states that: "For a fluid element, the time derivative of the momentum in j-direction is equal to the sum of the external forces acting in this direction

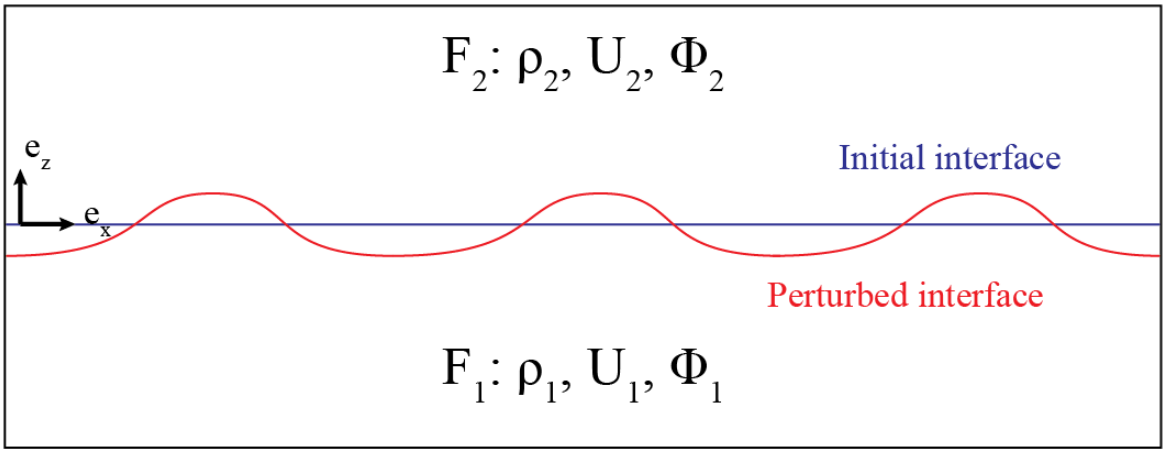

Figure 5: Geometry of the gravity wave problem.

on the fluid element, plus the molecular-dependent input of momentum per unit time". This translates as:

$$\rho(\frac{\partial \boldsymbol{u}}{\partial t} + \boldsymbol{u}\boldsymbol{\nabla}\boldsymbol{u}) = \boldsymbol{\nabla}P + \boldsymbol{\nabla}\boldsymbol{\tau_{ij}} + \boldsymbol{f}$$

$\boldsymbol{f}$ is the body force (in this case only gravity force) and the shearing tensor $\boldsymbol{\tau_{ij}} = 0\boldsymbol{\delta_{ij}}$ for inviscid fluids.

A.3 Perturbation

Suppose a small perturbation of the interface from the horizontal (Figure 5):

$$\xi(x, y, t)\boldsymbol{e_z}$$

Small is taken in consideration to the only available scale in the problem: u (recall the geometry is only an infinite horizontal interface at the boundary between two infinite fluids). Thus an argument of smallness would be that the acceleration produced by the perturbation is smaller than the velocity. From Newton's second law (16), and given a buoyancy driven force:

$$g'\xi << \rho\frac{\partial \boldsymbol{u_{1,2}}}{\partial x} = \rho U_{1,2} \tag{16}$$

with $g' = g\frac{\rho_f - \rho_s}{\rho_f}$ the specific gravity, i.e. the buoyancy-corrected weight. Drazin and Reid (2004) rather propose as a smallness condition that $g\xi << u_{1,2}^2$ and $\frac{\partial \xi}{\partial x,y} << 1$.

The perturbation of the interface is reflected as a small perturbation in the velocity potential (14) as:

$$\begin{aligned} \phi_1 &= U_1 x + \phi_1'(x, y, t) \text{ for } z < \xi \\ \phi_2 &= U_2 x + \phi_2'(x, y, t) \text{ for } z > \xi \end{aligned} \tag{17}$$

In case of small perturbations, one can neglect products of small quantities $(\phi'_{1,2}, \xi)$. The potential can then be developed in a Taylor series, such that:

$$[\phi'_{1,2}]_{z=\xi} = [\phi'_{1,2}]_{z=0} + \xi \left[\frac{\partial \phi'_{1,2}}{\partial z}\right]_{z=0} + H.O.T \tag{18}$$

H.O.T. referring to "higher order terms", i.e. products of small quantities neglected for the first order linearization.

A.4 Boundary conditions

1) One can make the assumption that the small perturbation alters the flow in a finite region such that a boundary condition at infinite is:

$$\begin{aligned} \phi_1 &= U_1 x \text{ for } z \to -\infty \\ \phi_2 &= U_2 x \text{ for } z \to +\infty \end{aligned} \tag{19}$$

2) The fluid just above and below the interface must move with the interface, otherwise it would create voids or overlaps, such that a boundary condition is:

$$u_{z1} = u_{z2} = \frac{D\xi}{Dt} \text{ at } z \to \xi \tag{20}$$

Recall that ξ is not function of elevation. Moreover, since the tangential velocities are discontinuous, (20) is valid in each fluid only and thus writes:

$$\frac{\partial \phi_{1,2}}{\partial z} = \frac{\partial \xi}{\partial t} + u_{x(1,2)} \frac{\partial \xi}{\partial x} + u_{y(1,2)} \frac{\partial \xi}{\partial y} \text{ at } z \to \xi \tag{21}$$

3) Moreover, at the interface, the normal stress has to be continuous, thus for a fluid, the pressure is continuous. This can be translated from the momentum equation (16), by recalling that $\boldsymbol{u}$ derives from the potential ϕ (14):

$$\rho \left(\frac{\partial \boldsymbol{\nabla} \phi}{\partial t} + \boldsymbol{u} \boldsymbol{\nabla} \boldsymbol{u} \right) = \boldsymbol{\nabla} P + \boldsymbol{f}$$

Inverting the time and spatial derivatives through the Leiniz theorem:

$$\rho \left(\boldsymbol{\nabla} \frac{\partial \phi}{\partial t} + \boldsymbol{u} \boldsymbol{\nabla} \boldsymbol{u} \right) = \boldsymbol{\nabla} P + \boldsymbol{f}$$

And integrating over the volume:

$$\rho \left(\frac{\partial \phi}{\partial t} + \frac{1}{2} \boldsymbol{u}^2 \right) = P + \rho g z + C$$

C being an integration constant and $\boldsymbol{u}^2$ is a scalar product. The condition is that the pressure must be equal in F_1 and F_2 at the interface, thus:

$$\rho_1 \left(\frac{\partial \phi_1}{\partial t} + \frac{1}{2}(\boldsymbol{\nabla}\phi_1)^2 + gz \right) + C_1 = \rho_2 \left(\frac{\partial \phi_2}{\partial t} + \frac{1}{2}(\boldsymbol{\nabla}\phi_2)^2 + gz \right) + C_2 \text{ at } z = \xi \tag{22}$$

4) The same condition needs to be satisfied for the initial flow before pertubation as well, so that (22) similarly applies, and replacing ϕ by its constant value:

$$\rho_1(\frac{1}{2}(U_1^2 + gz) + C_1 = \rho_2(\frac{1}{2}(U_2^2 + gz) + C_2 \text{ at } z = 0$$

And since the condition is for $z = 0$, this gives a relation for the two constants:

$$\frac{1}{2}\rho_1 U_1^2 + C_1 = \frac{1}{2}\rho_2 U_2^2 + C_2 \tag{23}$$

A.5 Linearization

The set of equations (13) to (23) poses the entire problem. Linearization of the set permits an analytic resolution.

The conditions of continuity and incompressibility (15) apply to the initial potential as well as to the perturbed potential (17), so that:

$$\begin{aligned} \triangle\phi_1' &= 0 \text{ for } z \leq \xi \\ \triangle\phi_2' &= 0 \text{ for } z \geq \xi \end{aligned} \tag{24}$$

The boundary condition (19) at ∞, given the perturbation of the potential (17) with the unperturbed $\phi_{1,2}$ constant by definition simplifies into:

$$\begin{aligned} \nabla\phi_1' &\to 0 \text{ for } z \to -\infty \\ \nabla\phi_2' &\to 0 \text{ for } z \to +\infty \end{aligned} \tag{25}$$

Developing the boundary condition at the interface (21) with: -the definition of the perturbed potential (17), -the unperturbed $\phi_{1,2}$ are constant over z by definition of the problem, -using the Taylor series (18) for $\frac{D\xi}{Dt}$ and neglecting products of small quantities:

$$\frac{\partial \phi_{1,2}'}{\partial z} = \frac{\partial \xi}{\partial t} + u_{1,2}\frac{\partial \xi}{\partial x} \text{ at } z = \xi \tag{26}$$

Neglecting products of small quantities in (22) and replacing the definition of the potential (17):

$$\rho_1 \left(\frac{\partial \phi_1'}{\partial t} + U_1\frac{\partial \phi_1'}{\partial x} + \frac{1}{2}U_1^2 + g\xi \right) + C_1 = \rho_2 \left(\frac{\partial \phi_2}{\partial t} + U_2\frac{\partial \phi_2'}{\partial x} + \frac{1}{2}U_2^2 + g\xi \right) + C_2 \text{ at } z = \xi$$

which simplifies with the equality in (23) into:

$$\rho_1 \left(\frac{\partial \phi_1'}{\partial t} + U_1\frac{\partial \phi_1'}{\partial x} + g\xi \right) = \rho_2 \left(\frac{\partial \phi_2}{\partial t} + U_2\frac{\partial \phi_2'}{\partial x} + g\xi \right) \text{ at } z = \xi \tag{27}$$

A.6 Solution

The solution of the surface perturbation shall be a wave. Also, if other solutions exist, they could be decomposed into a Fourrier series, ending as waves. Moreover, geophysics is almost always resolved with waves. Thus a solution is searched with the form:

$$\begin{aligned} \xi &= \tilde{\xi}\exp(i(kx+ly)+st) \\ \phi_1' &= \tilde{\phi_1'}(z)\exp(i(kx+ly)+st) \\ \phi_2' &= \tilde{\phi_2'}(z)\exp(i(kx+ly)+st) \end{aligned} \tag{28}$$

The problem is now simply to resolve an ordinary differential system in z. Eq. (24) is a Laplace's equation whose solutions are of the form:

$$\tilde{\phi_{1,2}'} = A_{1,2}e^{-Kz} + B_{1,2}e^{Kz} \tag{29}$$

with $K = (k^2+l^2)^{1/2}$ the total wavenumber and $A_{1,2}$ two constants. Given the boundary condition (25), the solution must vanish in + resp. - ∞ for F_1 resp. F_2, and so:

$$\begin{aligned} \tilde{\phi_1'}(z) &= A_1 e^{Kz} \\ \tilde{\phi_2'}(z) &= A_2 e^{-Kz} \end{aligned} \tag{30}$$

Now from eq. (26):

$$\begin{aligned} A_1 K e^{Kz} e^{(i(kx+ly)+st)} &= (s\tilde{\xi} + U_1 ik\tilde{\xi})e^{(i(kx+ly)+st)} \\ -A_2 K e^{Kz} e^{(i(kx+ly)+st)} &= (s\tilde{\xi} + U_2 ik\tilde{\xi})e^{(i(kx+ly)+st)} \quad \text{at } z=\xi \end{aligned} \tag{31}$$

or, removing the equal harmonic terms, and taking into account that in the first exponential $z = \xi$, and this term can be neglected with a Taylor development:

$$\begin{aligned} A_1 &= (s+U_1 ik)\tilde{\xi}/K \\ A_2 &= -(s+U_2 ik)\tilde{\xi}/K \end{aligned} \tag{32}$$

Similarly resolving (27) by replacing the form of the solution given in (28) and in (32), one finds:

$$\rho_1[Kg + (s+ikU_1)^2] = \rho_2[Kg - (s+ikU_2)^2] \tag{33}$$

which is a simple quadratic function. The solution is straightforward to resolve with the discriminant method and leads:

$$s = -ik\frac{\rho_1 U_1 + \rho_2 U_2}{\rho_1+\rho_2} \pm \left[\frac{k^2\rho_1\rho_2(U_1-U_2)^2}{(\rho_1+\rho_2)^2} - \frac{Kg(\rho_1-\rho_2)}{\rho_1+\rho_2}\right]^{1/2} \tag{34}$$

In order to find the result of a simple gravity wave, the coefficient s must be imaginary in order to correspond to a pulsation (w) associated with an oscillation of the surface. Consider the simple case of an unidirectional wave ($K = k$), and no difference in velocities of the flows ($u_1 = u_2$). Moreover, given the absence of a bed, and thus reference in the

problem, the velocity can be set zero. For a gravity wave, the denser fluid needs to be underneath the light one, thus $\rho_1 > \rho_2$. These conditions grant the existence of a gravity wave and the relation between the velocity ($c = w/k$) and wavelength ($\lambda = 2\pi/k$) found in most textbooks and used for the interpretation of the sedimentary record is then:

$$c^2 = \frac{g(\rho_1 - \rho_2)}{k(\rho_1 + \rho_2)} = \frac{g(\rho_1 - \rho_2)}{\rho_1 + \rho_2}\frac{\lambda}{2\pi} \tag{35}$$

If $\rho_1 < \rho_2$ this would have produced a Rayleigh-Taylor instability, with an exponential sink of the interface instead of a pulsation:

$$s = \pm \left[-\frac{kg(\rho_1 - \rho_2)}{\rho_1 + \rho_2} \right]^{1/2} \tag{36}$$

References

-

Alexander J., Bridge J. S., Cheel R. J., Leclair S. F. (2001). Bedforms and associated sedimentary structures formed under supercritical water flows over aggrading sand beds. Sedimentology, 48(1), 133-152.

Allen J. R.L. (1984). Sedimentary Structures, their Character and Physical Basis, Vol. 1. Developments in Sedimentology, 30, 17-22.

Andrews B., Manga M. (2012). Experimental study of turbulence, sedi- mentation, and coignimbrite mass partitioning in dilute pyroclastic density currents. J Volcanol Geotherm Res 225-226:30-44

Brand B.D., Clarke A.B., Semken S. (2009). Eruptive conditions and depo- sitional processes of Narbona Pass Maar volcano, Navajo volcanic field, Navajo Nation, New Mexico (USA). Bull Volcanol 71:49-77

Brand B.D., Clarke A.B. (2012). An unusually energetic basaltic phreatomagmatic eruption: using deposit characteristics to constrain dilute pyroclastic density current dynamics. J Volcanol Geotherm Res 243-244:81-90

Carlson R. H., Roberts W. A. (1963). Project Sedan, Mass Distribution and Throwout Studies. BOEING CO SEATTLE WA.

Cartigny M. (2012). Morphodynamics of supercritical high-density turbidity currents (Vol. 10). Utrecht University, Faculty of Geosciences, Department of Earth Sciences.

Chanson H. (2009). Current knowledge in hydraulic jumps and related phenomena. A survey of experimental results. European Journal of Mechanics-B/Fluids, 28(2), 191-210.

Cole P.D. (1991). Migration direction of sand wave structures in pyroclastic-surge deposits: implications for depositional processes. Geology 19:1108-1111

Crowe B.M., Fisher R.V. (1973). Sedimentary structures in base-surge deposits with special reference to cross-bedding, Ubehebe Craters, Death Valley, California. Geol Soc Am Bull 84:663-682

Douillet G.A., Pacheco D.A., Kueppers U., Tsang-Hin-Sun E., Dingwell D.B. (2013b). Dune bedforms produced by the 2006 pyroclastic density currents at Tungurahua volcano, Ecuador. Bull. Volcanol. 75, 762.

Douillet G. A., Rasmussen K. R., Kueppers U., Lo Castro D., Merrison J. P., Iversen J. J., Dingwell D. B. (2014). Saltation threshold for pyroclasts at various bedslopes: Wind tunnel measurements. Journal of Volcanology and Geothermal Research, 278, 14-24.

Douillet G. A., Tsang-Hin-Sun ., Kueppers U., Dingwell D. B. (Submitted). Syn-eruptive soft-sediment deformation in deposits of dilute pyroclastic density currents: granular shear, impacts and shock waves triggers. Solid Earth.

Drazin P.G., Reid W.H. (2004). Hydrodynamic stability. Cambridge university press.

Druitt T.H. (1992). Emplacement of the 18 May 1980 lateral blast deposit ENE of Mount St. Helens, Washington. Bull Volcanol 54:554-572

Duller R.A., Mountney N.P., Russell A.J., Cassidy N.C. (2008). Architectural analysis of a volcaniclastic jokulhlaup deposit, southern Iceland: sedimentary evidence for supercritical flow. Sedimentology, 55(4), 939-964.

Fisher R.V., Waters A.C. (1969). Bed forms in base-surge deposits: lunar implications. Science, 165(3900), 1349-1352.

Fisher R.V., Waters A.C. (1970). Base surge bed forms in Maar volcanoes. Am J Sci 268:157-180

Frechen. (1971). Siebengebirge am Rhein, Laacher Vulkangebiet, Maargebiet der Westeifel, Vulkanologischpetrographische Exkursionen. Gebr. Borntraeger, Berlin-Stuttgart.

Froude M. (2014). PhD dissertation. University of East Anglia, School of Environmental Sciences (United Kingdom)

Gencalioglu-Kuscu G., Atilla C., Cas R.A.F., Kuscu I. (2007). Base surge deposits, eruption history, and depositional processes of a wet phreatomagmatic volcano in Central Anatolia (Cora Maar). J Volcanol Geotherm Res 159:198-209

Gilbert G.K., Murphy E.C. (1914). The transportation of debris by running water (No. 86). US Government Printing Office.

Guyon E., Hulin J.P., Petit L. (2002). Hydrodynamique physique. EDP Sciences, 2001 - 674 pages

Hand B.M. (1969). Antidunes as trochoidal waves. Journal of Sedimentary Research, 39(4).

Hand B.M. (1974). Supercritical flow in density currents. Journal of Sedimentary Research, 44(3).

Huang H., Imran J., Pirmez C., Zhang Q., Chen G. (2009). The critical densimetric Froude number of subaqueous gravity currents can be non-unity or non-existent. Journal of Sedimentary Research, 79(7), 479-485.

Kennedy J.F. (1961). Stationary waves and antidunes in alluvial channels. California Institute of Technology, Pasadena, CA, USA.

Kennedy J.F. (1963). The mechanics of dunes and antidunes in erodible-bed channels. Journal of Fluid Mechanics, 16(04), 521-544.

Kostic S., Parker G. (2007). Conditions under which a supercritical turbidity current traverses an abrupt transition to vanishing bed slope without a hydraulic jump. Journal of Fluid Mechanics, 586, 119-145.

Kostic S. (2011). Modeling of submarine cyclic steps: Controls on their formation, migration, and architecture. Geosphere, 7(2), 294-304.

Kostic S. (Submitted). Submarine Upper-Regime Bedforms: Hydrodynamic Response of Turbidity Currents to Fine-Grained Sediment Waves, submitted to Geosphere.

Kumar R. (2012). Derivation of the Navier-Stokes equations. 11th indo-german winter academy. (Available online)

Lang J., Winsemann J. (2013). Lateral and vertical facies relationships of bedforms deposited by aggrading supercritical flows: from cyclic steps to humpback dunes. Sedimentary Geology, 296, 36-54.

Mattson P.H., Alvarez W. (1973). Base surge deposits in Pleistocene volcanic ash near Rome. Bull Volcanol 37(4):553-572

Middleton G.V. (1965). Antidune cross-bedding in a large flume. Journal of Sedimentary Research, 35(4).

Moore J.G. (1967). Base surge in recent volcanic eruptions. Bull Volcanol 30(1):337-363

Moore J.G., Nakamura K., Alcaraz A. (1966). The 1965 eruption of Taal Volcano. Science 151:955-960

Nocita B.W. (1988). Soft-sediment deformation (fluid escape) features in a coarse-grained pyroclastic-surge deposit, north-central New Mexico. Sedimentology, 35(2), 275-285.

Plastino A.R., Muzzio J.C. (1992). On the use and abuse of Newton's second law for variable mass problems. Celestial Mechanics and Dynamical Astronomy, 53(3), 227-232.

Prave A.R. (1990). Clarification on some misconceptions about antidune geometry and flow character. Sedimentology 37: 1049-1052

Richards A.F. (1959). Geology of the Islas Revillagigedo, Mexico. 1. Birth and development of Volcano Brcena, Isla San Benedicto. Bull Volcanol 22(1):73-123

Rowley P.D., MacLeod N.S., Kuntz M.A., Kaplan A.M. (1985). Proximal bedded deposits related to pyroclastic flows of May 18, 1980, Mount St. Helens, Washington. Geol Soc Am Bull 96(11):1373-1388

Rowley P. D., MacLeod N. S., Kuntz M. A., Kaplan A. M. (1985). Proximal bedded deposits related to pyroclastic flows of May 18, 1980, Mount St. Helens, Washington. Geological Society of America Bulletin, 96(11), 1373-1383.

Schmincke H.U., Fisher R.V., Waters A.C. (1973). Antidune and chute-and- pool structures in the base surge deposits of the Laacher See area, Germany. Sedimentology 20:553-574

Valentine GA (1987). Stratified flow in pyroclastic surges. Bull Volcanol 49:616-630

Sequeiros O. E., Spinewine B., Garcia M. H., Beaubouef, R. T., Sun, T., Parker, G. (2009). Experiments on wedge-shaped deep sea sedimentary deposits in minibasins and/or on channel levees emplaced by turbidity currents. Part I. Documentation of the flow. Journal of Sedimentary Research, 79(8), 593-607.

Sigurdsson H., Carey S.N., Fisher R.V. (1987). The 1982 eruption of E1 Chichon volcano, Mexico (3): physical properties of pyroclastic surges. Bull Volcanol 49:467-488

Spinewine B., Octavio E., Sequeiros O.E., Garca M.H., Beaubouef R.T., Sun T., Savoye B., Parker G. (2009). Experiments on wedge-shaped deep sea sedimentary deposits in minibasins and/or on channel levees emplaced by turbidity currents. Part II. Morphodynamic evolution of the wedge and of the associated bedforms. J Sed Res 79(8):608- 628

Sulpizio R., De Rosa R., Donato P. (2008). The influence of variable topography on the depositional behaviour of pyroclastic density currents: the examples of the Upper Pollara eruption (Salina Island, southern Italy). J Volcanol Geotherm Res 175(3):367-385

Valentine G.A. (1987). Stratified flow in pyroclastic surges. Bull Volcanol 49:616-630

Vallis G. K. (2006). Atmospheric and oceanic fluid dynamics: fundamentals and large-scale circulation. Cambridge University Press.

Walker R. G. (1967). Upper flow regime bed forms in turbidites of the Hatch Formation, Devonian of New York State. Journal of Sedimentary Research, 37(4).

Waters A. C., Fisher R. V. (1971). Base surges and their deposits: Capelinhos and Taal volcanoes. Journal of Geophysical Research, 76(23), 5596-5614.

Wynn R.B., Stow D.A.V. (2002). Classification and characterisation of deep- water sediment waves. Mar Geol 192:7-22

Yokokawa M., Hasegawa K., Kanbayashi S., Endo N. (2010). Formative conditions and sedimentary structures of sandy 3D antidunes: an application of the gravel step-pool model to fine-grained sand in an experimental flume. Earth Surface Processes and Landforms, 35(14), 1720-1729.

This page was intentionally left blank.

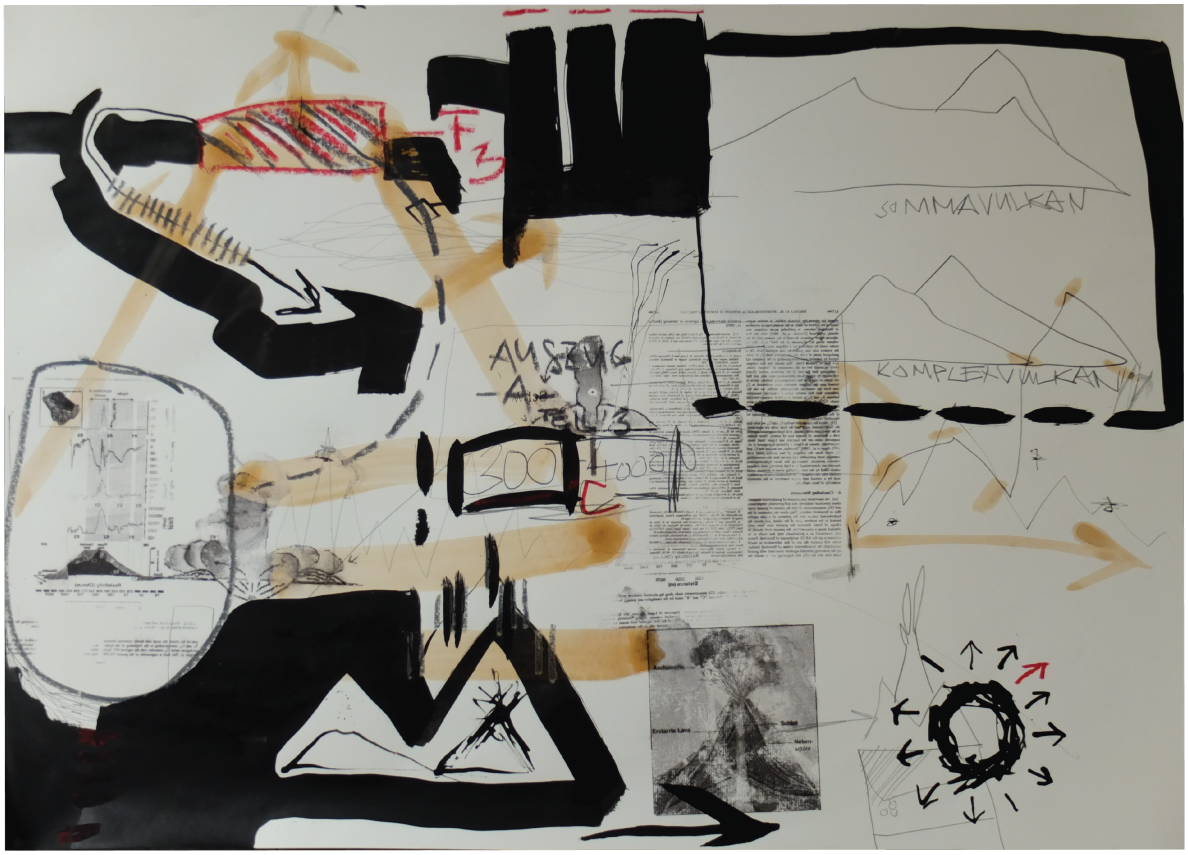

Figure 2.6: Painting, drawing and collage by Almut Winkler interacting with photocopies of Finizola et al. (2010). Almut Winkler (2014)

This page was intentionally left blank.

Chapter 3

Dune bedforms produced by dilute pyroclastic density currents from the August 2006 eruption of Tungurahua volcano, Ecuador

This chapter was published in the Journal "Bulletin of Volcanology" in 2013 together with chapter 1. It describes and discusses the genesis of dune bedforms forming the overbank deposits of the August 2006 eruption of Tungurahua volcano.

This page was intentionally left blank.

Bull Volcanol (2013) 75:762
DOI 10.1007/s00445-013-0762-x

RESEARCH ARTICLE

Dune bedforms produced by dilute pyroclastic density currents from the August 2006 eruption of Tungurahua volcano, Ecuador

Guilhem Amin Douillet · Daniel Alejandro Pacheco · Ulrich Kueppers · Jean Letort · Ève Tsang-Hin-Sun · Jorge Bustillos · Minard Hall · Patricio Ramón · Donald B. Dingwell

Received: 17 February 2013 / Accepted: 17 September 2013 / Published online: 13 October 2013

Abstract A series of pyroclastic density currents were generated at Tungurahua volcano (Ecuador) during a period of heightened activity in August 2006. Dense pyroclastic flows were confined to valleys of the drainage network, while dilute pyroclastic density currents overflowed on interfluves where they deposited isolated bodies comprising dune bedforms of cross-stratified ash exposed on the surface. Here, the description, measurement, and classification of more than 300 dune bedforms are presented. Four types of dune bedforms are identified with respect to their shape, internal structure, and geometry (length, width, thickness, stoss and lee face angles, and stoss face length). (1) "Elongate dune bedforms" have smooth shapes and are longer (in the flow direction) than wide or thick. Internal stratification consists of stoss-constructional, thick lensoidal layers of massive and coarse-grained material, alternating with bedsets of fine laminae that deposit continuously on both stoss and lee sides forming aggrading structures with upstream migration of the crests. (2) "Transverse dune bedforms" show linear crests perpendicular to the flow direction, with equivalent lengths and widths. Internally, these bedforms exhibit finely stratified bedsets of aggrading ash laminae with upstream crest migration. Steep truncations of the bedsets are visible on the stoss side only. (3) "Lunate dune bedforms" display a barchanoidal shape and have stratification patterns similar to those of the transverse ones. Finally, (4) "two-dimensional dune bedforms" are much wider than long, exhibit linear crests and are organized into trains. Elongate dune bedforms are found exclusively in proximal deposition zones. Transverse, lunate, and two-dimensional dune bedforms are found in distal ash bodies. The type of dune bedform developed varies spatially within an ash body, transverse dune bedforms occurring primarily at the onset of deposition zones, transitioning to lunate dune bedforms in intermediate zones, and two-dimensional dune bedforms exclusively on the lateral and distal edges of the deposits. The latter are also found where flows moved upslope. Elongate dune bedforms were deposited from flows with both granular-based and tractional flow boundaries that possessed high capacity and competence. They may have formed in a subcritical context by the blocking of material on the stoss side. We do not interpret them as antidune or "chute-and-pool" structures. The dimensions and cross-stratification patterns of transverse dune bedforms are interpreted as resulting from low competence currents with a significant deposition rate, but we rule out their interpretation as "antidunes". A similar conclusion holds for lunate dune bedforms, whose curved shape results from a sedimentation rate dependent on the thickness of the

Editorial responsibility: V. Manville

Electronic supplementary material The online version of this article (doi:10.1007/s00445-013-0762-x) contains supplementary material, which is available to authorized users.

G. A. Douillet (✉) · U. Kueppers · D. B. Dingwell
Earth & Environmental Sciences, Ludwig-Maximilians-Universität (LMU), Munich, Germany
e-mail: g.douillet@min.uni-muenchen.de

D. A. Pacheco · J. Bustillos · M. Hall · P. Ramón
Instituto Geofísico, Escuela Politécnica Nacional, Quito, Ecuador

J. Letort · È. Tsang-Hin-Sun
Ecole et Observatoire des Sciences de la Terre, Université de Strasbourg, Strasbourg, France

J. Letort
Laboratoire de Géophysique Interne et Tectonophysique (LGIT), Grenoble, France

È. Tsang-Hin-Sun
Laboratoire de Géosciences Marines, Université de Brest, Brest, France

bedform. Finally, two-dimensional dune bedforms were formed where lateral transport exceeds longitudinal transport; i.e., in areas where currents were able to spread laterally in low velocity zones. We suggest that the aggrading ash bedsets with upstream crest migration were formed under subcritical flow conditions where the tractional bedload transport was less important than the simultaneous fallout from suspension. This produced differential draping with no further reworking. We propose the name "regressive climbing dunes" for structures produced by this process. A rapid decrease in current velocity, possibly triggered by hydraulic jumps affecting the entire parent flows, is inferred to explain their deposition. This process can in principle hold for any kind of particulate density current.

Keywords Pyroclastic dune bedforms · Antidune · Aggrading structures · Regressive climbing dunes · Tungurahua

Introduction

Pyroclastic density currents

Pyroclastic density currents (PDCs) are gas particle flows produced during explosive eruptions (Druitt 1996). They exhibit a wide range of particle concentration, grain size distribution, and temperature, and they vary in concentration gradient, flow density, and transport mechanisms (Sparks 1976; Burgisser and Bergantz 2002).

Pioneer authors classified PDCs into three end-members based on deposit characteristics: (1) flow (massive, unsorted, coarse-grained, and topography-confined deposits from "dense pyroclastic flows"), (2) surge (often cross-stratified, relatively sorted, finer grained, and topography-influenced deposits from laterally moving, low particle concentration "dilute PDCs"; Wohletz and Sheridan 1979; Walker 1984), and (3) fall (stratified or massive, sorted draping deposits from "fallout"). It has been emphasized that deposits mainly reflect basal boundary zone processes (Carey 1991; Branney and Kokelaar 1997), and a classification into granular, tractional, and direct fallout-dominated boundary flows has been adopted by Branney and Kokelaar (2002, Chap. 4). Other classifications define two groups: inertia-dominated and gravitation-dominated flows (Doronzo 2012). All of these terms are relevant for aspects of this study but they only represent conceptual end-members. The different transport mechanisms are probably gradational in nature, and PDCs are likely continuously stratified flows with different types of particle support (Rowley et al. 1985; Valentine 1987; Burgisser and Bergantz 2002), that can evolve both in time and space (Wohletz and Sheridan 1979; Branney and Kokelaar 2002, Chap. 6; Sulpizio et al. 2008).

Here, we describe the dune bedforms and cross-stratification patterns found in the deposits of dilute PDCs generated at Tungurahua volcano (Ecuador) in August 2006. The excellent preservation of the surface shape of the bedforms makes it a unique outcrop, enabling analysis of their spatial distribution and relationships with inferred current dynamics.

Dune bedforms in deposits of dilute PDCs

Terminology

We term dune bedforms (DBs) the decimeter- to decameter-scale undulations on the surface of the deposits. We use this name in a purely descriptive way, following "bed form" as defined in Bridge and Demicco (2008, p. 157) as "a single geometric element, such as a ripple or a dune", as "dune form" was used in Mattson and Alvarez (1973). DB is equivalent to "sand-wave" (Wohletz and Sheridan 1979; Allen 1982; Sigurdsson et al. 1987; Cole 1991; Druitt 1992), a term avoided in this study because it is loosely defined (bedforms are not waves), and to prevent confusion with the term "sediment wave" (kilometer-scale undulations in turbidites; Wynn and Stow 2002). We avoid using simply "dune" since it has a genetic connotation (a dune is deposited from a subcritical flow across interaction with a flow-free boundary; Bridge and Demicco 2008, pp. 163 and 169). We use "length" to describe the distance from the onset to the end of the DB in a direction perpendicular to the crest (i.e., parallel to the flow direction) rather than "wavelength" that refers to the spacing between successive crests in repetitive trains of bedforms exclusively (conventional crest-to-crest wavelength; Fig. 1). "Thickness" is preferred to "amplitude", since the DBs potentially did not reach equilibrium before deposition ended. "Width" refers to the extent of the DB parallel to the crest. The stoss side faces upstream and the lee downstream (Fig. 1). Cross-stratifications are strata inclined with respect to an underlying plane bed and record the temporal evolution of a bedform (Fig. 2). "Lamina" refers to a millimeter-scale strata, "bedset" to a group of laminae that follow a common pattern and a "layer" represents

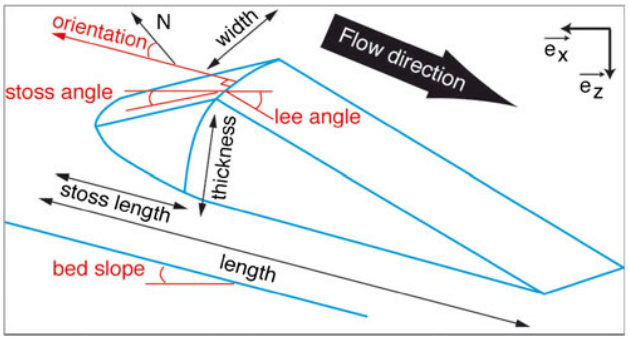

Fig. 1 Sketch of the measurements carried out on bedforms: stoss and lee face angles taken to the horizontal, width, crest orientation, stoss face length, length, and thickness of exposed bedform

a single, thick (>1 cm) and massive strata. We speak of "constructional features" when part of the laminations are preserved so that a bedform partly "climbs" on its neighbour during migration (such as climbing or drift cross-laminations). "Aggrading features" is used when preservation occurs on both sides of the bedform so that individual strata can be followed from the stoss to the lee side across the crest, resulting in the complete expression of the original geometry of the bedforms. In that case, the crests of successive strata forming a DB can be shifted laterally with respect to each other, leading to upstream or downstream crest-migrating structures (also termed regressive and progressive, respectively). Note that up- or downstream migration of a crest should not be confused with migration of the whole structure. Indeed, in contrast to most fluvial and aeolian bedforms, there is no migration of the whole structure because accretion occurs on both sides of the bedform. "Stoss-aggradation" indicates that the stoss face is subjected to more aggradation than the lee, inducing upstream crest migration during growth of the bedform ("regressive"). "Formsets" are bedsets that have the overall shape of a bedform (Fig. 2).

Interpretations

Cross-stratification within PDC deposits was recognized as a primary feature from observations of DBs produced by nuclear test base surges and modern dilute PDCs (Moore et al. 1966; Moore 1967). DBs produced by dilute PDCs can exhibit: (1) very steep or very low face angles on both sides of a DB, (2) very common aggrading nature with up- or downstream migration of successive crests and appearance of cross-stratification within formsets, (3) successive individual laminae with heterogeneous grain size distributions, (4) steep truncations covered by stoss-aggrading lensoidal layers. Many interpretations and suggestions regarding the formation of PDC DBs have been put forward, as described below, but controversy remains.

(a) Climbing dunes

Aggrading cross-bedding (with both migration directions) is ubiquitous in the dilute PDC sedimentary record (Fig. 3 of Fisher and Waters (1969); Fig. 7 of Mattson and Alvarez (1973); types III and IV of Schmincke et al. (1973), Fisher (1977), Yokoyama and Tokunaga (1978), Wohletz and Sheridan (1979), Allen (1982, p. 425), and Sohn and Chough (1989); types A, B, C of Cole (1991) and Fig. 2 of Dellino et al. (2004)). These characteristics have often been described and/or interpreted as "climbing dunes" (Walker 1984; Sohn and Chough 1989; Cagnoli and Ulrich 2001). Note however that "climbing dune" is not a descriptive term for "aggrading DB" as it contains an intrinsic interpretation as "lower flow regime" bedform, as used by Sohn and Chough (1989). Climbing dunes form under high deposition rates (Allen 1970; Ghienne et al. 2010), as noted in the PDC environment by Walker (1984), who observed that "the environment in which climbing dune-bedded surge deposits form is a strongly depositional one: the surges were heavily laden, and as they slowed down they rapidly shed their load".

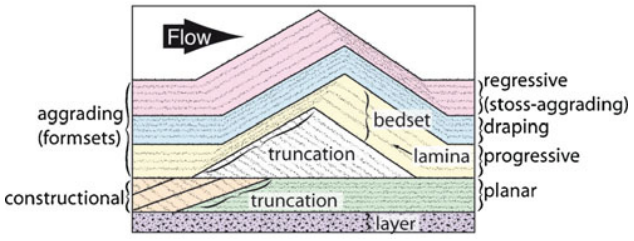

Fig. 2 Nomenclature for the different cross-stratification patterns. *Colors* refer to a group with similar characteristics

(b) Antidunes

According to fluid dynamics, antidunes are related to stationary gravity waves trapped at density interfaces (Prave 1990; Alexander et al. 2001). Gravity waves only form if there is a free-density interface that can oscillate (e.g., water and air (Alexander et al. 2001; Duller et al. 2007); a density current and an ambient fluid (Hand 1974; Spinewine et al. 2009)). For a gravity wave to become stationary over a bed, wave velocity must equal flow velocity, but in the opposite direction. This condition happens in the transcritical regime (Froude number close to 1; Guyon et al. 2001, p. 289; Duller et al. 2007).

In PDC sedimentology, "antidune" was initially used as a descriptive term for low-angle, meter-scale, cross-stratifications inclined at angles less than the repose angle on both sides resembling standing waves (in fact, stationary waves!) with aggrading patterns, i.e., without a meaning in terms of fluid dynamics (Fisher and Waters 1969, 1970; Waters and Fisher 1971). Subsequent usage adopted the fluid dynamics connotation, thus turning into an interpretation (Crowe and Fisher 1973; Mattson and Alvarez 1973; Schmincke et al. 1973).

Confusion has since arisen and "antidune" has been variously used as (1) a descriptive term for DBs showing upstream crest migration, (2) DBs with aggrading bedsets, (3) low-angle cross-stratifications, or as (4) a fluid dynamics interpretation for different kinds of DB cross-stratifications in PDCs (Fisher 1977; Yokoyama and Tokunaga 1978; Wohletz and Sheridan 1979; Walker et al. 1981; Fisher et al. 1983; Suthren 1985; Sohn and Chough 1989; Charland and Lajoie 1989; Gianneti and Luongo 1994; Brand and White 2007; Gençalioğlu-Kuşcu et al. 2007; Brand et al. 2009; Brand and Clarke 2009, 2012; Kelfoun et al. 2009; Andrews and Manga 2012). Similarly, the term "chute and pool" has been variously used as an interpretative/descriptive term for stoss aggrading, lensoidal layers laying on steep truncations,

even if "chute and pool" should exclusively be reserved as interpretation of deposits produced by hydraulic jumps (Schmincke et al. 1973).

(c) Basal boundary processes

In contrast to a structure fully ruled by the fluid-phase dynamics, it has been suggested that the formation of DBs was controlled by the basal flow-bed boundary (Branney and Kokelaar 2002, Chap. 4). Cohesive effects due to water content have been pointed to as a possible source for stoss-aggrading bedforms unrelated to gravity waves (e.g., Allen 1982, pp.428–429), but the observation that both up- and downstream migration occurs during single events excludes this (Cole 1991; Druitt 1992). Other types of distrainment effects (the opposite of entrainment) might however have an influence on the formation of DBs. Deposits are thus often interpreted in terms of a basal boundary zone (Branney and Kokelaar 2002, Chap. 4). Several studies suggested boundary zones intermediate between two end members. A tractional boundary that is inhibited by a high basal clast concentration is thought to account for fine-grained, massive or faintly stratified beds (Branney and Kokelaar 1997; Brown and Branney 2004; Sulpizio et al. 2010). Tractional and fallout boundaries are inferred for faint, low-angle cross-stratifications with fallout grain characteristics (Valentine and Giannetti 1995; Wilson and Hildreth 1998). Under water, "raining" sediment seems to inhibit cross-bedding development for antidunes but not lower stage bedforms (Arnott and Hand 1989), whereas a high fines concentration eases the formation of cross-lamination (Simons et al. 1963), and rapidly depositing suspensions from a density current produce poorly graded deposits (Sumner et al. 2008).

(d) Particulate density currents and pulsating nature

It is often hypothesized that dilute PDCs have pulsating behavior (Wohletz and Sheridan 1979; Valentine 1987; Sohn and Chough 1989; Sulpizio and Dellino 2008) and that this might trigger formation of stoss-aggrading bedforms unrelated to antidunes (Collela and Hiscott 1997; Vasquez and Ort 2006; Sulpizio et al. 2007; Sulpizio and Dellino 2008). Dilute pulses would lose their kinetic energy rapidly (Wohletz 1998), each pulse producing a single lamina or bedset by stepwise deposition (Walker 1984; Cole 1991; Sulpizio et al. 2007). Vasquez and Ort (2006) interpreted the succession of truncated bedsets and overlying capping sets as indication of waning flows with a leading head and slower tail. Stoss-aggrading structures are typical of the PDC record, but also widely observed in turbidites at the kilometer scale (Nakajima and Satoh 2001; Wynn and Stow 2002), the meter scale (Mulder et al. 2009; Ponce and Carmona 2011), in experimental particulate density currents (Kubo and Nakajima 2002; Spinewine et al. 2009) and in sub- and proglacial fan deposits (Ghienne et al. 2010; Girard et al. 2012; Lang and Winsemann 2013). Such features are almost absent from other environments, suggesting that the particulate–density–current nature of the parental flows might be the source for stoss-aggrading bedforms (Rowley et al. 1985).

Spatial evolution

DBs are found to evolve in dimension (Douillet et al. 2013 and references therein), shape, and internal structure within deposits of the same eruption. Plate 24 of Richards (1959) shows DBs formed only after a break in slope, being absent above the break. The 1980 Mt. St. Helens (USA) eruption produced low-angle DBs (Fisher 1990) whose shape evolved downstream from hummocks to transverse shapes in the downstream direction (Hoblitt et al. 1981), and internal organization showing downstream crest migration on the stoss faces of ridges and upstream crest migration on ridge lee faces (Druitt 1992). Similarly, DBs from the 1982 eruption of El Chichón (México) have successive crests migrating upstream in proximal zones but migrating downstream in distal zones, interpreted as a result of downstream decrease in flow velocity (Sigurdsson et al. 1987). At Laacher See volcano (Germany), lensoidal layers aggrading on the upstream face of steep truncations interpreted as "chute-and-pool" structures were observed in more proximal zones than DB cross-stratifications with up- and downstream crest migration in distal zones (Schmincke et al. 1973). In contrast, at Roccamonfina (Italy) and Sugarloaf Mountain (USA) volcanoes, "chute-and-pool" structures as well as up- or downstream crest-migrating DB cross-stratifications occur within meters of each other (Cole 1991). In terms of their organization, DBs can also form composite bedforms built up by several successive DBs (e.g., Sigurdsson et al. 1987) or show a certain degree of repeatability in the downstream direction, suggesting periodic morphologies (Hoblitt et al. 1981).

The 2006 eruption of Tungurahua

Tungurahua is an active andesitic stratovolcano of the eastern Cordillera of the Northern Volcanic Zone in Ecuador (Hall et al. 1999, 2008; Le Pennec et al. 2008). The current period of activity began in 1999, reaching a paroxysm in July and August 2006, with generation of PDCs flowing down to populated areas, causing fatalities and severe damage to infrastructure and the agricultural sector. The 2006 PDCs were well-monitored and the deposits documented (Kelfoun et al. 2009; Samaniego et al. 2011; Eychenne et al. 2012; Douillet et al. 2013).

The July 14–16 PDCs flowed on the N-NW flanks. The more voluminous August 16–17 PDCs deposited on the N, W, and SW flanks, covering the July deposits. This paper focuses on the

August deposits. The eruption lasted for less than 8 h and about five PDCs reached the study areas at approximate flow front velocities of 30 m/s (inferred from seismic records; Kelfoun et al. 2009). The generation of the PDCs is believed to have resulted from the episodic destabilization of erupted products accumulated near the vent. Drainage channels directed the PDCs, confining the dense pyroclastic flows (Kelfoun et al. 2009). Cross-stratified, ash dominated deposits are found on the outer interfluves of valley curves and downstream of cliffs (Douillet et al. 2013). The cross-stratified deposits can be divided into a proximal (*P-Xst*) and distal (*D-Xst*) facies associations. On the upper flanks, *P-Xst* deposits are the signature of successive input from dense pyroclastic flows and dilute PDCs. On the lower flanks, the *D-Xst* deposits outcrop as isolated patches 100 s of meters broad and several meters thick that we refer to as "ash bodies" (Douillet et al. 2013). DBs produced by the eruption (C. Robin, personal communication) cover most of the surface of the *Xst* deposits, draped by a centimeter-thick fall layer confirming their pristine outer shapes (November 2010).

Data

Measurements

We measured the shape characteristics on the outer surface of more than 300 DBs from different depositional ash bodies. Since the outer surface corresponds either to a final lamina or truncation, our dataset should be comparable to others from cross-sections. The orientation of the crest and six shape parameters: length, thickness, width, stoss face length, stoss face slope angle, and lee face slope-angle were measured from eyewitness definition in the field (Fig. 1). Stoss and lee face slope angles are given here referred to the horizontal (i.e., not corrected for the mean underlying bed slope angle). Ripple index (RI; corresponding to the ratio of length over thickness) and ripple symmetry index (RSI; ratio of length of long face over length of short face) were calculated following Tanner (1967). High RI values characterize flat DBs, high RSI values asymmetrical DBs. The RSI ratio is always >1: i.e., it does not distinguish whether the stoss or the lee face is longer. For Tungurahua, where DBs may exhibit a longer stoss or longer lee face, we allocated a sign to the RSI (termed signed RSI: "S-RSI"):

"S−RSI" = RSI if the stoss face is the longest;

"S−RSI" = −RSI if the lee face is the longest;

The six shape parameters are presented in four graphs (Fig. 3). The length vs. thickness data (Fig. 3a) follow a logarithmic trend that fits with other DB datasets from the literature and are in the middle range of sizes. Length versus width data (Fig. 3b) permit recognition of different shape patterns (see "Dune bedform types" section). In aeolian and subaqueous environments, a gentle stoss face ruled by erosion (theoretically) follows a steep lee face angle determined by the repose angle of the particles. However, at Tungurahua, the stoss and lee face slope angles vary significantly (Fig. 3c) and either side can be steeper. Laboratory measurements of the dynamic and static repose angles of dry bulk ash are 32° and 41°, respectively, and 38° and 52° for the fraction <250 μm. The majority of DBs from Tungurahua have negative S-RSI values, indicating longer lee than stoss faces (Fig. 3d), though this can be an effect of the strong dip of the underlying bed (between 10° and 25°). A scattered relation between RI and S-RSI is visible, indicating that flat bedforms tend to be more asymmetrical (Fig. 3d).

Dune bedform types

In the field, each DB was given a descriptive classification based on its overall morphology. Four common types were defined (Figs. 4, 5, 6, and 7): "elongate", "transverse", "lunate", and "two-dimensional". Cross-sections permit linkage of external shapes with internal stratification patterns. The main quantitative characteristics are listed in Table 1 and the six shape parameters grouped by color according to the DB type in Fig. 3.

Elongate

DBs from the *P-Xst* zone (see Douillet et al. 2013) are grouped under the term "elongate" as a reference to their usual shape. Usually, they are longer than wide, are the flattest (high RI) and have low-angle stoss faces. They produce only a slight bump on the surface of the deposits with diffuse crests that may be difficult to trace and have short stoss faces (high S-RSI), possibly because they formed on the steepest slopes (Figs. 3c, d and 4.

Internally (Fig. 4b–e), elongate DBs shows aggrading patterns with a composite nature alternating between three lithofacies: (*lensmBLA-facies*, *xsbAL-facies*, and *mbAL-facies*). The *lensmBLA-facies* consists of coarse-grained and massive layers made of an unsorted mixture of ash, lapilli, and blocks up to 10 cm in diameter. It sometimes shows gradational grain size changes. The layers vary between 3 and 20 cm in thickness and have a lensoidal shape. They thicken on the lower part of the stoss side and thin to the crest and on the lee, sometimes until they disappear, inducing an overall upstream migration of successive crests. The *xsbAL-facies* consists of ash and lapilli bedsets that are crudely to diffusely laminated. Laminations usually show smooth crests and build up stoss-aggrading bedsets. The *mbAL-facies* is similar in grain size and bedset dimensions to the *xsbAL-facies*, but massive. The contact between the three facies types can be sharp or gradational, and they may occur in

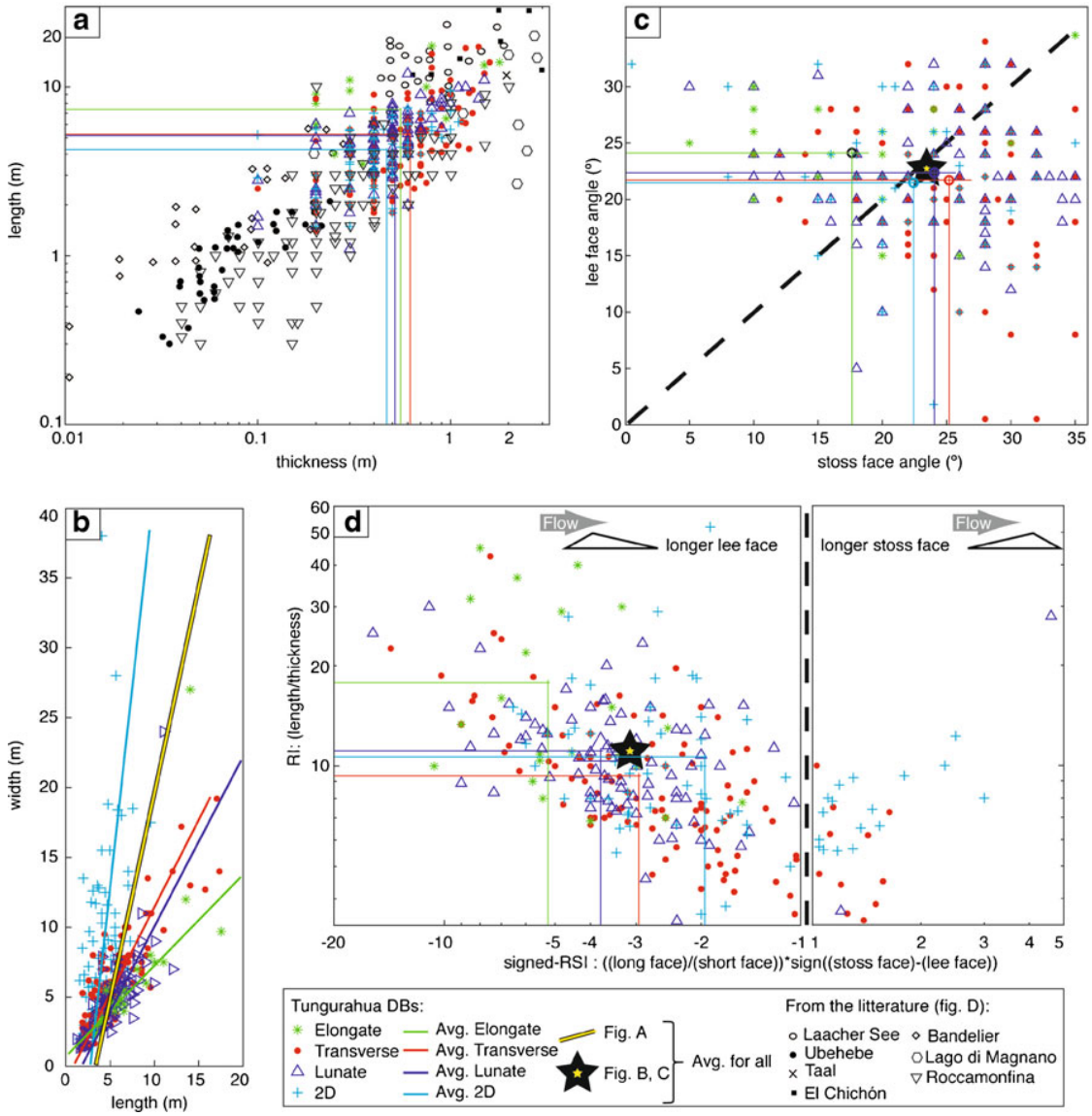

Fig. 3 Dimensions of dune bedforms by types. **a** Length versus thickness, compared with outcrops from Ubehebe Crater (Crowe and Fisher 1973); Taal volcano (Waters and Fisher 1971); Laacher See (Schmincke et al. 1973); Bandelier Tuff and El Chichón (Sigurdsson et al. 1987); Bolsena caldera, Vico caldera, Baccano crater, and Martignano crater—all four grouped under "Lago di Magnano"—(Mattson and Alvarez 1973); Roccamonfina (Gianneti and Luongo 1994); and Cora Maar (Gençalioğlu-Kuşcu et al. 2007). **b** Length versus width with linear regression. **c** Lee versus stoss face angles measured with respect to the *horizontal line*. The *dotted line* denotes equal lee and stoss angles. **d** Ripple index (length over width) as a function of signed ripple symmetry index (long face length over short face length, with negative sign indicating lee face longer than stoss)

any order with the final strata forming a DB being made of any of the three facies. No correlation between different bedforms was possible. In one outcrop, a centimeter-thick, draping deposit of lapilli-sized ash aggregates without matrix was found intercalated between a *lensmBLA* layer and *xsbAL* bedset.

Elongate DBs seem to nucleate without apparent underlying topography, but in gullies with deep exposure it is striking that the root of a bedform can be located several meters below the base of the surface expression. In that case, the structure alternates between several episodes of each facies, has truncations on stoss sides, but remains stable regarding its overall location.

Transverse

Transverse DBs have linear crests perpendicular to the (inferred) flow direction (Fig. 5a). Of all DBs, they show the broadest size variation and are characterized as relatively equivalent with respect to width versus length (Fig. 3, Table 1).

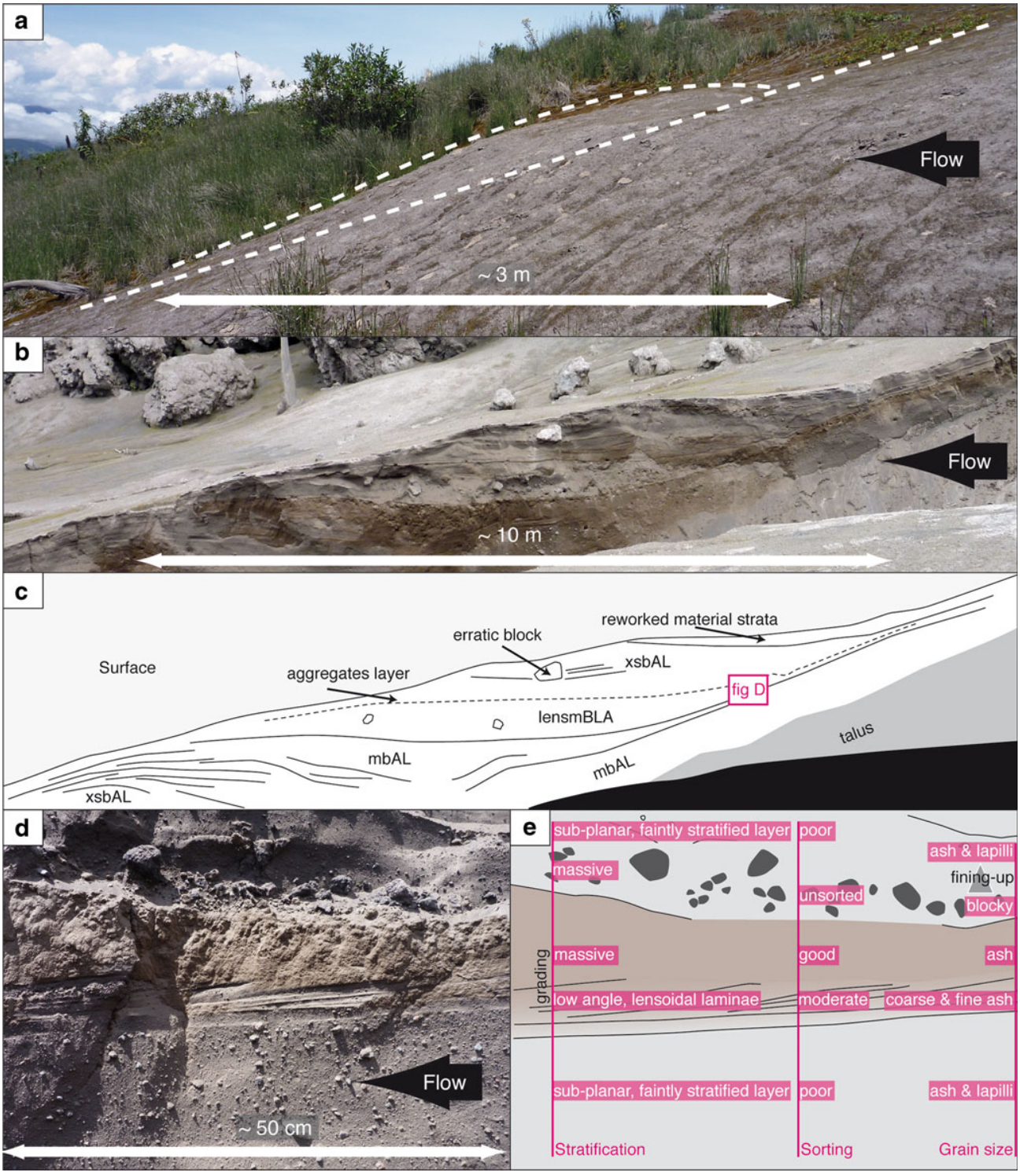

Fig. 4 Photographs of **a** the outer shape of an elongate dune bedform, **b** the internal structure of another elongate dune bedform, with **c** interpretation, and **d** zoom into the stratae with **e** interpretation. Note the (1) aggrading lensoidal layers with upstream migration of the crest, (2) intercalation of massive layers ash or blocky material and cross stratified laminae

They have sharp crests and steep, straight faces (combined with low RI), and the stoss being often steeper than the lee.

Internal cross-stratification is formed by several crudely stratified bedsets of subcentimetric laminae of ash and of

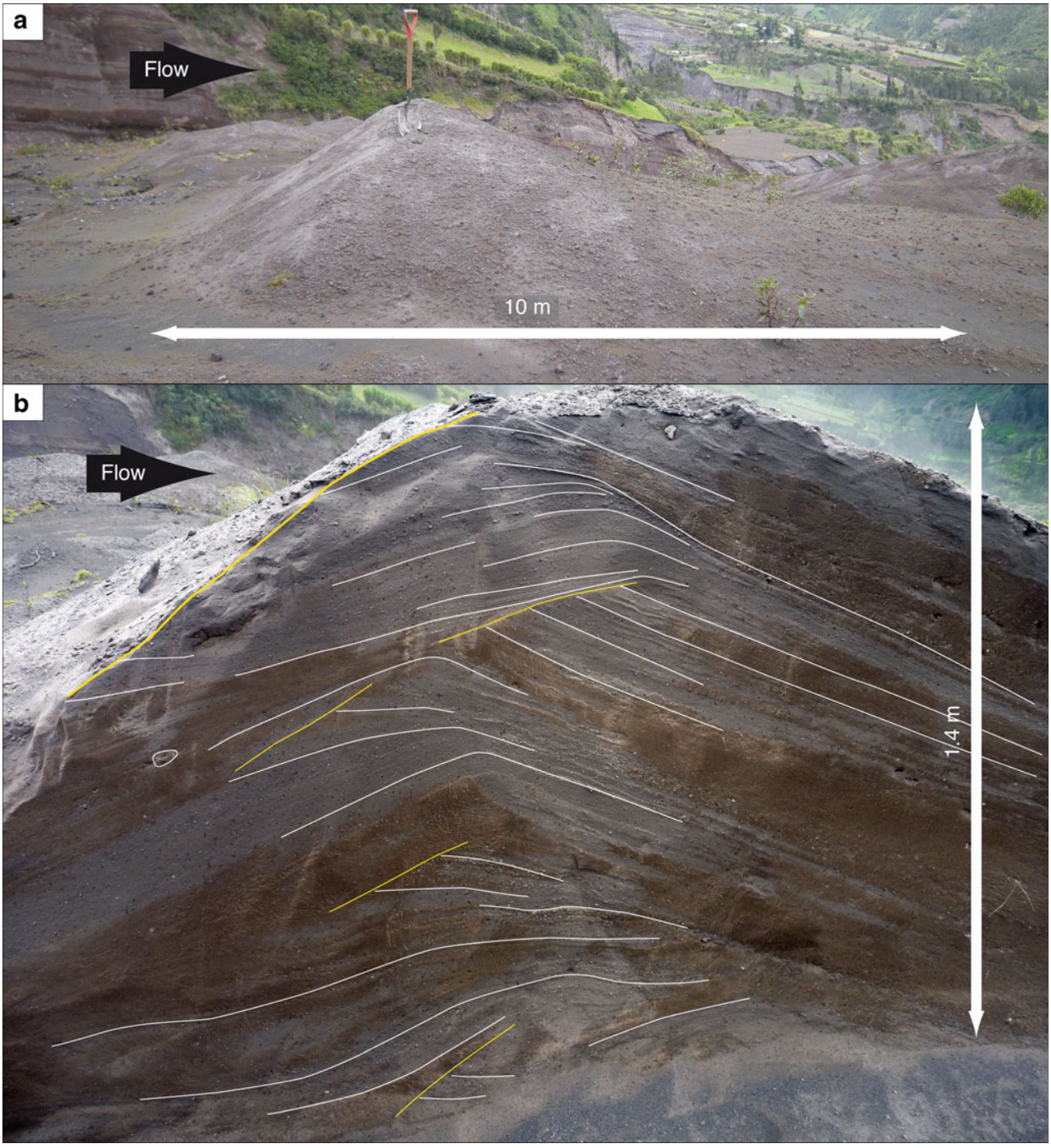

Fig. 5 Photographs of **a** the outer shape of a transverse dune bedform (shovel 1 m length) and **b** its internal structure. Note the (1) aggrading bedsets with upstream migration of the crest, (2) episodic truncations on the stoss side with angle steeper than the laminae, (3) absence of truncations on the lee side, and (4) the basal laminations at the base of the structure

coarse ash (similar to the *xsbAL-facies* from elongates). Within a bedset, stoss aggradation dominates and induces an upstream crest migration. The aggrading bedsets are episodically truncated on stoss sides, but never on lee sides. These erosional episodes tend to sharpen the structures as the discordance planes are steeper than the aggrading bedsets.

Lunate

Lunate DBs have a barchanoidal shape; that is, their crests are crescent-shaped and convex upstream (Fig. 6a). They have a thick body and thinning tails on the lateral ends (horns). We avoid the term "barchanoid" because barchan dunes form in

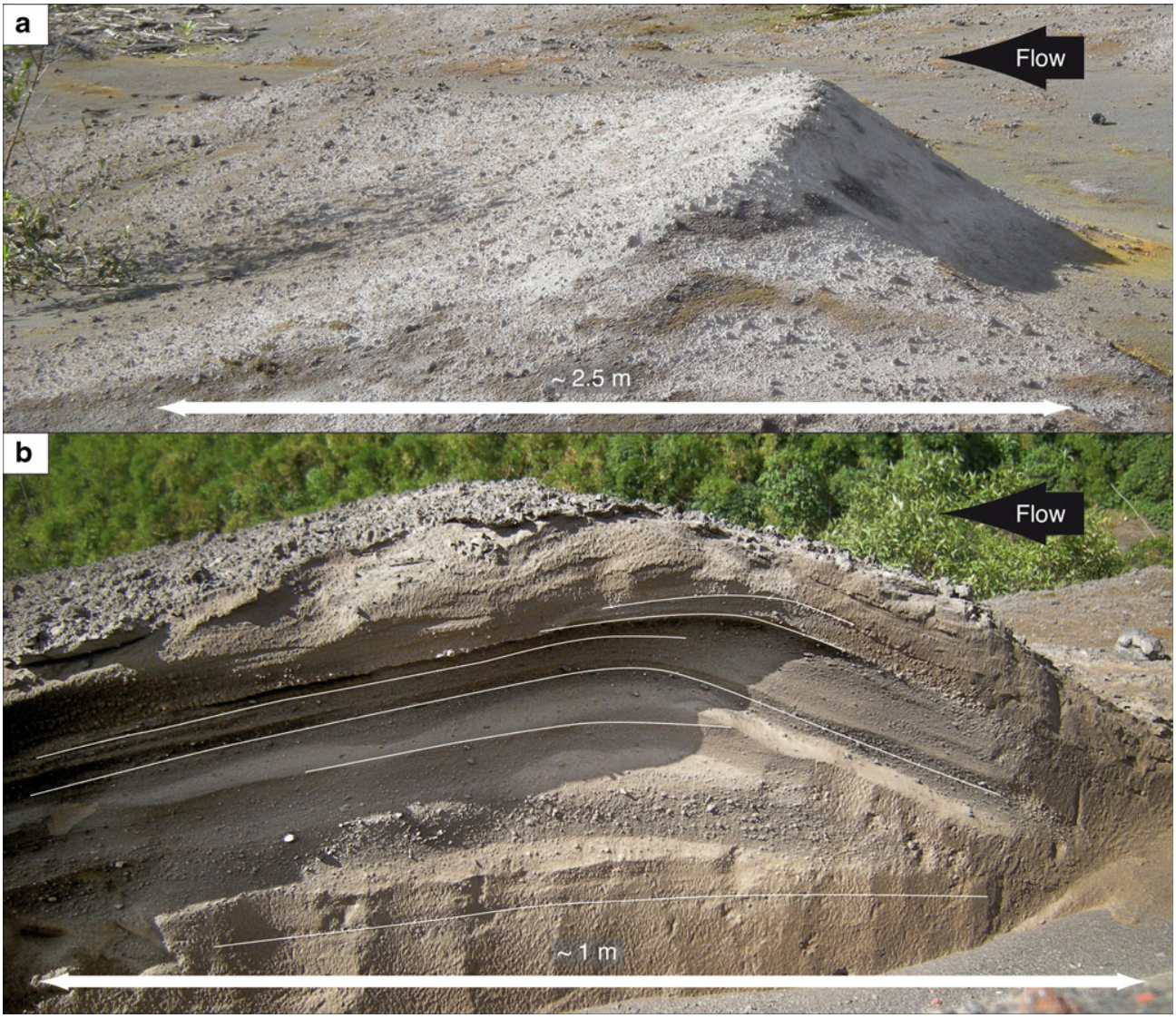

Fig. 6 Photograph of **a** the outer shape of a lunate dune bedform and **b** internal structure in another lunate dune bedform. Note: (1) aggrading structure, (2) upstream migration of the crest, and (3) variation in grain size between individual laminae

conditions of very low sediment supply. Lunate DBs have slightly smaller dimensions than elongate and transverse DBs. The face angles and average RI are comparable to those of transverse DBs (steep sided bedforms), but S-RSI and RSI are slightly greater than for transverse DBs (more asymmetrical; due to the long tails).

Internally, the observed cross-stratification is similar to the transverse type with stoss-aggrading bedsets, sharp crests and straight laminations on each side (Fig. 6b). The DBs seem to nucleate from flat streambeds and are thus not controlled by the underlying bed morphology.

Two-dimensional

The term "two-dimensional" (2D, Fig. 7) refers to 2D ripples that show similar characteristics: (1) linear crests perpendicular to the flow direction, (2) width greater than length, (3) organization in spatially recurring patterns in the flow direction (in train), and (4) almost symmetrical faces (Bridge and Demicco 2008, p. 231). Though both have linear crests, 2D DBs clearly distinguish from transverse on the length versus width graph (Fig. 3b). Face angles and average RI are in the middle range, but RI varies much more in this type (large 2D DBs are usually steep whereas smaller ones tend to be flat; Fig. 8a). 2D DBs have the smallest average thickness and S-RSI and RSI (most symmetrical), and the highest number of DBs with longer stoss face (positive S-RSI). They are organized in a spatially recurring pattern in the downstream direction (organization in train) and as such, can be given a wavelength (crest-to-crest distance; Fig. 7). The internal stratification patterns are not documented.

Fig. 7 Photograph of two dimensional dune bedforms. Note the significant width and short length as well as the repetition, in train in the downstream direction, of the same shape patterns

Other types of DBs

Other patterns have been observed but not investigated systematically (Fig. 7; group "other" in Electronic supplementary material (ESM) Table 2). Sporadic linguoid DBs are randomly distributed (crescentic crest but body pointing downstream, i.e., concave upstream; Fig. 8c). A single longitudinal DB (long crest parallel to flow direction; Cooke et al. 1993) has been found at the edge of the dense pyroclastic flow path behind a standing tree (1 m diameter; Fig. 8d). The apparent grain size of this DB is coarser and less sorted than the other types, including blocks of up to 10 cm. The DB is 19.5 m long (parallel to flow), 4.8 m wide (perpendicular to flow), and 1.3 m thick. It is located close to transverse and lunate DBs. Numerous composite structures resulting from the superposition of several DBs have been observed (Fig. 8e), with imbrications of both small and large DBs, superimposed on the lee face of one another. Other types of composite shapes have diverging and doubled crests, either resulting from the splitting of an initial DB or rather from the merging of two DBs with different orientation. "V shaped" DBs occur in zones dominated by lunate and 2D DBs. Steeply incised, very local truncations filled with massive ash are also observed (Fig. 8b). The virtual absence of ripple-sized cross-lamination is noteworthy.

Granulometry

Twenty-six samples were collected on the stoss and lee sides of 13 DBs from different deposition zones (see Douillet et al. 2013). Stoss samples are slightly better sorted and coarser grained (average σ, 1.42; Md, 2.87) than lee ones (average σ, 1.58; Md, 2.82; Fig. 9). This generally supports the inference that cross-stratification is related to tractional processes: stoss faces being slightly more exposed to traction, they have a tendency to be fines depleted (coarsening the median grain size and improving the sorting; Nakajima and Satoh 2001).

Spatial distribution

The four DB types are observed to outcrop with a spatial evolution, analyzed for the main deposition zones (Chontal (Fig. 10) and Achupashal (Fig. 11)). A general description and interpretation of the dilute PDC deposits can be found in Douillet et al. (2013).

Proximal zone

The proximal cross-stratified deposits outcrop as a wide sheet on the overbanks of smoothly incised valleys on the steep (up to 25°) upper slope of the volcano. There, dilute PDCs are interpreted to derive from the dense flows by air entrainment and the depositional area was affected by both dilute and dense flows. Although their shape can vary, DBs of this zone have all been grouped as "elongates", a choice justified by their clear deviation from the other types in quantitative measurements and the fact that their composite stratification patterns have not been observed in other deposition zones. They occur in isolation at large distances from each other and no downstream size decrease is apparent.

Distal zones

In distal zones, PDCs were confined mainly to deep channels of the drainage network. While dense pyroclastic flow

Table 1 Average quantitative characteristics of the dune bedforms by types

DB type/measure	Length (m)			Width (m)			Thickness (m)			Stoss (°)			Lee (°)			RI			S-RSI			RSI		
	Max	Min	Mean	Max	Min	Mean	Max	Min	Mean	Max	Min	Mean	Max	Min	Mean	Max	Min	Mean	Max	Min	Mean	Max	Min	Mean
Elongate	*17.5*	*3.2*	*7.4*	27	2.4	6.5	*1.8*	*0.2*	0.55	*35*	5	17.6	*35*	*15*	*24.1*	45	*6.8*	*17.9*	−1.5	−10.7	−5.2	10.7	*1.6*	*5.2*
Transverse	17.3	1.4	5.3	**19.2**	**1.4**	5.8	1.6	**0.1**	*0.61*	*35*	*10*	*25.2*	34	**0**	21.7	42.5	3.4	**9.4**	1.6	−14	−2.9	14	**1**	3.2
Lunate	12	**1.1**	5.2	24	**1.4**	**4.9**	1.5	**0.1**	0.51	*35*	5	24	**32**	5	22.4	**30**	**3.3**	11.2	*4.6*	**−15.7**	−3.7	*15.7*	1.1	3.9
2D	**9.5**	1.5	**4.3**	*38*	2	*9.3*	**1.1**	**0.1**	**0.46**	*35*	**0**	22.4	**32**	10	**21.5**	*52*	3.6	10.7	3	*−6.5*	*−1.9*	**6.5**	**1**	**2.7**
all	17.5	1.1	5.2	41	1.4	6.5	2	0.1	0.55	*35*	0	23.7	35	0	22	52	3.3	10.8	4.6	−15.67	−3.1	15.7	1	3.41

deposits are confined to thalwegs, cross-stratified, isolated, wedge-shaped ash bodies a few hundred meters across outcrop on the outer overbanks of valley curves. Deposition is related to dilute PDCs that overflowed the valleys, and possibly experienced a hydraulic jump of the entire current or at least strong deceleration during deposition. DBs with the largest dimensions are observed at the upstream onset of the ash bodies. A decrease in length, thickness, and width of the DBs (grayscale in Figs. 10 and 11) follows the currents' direction, reconstructed from their orientation, together with an evolution from transverse, to lunate, to 2D shapes.

(a) Chontal

The Chontal ash body is bordered by two curving valleys and was deposited by dilute PDCs overflowing from both of them (Fig. 10). A clear evolution of the DB type is visible: At the upstream limit (SW), only large transverse DBs outcrop, organized in train with the sharp onset of the ash body (the only transverse DBs observed in train). Close to the eastern valley, DBs are smaller and lunate shapes occur together with transverse ones. 2D DBs are exclusively found on the edge of the DB field, where spreading of the flows was possible. At the downstream end of the ash body, DBs diminish in size until no more DBs outcrop (November 2010).

(b) Cusua

The Cusua ash body is located on the outer overbank of a valley curve (Fig. 11b). The northern border is forced by a topographic barrier that blocked spreading. Shape evolution of the DBs is less pronounced than for Chontal, but still noticeable. Transverse DBs are distributed across the entire ash body but dominate at the upstream limit. Lunate DBs occur in the middle and lower part of the ash body but are absent near the upstream limit. 2D DBs are mainly located on the southern and western edges of the ash body, i.e., away from the source and from the topographic barrier, where flows were free to spread. Only one 2D DB was found in the northern part.

(c) Chacauco

At the base of the volcanic edifice, dilute PDCs "jumped" the Chambo River and reached the village of Chacauco on the opposite bank. There, topography sloped counter to the flow direction, forcing slowing, and spreading of the currents. Only 2D DBs (except 2 transverse) developed and formed concentric trains away from the source valley (Fig. 11a).

Interpretation

Flow conditions during deposition of PDCs affect the sedimentary record, providing the opportunity to infer the

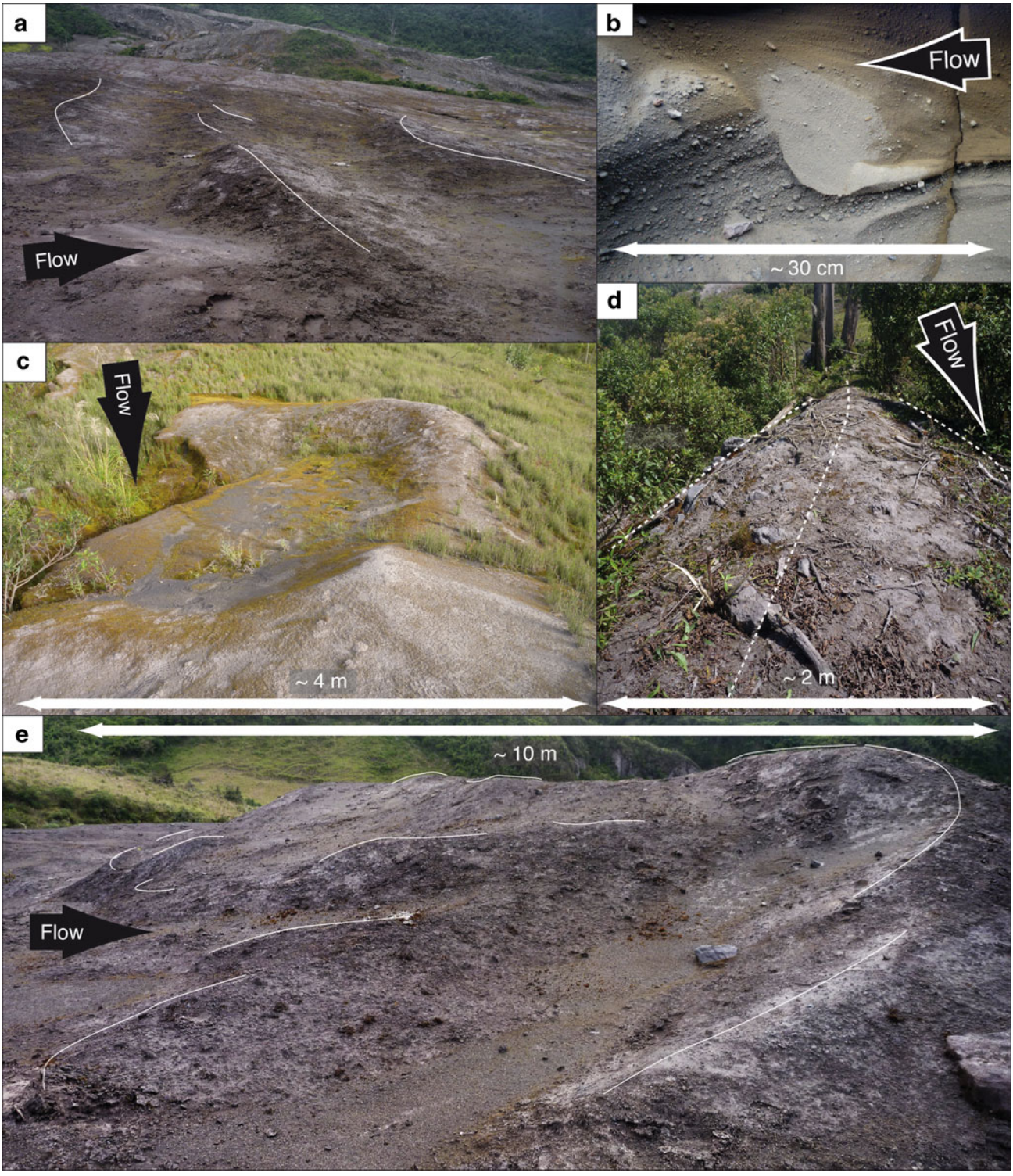

Fig. 8 **a** Small-scale 2D DB train, **b** cut-and-fill structure of faintly stratified ash and lapilli, **c** crescentic DB or alternatively the crater from the impact of a large block, **d** longitudinal DB behind a tree (the base of the tree is not visible), **e** composite DB cluster formed with several imbricated crests

dynamics of the parent currents. However, caution must be exercised when interpreting the sedimentary record, since different conditions may produce similar bedforms. The accent should always be put on a careful description independent of any interpretation. In the following section, we distinguish between dunes and antidunes and discuss the antidune interpretation for the DBs at Tungurahua. We then individually interpret each DB type and suggest a new

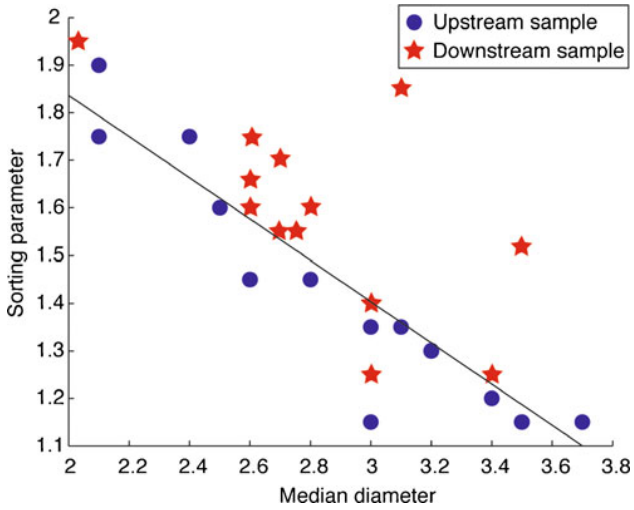

Fig. 9 Sorting parameter versus median diameter of material sampled on pairs of stoss and lee sides from 13 dune bedforms. Stoss samples are better sorted and coarser-grained, arbitrary line separates most stoss vs. lee points

interpretative term: "regressive climbing dune" for the stoss aggrading, steep sided, and regressive bedsets found in distal areas.

Fluid dynamics of antidunes, dunes, and climbing dunes

In the past decades, many DBs in the deposits of PDCs have been described and/or interpreted as antidunes or climbing dunes. Both terms however refer to strict fluid dynamics

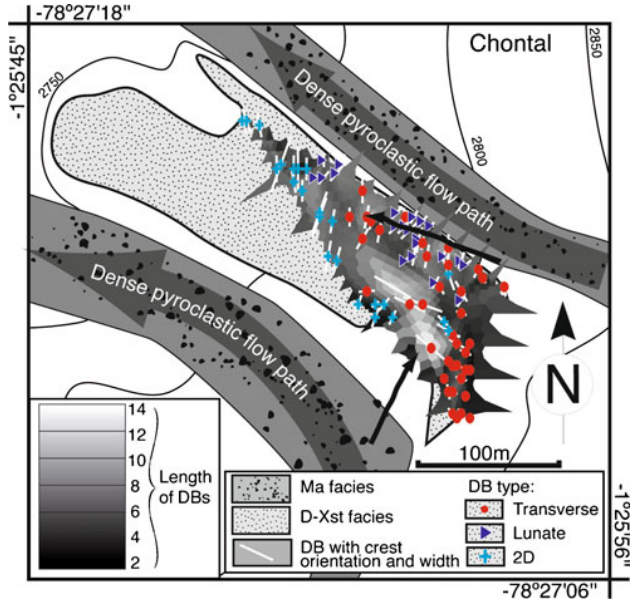

Fig. 10 Map of Chontal ash body. The thickness of dune bedforms is represented in *grayscale* and the orientation of the crests as well as the width of individual dune bedforms are given by white lines (see Douillet et al. 2013)

considerations, and are thus interpretative terms of the growth of a sedimentary structure. Dunes (including climbing dunes!) are exclusively the product of subcritical flows, whereas antidunes are related to trans- and supercritical flows and stationary gravity waves (Bridge and Demicco 2008, p. 181).

When sedimentation occurs at the base of a stationary gravity wave, an antidune can be produced with its shape and wavelength related to those of the gravity wave at the density interface (Hand 1969; Kubo and Nakajima 2002). The wavelength may be used to derive information on flow velocity and thickness as well as the density interface (Prave 1990). If the gravity wave is not perfectly stationary, the coupled antidune/gravity wave moves together and the antidune can migrate upstream or downstream, i.e., up- or downstream migration is not indicative of the flow regime (Kubo and Nakajima 2002; Spinewine et al. 2009).

Dunes *sensus stricto* consist of DBs produced under subcritical conditions (Froude number, <1; Bridge and Demicco 2008, p. 163). An open flow (i.e., with a free upper surface) in subcritical regime decreases in thickness and accelerates over an increase in streambed elevation (Branney and Kokelaar 2002, p. 19; Guyon et al. 2001, p. 289). As such, its capacity and competence will increase, possibly leading to erosion on the stoss face of a DB. Beyond the "crest", the decrease in streambed elevation leads to flow deceleration and thickness increase, possibly inducing deposition on the lee face.

Constructional cross-stratification (such as climbing cross-laminations) is produced when the angle of climb equals or exceeds the angle of the stoss side, indicating more aggradation than erosion (Bridge and Demicco 2008, p. 176). Whereas climbing ripples are common in the sedimentary record, climbing dunes are rarer. Examples are found in turbidites, glaciogenic subaqueous fans or glacial outburst flood deposits, and dilute PDC deposits (Ghienne et al. 2010 and references therein). All of these are related to particle-driven density currents. If the deposition rate supersedes erosion on the stoss side, the latter is not completely eroded during migration, stoss side laminae are preserved, aggrading structures are produced and the full geometry of the original structure is observed. The angle of climb depends on the ratio of deposition to bedload transport (Allen 1970): the more deposition (from suspended load), the steeper the angle of climb. In the extreme case, laminae would emplace as fallout and drape the bedform to produce symmetrical structure on the pre-existing bedform with no bedload (lateral) transport (Ashley et al. 1982). It is thus not possible to explain upstream crest migrating structures with this scheme because deposition must be more important on the lee than on the stoss face for a dune (subcritical regime).

In the case of a thick homogenous flow (e.g., for a water–air interface, when the flow depth is greater than twice the wavelength of the bedform; Bridge and Demicco 2008, p. 181), antidunes cannot form because there is no interface close

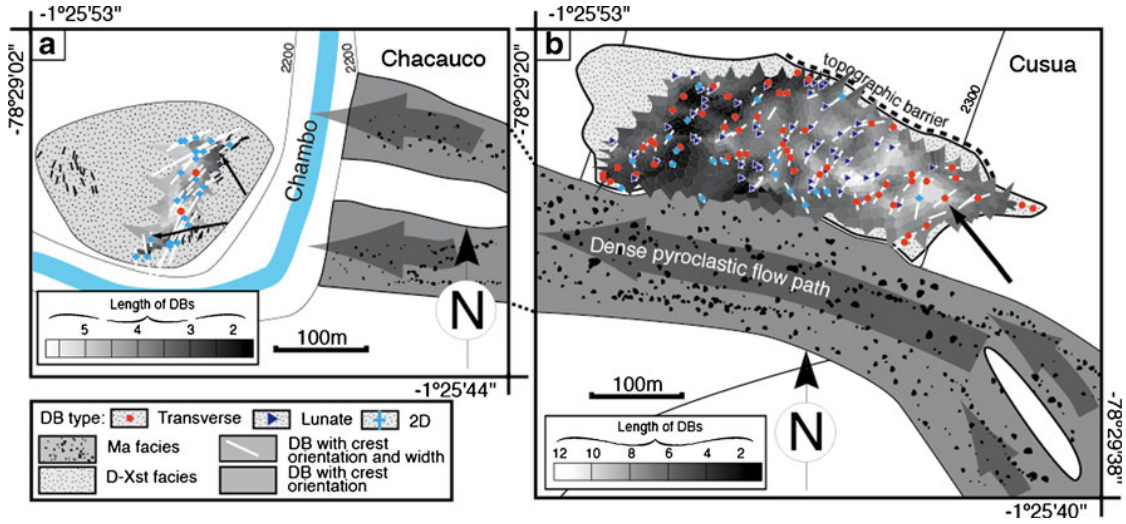

Fig. 11 Maps of ash bodies in Achupashal valley. **a** Lowermost zone of Chacauco ash body. **b** Cusua ash body. Dune bedform types follow the same coding as for Fig. 10

to the bed that can trap internal gravity waves and shape the bed. Yet, DBs can be active without a free boundary. Indeed, a positive streambed morphology will reduce the section of the flow and cause acceleration over the stoss face whereas deceleration is experienced on the lee with possible formation of a separation vortex for a short distance downstream. Thus, a downstream migrating DB can be produced. In such a case, the DB does not hold information on the flow thickness. Distinction between DBs related to a flow interface (Bridge and Demicco 2008, p. 169; Lorenz et al. 2010) and DBs related to self-production of a separation vortex on the lee (as is often the case for aeolian dunes) is an important issue in understanding flow stratification within dilute PDCs.

We believe that the development of stationary gravity waves of meter-scale wavelength is unlikely in dilute PDCs. Indeed, stationary waves require relative steadiness and static stability and dilute PDCs are thought to be highly turbulent, pulsatile and unsteady flows, at least near the base (Kieffer and Sturtevant 1988; Andrews and Manga 2012). The existence of a sharp internal flow interface within dilute PDCs is questionable and it seems more likely that they show a continuous density gradient, not prone to trap internal gravity waves. Moreover, stoss-aggrading bedforms, often seen as indicators of stationary gravity waves, are not necessarily related to antidunes, since deposition of particles is not simply driven by the dynamics of the fluid phase (Nakajima and Satoh 2001). Indeed, when a subcritical current flows over positive topography, deposition may be caused even if the flow itself accelerates, because the increase in flow velocity (and turbulent entrainment) might be not insufficient to carry the particles over the obstacle (Kubo and Nakajima 2002). Dilute PDCs may be especially prone to such a scenario, because particles are gas-supported, and the entrainment of particles by gas with low viscosity is not as strong as by water.

Using geometrical relationships of the DBs, we demonstrate the inadequacy of interpreting steep DBs as antidunes: we observed DBs with a length of 10 m, a stoss angle of 35° and a thickness of 1.6 m. The wavelength of a (stationary) gravity wave trapped at a density interface needs to be at least 12 times greater than the thickness of the underflow and this ratio increases with the density contrast (Hand et al. 1972; Prave 1990). Thus, a 10 m long DB, associated with a 10 m wavelength stationary gravity wave, would imply an underflow thinner than 0.8 m. It is rather unlikely that a 0.8 m thick flow would stay in supercritical conditions while climbing a 1.6 m high slope at 35° and produce a gravity wave with amplitude (equal to the thickness of the DB) twice that of the flow thickness. Thus, it seems unlikely that steep DBs are antidunes. Furthermore, truncations are observed only on laminae of the stoss side and never on the lee side. This shows that these truncations are not related to antidune formation. Indeed, if these structures were produced by a gravity wave moving slightly upstream (to account for the upstream migration of the crests), one should observe truncations on the lee sides, or the wavelength of the gravity wave should increase during building of the cross-stratification. Thus, neither the steep transverse, nor the lunate nor 2D DBs can be interpreted as antidunes.

Dune bedform types

Elongates

In elongate DBs, the *lensmBLA-facies* layers are interpreted to be related to dense flows, since dilute PDCs would be unlikely

to be able to transport the largest blocks. In contrast, the *xsbAL-facies* bedsets derive from fully dilute PDCs with tractional flow boundaries, and the *mbAL-facies* from dilute PDCs where the rate of supply exceeded the rate of deposition, favoring the development of a concentrated zone that inhibited stratification (Branney and Kokelaar 1997; Sulpizio et al. 2010), possibly with a traction carpet (Sohn 1997; Fig. 12a–d). The borders between the facies within a DB can be sharp or gradational, showing that the flow types could evolve into each other or occur individually. These interpretations are supported by the exclusive location of elongate patterns in proximal zones, where PDCs were barely confined by topography and a gradation between dense pyroclastic flows and dilute PDCs is to be expected, and by their absence in distal zones, where only dilute PDC occurred. The coarseness and flatness of the *lensmBLA-facies* lensoidal layers suggest a high capacity (ability to transport) and competence (erosiveness) of the flows, otherwise, the layers would build more steeply. The intercalated *xsbAL-facies* bedsets are steeper and similar to distal patterns, though they tend to grade from (or into) *mbAL-facies*.

The flat and upstream migrating patterns of *lensmBLA-facies* found in elongate DBs are strikingly similar to: (1) structures produced in experimental subaqueous density currents

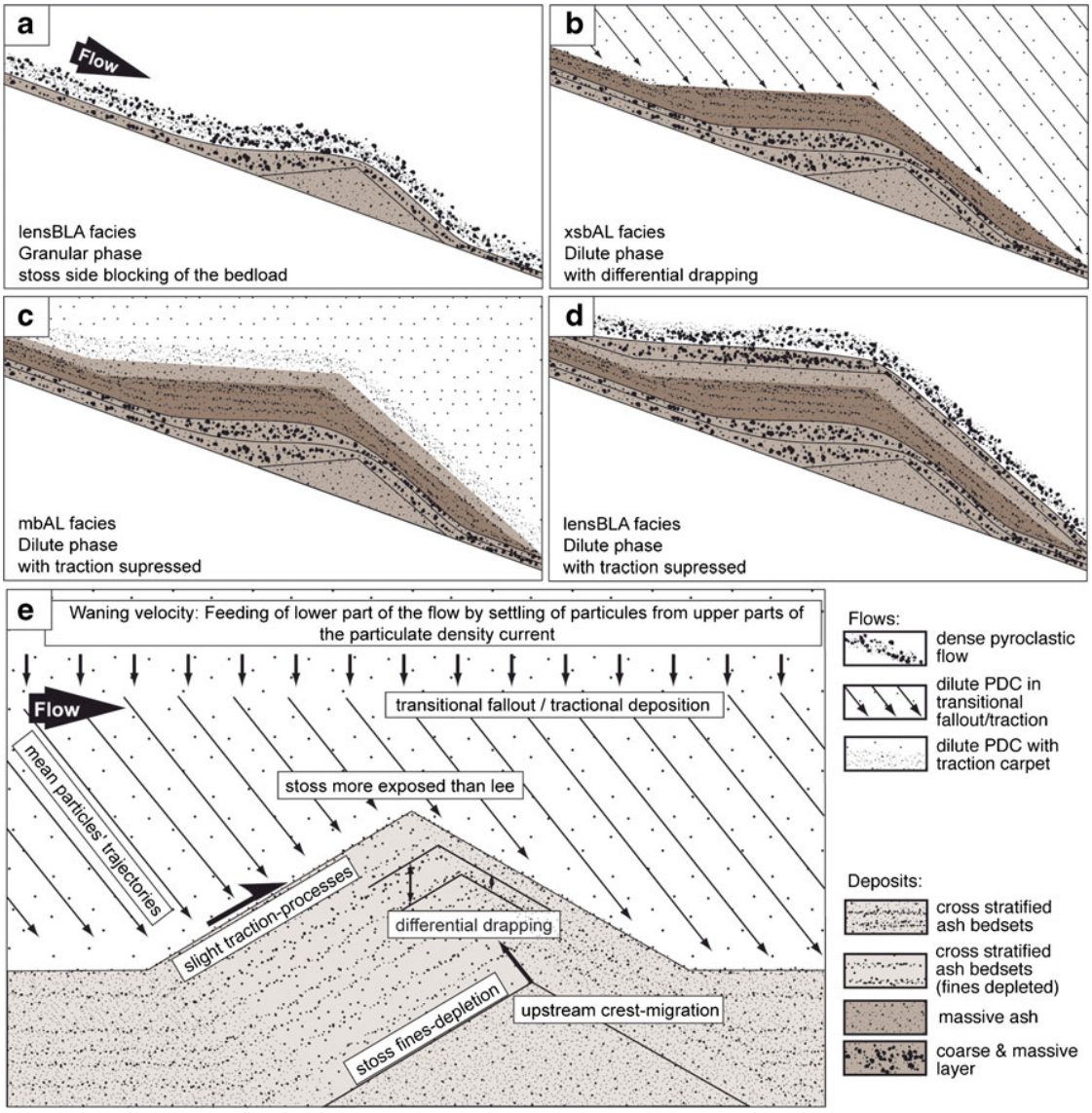

Fig. 12 Interpretative sketch of **a**, **b**, **c**, and **d**, the formation of elongate DBs by successive flows, and **e**: regressive climbing dune. Currents are represented with grains only, deposits with grains, and background colors. **a** Granular phases deposit *lensmBLA* layers; **b** dilute phase deposits *xsbAL* bedset; **c** dilute phase with traction suppressed by high basal concentration deposits *mbAL* bedset; **d** granular phase deposits *lensmBLA* layer. **e** Regressive climbing dunes are formed by the differential exposition between stoss and lee faces, in turns driven by the mean particle trajectories that have a fall and a lateral component, together with little traction after initial landing

interpreted as cyclic steps (Fig. 6a of Spinewine et al. 2009), (2) types I and II DBs from Schmincke et al. (1973), interpreted as "chute-and-pool" structures, and (3) antidunes produced in water tanks (Hand 1974; Fig. 5 in Cheel (1990)). Moreover, they only occur in steep proximal zones. These factors may contribute to their diagnosis as antidunes or "chute-and-pool" structures. However, contrary to the Schmincke et al. (1973) "chute-and-pool" structures, the elongate DBs do not aggrade against the stoss face of a truncation surface, but nucleate without any apparent initial streambed topography. Yet "chute-and-pool" structures (an end-member of cyclic steps) have a length related to their grain size (Alexander 2008), and as such, different layers should have similar granulometry, or show truncations, which is not observed at Tungurahua.

Concerning interpretation as antidunes, only the *lensmBLA-facies* layers have the lensoidal, stoss-aggrading shape that would favor this interpretation. However, these are related to dense pyroclastic flows. The draping layer of accreted-ash lapillis found intercalated between coarser layers is interpreted as a fallout deposit, showing that such DBs continued their growth over different pulses or flows, as suggested by Walker (1984), Cole (1991), and Sulpizio et al. (2007). It seems unlikely that two stationary gravity waves of the same wavelength would emplace at the same place (they are free boundary related) for two different flows and contribute to the growth of a single antidune (unless interaction of the second flow with the DB produced a "forced" stationary wave). Rather than assign these as antidunes, we suggest that the bedslope decrease induced on the stoss side of the bedform would lead to blocking of parts of the bedload causing stoss-aggradation without the flow necessarily being in a trans- or supercritical condition, as suggested for turbidites (basal lenses of Ponce and Carmona 2011). The *xsbAL-facies* bedsets have similar characteristics to the distal DBs, and the same argument holds (see below).

Transverse

Transverse DBs are formed by finely laminated bedsets of ash, indicating emplacement by turbulent and fully dilute currents with a tractional basal flow boundary. Since the number of bedsets found within a single DB exceeds the likely number of PDCs having flowed in the zone, each bedset (and not each laminae, as suggested by Cole (1991) or Sulpizio et al. (2007)) most probably relates to individual pulses within a single PDC rather than to individual PDCs. Within each pulse, turbulence eddies produce the lamination (Bridge and Demicco 2008, Chap. 3).

Bedset truncation steepens the structures. These truncations cannot result from simple collisions of saltons during saltation, which should produce a flat erosive plane, as in the aeolian context. Rather, we suggest that these truncations are linked with high-energy bursts linked to single eddies.

The transverse DBs (with steep stoss- and lee-sides angles close to the repose angle) suggest low capacity and/or slow flows, otherwise, such steep unconsolidated structures would be eroded. Moreover, the structures are mainly aggrading, with construction on both sides. The currents must thus have had an entirely depositional dynamic with much higher particle concentrations than the saturated transport capacity.

Lunate

The similarity in internal structure of lunate and transverse DBs as well as their spatial proximity leads to the same interpretation of the flows producing them: turbulent, fully dilute, low capacity flows with a tractional basal flow boundary, entirely depositional dynamics with higher particle concentration than the saturated transport capacity, and each bedset corresponding to a pulse.

The shape is however strikingly different and can result from a process influenced by the thickness of the obstacle: possibly, the thicker the obstacle, the more it blocks the current and promotes stoss aggradation. As the thin parts block fewer particles, they are less subject to stoss side aggradation, and the crests of the tails migrate upstream at slower rates. This does not explain why some DBs become lunate and others transverse. Moreover, lunate shapes are located at Chontal where currents emanated from two valleys with different directions, and in lower zones of Cusua, but are absent in the uppermost zones where currents were more likely unidirectional. Thus they possibly result from currents with different directions. Information on their 3D internal structure is required to ensure that the tails are not the remains of late-stage erosion of a larger DB, or contain evidence of two current directions.

2D

2D DBs may form when lateral transport is more important than downstream transport. Numerical simulations from a random bed configuration with the constraint that lateral transport exceeds downstream transport result in formation of 2D DBs (Rubin 2010). This is particularly interesting at Tungurahua as 2D DBs are found on the unconfined edges of ash bodies, where flows are likely to spread, thus having a strong lateral component. Similarly, the Chacauco ash body dips against flow direction and forces lateral spreading of the flows.

Even if they have periodic morphologies and are the most symmetrical, the emplacement of 2D DBs on the lower and outer edges of deposition zones (and downstream from transverse and lunate DBs) is not in agreement with interpretation as antidunes.

Composite DBs

The "V" shaped DBs sporadically observed may result from the convergence of two small 2D DBs with different orientations during a single event, or successive currents with different flow directions. They could also represent extreme cases of lunate DBs; systematic cross sections are needed to constrain their genesis.

Contrary to previous suggestions for other similar features (Nemoto and Yoshida 2009), the composite DBs at Tungurahua are not interpreted here as antidunes, since it is unlikely that several stationary gravity waves would occur at the same place to produce accreting structures. In the aeolian context, composite ripples are interpreted as a transitory state in the organization of fully developed trains (Anderson 1990). Accordingly, composite DBs at Tungurahua are interpreted as DBs that did not reach equilibrium by the end of the events.

The longitudinal dune observed behind a tree at the edge of the pathway of dense pyroclastic flows is formed by massive, unsorted, and coarse deposits. It is interpreted as deposited from a dense flow in the pressure shadow of the tree rather than by tractional currents.

Regressive climbing dunes

Here, we introduce and justify a new interpretative term "regressive climbing dunes". The aggrading nature of both transverse and lunate DBs cannot be interpreted as climbing dunes, since climbing dunes never show upstream crest migration (see "Interpretations" section). Similar structures have been observed in turbidites (Mulder et al. 2009; Ponce and Carmona 2011) even if a controversy exists regarding their interpretation (Higgs 2011). One interesting interpretation invokes differential draping from suspended load to account for upstream migrating structures (Nakajima and Satoh 2001; Kubo and Nakajima 2002; Ponce and Carmona 2011). The similarity between PDCs and turbidity currents is that they are both particulate density currents and as such, the agent of excess density (the particles) is not a conserved quantity (particles can deposit or be entrained). Since a density current is accelerated by its greater density than the ambient medium, it should decelerate when deposition begins, in turn further increasing deposition and so on (e.g., the dilute PDC pulses depositing laminae "en masse" of Sulpizio et al. (2007)). Ponce and Carmona (2011) use the term differential draping for stoss-aggrading bedforms deposited from turbidity currents. We suggest that this "differential draping" also occurs for DBs in dilute PDCs. The increased sedimentation on the stoss face would result from the suspended charge that deposit. Since deposition decreases flow energy for a particulate density current, freshly landed particles cannot be further transported as bedload. The trajectory of particles depositing from suspended load being the combination of a vertical fall component and a lateral transport component, the stoss side of the bedform is more exposed than the lee side (Fig. 12e). In the case of direct deposition from suspension without a splashing effect and no further transport (e.g., saltation), the stoss face would experience more aggradation than the lee. This implies rapidly decelerating and slow currents to reduce bedload transport and lead to major direct sedimentation of the suspended load (as suggested by Ponce and Carmona (2011)). Such a process may be triggered if basal parts of the flow benefit from high rates of supply by settling of particles from the upper parts of the flow, favoring saturated transport at the boundary (but still below granular boundary conditions).

Fine-grained and finely laminated, aggrading and upstream crest migrating structures are thus transitional between direct fallout and tractional flow boundary processes, with the traction base not inhibited by high supply rates. This is in accordance with the interpretation that hydraulic jumps of the entire PDCs led to emplacement of the cross-stratified ash wedges (see Douillet et al. 2013, also suggested in glacial outburst deposits by Ghienne et al. (2010)). We introduce the term "regressive climbing dunes" for aggrading structures that exhibit upstream migration of the crests due to high supply and deposition from suspension (differential drapping) but little bedload reworking, in subcritical conditions (i.e., unrelated to antidunes). "Regressive climbing dunes" are in agreement with different conceptual models of waning flows (Cole 1991; Walker 1984; Sulpizio et al. 2007; Vasquez and Ort 2006; Ponce and Carmona 2011). This term includes a genetic interpretation and is interpretative, not descriptive. It also applies for other types of particulate density currents such as turbidity currents or hyperpycnal flows.

Conclusion

The genesis of DBs deposited from dilute PDCs deserves further investigation. In particular, a better understanding of their link to a flow interface (at an upper flow boundary, like for fluvial dunes) or basal flow boundary (like for aeolian ripples) is required. It is therefore fundamental to differentiate between descriptive patterns (e.g., foreset/backset lamination, aggrading structure, evolution of laminae thickness, truncations, steepness to bed, or horizontal) and interpretations (e.g., dunes, antidunes, climbing dunes, and "chute-and-pool" structures). Interpretation as antidunes is not straightforward for DBs in PDC deposits.

Cross-stratified dune bedforms produced by pyroclastic density currents during the August 2006 eruption at Tungurahua volcano have been described. Four types of dune bedforms have been qualitatively defined—elongate, transverse, lunate, and two-dimensional—and quantitatively distinguished based on more than 300 measurements of shape characteristics.

The development of each type of dune bedforms varies spatially and records different conditions. In proximal zones, elongate dune bedforms correspond to a separate sedimentary environment in the proximal areas, dominated by the interaction between granular based and tractional flow boundaries. There, flows were topographically unconfined and the deposits are the record of the mixed and successive influence of dense pyroclastic flows (*lensmBLA-facies*) and dilute PDCs (*xsbAL- and mbAL-facies*), indicating currents with a strong capacity and competence. The stoss-aggrading, lensoidal layers of *lensmBLA-facies* of these dune bedforms are not interpreted as "chute-and-pool" or antidune structures. They likely result from stoss-side blocking of material transported as bedload. Elongate patterns are absent in the distal record, where dense pyroclastic flows were confined to valley thalwegs and only dilute PDCs acted on sedimentation.

Transverse and lunate DBs are found in the ash bodies of the distal environment, where only dilute PDCs overflowed and deposited. These zones are dominated by direct fallout and tractional flow boundary processes, with dilute PDCs having a significant deposition rate and with particle concentrations above the saturated transport conditions. These zones probably record hydraulic jumps responsible for a sudden deceleration of the flows (Douillet et al. 2013). Transverse dune bedforms grew at the onset of the deposition zones as a result of highly depositional currents with low competence. Lunate dune bedforms are related to currents whose sedimentation rates are related to the thickness of the dune bedform: the thicker the obstacle, the more stoss-face aggradation it experiences. Alternatively, they might form in the presence of two current directions. Two dimensional dune bedforms outcrop on the edges of deposition zones and where the deposition areas dipped against flow direction. In both cases, significant lateral spreading of the PDCs occurred.

We do not interpret the transverse, lunate and two-dimensional dune bedforms as antidunes. Rather, these three types of dune bedforms are the expression of highly depositional dynamics and seem to be an extreme case of climbing dune. A low bedload transport component and major direct sedimentation from suspended load during waning phases of the currents led to upstream migration of the crests under subcritical flow conditions. We suggest the term "regressive climbing dunes" for bedforms produced by such a process, which might occur in all types of particulate density currents.

Acknowledgments Drs. Manville, Sulpizio, and Cioni are acknowledged for valuable reviews; Prof. Andreotti for discussion; our colleagues from Instituto Geofísico, Quito, for discussion, information, and help during field work; Yan Lavallée for editing the manuscript; and Jean-Rémi Dujardin for editing the photographs. We are indebted to the following (partial) funding sources: Alsatian grant BOUSSOLE (GAD); the grant THESIS from the Elite Network of Bavaria (GAD); the Deutsche Forschungsgemeinschaft grant KU2689/2-1 (GAD, UK), the Deutsche Forschungsgemeinschaft grant LA 2651/1-1 (UK, YL); a Research Professorship (LMUexcellent) of the Bundesexzellenzinitiative (DBD); an advanced grant from the European Research Council–EVOKES (DBD). GAD and DAP thank the bomberos from Baños and Patate for rescue during fieldwork.

References

Alexander J (2008) Bedforms in Froude-supercritical flow. Marine and River Dune Dynamics, Leeds, pp 1–5, 1–3 April 2008

Alexander J, Bridge JS, Cheel RJ, Leclair S (2001) Bedforms and associated sedimentary structures formed under supercritical water flows over aggrading sand beds. Sedimentology 48:133–152

Allen JRL (1970) A quantitative model of climbing ripples and their cross laminated deposits. Sedimentology 14:5–26

Allen JRL (1982) Sedimentary structures. Their character and physical basis. Elsevier, Amsterdam, p 663

Anderson RS (1990) Eolian ripples as examples of self-organization in geomorphological systems. Earth Sci Rev 29:77–96

Andrews B, Manga M (2012) Experimental study of turbulence, sedimentation, and coignimbrite mass partitioning in dilute pyroclastic density currents. J Volcanol Geotherm Res 225–226:30–44

Arnott RWC, Hand BM (1989) Bedforms, primary structures and grain fabric in the presence of suspended sediment rain. J Sed Res 59:1062–1069

Ashley GM, Southard JB, Boothroyd JC (1982) Deposition of climbing-ripple beds: a flume simulation. Sedimentology 29:67–79

Brand BD, Clarke AB (2009) The architecture, eruptive history, and evolution of the Table Rock Complex, Oregon: from a Surtseyan to an energetic maar eruption. J Volcanol Geotherm Res 180:203–224

Brand BD, Clarke AB (2012) An unusually energetic basaltic phreatomagmatic eruption: using deposit characteristics to constrain dilute pyroclastic density current dynamics. J Volcanol Geotherm Res 243–244:81–90

Brand BD, White CM (2007) Origin and stratigraphy of phreatomagmatic deposits at the Pleistocene Sinker Butte Volcano, Western Snake River Plain, Idaho. J Volcanol Geotherm Res 160:319–339

Brand BD, Clarke AB, Semken S (2009) Eruptive conditions and depositional processes of Narbona Pass Maar volcano, Navajo volcanic field, Navajo Nation, New Mexico (USA). Bull Volcanol 71:49–77

Branney MJ, Kokelaar P (1997) Giant bed from a sustained catastrophic density current flowing over topography: Acatlán ignimbrite, Mexico. Geology 25(2):115–118

Branney MJ, Kokelaar P (2002) Pyroclastic density currents and the sedimentation of ignimbrites. Geological Society Memoir no. 27. viii+143 pages

Bridge JS, Demicco RV (2008) Earth surface processes, landforms and sediment deposits. Cambridge: Cambridge University Press. 815p. ISBN-10:0-521-85780-5

Brown RJ, Branney MJ (2004) Bypassing and diachronous deposition from density currents: evidence from a giant regressive bed form in the Poris ignimbrite, Tenerife, Canary Islands. Geology 32:445–448

Burgisser A, Bergantz GV (2002) Reconciling pyroclastic flow and surge: the multiphase physics of pyroclastic density currents. Earth Planet Sci Lett 202:405–418

Cagnoli B, Ulrich TJ (2001) Ground penetrating radar images of unexposed climbing dune-forms in the Ubehebe hydrovolcanic field (Death Valley, California). J Volcanol Geotherm Res 109: 279–298

Carey SN (1991) Transport and deposition of tephra by pyroclastic flows and surges. In: Fisher, RV, Smith GA (eds). Sedimentation in volcanic settings. SEPM Special Publication No 45:39–57

Charland A, Lajoie J (1989) Characteristics of pyroclastic deposits at the margin of Fond Canonville, Martinique, and implications for the transport of the 1902 nuées ardentes of Mt. Pelée. J Volcanol Geotherm Res 38:97–112

Cheel RJ (1990) Horizontal lamination and the sequence of bed phases and stratification under upperflow-regime conditions. Sedimentology 37:517–529

Cole PD (1991) Migration direction of sand wave structures in pyroclastic-surge deposits: implications for depositional processes. Geology 19:1108–1111

Collela A, Hiscott RN (1997) Pyroclastic surges of the Pleistocene Monte Guardia sequence (Lipari Island, Italy): depositional processes. Sedimentology 44:47–66

Cooke R, Warren A, Goudie A (1993) Desert geomorphology. UCL Press, London, p 526

Crowe BM, Fisher RV (1973) Sedimentary structures in base-surge deposits with special reference to cross-bedding, Ubehebe Craters, Death Valley, California. Geol Soc Am Bull 84:663–682

Dellino P, Isaia R, Veneruso M (2004) Turbulent boundary layer shear flows as an approximation of base surge at Campi Flegrei (Southern Italy). J Volcanol Geotherm Res 133:211–228

Doronzo DM (2012) Two new end members of pyroclastic density currents: forced convection-dominated and inertia-dominated. J Volcanol Geotherm Res 219–220:87–91

Douillet GA, Tsang-Hin-Sun E, Kueppers U, Letort J, Pacheco DA, Goldstein F, Von Aulock F, Lavallée Y, Hanson JB, Bustillos J, Robin C, Ramón P, Hall M, Dingwel DB (2013) Sedimentology and geomorphology of the deposits from the August 2006 pyroclastic density currents at Tungurahua volcano, Ecuador. Bull Volcanol 75:765. doi 10.1007/s00445-013-0765-7

Druitt TH (1992) Emplacement of the 18 May 1980 lateral blast deposit ENE of Mount St. Helens, Washington. Bull Volcanol 54:554–572

Druitt TH (1996) Pyroclastic density currents. In: Gilbert JS, Sparks RSJ (eds) The physics of explosive volcanic eruptions, vol 145. Geological Society, London, pp 145–182

Duller RA, Mountney NP, Russell AJ (2007) Architectural analysis of a volcaniclastic Jo¨ Kulhlaup deposit, Southern Iceland: sedimentary evidence for supercritical flow. Sedimentology 55:939–964

Eychenne J, Lepennec JL, Troncoso L, Gouhier M, Nedelec JM (2012) Causes and consequences of bimodal grain-size distribution of tephra fall deposited during the August 2006 Tungurahua eruption (Ecuador). Bull Volcanol 74(1):187–205

Fisher RV (1977) Erosion by volcanic base-surge density currents: U-shaped channels. Geological Society of America Bulletin 88(9):1287–1297

Fisher RV (1990) Transport and deposition of a pyroclastic surge across an area of high relief: the 18 May 1980 eruption of Mount St. Helens, Washington. Geol Soc Am Bull 102:1038–1054

Fisher RV, Waters AC (1969) Bed forms in base surge deposits: lunar implications. Science 165:1349–1352

Fisher RV, Waters AC (1970) Base surge bed forms in Maar volcanoes. Am J Sci 268:157–180

Fisher RV, Schmincke HU, Van Bogaard P (1983) Origin and emplacement of a pyroclastic flow and surge unit at Laacher See, Germany. J Volcanol Geotherm Res 17:375–392

Gençalioğlu-Kuşcu G, Atilla C, Cas RAF, Kuşcu İ (2007) Base surge deposits, eruption history, and depositional processes of a wet phreatomagmatic volcano in Central Anatolia (Cora Maar). J Volcanol Geotherm Res 159:198–209

Ghienne JF, Girard F, Moreau J, Rubino JL (2010) Late Ordovician climbing-dune cross-stratification: a signature of outburst floods in proglacial outwash environments? Sedimentology 57(5):1175–1198

Gianneti B, Luongo G (1994) Trachyandesite scoria-flow and associated trachyte pyroclastic flow and surge at Roccamonfina Volcano (Roman Region, Italy). J Volcanol Geotherm Res 59:313–334

Girard F, Ghienne JF, Rubino JL (2012) Occurrence of hyperpycnal flows and hybride vent beds related to glacial outburst events in a Late Ordovician proglacial delta (Murzuq basin, SW Libya). J Sed Res 82:688–708

Guyon E, Hulin JP, Petit L (2001) Hydrodynamique physique. Edition CNRS. ISBN-10:2-86883-502-3

Hall ML, Robin C, Beate B, Mothes P, Monzier M (1999) Tungurahua Volcano, Ecuador: structure, eruptive history and hazards. J Volcanol Geotherm Res 91(1):1–21

Hall ML, Samaniego P, Le Pennec JL, Johnson JB (2008) Ecuadorian Andes volcanism: a review of Late Pliocene to present activity. J Volcanol Geotherm Res 176(1):1–6

Hand BM (1969) Antidunes as trochoidal waves. J Sediment Petrol 39: 1302–1309

Hand BM (1974) Supercritical flow in density currents. J Sed Petr 44(3): 637–648

Hand BM, Middleton GV, Skipper K (1972) "Antidune cross-stratification in a turbidite sequence, Cloridome Formation, Gaspé, Quebec. By Skipper (1971) Sedimentology" discussion. Sedimentology 18(1–2):135–138

Higgs R (2011) 'Hummocky cross-stratification-like structures in deep-sea turbidites: Upper Cretaceous basque basins (Western Pyrénées, France). By Mulder et al. (2009), Sedimentology' Discussion. Sedimentology 58:566–570

Hoblitt RP, Dan Miller C, Vallance JM (1981) Origin and stratigraphy of the deposits produced by the May 18 directed blast. In: Lipman PW, Mullineaux DR (eds) The 1980 eruptions of Mount St. Helens, Washington, USGS Prof. Papers 1250

Kelfoun K, Samaniego P, Palacios P, Barba D (2009) Testing the suitability of frictional behaviour for pyroclastic flow simulation by comparison with a well-constrained eruption at Tungurahua volcano (Ecuador). Bull Volcanol 71(9):1057–1075

Kieffer SW, Sturtevant B (1988) Erosional furrows formed during the lateral blast at Mount St. Helens, May 18, 1980. J Geophys Res 93(B12):14793–14816

Kubo Y, Nakajima T (2002) Laboratory experiments and numerical simulation of sediment-wave formation by turbidity currents. Mar Geol 192:105–121

Lang J, Winsemann J (2013) Lateral and vertical facies relationships of bedforms deposited by aggrading supercritical flows: from cyclic steps to humpback dunes. Sediment Geol 296:36–54

Le Pennec JL, Jaya D, Samaniego P, Ramón P, Yánez SM, Egred J, van der Plicht J (2008) The AD 1300–1700 eruptive periods at Tungurahua volcano, Ecuador, revealed by historical narratives, stratigraphy and radiocarbon dating. J Volcanol Geotherm Res 176:70–81

Lorenz RD, Claudin P, Andreotti B, Radebaugh J, Tokano T (2010) A 3km atmospheric boundary layer on Titan indicated by dune spacing and Huygens data. Icarus 205:719

Mattson PH, Alvarez W (1973) Base surge deposits in Pleistocene volcanic ash near Rome. Bull Volcanol 37(4):553–572

Moore JG (1967) Base surge in recent volcanic eruptions. Bull Volcanol 30(1):337–363

Moore JG, Nakamura K, Alcaraz A (1966) The 1965 eruption of Taal Volcano. Science 151:955–960

Mulder T, Razin P, Faugeres JC (2009) Hummocky cross-stratification-like structures in deep-sea turbidites: Upper Cretaceous basque basins (Western Pyrénées, France). Sedimentology 56:997–1015

Nakajima T, Satoh M (2001) The formation of large mudwaves by turbidity currents on the levees of the Toyama deep-sea channel, Japan Sea. Sedimentology 49:435–463

Nemoto Y, Yoshida S (2009) Nested architecture of pyroclastic bedforms generated by a single flow event, Outcrop examples from the Izu

volcanic islands. American Geophysical Union, Japan, Fall Meeting 2009, abstract #V23C-2078

Ponce JJ, Carmona N (2011) Coarse-grained sediment waves in hyperpycnal clinoform systems, Miocene of the Austral foreland basin, Argentina. Geology 39:763–766

Prave AR (1990) Clarification on some misconceptions about antidune geometry and flow character. Sedimentology 37: 1049–1052

Richards AF (1959) Geology of the Islas Revillagigedo, Mexico. 1. Birth and development of Volcano Bárcena, Isla San Benedicto. Bull Volcanol 22(1):73–123

Rowley PD, MacLeod NS, Kuntz MA, Kaplan AM (1985) Proximal bedded deposits related to pyroclastic flows of May 18, 1980, Mount St. Helens, Washington. Geol Soc Am Bull 96(11):1373–1388

Rubin DM (2010) A unifying model of planform straightness of ripples and dunes in air and water American Geophysical Union, Fall Meeting 2010, abstract #EP43F-07

Samaniego P, Le Pennec JL, Robin C, Hidalgo S (2011) Petrological analysis of the pre-eruptive magmatic process prior to the 2006 explosive eruptions at Tungurahua volcano (Ecuador). J Volcanol Geotherm Res 199(1–2):69–84

Schmincke HU, Fisher RV, Waters AC (1973) Antidune and chute-and-pool structures in the base surge deposits of the Laacher See area, Germany. Sedimentology 20:553–574

Sigurdsson H, Carey SN, Fisher RV (1987) The 1982 eruption of E1 Chichon volcano, Mexico (3): physical properties of pyroclastic surges. Bull Volcanol 49:467–488

Simons DB, Richardson EV, Haushild, WL (1963) Some effects of fine sediment on flow phenomena. U.S. Geol Surv Water Supply Pap 1498G-47

Sohn YK (1997) On traction carpet sedimentation. J Sed Res 67(3):502–509

Sohn YK, Chough SK (1989) Depositional processes of the Suwolbong tuff ring, Cheju Island (Korea). Sedimentology 36:837–855

Sparks RSJ (1976) Grain size variations in ignimbrites and implications for the transport of pyroclastic flows. Sedimentology 23:147–188

Spinewine B, Octavio E, Sequeiros OE, García MH, Beaubouef RT, Sun T, Savoye B, Parker G (2009) Experiments on wedge-shaped deep sea sedimentary deposits in minibasins and/or on channel levees emplaced by turbidity currents. Part II. Morphodynamic evolution of the wedge and of the associated bedforms. J Sed Res 79(8):608–628

Sulpizio R, Dellino P (2008) Sedimentology, depositional mechanisms and pulsating behaviour of pyroclastic density currents. In: Gottsman J, Marti J (eds). Calderas volcanism: analysis, modelling and response. Devel Volcanol 10:57–96

Sulpizio R, Mele D, Dellino P, La Volpe L (2007) Deposits and physical properties of pyroclastic density currents during complex Subplinian eruptions: the AD 472 (Pollena) eruption of Somma-Vesuvius, Italy. Sedimentology 54:607–635

Sulpizio R, De Rosa R, Donato P (2008) The influence of variable topography on the depositional behaviour of pyroclastic density currents: the examples of the Upper Pollara eruption (Salina Island, southern Italy). J Volcanol Geotherm Res 175(3):367–385

Sulpizio R, Bonasia R, Dellino P, Mele D, Di Vito MA, La Volpe L (2010) The pomici di avellino eruption of somma-vesuvius (3.9 ka BP). Part II: Sedimentology and physical volcanology of pyroclastic density current deposits. Bull Volcanol 72(5):559–577

Sumner EJ, Amy LA, Talling PJ (2008) Deposit structure and processes of sand deposition from decelerating sediment suspensions. J Sed Res 78:529–547

Suthren RJ (1985) Facies analysis of volcaniclastic sediments: a review. Geol Soc London Spec Publ 18(1):123–146. doi:10.1144/GSL.SP.1985.018.01.07

Tanner WF (1967) Ripple mark indices and their uses. Sedimentology 9: 89–104

Valentine GA (1987) Stratified flow in pyroclastic surges. Bull Volcanol 49:616–630

Valentine GA, Giannetti B (1995) Single pyroclastic beds deposited by simultaneous fallout and surge processes: Roccamonfina volcano, Italy. J Volcanol Geotherm Res 64:129–137

Vasquez JA, Ort MH (2006) Facies variation of eruption units produced by the passage of single pyroclastic surge currents, Hopi Buttes volcanic field, USA. J Volcanol Geotherm Res 154:222–236

Walker GPL (1984) Characteristics of dune-bedded pyroclastic surge bedsets. J Volcanol Geotherm Res 20(3–4):281–296

Walker GPL, Wilson CJN, Froggatt PC (1981) An ignimbrite veneer deposit: the trail of a pyroclastic flow. J Volcanol Geotherm Res 9:409–421

Waters A, Fisher RV (1971) Base surges and their deposits: Capelinhos and Taal volcanoes. J Geophys Res 76:5596–5614

Wilson CJN, Hildreth V (1998) Hybrid fall deposits in the Bishop Tuff, California: a novel pyroclastic depositional mechanism. Geology 26:7–10

Wohletz KH (1998) Pyroclastic surges and compressible two-phase flow. In: Freundt A, Rosi M (eds) From magma to tephra: modelling physical processes of explosive volcanic eruptions. Elsevier, Amsterdam, pp 247–311

Wohletz KH, Sheridan MF (1979) A model of pyroclastic surge. Geological Society of America 180:177–194

Wynn RB, Stow DAV (2002) Classification and characterisation of deep-water sediment waves. Mar Geol 192:7–22

Yokoyama S, Tokunaga T (1978) Base-surge deposits of Mukaiyama Volcano, Nii-jima, Izu Islands. Bull Volcanol Soc Jpn 23:249–262

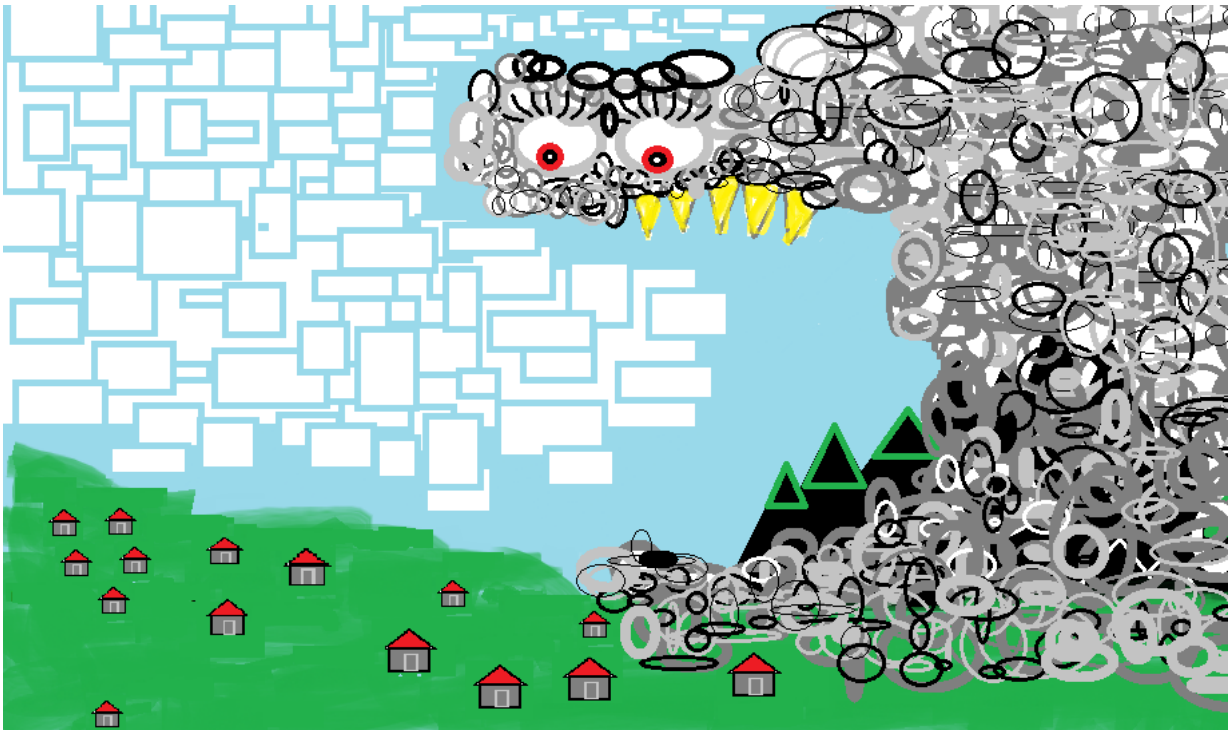

Figure 3.13: Numerical drawing based on the co-PDC ash clouds from the 1 February 2014 eruption of Tungurahua. Note the oval representation of PDCs (suggesting turbulence), whereas the surrounding fluid is represented by rectangles (density stratified atmosphere). The eruptive cloud is trapped at a density interface in the atmosphere and spreads as hypopycnal flow. The overall shape resembles nuclear tests clouds (base surges). The lower density of ovals in distal co-PDC clouds reflect lower particle concentration or scale of turbulence. Guillaume Herbertz (2014).

This page was intentionally left blank.

Part III

Boundary layer processes

Chapter 4

Saltation threshold for pyroclasts at various bedslopes: Wind tunnel measurements

This chapter was published in the "Journal of Volcanology and Geothermal Research" in 2014. It presents wind tunnel measurements of the saltation threshold for pyroclasts. The results may be used to retrieve quantitative information on the basal boundary conditions of pyroclastic density currents.

This page was intentionally left blank.

Journal of Volcanology and Geothermal Research 278–279 (2014) 14–24

Contents lists available at ScienceDirect

Journal of Volcanology and Geothermal Research

journal homepage: www.elsevier.com/locate/jvolgeores

Saltation threshold for pyroclasts at various bedslopes: Wind tunnel measurements

Guilhem Amin Douillet [a,*], Keld R. Rasmussen [b], Ulrich Kueppers [a], Deborah Lo Castro [c], Jon P. Merrison [d], Jacob J. Iversen [d], Donald B. Dingwell [a]

[a] Earth & Environmental Sciences, Ludwig Maximilian University, Munich, Germany
[b] Institute of Geocience, University of Aarhus, Denmark
[c] Istituto Nazionale di Geofisica e Vulcanologia, Sezione di Catania, Italy
[d] Institute of Physics and Astronomy, University of Aarhus, Denmark

ARTICLE INFO

Article history:
Received 2 August 2013
Accepted 27 March 2014
Available online 12 April 2014

Keywords:
Pyroclasts
Wind tunnel
Saltation threshold
Surface roughness

ABSTRACT

Pyroclastic density currents represent one of the most destructive hazards associated with explosive volcanism. This destructive nature does not only urge the need for but also prevents the obtainment of in situ measurements of their physical characteristics. The resulting deposits offer, however, evidence of the physics of their sedimentation phase. Deposits of dilute pyroclastic density currents frequently exhibit repeated cycles of deposition and erosion, yielding insights into the turbulent shearing along the ground. The utilization of such field observations can be greatly enhanced by the calibration of physical properties of such flows under well-constrained laboratory conditions. Here, wind tunnel measurements were performed using pyroclastic particles. The saltation threshold and surface roughness length were calculated for wind above a pyroclastic bed. The results serve as an aid in linking field observations to quantitative values of turbulent shear at the base of a flow. Scoria and pumice particles were investigated as a function of grain size (1 ϕ fractions between 0.125 and 4 mm), as well as the influence of bedslope (−20° to +25° in 10° steps). The results point to the dominant control of density, grain size and, contrary to previous assumptions, differ moderately from results obtained for round beads. Properly utilized, the dataset enables the establishment of a link between the grain size of natural deposits and the shearing extant during their emplacement. Depending on the type of sedimentary structure observed in the field, the saltation threshold can be used as a minimal or a maximal shearing limit during emplacement of dilute pyroclastic density current deposits. Stoss-aggrading laminations likely involve the saltation threshold as an upper limit, whereas for truncation events it must have been overcome. The effect of particle concentration within the flow, a critical parameter for pyroclastic density currents and the extent of validity of the data, are discussed.

1. Introduction

1.1. Particle transport

When a fluid flowing over an erodible bed reaches a certain speed profile, known as the fluid threshold, loose particles on the bed begin to move. Erosion, transport and deposition of particles may occur in all kinds of flows (atmospheric, fluvial, tidal and marine currents; turbidity currents; snow avalanches and, of particular interest here, pyroclastic density currents). As all clastic sediments have been transported and deposited, these processes are fundamental. They shape the landscape, deplete some areas of their soil and yield vast sedimentary deposits elsewhere (covering 70% of the Earth surface). Ripples and dunes form from the cm to the km scale, in aqueous, aeolian and even extraterrestrial environments.

Particle motion in a fluid can be understood as occurring via three main conceptual transport mechanisms: 1) rolling/creep occurring when particles move without leaving the bed, 2) saltation consisting of one or several particle jumps and 3) suspension, where the fluid turbulence fully supports the clasts that therefore exhibit no interaction with the ground.

1.2. Pyroclastic density currents

During explosive volcanic eruptions as well as catastrophic lava-dome collapses, newly-formed particles (pyroclasts) can be transported down the volcanic edifice as dilute particulate density currents, supported by a fluid phase consisting of a mixture of volcanic gas and entrained air (Carey, 1991; Druitt, 1996). Those pyroclastic density currents (PDCs) can flow at hundreds of km/h at temperatures of several

* Corresponding author. Tel.: +49 89 21804272; fax: +49 89 21804176.
E-mail address: g.douillet@min.uni-muenchen.de (G.A. Douillet).

http://dx.doi.org/10.1016/j.jvolgeores.2014.03.011

hundred °C). They thus pose a threat to local populations and infrastructure and can drastically alter the environment (Tanguy et al., 1998). As with any particle-laden flow, dilute PDCs can produce a range of sedimentary structures, including dune bedforms, erosive planes and massive deposits (Branney and Kokelaar, 2002; Douillet et al., 2013a). From a sedimentological point of view, PDCs can be classified based on the processes occurring at their base. Branney and Kokelaar (2002) defined four different kinds: granular, fluid-escape, tractional or fallout-dominated flow boundary zones. Where tractional processes can be inferred from the deposits, generally by the presence of cross-stratification (Douillet et al., 2013b) and a granulometry dominated by ash and lapilli (i.e. particle diameter <6.4 cm, Walker, 1971), particles are believed to undergo transport driven by the fluid phase down to the base of the flow. Each individual particle was thus subject to rolling, saltation and direct fall before deposition. From a theoretical point of view, dilute PDCs are regarded as turbulent, density-stratified, convecting gas-particulate flows (Valentine, 1987; Burgisser and Bergantz, 2002). Because of their opaque and hazardous nature, the internal processes are largely derived from direct observation during their flow and therefore much of our understanding must come from detailed analysis of their deposits. This situation creates a significant role for appropriate laboratory measurements in order to infer insights into flow conditions from the sedimentary record.

1.3. Wind-blown saltation

Saltation is a fundamental transport mechanism on a wind tractional flow boundary, typically accounting for 75% or more of the total mass transport (Bagnold, 1941). Moreover, since suspended particles do not interact with the bed, saltation is also the main mechanism of energy transfers between the flow and the bed (Owen, 1964). Even creeping/rolling particles indirectly extract energy from the wind flow via impacting saltating particles that transfer a fraction of their forward momentum (Bagnold, 1941; Merrison, 2012). Thus, saltation is the main process occurring at a tractional bed interface with particle transport.

Close to a rough boundary, small-scale turbulence generates a mixed layer where the shear stress (τ) can be assumed constant:

$$\tau = \rho u^{*\wedge}2 \quad (1)$$

with u^* (m/s), is a parameter called the shear (or friction) velocity and ρ the air density. Since the observation scale is much larger than the turbulent time scale, one can parameterize the shear stress by an eddy diffusivity, the size of which is proportional to the distance from the surface (Vallis, 2006, pp. 409–413; Durán et al., 2011):

$$\tau = \rho u^{*} \kappa z dU_z/dz \quad (2)$$

with U_z the average streamwise velocity component. The Von Karman constant κ generally has the value 0.4. Combining Eqs. (1) and (2), we get $dU_z/dz = u^*/\kappa\, z$, which integrates to define the logarithmic boundary layer known as the "Law of the Wall":

$$U_z = u^{*} \ln(z/z_0)/\kappa \quad (3)$$

z_0 (dimension of a length) is an integration constant called the aerodynamic surface roughness length (Garratt, 1992). It corresponds to the conceptual height above the bed where the wind speed extrapolated from Eq. (3) decreases to zero (the rougher the bed the larger the value of z_0). Whereas u^* is related to the velocity gradient of the wind-speed profile (slope of the logarithmic profile), z_0 relates to the roughness of the bed and those two parameters together completely define a logarithmic boundary layer. Other expressions of a velocity profile are available to account for secondary effects, but the logarithmic expression is recommended for evaluating shear velocities (see Bauer et al., 2004 and references therein).

For a dynamically fully rough wind over a fixed sand surface composed of uniform grains, Bagnold (1941) found empirically that:

$$z_0 = D_p/30 \quad (4)$$

where D_p is particle diameter. For non-uniform sand, D_p is replaced by D_g being some linear measure of the basal roughness elements (usually 2^*D_{50} or D_{90} where the subscript refers to the percentage of the population that is finer than the indicated size, Church et al., 1990; Nikuradse, 1933; Bauer et al., 2004 and references therein). Note however that for a saltating bed, z_0 slightly depends on u^* (e.g. Owen, 1964; Rasmussen and Mikkelsen, 1990; Sherman, 1992; Rasmussen et al., 1996; Durán et al., 2011).

Conceptually, five forces act on a clast subjected to a flow (Durán et al., 2011; Merrison, 2012): 1) drag force depending on particle shape and the flow speed, parallel to flow direction; 2) lift force depending on particle shape and driven by the pressure difference between the base and the top of the particle, (i.e. shear velocity), perpendicular to the bed; 3) torque force depending on particle shape and driven by the speed

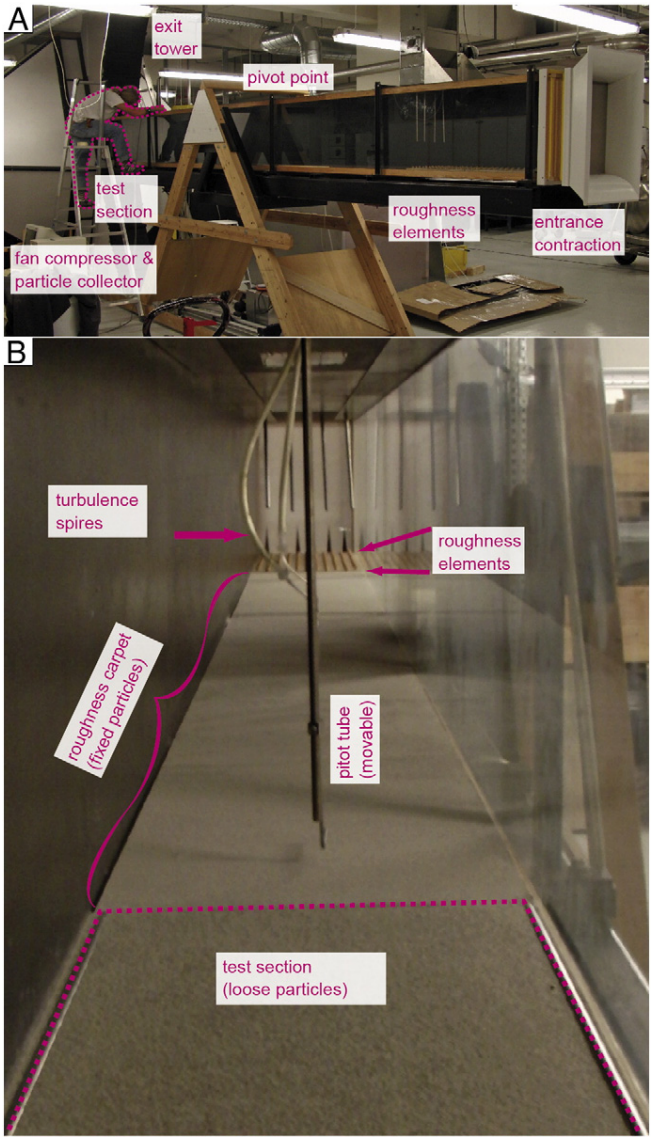

Fig. 1. Wind tunnel used in the study. A) View from the outside with the different sections. Note the pivot point that permits inclination. B) Inner view with the different sections (particles are 1–2 mm pumice). Note: loose bed in front and corresponding roughness carpet in the back.

difference between the base and the top of the particle, (i.e. shear velocity), induce a rotation; 4) adhesive forces including electrification, and other effects, linearly dependent on grain diameter, and other unidentified parameters, active on the contact points; and 5) gravitational forces depending on the density and volume of the particles.

Below a threshold shear velocity, the drag and lift forces are insufficient to counteract the weight of the particle and no motion occurs.

The fluid static saltation threshold (SST — U^*_0) is the threshold where particles start to move in saltation under the fluid shear stress alone (Durán et al., 2011). It is characterized by the minimal speed profile that initiates saltation of particles from a state of repose. For large particles such as sand-sized material, adhesive forces can be largely neglected, and the threshold is dominated by gravitational and torque forces (i.e. motion will be initiated by brief rolling leading to saltation, Durán et al., 2011; Merrison, 2012). The critical shear stress for transport depends on the drag coefficient, the vertical velocity profile near the bed and the characteristics of the particle bed. Bagnold also defined the impact (dynamic) threshold for saltation which is the minimum shear stress (speed profile) for which an already saltating bed can be maintained in saltation. The distinction is required by the fact that there is an amount of energy that must be transferred to initiate saltation, but once saltation has begun, the impacting particles will transfer part of their energy to particles in repose, possibly ejecting new particles (known as the splashing effect, Creyssels et al., 2009; Kok and Renno, 2009; Durán et al., 2011).

1.4. State of the art

The first physically-based intensive studies of wind-blown sand transport were conducted by Bagnold (1941). Iversen et al. (1976) measured the SST for blowing wind over different types of clast shapes, grain sizes and densities. Iversen and Rasmussen (1994, 1999) investigated the effect of bedslope on saltation threshold and mass transport. Those experiments provided the motivation for the present work, to provide an erosion threshold for pyroclasts that can be compared to field-based grain size data. A large number of studies on grain sizes of pyroclastic deposits are available (e.g., Sparks, 1976; Walker, 1984), yet these data remain underexploited in terms of the quantitative relations that might be derived for the flow parameters.

Some efforts have been made to relate field features to quantitative dilute PDC flow parameters related to the boundary layer. The shape of erosive furrows, for example, has been linked to the size of boundary layer eddies and used to derive flow velocities (Kieffer and Sturtevant, 1988). Dilute PDCs are particle-laden flows with dominant fluid–particle interactions and minor particle–particle support. Depending on the transport hypothesis, one of two approaches can be applied to link their deposits to flow parameters: 1) the sediment was emplaced from turbulent suspension transport (suspension criterion) or 2) the sediment was emplaced in a tractional boundary with saltation and thus must have been transported by the fluid-phase turbulent shear at the flow boundary (Shields criterion). The suspension criterion suggests that particles deposited from dilute flows must have been transported in suspension, thus the flow turbulence scales the terminal fall velocity of the transported material (Middleton, 1976; Dellino and La Volpe, 2000). The use of the Rouse number is an alternative formulation of this problem (e.g. Valentine, 1987). However, for deposits of supposedly dilute PDCs, the use of the suspension criterion applied to the coarsest clasts found will lead to unrealistic velocity values if flow density is not taken into account (Sparks, 1983; Walker and McBroome, 1983; Lajoie et al., 1989). Moreover, the settling velocity of pyroclasts is difficult to calculate (Walker et al., 1971; Sparks et al., 1978; Bonadonna et al., 1998; Dellino et al., 2005), thus the suspension criterion requires

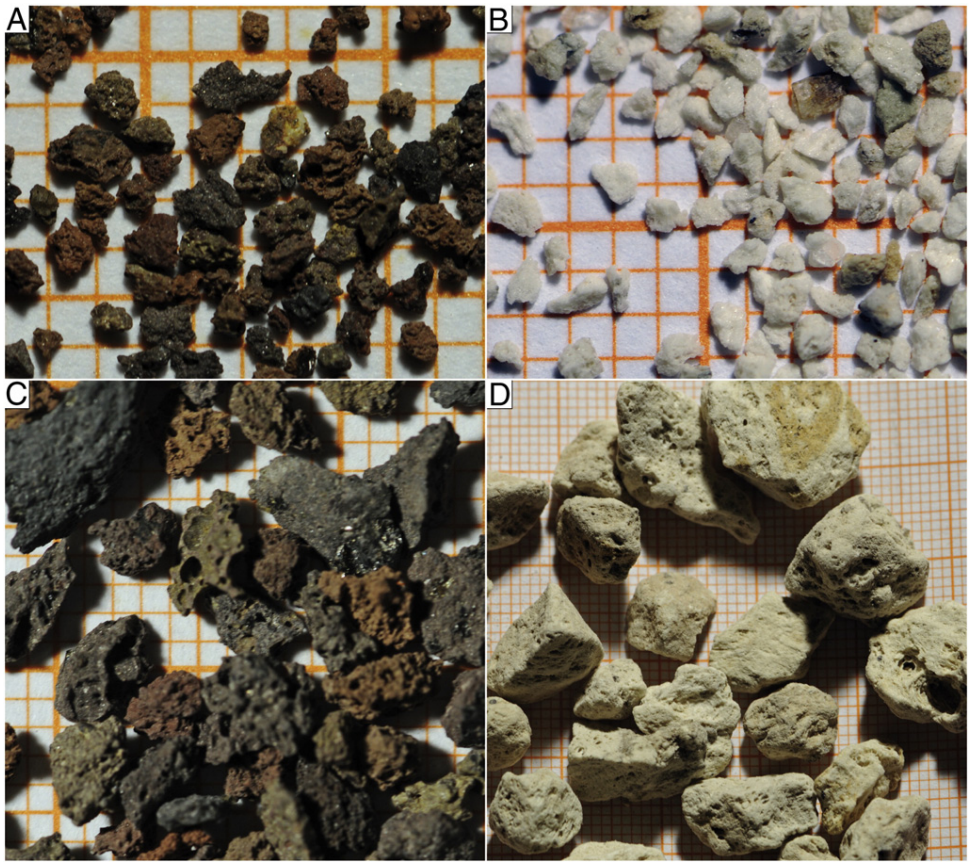

Fig. 2. View of the pyroclasts. Background grid is in mm. Particles: A) 0.5–1 mm scoria; B) 0.5–1 mm pumice; C) 2–4 mm scoria; D) 4–16 mm pumice. Note: vesiculated nature and angular shapes.

the estimation of both flow density and particle terminal fall velocities. On the other hand, the Shields criterion consists of the minimal shearing necessary to onset particle motion (Shields, 1936; Miller et al., 1977). Dellino et al. (2004a) applied the Shields criterion to cross-stratified deposits and the suspension criterion on directly overlying deposits in order to completely constrain the parental transitory flow (with response on the ethics by Le Roux, 2005). They later applied this method to the coarse- and fine-grained modes of the same layer, assuming a bedload and suspension transport for the modes (Dellino et al., 2008). In practice, both methods provide a threshold value for the horizontal shear velocity.

Here, we present a set of wind tunnel measurements at variable bedslope in order to characterize the static saltation threshold and surface roughness for pyroclastic particles of different density and grain size. Under the assumption that PDC deposits reflect boundary layer processes during emplacement, this dataset is well-suited to enhance our quantitative understanding of PDC dynamics.

2. Method

2.1. Wind tunnel measurements

In this study, we used a wind tunnel with adjustable bed inclination (Fig. 1, described by Iversen and Rasmussen, 1994). Because of the sloping possibility, the length is only 6 m and the flow thus needs to be adjusted immediately to the downwind equilibrium. A set of turbulence-generating spires and roughness blocks (on the first 80 cm) are placed at the upstream end of the tunnel. In the following 4 m in downwind direction, a roughness array is created on the bed. The roughness array consists of a board with a flat bed of particles glued on it and a roughness array was prepared for each sample type so that a fully developed turbulent wind profile in equilibrium with each sample type was achieved. The downstream end of the section consisted of a ca. 1 cm thick layer of loose samples on a length of 1 m.

The SST was measured by gradually increasing wind speed (blindly, i.e. without knowing the value) in the tunnel until a small but continuous amount of particles began to saltate at the downstream end of the test section. The observation was performed visually with the help of a laser beam that highlighted saltons. The criterion was that more than one particle would begin to saltate within a 5 s time-window during at least 1 min (thereby ensuring that not only the most unstable particle would move). The wind profile was then recorded at the downstream end of the roughness carpet using a pitot tube connected to a precision manometer. This method was previously applied by Iversen and Rasmussen (1994), who validated their results by comparing them with those obtained in a 15 m-long wind tunnel.

2.2. Particles

In order to evaluate the influence of particle characteristics on their saltation threshold and surface roughness, two kinds of natural pyroclasts from the East Eifel volcanic area (Germany) were used (Fig. 2). Pumice particles from the Laacher See eruption were provided (pre-washed with heavy water and pre-sieved), by ROTEC GmbH & Co. KG (Mühlheim–Kärlich), scoriaceous fragments of a porous lava flow ("Schaumlava") were provided by Paul Link GmbH & Co. KG (Kretz). Wet mechanic sieving in one ϕ intervals was performed (0.125 mm–16 mm).

Matrix densities were measured by Helium pycnometry (Ultrapyc from Quantachrome) utilizing ca. 30 g of particles from each fraction (Fig. 3A). Density is stable between the different size fractions with an average of 2.5 g/cm^3 and 1.4 g/cm^3 for the scoria and pumice particles, respectively. The pumice particles were found to float on water for several days.

Four shape parameters were derived from measurements of hundreds of single particles with a Retsch Camsizer: sphericity (avg. 0.81 ± 0.07), symmetry (avg. 0.87 ± 0.02), aspect ratio (avg. 0.68 ± 0.04) and convexity (avg. 0.98 ± 0.01) (Table 1, Fig. 3B–E). All samples show similar values. This similarity might be a consequence of the large number of particles analyzed for each sample type (>500).

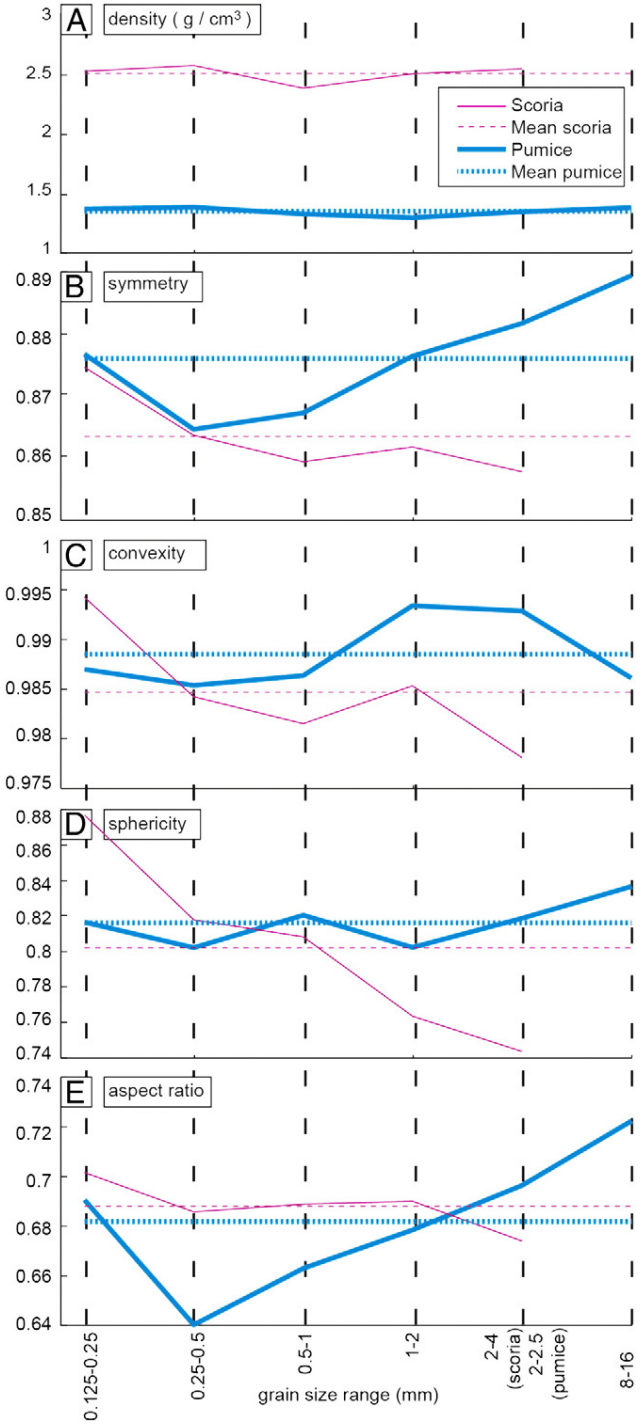

Fig. 3. Averaged particle parameters by samples. A) Density, B) to E) shape parameters.

3. Data

3.1. Static saltation threshold

Wind profiles recorded at the SST at zero bed slope show typical log-linear turbulent curves following the law of the wall (Fig. 4). Repeated

Table 1
Shape parameters for all particle types derived from averaged Camsizer measurements and densities.

Grain size (mm)	Sphericity	Symmetry	Aspect ratio	Convexity	Density ($kg \cdot m^{-3}$)
Scoria					
0.25–0.125	0.8767	0.8745	0.7015	0.9942	2531
0.5–0.25	0.8177	0.8635	0.6858	0.9841	2580
1–0.5	0.8081	0.8593	0.6889	0.9814	2391
2–1	0.7634	0.8616	0.69	0.9852	2511
4–2	0.7435	0.8576	0.6741	0.978	2552
Mean	0.8019	0.8633	0.6880	0.9846	2513
Pumice					
0.25–0.125	0.8164	0.8766	0.6906	0.9869	1383
0.5–0.25	0.802	0.8645	0.6405	0.9853	1398
1–0.5	0.8203	0.8671	0.6631	0.9863	1340
2–1	0.8022	0.8763	0.6785	0.9933	1309
2.5–2	0.8186	0.8816	0.6964	0.9928	1359
16–8	0.8365	0.8893	0.7222	0.986	1394
Mean	0.8160	0.8759	0.6819	0.9884	1364

Table 2
Results of the windtunnel measurements. Abbreviations: GS up/low: upper and lower grain size range; u^*: shear velocity; ⊙: threshold Shields number; z_0: surface roughness length; v_{10cm} and v_{100cm}: extrapolated velocity at 10 and 100 cm above the bed, respectively, following Eq. (3); Rep.: number of repetition of the whole measurements used for averaging.

GS up (mm)	GS low (mm)	u^* (m/s)	⊙	z^0 (mm)	v^{10cm} (m/s)	v^{100cm} (m/s)	rep.
Scoria							
0.25	0.125	0.2046	0.1728	0.1765	4.86	6.01	1
0.5	0.250	0.2856	0.1386	0.2395	6.57	8.18	2
1	0.5	0.4596	0.1932	0.5205	9.7	12.28	3
2	1	0.6574	0.3142	2.9249	11.12	14.81	2
4	2	0.6852	0.1887	3.1374	11.47	15.32	1
Pumice							
0.25	0.125	0.0629	0.1042	0.1563	1.51	1.87	2
0.5	0.25	0.0546	0.0466	0.0793	1.41	1.71	3
1	0.5	0.0979	0.0381	0.1596	2.35	2.9	1
2	1	0.4359	0.1545	1.4294	7.93	10.38	3
2.5	2	0.4675	0.1845	2.5799	8.05	10.67	2
16	8	0.6808	0.0835	8.0416	9.83	13.66	1

measurements show consistent results, demonstrating the reliability of the set-up. Shear velocities were estimated from log-linear best-fit regressions of the data (Eq. (3), Table 2). Estimates of surface roughness lengths were derived directly from the best-fit regression parameters generated for estimating shear velocities (as the height where the profile crosses the zero velocity line, Table 2).

The shear velocities for the SST are compared to standard curves for different clast densities and shapes (Fig. 5 from Iversen et al., 1976). Both scoria and pumice samples of all grain sizes plot within the field for round particles of similar densities, thus the SST seems to be little affected by the high angularity and other specificities of the pyroclasts.

The Shields number (⊙) is often used as a dimensionless criterion for motion:

$$\odot = \rho_f (u^*)^2 / \left(\rho_p - \rho_f\right) g\, D_p \quad (5)$$

Given all the values measured for the experiments, we calculated the threshold Shields number (Fig. 6). Values are in the smallest range of measured data, as expected for particles of large size (as defined in the aeolian research context—100 s μm). Indeed, the Shields number is a parameter based upon a simple model including only gravity and a lift type force, whereas for large grains, detachment occurs through

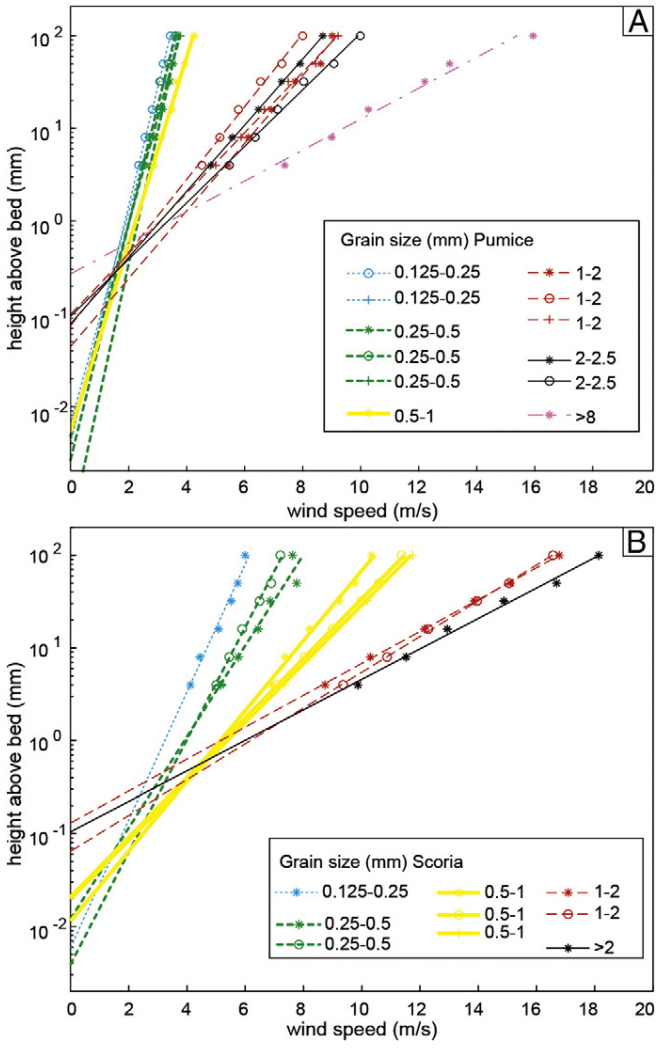

Fig. 4. Speed profiles at SST. Points are measurements, lines are logarithmic fits. Samples by colors, repeated samples have the same color. A) Pumice samples, B) scoria samples.

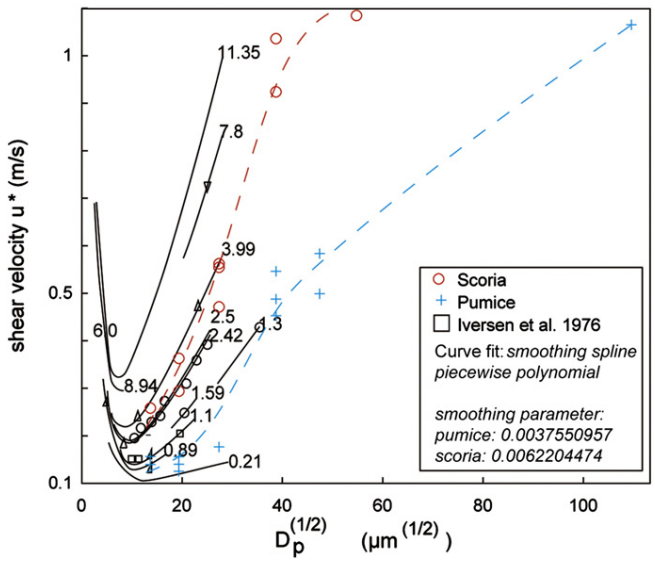

Fig. 5. Saltation threshold shear speeds as a function of grain diameter (square root). Data are compared to results from Iversen et al. (1976) in black, with numbers indicating densities of the studied material.

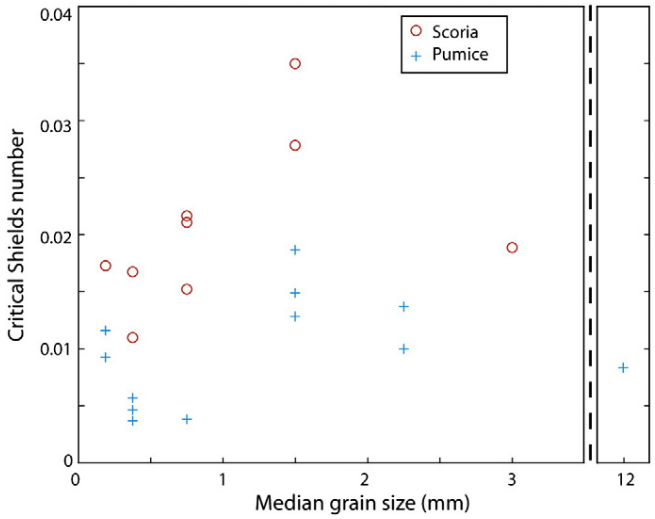

Fig. 6. Static threshold Shields numbers calculated from Eq. (5) and the measurement results for sample type and grain size. Values in table 3.

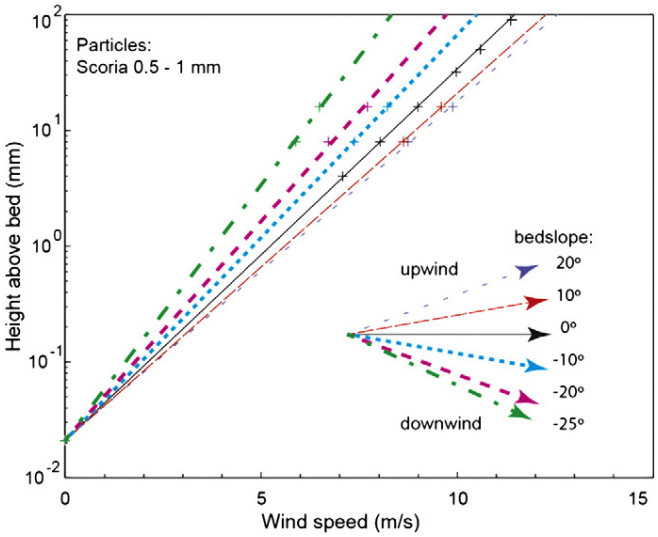

Fig. 8. Example of the slope influence for the 0.5–1 mm scoria samples. Color coding indicates the bedslope. Surface roughness lengthscale is fixed to the no-slope value.

rolling, which has only a weak dependence upon size. The Shields number might thus be inappropriate for particle transport in PDCs.

3.2. Surface roughness

Empirically, it was observed that the surface roughness length roughly obeys Eq. (4), thus solely depending on grain characteristics. There is some scatter in the extrapolated surface roughness length for the pyroclasts (Fig. 7). While the larger clasts fit reasonable well in the range expected some of the values obtained for the smaller pumice particles (<1 mm) are lower than expected. This may be due to a larger measurement uncertainty for fines: the lowest measurement height is fixed by the size of the sensor, and extrapolation to the zero wind speed must thus be longer for the smaller speed gradient above the finest particles.

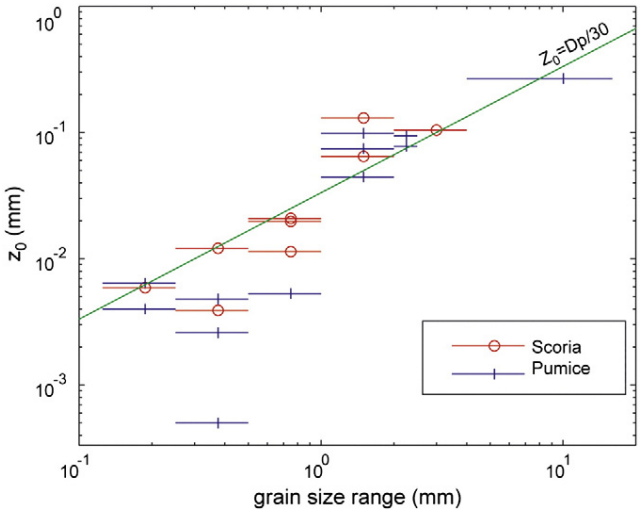

Fig. 7. Surface roughness lengthscale (z_0) as a function of grain size range. The horizontal bars indicate the grain range of each sample. Green line follows Eq. (4) with the mean diameter.

3.3. Inclined profiles

The SST was similarly observed for measurements with an inclined bed and velocities measured at two different heights. Since the particles for horizontal and inclined tests are the same, the surface roughness lengths were assumed to be unaffected by inclination and taken as those from the zero-slope results. This assumption was previously verified on the same set-up by Rasmussen et al. (1996). The SSTs are affected only because gravity forces act with or against the wind influence (Fig. 8, Table 3). In order to compare the threshold values and eliminate systematic parasitic effects, sloping results are normalized to the zero-slope SST (Fig. 9). A discussion on the effects of slope on the SST is available in Iversen and Rasmussen (1994) for sand particles. In our experiments, the SST can be increased by up to 82% when the slope acts against flow direction compared to the minimum (downflow) results, and is on average greater by 50%. Both sample types exhibit the same trend and no clear trend regarding grain size was discerned.

Table 3
Values of shear velocity for different bedslope angles and all samples. Positive bedslope value: slope acts against flow direction. GS up/low: upper and lower grain size range (mm).

	Angle (°)	20	10	0	−10	−20	−25
GS up	GS low	u* value	u* value	u* value	u* value	u* value	u* value
Scoria							
0.25	0.125	0.2756	0.2731	0.2584	0.2223	0.2065	0.1836
0.50	0.25	0.3892	0.3775	0.3631	0.3250	0.2702	0.2682
0.50	0.25	0.3362	0.3298	0.2941	0.2725	0.2402	0.2266
1.00	0.50	0.5526	0.5232	0.4714	0.4355	0.3451	0.3316
1.00	0.50	0.6076	0.5933	0.5547	0.5077	0.4712	0.4027
2.00	1.00	1.1204	1.0669	1.0361	0.8365	0.7400	0.6162
2.00	1.00	1.0647	1.0290	0.9240	0.9029	0.8044	0.6894
4.00	2.00	NO DATA	1.2409	1.0846	1.0421	0.9522	0.8553
Pumice							
0.25	0.125	0.1612	0.1560	0.1395	0.1416	0.1305	0.1243
0.50	0.25	0.1315	0.1266	0.1253	0.1132	0.1080	0.0959
1.00	0.50	0.2139	0.2073	0.1765	0.1748	0.1594	0.1456
2.00	1.00	0.4938	0.4851	0.4877	0.4474	0.3982	0.3482
2.00	1.00	0.5457	0.5362	0.4528	0.4567	0.3979	0.3713
2.5	2.00	0.5996	0.5879	0.4990	0.5117	0.4517	0.4093

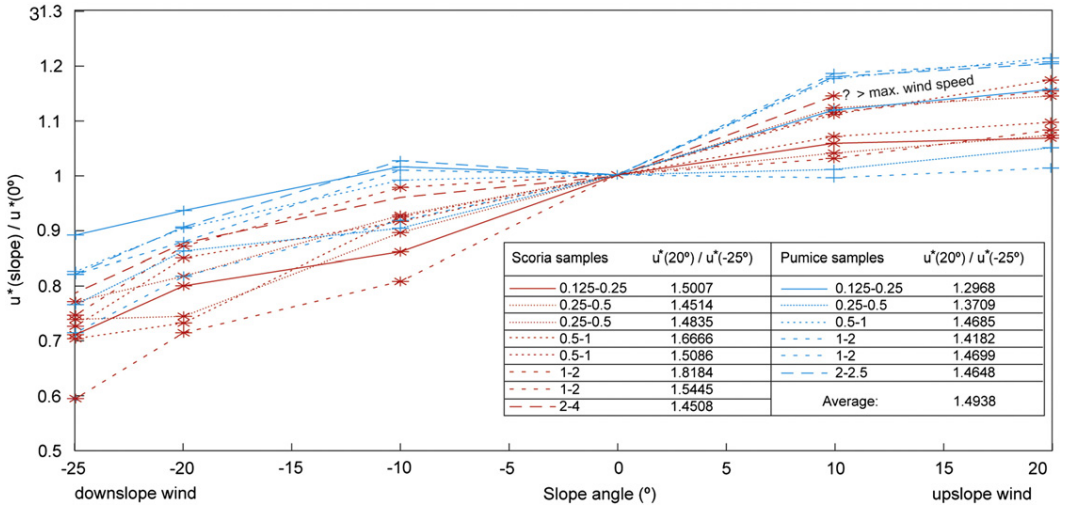

Fig. 9. Influence of slope on the static saltation threshold normalized by the no-slope threshold. Inlet table gives the ratio between maximal downslope and upslope results. Results presented for both scoria and pumice particles.

4. Discussion

4.1. Considerations for use

A link between pyroclast grain size and the associated SST has been measured with a wind tunnel in order to serve as a reference for field studies. Nevertheless, the use of the results is not straightforward and requires careful consideration. The data presented here are for pure wind, without particle load and they are only relevant in the vicinity of the bed interface. Even very dilute PDCs are likely to be highly loaded in particles saltating or in suspension, with various grain sizes.

4.1.1. Boundary processes

Our data relate to near bed boundary processes at the sedimentation interface and the surface roughness lengths are for wind exposed to grain-scale topography. We refrain from extrapolation to a larger part of a PDC's thickness.

A simple logarithmic profile is valid in the vicinity of the bed, but it is most likely that the basal roughness elements influencing on the turbulence for a whole PDC consist of trees, large bedforms and geomorphological features (Dellino et al., 2004b). In that case, an additional term "d_0" (displacement length) is needed in Eq. (3) to correct for surfaces with large roughness elements that account for a considerable part of the wall friction (Grimmond and Oke, 1998):

$$U_z = u^* \ln((z-d_0)/z_0)/\kappa$$

Even so, the law of the wall is valid in the vicinity of the boundary only, and a velocity profile is likely to reach a freestream velocity or follow some Kolmogorov model in its outer parts (defect layer). Dilute PDCs are complex, with density stratification, convection, and flow regime changes interacting with turbulent eddies at a range of scale (Valentine, 1987; Burgisser and Bergantz, 2002; Andrews and Manga, 2012), so that our data should only be used as an instantaneous shear threshold near the bed, that is intermittently reached via the flow's large-scale turbulence.

4.1.2. Flow density

For a given speed, flow density and shearing are positively correlated. This needs to be addressed, especially in the PDC context, because: 1) elevated temperatures lead to decreased gas densities and 2) the particle volumetric concentration can increase the bulk density of the flow (Boudon and Lajoie, 1989). Consequently, the shear velocities presented here need to be converted in flow velocities by carefully taking into account the density of the flow. Table 4 summarizes the flow density for different concentrations and air at 25 °C (ambient air), 100 °C (liquid water limit), 230 °C (wood scorches—Bradbury, 1953), 270 °C (wood carbonizes—Lullin, 1925), and 450 °C (highest temperature encountered in the literature by the authors, Lacroix, 1904).

Air density depends upon temperature as:

$$\rho_{air} = M_{mol}P/(RT) \quad (6)$$

with $M_{mol} = 0.029$ kg/mol the molecular mass of air, $R = 8.314$ J/(mol·K) the ideal gas constant, P taken at 1.013 hPa the atmospheric pressure, and T the temperature in Kelvins.

The particle volumetric concentration is probably the most difficult value to assess. Doronzo and Dellino (2011) used a value of 3.7% at 1 m above the ground for their numerical simulations, a value based on deposit analysis and experiments (Dellino et al., 2008). However, probably only the finest, suspended fraction of the particles can be considered as increasing the density of the fluid whereas larger particles are more likely to be in (partial) interaction with the ground contact zone and participate in boundary layer saturation (Simons et al., 1963). Doronzo and Dellino (2011) used a grain size distribution containing 4.6% of particles with a diameter of 63 μm, the remaining 95.4% with a diameter of 1.4 cm and above. We can thus also consider the case where only particles of 63 μm and less contribute to the flow density.

Considering,

$$\rho_{flow} = C\rho_p + (1-C)\rho_f \quad (7)$$

with C the particle volumetric concentration.

Table 4 summarizes the different densities depending on temperature and particle volumetric concentration. It clearly shows the dominant influence of particle concentration over temperature. Although density of a pure wind can double in the temperature range of PDCs,

Table 4
Values of flow density ($kg \cdot m^{-3}$) calculated for different temperatures (T(°C)) following Eq. (6) and volumetric particle concentrations (C(%)) following Eq. (7). For particle concentrations above 0, the value is given for a particle density of 1300 and 2500 $kg \cdot m^{-3}$.

T(°C)\C(%)	0	0.17	1	3.7
25	1.19	3.39/5.43	14.17/26.17	49.24/93.64
100	0.95	3.15/5.20	13.94/25.94	49.01/93.41
230	0.7	2.91/4.96	13.70/25.70	48.78/93.18
270	0.65	2.86/4.90	13.64/25.64	48.73/93.13
450	0.49	2.70/4.74	13.48/25.48	48.57/92.97

particle concentration mostly governs the flow density and leads to increases with a factor of 200 between our extreme examples. As a comparison, Brand and Clarke (2012) used densities of 3, 7 and 11 kg/m^3 on their analysis based on Wohletz (1998).

Given that the SST is a shearing threshold (thus the threshold parameter is τ and not u^*), it appears from (Eq. 1) that the shear velocity, (and so the slope of the velocity profile) at a given shear stress is controlled by the root of the bulk flow density, so that:

$$u^*(\rho_i) = u^*(\rho_0)(\rho_0/\rho_i)^{\wedge}(1/2) \quad (8)$$

As a first approximation, the values of SST can thus simply be corrected by taking an adequate flow density, and the new shear velocity applied to calculate the wind profile. Note, however, that the saltation threshold increases itself up to a factor 2 due to the particle-to-fluid density-ratio in a more complicated manner, probably as an effect of the relative energy with which particles interact with each other (Iversen et al., 1987).

4.1.3. Saturated flux

A saltating bed transports a given flux of particles, depending on the wind profile (Zheng et al., 2004; Creyssels et al., 2009), or in other terms, it reaches a maximal transport capacity, i.e. a saturated flux (Durán and Hermann, 2006). The particle concentration and its effects on entrainment and erosion capability are especially relevant for dilute PDCs with load greater than aeolian transport.

During saltation, the moving grains extract momentum from the air, and so the shear stress in the saltation layer can be divided into the grain-borne and air-borne shear stress. As long as the saturation flux is not reached, more grains are entrained, and a transfer from air-borne to grain-borne shear stress occurs. At saturation, no additional grains can be put in motion and the air-borne shear stress is reduced just below the saltation threshold (Owen, 1964; Iversen and Rasmussen, 1999; Durán et al., 2011). Several models have been suggested for saturated transport (Andreotti, 2004; Zheng et al., 2004; Durán and Hermann, 2006; Durán et al., 2011 – chap 4.3 – and references therein), and are beyond the scope of the data presented herein. In most models, even if the velocity profile *above* the saltation layer could indicate that the saltation threshold is exceeded, no additional particles will be entrained if the fluid *in* the saltation layer has already reached saturation. Saturation would be an equilibrium state with continuous exchange of particles between the bed and fluid phase (entrainment and deposition) but no net erosion. Saturated transport is a fundamental aspect for decelerating dilute PDCs, whose total transport capacity will reduce downflow.

Experiments on the influence of settling particles on the formation of cross-laminations in aqueous flows seem to indicate that 1) cross-lamination is inhibited for antidunes but not for lower stage bedforms (Arnott and Hand, 1989), 2) high deposition rates from the suspended load in density currents will produce poorly-graded deposits (Sumner et al., 2008) and 3) high concentrations of fine particles ease the formation of cross-lamination (Simons et al., 1963). Several studies have suggested that a tractional boundary is inhibited by high basal clast concentration, which is thought to account for fine-grained, massive or faintly stratified beds (Branney and Kokelaar, 1997; Brown and Branney, 2004; Sulpizio et al., 2010). The current lack of knowledge on the saturated flux and the uncertainties of application it entails should be kept in mind when applying the present dataset to PDCs.

Finally, the presence of particles landing from the upper parts of a PDC on the ground contact zone may, in some cases, induce mobilization of the bed that would otherwise not move. Indeed, particles falling and bouncing from the upper part of the flow are an input of energy to the interface and might eject other particles during impact, like the splashing effect for saltons. As such, the dynamic saltation threshold (the speed to maintain an already saltating bed in saltation, Iversen and Rasmussen, 1994) might provide results closer to what corresponds to a PDC boundary with landing particles from the upper part. The ratio of dynamic to static threshold is about 0.7 (Iversen and Rasmussen, 1994).

4.2. Application to PDC deposits

4.2.1. Cross-bedding type

At least three types of cross-bedding can be recognized in PDC deposits: 1) "partially erosive cross-lamination", 2) "differential draping laminations", and 3) "non-laminated cross-bedding" (Branney and Kokelaar, 2002; Douillet et al., 2013a, 2013b; Fig. 10).

The "partially erosive cross-laminations" consist of all those kinds of bedforms that show truncations, e.g. stoss-eroded dune bedforms, the so-called "chute and pool" type of bedding, or any erosive plane (Fig. 10A). In such cases, it can be inferred that previously deposited particles have been remobilized. Provided that it can be inferred that a dilute flow eroded the former deposits, one can relate the grain size of the deposits to the associated SST as a minimum value. Indeed, no particles would move below the threshold.

The "differential draping laminations" consist of those bedsets aggrading on both sides of a bedform in an asymmetrical manner (e.g. climbing dunes and stoss-depositional dune bedforms, Fig. 10B). Recent interpretation has suggested that stoss-aggrading dune bedforms are produced by a transitional process between direct fallout and tractional current in dilute PDCs with preferential draping on the stoss side but little tractional component (Douillet et al., 2013b). In such a case, the SST would thus represent an upper limit for the formation of dune bedforms by differential draping, since passing the threshold would imply a major influence of tractional processes.

Finally, for the "non-laminated cross-bedding" type, it should be stated clearly that not all cross-bedding within PDC deposits has been deposited from dilute PDCs with a tractional boundary. If the smallest strata forming a sedimentary structure are more than a few mm thick and indeed represent thin, massive layers, then caution must be taken during interpretation (Fig. 10C). Such layers might be emplaced from a granular-based flow boundary, possibly dense pyroclastic flows. The same applies for very diffuse laminations (Fig. 10D), where the structure can represent a deposit from a dilute PDC with a high particle concentration at its base (traction carpet, Sohn, 1997). Even if the fluid phase dominated most of the flow, particles might deposit with none or all diffuse lamination because high deposition rates or bedload transport would completely saturate the boundary, inhibiting cross-stratification. In that case, even if the SST is reached, it cannot affect the sediment bed, because a thin traction carpet would "reptate" between the fluid phase and the actual deposit. This case might to some extent be similar to the model by Andreotti (2004).

4.2.2. Stoss-aggrading dune bedforms

The results of the inclined-bed measurements bring a new view on the formation of stoss-aggrading dune bedforms that have successive crest migrating upstream. These structures are typical for the dilute PDC record (Fig. 10B). They are often observed on the steep flanks of volcanoes and they exhibit both stoss and lee face angles dipping from 0 to more than 35° to the horizontal (Douillet et al., 2013b). Typical wind-blown dunes on the other hand are relatively simpler systems where particles are eroded and transported on a gentle stoss side, and deposited on the steeper lee side at the repose angle. The genesis of stoss-aggrading dune bedforms produced from PDCs has been variously interpreted as antidunes (indicating stationary gravity waves, Fisher and Waters, 1969; Crowe and Fisher, 1973), as a plastering effect (indicating liquid water content in the flow, Allen, 1982), as the result of en-masse deposition of individual pulses (Sulpizio et al., 2007) or as a differential draping effect due to high direct sedimentation from the suspended load (Douillet et al., 2013b).

From the inclined measurements it appears that, in order to produce erosion on the stoss side and deposition on the lee side, as is the case for

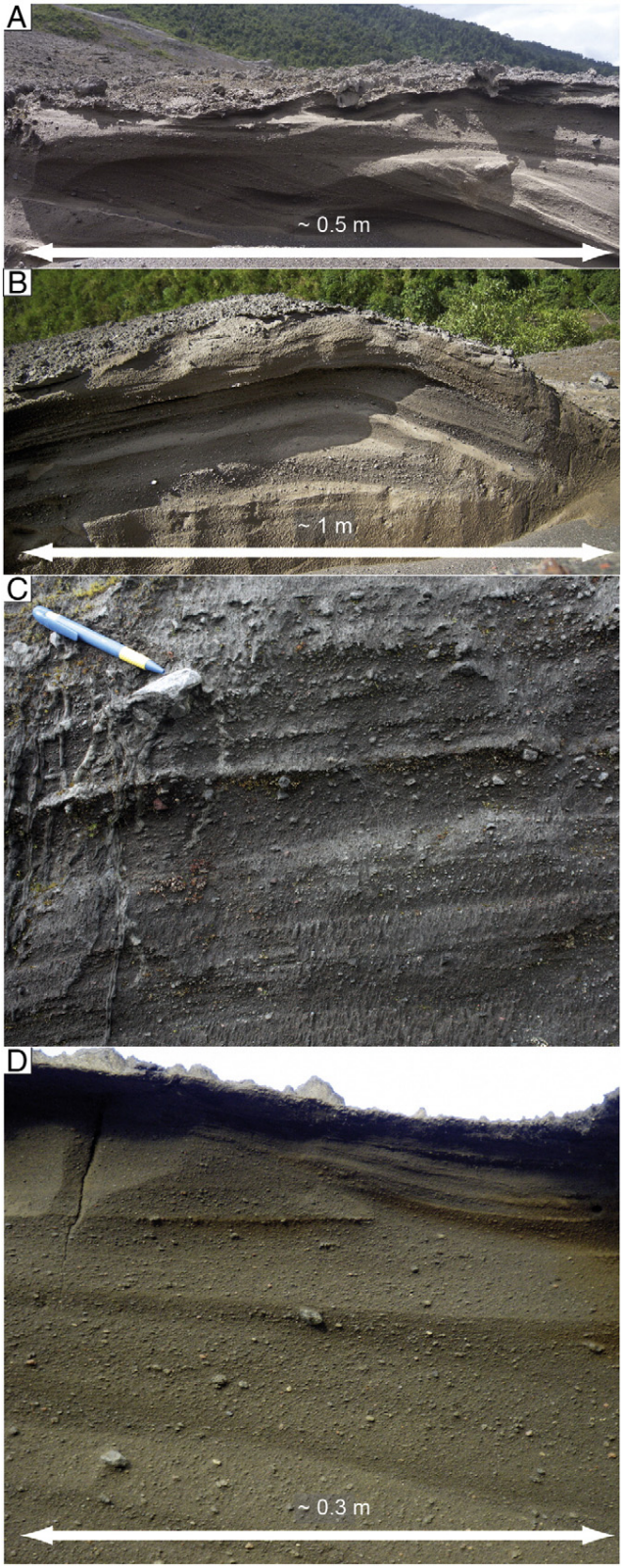

Fig. 10. Examples of PDC deposits. A) truncated laminations covered by planar lamination. B) Stoss-aggrading dune bedform showing differential draping. C) Cross-bedding made from thin layers rather than laminae. D) Very diffuse lamination. All outcrops from the deposits of the 2006 eruption of Tungurahua volcano (see Douillet et al., 2013a, 2013b).

typical dunes, the shear velocity must be more than 50% higher on the stoss face for PDC bedforms (difference between upslope and downslope wind threshold—inset in Fig. 9). Unless a detachment eddy is produced above the lee face, it however seems unlikely that such difference would occur between the stoss and the lee side. This rules out antidunes (i.e. bedforms related to stationary gravity waves, Prave, 1990) as an interpretation. For dune bedforms produced by traction in pure fluids (aeolian wind, water flows), no deposition can occur on the stoss side, because material is not available from the flow directly, it first needs to be put in transport (eroded from the stoss side), and only thereafter can be deposited (on the lee side). In the case of dilute PDCs however, the sediment is present everywhere in the flow, settling from the upper parts of the PDC, and thus, as long as the 50% shear velocity decrease between the stoss and lee are not satisfied, stoss aggradation will be more important than lee aggradation. Any shear difference lower than 50% would not permit to produce downstream migrating bedforms, and erosion would be less pronounced on the stoss than the lee side (or, under aggrading conditions, there would be more stoss aggradation). This can explain the widespread occurrence of stoss-aggrading bedforms in PDCs. Moreover, this process is actually not limited to PDCs, but includes other particle-laden flows and particulate density currents (sediment-laden hyperpicnal flows, turbidity currents), and indeed, similar bedforms occur in their deposits (Douillet et al., 2013b; Lang and Winsemann, 2013).

4.2.3. Example of flow velocities inferred from PDC deposits

We use field observations from the 2006 PDC deposits at Tungurahua volcano (Douillet et al., 2013a, 2013b) as an example of a simple approach: The presence of slightly burned wood fragments is taken as a hint for a flow temperature of 270 °C. Abundant aggrading cross-bedding suggests high particle concentration but within a tractional boundary zone (particle concentration of 3.7%). Scoria and dense clasts form most of the deposits (particle density taken 2500 kg/m^3). This corresponds to a flow density of 93.13 kg/m^3. Freshly emplaced loose cross-stratified bedsets containing laminations with particles up to ca. 1 to 2 mm diameter have been eroded repeatedly. For a pure wind at ambient temperature this would correspond to a shear velocity of 0.6574 m/s, and a velocity of 11.12 and 14.81 m/s at 10 and 100 cm above the bed, respectively (Table 2). Correcting for the flow density indicated above, the shear velocity becomes 0.0743 m/s and the velocities become 1.26 and 1.67 m/s at 10 and 100 cm above the bed, respectively. This corresponds to a decrease of one order of magnitude, leading to very low shear velocities for entrainment of particles.

The measured (and corrected) SST shear velocities and near bed flow velocities obtained from our study are thus at the lowermost limit of velocities usually inferred for dilute PDC deposits. Walker (1984) interpreted the grain size and sedimentary structures found within dilute PDC deposits as indicative of weak and slow flows, fully supported by our measurements. One should keep in mind that in order for a sedimentary structure to form, sedimentation should be possible (i.e. if a flow is too fast, it is unlikely to deposit). For example, Brand and Clarke (2012) observed 20 m-long structures interpreted as antidunes, from which they inferred layer-averaged flow velocities of 30–80 m/s. For layers showing a kink in their bedslope angle (interpreted as chute and pool structures) they inferred layer-averaged flow velocities of 52–73 m/s. From our measurements, the near bed velocities at saltation threshold with the flow density they use (7 kg/m^3) for 8–16 mm diam. pumice particles (as we observe from their pictures) would result in a shear velocity of 0.2807 m/s and velocities of 1.73 and 3.30 m/s at 10 and 100 cm height above the bed, respectively (Table 2). For 2–4 mm diam. scoria particles, velocities of 2.37 and 3.95 m/s would be acting at 10 and 100 cm height above the bed, respectively. Above these velocities, the flow should be over-saturated to force deposition or erosion should occur. It is complex to compare layer-averaged velocities with near bed values, but our results bring a new perspective on the *sedimentation* phases of a dilute PDC. We do not exclude fast flow velocities for dilute PDCs, such as the 235 m/s obtained by Kieffer and Sturtevant (1988)

for the Mount St. Helens blast, but as they did, such velocities should only be associated with erosional, and not depositional features.

5 . Conclusion and overview

We performed wind tunnel measurements of the shear velocity at the saltation threshold and the surface roughness length scale for pyroclastic particles. The dataset was measured for different types of particles, different grain sizes and at various slope angles to account for the variety of features observed in the field. Carefully used, the dataset permits linking of field characteristics (the grain size of a sedimentary structure) to quantitative flow parameters (the shear velocity necessary to put the particles in motion). The results also yield the order of magnitude of the shear velocities acting during deposition of PDCs, a valuable input for numerical models.

Several effects have to be taken into account in order to avoid over-interpretation or misuse of the dataset: the effect of the fluid-phase density has to be corrected and the influence of particle concentration and settling has to be addressed. Different scenarios can be envisaged and careful description and interpretation of the sedimentary record remains fundamental. Indeed, whereas insights for granular boundary flow would render the dataset inapplicable, the saltation threshold can be seen as an upper limit in the case of draping deposits or as a minimum if erosion plays a role and is due to the fluid-phase competence. These considerations taken into account, our dataset can provide valuable information on PDC dynamics.

The results of the influence of slope also provide new insights on the formation of stoss-aggrading structures deposited from dilute PDCs. The gravity-induced difference in the saltation threshold between a (upsloping) stoss side and (downsloping) lee side might indeed explain those structures. It also brings some new perspective on some deposit feature interpretation, and possibly over-estimated flow velocities for parental dilute PDCs.

Further effort will be needed in order to account for the specificities of PDCs. The dynamic saltation threshold and the influence of particle concentration within the flow should be a priority for future experimental designs. Although the measurements presented here represent but a first order approach towards the quantitative interpretation of deposits, this tool can also be powerful to constrain numerical input parameters and global understanding of pyroclastic density currents.

Acknowledgments

Olivier Roche and Pierfrancesco Dellino are acknowledged for valuable reviews. The pumice particles used in this study were kindly offered by ROTEC GmbH & Co. KG (Mühlheim-Kärlich), the scoria particles by Paul Link GmbH & Co. KG (Kretz). We are grateful to the ESA grant TNA2-Europlanet that supported the experiments in Aarhus. GAD and UK are financially supported by the Deutsche Forschungsgemeinschaft grant KU2689/2-1. GAD was partially funded by THESIS Elite Network of Bavaria. DBD acknowledges a Research Professorship (LMUexcellent) of the Bundesexzellenzinitiative and the support of the ERC Advanced Research Grant—EVOKES (No 247076).

References

Allen, J.R.L., 1982. Sedimentary Structures. Their Character and Physical Basis. Elsevier Science Publishers, Amsterdam (663 pages).
Andreotti, B., 2004. A two-species model of aeolian sand transport. J. Fluid Mech. 510, 47–70.
Andrews, B.J., Manga, M., 2012. Experimental study of turbulence, sedimentation, and coignimbrite mass partitioning in dilute pyroclastic density currents. J. Volcanol. Geotherm. Res. 225, 30–44.
Arnott, R.W.C., Hand, B.M., 1989. Bedforms, primary structures and grain fabric in the presence of suspended sediment rain. J. Sed. Res. 59.
Bagnold, R.A., 1941. The Physics of Blown Sand and Desert Dunes. William Morrow and Company, New York.
Bauer, B.O., Houser, C.A., Nickling, W.G., 2004. Analysis of velocity profile measurements from wind-tunnel experiments with saltation. Geomorphology 59, 81–98.
Bonadonna, C., Ernst, G.G.J., Sparks, R.S.J., 1998. Thickness variations and volume estimates of tephra fall deposits: the importance of particle Reynolds number. J. Volcanol. Geotherm. Res. 81, 173–187.
Boudon, G., Lajoie, J., 1989. The 1902 Pelean deposits in the Fort Cemetery of St. Pierre, Martinique: a model for the accumulation of turbulent nuées ardentes. In: Boudon, G., Gourgaud, A. (Eds.), Mount Pelee. J. Volcanol. Geotherm. Res., 38, pp. 113–130.
Bradbury, R., 1953. Fahrenheit 451 Ballantine Books.
Brand, B.D., Clarke, A.B., 2012. An unusually energetic basaltic phreatomagmatic eruption: using deposit characteristics to constrain dilute pyroclastic density current dynamics. J. Volcanol. Geotherm. Res. 243–244, 81–90.
Branney, M.J., Kokelaar, P., 1997. Giant bed from a sustained catastrophic density current flowing over topography: Acatlán ignimbrite, Mexico. Geology 25 (2), 115–118.
Branney, MJ., Kokelaar, P., 2002. Pyroclastic density currents and the sedimentation of ignimbrites. Geological Society Memoir no 27, London.
Brown, R.J., Branney, M.J., 2004. Bypassing and diachronous deposition from density currents: evidence from a giant regressive bed form in the Poris ignimbrite, Tenerife, Canary Islands. Geology 32, 445–448.
Burgisser, A., Bergantz, G.V., 2002. Reconciling pyroclastic flow and surge: the multiphase physics of pyroclastic density currents. Earth Planet. Sci. Lett. 202, 405–418.
Carey, S.N., 1991. Transport and deposition of tephra by pyroclastic flows and surges. Sedimentation in Volcanic Settings SEPM (Special Publication No 45.).
Church, M., Wolcott, J., Maizels, J., 1990. Palaeovelocity: a parsimonious proposal. Earth Surf. Process. Landf. 15, 475–480.
Creyssels, M., Dupont, P., Ould El Moctar, A., Valance, A., Cantat, I., Jenkins, J.T., Pasini, J.M., Rasmussen, K.R., 2009. Saltating particles in a turbulent boundary layer: experiment and theory. J. Fluid Mech. 625, 47–74.
Crowe, B.M., Fisher, R.V., 1973. Sedimentary structures in base-surge deposits with special reference to cross-bedding, Ubehebe Craters, Death Valley, California. Geol. Soc. Am. Bull. 84, 663–682.
Dellino, P., La Volpe, L., 2000. Structures and grain size distribution in surge deposits as a tool for modelling the dynamics of dilute pyroclastic density currents at La Fossa di Vulcano Aeolian Islands, Italy. J. Volcanol. Geotherm. Res. 96, 57–78.
Dellino, P., Isaia, R., La Volpe, L., Orsi, G., 2004a. Interaction between particles transported by fallout and surge in the deposits of the Agnano-Monte Spina eruption (Campi Flegrei, Southern Italy). J. Volcanol. Geotherm. Res. 133, 193–210.
Dellino, P., Isaia, R., Veneruso, M., 2004b. Turbulent boundary layer shear flows as an approximation of base surges at Campi Flegrei (Southern Italy). J. Volcanol. Geotherm. Res. 133, 211–228.
Dellino, P., Mele, D., Bonasia, R., Braia, G., La Volpe, L., Sulpizio, R., 2005. The analysis of the influence of pumice shape on its terminal velocity. Geophys. Res. Lett. 32, L21306.
Dellino, P., Mele, D., Sulpizio, R., La Volpe, L., Braia, G., 2008. A method for the calculation of the impact parameters of dilute pyroclastic density currents based on deposits particle characteristics. J. Geophys. Res. 113, B07206.
Doronzo, D.M., Dellino, P., 2011. Interaction between pyroclastic density currents and buildings: numerical simulation and first experiments. Earth Planet. Sci. Lett. 310, 286–292.
Douillet, G.A., Tsang-Hin-Sun, E., Kueppers, U., Letort, J., Pacheco, D.A., Lavallee, Y., Goldstein, F., Hanson, J.B., Bustillos, J., Robin, C., Ramón, P., Dingwell, D.B., 2013a. Cross-stratified, ash sedimentary wedges deposited from the 2006 dilute pyroclastic density currents at Tungurahua volcano, Ecuador. Bull. Volcanol. 75, 765.
Douillet, G.A., Pacheco, D.A., Kueppers, U., Tsang-Hin-Sun, E., Dingwell, D.B., 2013b. Dune bedforms produced by the 2006 pyroclastic density currents at Tungurahua volcano, Ecuador. Bull. Volcanol. 75, 762.
Druitt, T.H., 1996. Pyroclastic density currents. In: Gilbert, J.S., Sparks, R.S.J. (Eds.), The Physics of Explosive Volcanic Eruptions. Geological Society, London, Special Publications, 145, pp. 145–182.
Durán, O., Hermann, H., 2006. Modeling of saturated sand flux. J. Stat. Mech. 7, P07011.
Durán, O., Claudin, P., Andreotti, B., 2011. On aeolian transport: grain-scale interactions, dynamical mechanisms and scaling laws. Aeolian Res. 3, 243–270.
Fisher, R.V., Waters, A.C., 1969. Bed forms in base surge deposits: lunar implications. Science 165, 1349–1352.
Garratt, J.R., 1992. The Atmospheric Boundary Layer. Cambridge Atmospheric and Space Science Series.
Grimmond, C.S.B., Oke, T.R., 1998. Aerodynamic properties of urban areas derived from analysis of surface form. J. Appl. Meteorol. 38, 1262–1292.
Iversen, J.D., Rasmussen, K.R., 1994. The effect of surface slope on saltation threshold. Sedimentology 41, 721–728.
Iversen, J.D., Rasmussen, K.R., 1999. The effect of wind speed and bed slope on sand transport. Sedimentology 46, 723–731.
Iversen, J.D., Pollack, J.B., Greeley, R., White, B.R., 1976. Saltation threshold on Mars: the effect of interparticle force, surface roughness, and low atmospheric density. Icarus 29, 381–393.
Iversen, J.D., Greeley, R., Marshall, J.R., Pollack, J.B., 1987. Aeolian saltation threshold: the effect of density ratio. Sedimentology 34, 699–706.
Kieffer, S.W., Sturtevant, B., 1988. Erosional furrows formed during the lateral blast at Mount St. Helens, May 18, 1980. J. Volcanol. Geotherm. Res. 93 (B12), 14793–14816.
Kok, J.F., Renno, N.O., 2009. A comprehensive model of steady state saltation (COMSALT). J. Geophys. Res. 114, D17204.
Lacroix, A., 1904. La Montagne Pelée et ses éruptions. Masson, Paris.
Lajoie, J., Boudon, G., Bourdier, J.L., 1989. Depositional mechanics of the 1902 pyroclastic nuée ardente deposits of Mt. Pelée, Martinique. J. Volcanol. Geotherm. Res. 38, 131–142.

Lang, J., Winsemann, J., 2013. Lateral and vertical relationships of bedforms deposited by aggrading supercritical flows: from cyclic steps to humpback dunes. Sediment. Geol. 296, 36–54. http://dx.doi.org/10.1016/j.sedgeo.2013.08.005.
Le Roux, J.P., 2005. Comments on "Turbulent boundary layer shear flows as an approximation of base surges at Campi Flegrei (Southern Italy), by Dellino et al. (2004). J. Volcanol. Geotherm. Res. 141, 331–332.
Lullin, A., 1925. Recherches sur les températures d'inflammation du bois et sur les enduits ignifuges. PhD Thesis Ecole Polytechnique fédérale Zurich.
Merrison, J.P., 2012. Sand transport, erosion and granular electrification. Aeolian Res. 4, 1–16.
Middleton, G.V., 1976. Hydraulic interpretation of sand size distributions. J. Geol. 84, 405–426.
Miller, M.C., McCave, I.N., Komar, P.D., 1977. Threshold of sediment motion under unidirectional currents. Sedimentology 24, 507–527.
Nikuradse, J., 1933. Stromungsgesetze in rauhen Rohren: VDI Forschungsheft 361. translation by National Advisory Committee on Aeronautics, Technical Memorandum No. 1292, Washington, DC, 1950.
Owen, P.R., 1964. Saltation of uniform grains in air. J. Fluid Mech. 20 (2), 225–242.
Prave, A.R., 1990. Clarification of some misconceptions about antidunes geometry and flow character. Sedimentology 37, 1049–1052.
Rasmussen, K.R., Mikkelsen, H.E., 1990. Wind Tunnel observations of aeolian transport rates. Acta Mech. 1 (Suppl. 2), 135–144.
Rasmussen, K.R., Iversen, J.D., Rautaheimo, P., 1996. Saltation and wind–flow interaction in a variable slope wind tunnel. Geomorphology 17, 19–28.
Sherman, D.J., 1992. An equilibrium relationship for shear velocity and apparent roughness length in aeolian saltation. Geomorphology 5, 419–431.
Shields, A., 1936. Application of similarity principles and turbulence research to bed-load movement. Mitteilungen der Preussischen Versuchsanstalt fur Wasserbau und Schifbau, Berlin. In: Ott, W.P., van Uchelen, J.C. (Eds.), California Inst. Tech., W.M. Keck Lab. of Hydraulics and Water Resources, Rept. No. 167.
Simons, D.B., Richardson, E.V., Haushild, W.L., 1963. Some effects of fine sediment on flow phenomena. U. S. Geol. Surv. Water Supply Pap. 1498-G (47 pp.).
Sohn, Y.K., 1997. On traction carpet sedimentation. J. Sed. Res. 67 (3), 502–509.
Sparks, R.S.J., 1976. Grain size variations in ignimbrites and implications for the transport of pyroclastic flows. Sedimentology 23, 147–188.
Sparks, R.S.J., 1983. Mont Pelée Martinique May 8 and May 20 1902 pyroclastic flows and surges—discussion. J. Volcanol. Geotherm. Res. 19, 175–184.
Sparks, R.S.J., Wilson, L., Hulme, G., 1978. Theoretical modeling of the generation, movement and emplacement of pyroclastic flows by column collapse. J. Geophys. Res. 83, 1727–1739.
Sulpizio, R., Mele, D., Dellino, P., La Volpe, L., 2007. Deposits and physical properties of pyroclastic density currents during complex Subplinian eruptions: the AD 472 (Pollena) eruption of Somma-Vesuvius, Italy. Sedimentology 54, 607–635.
Sulpizio, R., Bonasia, R., Dellino, P., Mele, D., Di Vito, M.A., La Volpe, L., 2010. The pomici di avellino eruption of Somma-Vesuvius (3.9 ka BP). Part II: sedimentology and physical volcanology of pyroclastic density current deposits. Bull. Volcanol. 72 (5), 559–577.
Sumner, E.J., Amy, L.A., Talling, P.J., 2008. Deposit structure and processes of sand deposition from decelerating sediment suspensions. J. Sed. Res. 78, 529–547.
Tanguy, J.C., Ribière, C., Scarth, A., Tjetjep, W.S., 1998. Victims from volcanic eruptions: a revised database. Bull. Volcanol. 60, 137–144.
Valentine, G.A., 1987. Stratified flow in pyroclastic surges. Bull. Volcanol. 49, 616–630.
Vallis, G.K., 2006. Atmospheric and Oceanic Fluid Dynamics—Fundamentals and Large Scale Circulation. Cambridge University Press (ISBN: 978-0-521-84969-2).
Walker, G.P.L., 1971. Grain-size characteristics of pyroclastic deposits. J. Geophys. Res. 79, 619–714.
Walker, G.P.L., 1984. Characteristics of dune-bedded pyroclastic surge bedsets. J. Volcanol. Geotherm. Res. 20, 281–296.
Walker, G.P.L., McBroome, L.A., 1983. Mount St. Helens 1980 and Mount Pelée 1902—flow or surge. Geology 11, 571–574.
Walker, G.P.L., Wilson, L., Bowell, E.L.G., 1971. Explosive volcanic eruptions—I. The rate of fall of pyroclasts. Geophys. J. R. Astron. Soc. 22, 377–383.
Wohletz, K.H., 1998. Pyroclastic surges and compressible two-phase flow. In: Freundt, A., Rosi, M. (Eds.), From Magma to Tephra. Elsevier, Amsterdam, p. 25.
Zheng, X., He, L., Wu, J., 2004. Vertical profiles of mass flux for windblown sand movement at steady state. J. Geophys. Res. 109, B01106. http://dx.doi.org/10.1029/2003JB002656.

This page was intentionally left blank.

Figure 4.11: Painting, drawing and collage by Almut Winkler interacting with photocopies of Douillet et al. 2014 and Finizola et al. 2006. Almut Winkler (2014).

This page was intentionally left blank.

Chapter 5

Syn-eruptive soft-sediment deformation in deposits of dilute pyroclastic density currents: granular shear, impact and shock wave triggers.

This chapter was in open discussion in the Journal "Solid Earth (EGU)" during the review process of the PhD. The final version was inserted in the manuscript after corrections from the jury. It describes soft sediment deformation structures found in deposits of dilute pyroclastic density currents. Their interpretation permits to retrieve important information about the flow, eruption, and deposition of dilute pyroclastic density currents.

Reference: *Douillet G.A., Taisne B., Tsang-Hin-Sun E., Müller S.K., Kueppers U., Dingwell D.B. 2015. Syn-eruptive, soft-sediment deformation of deposits from dilute pyroclastic density current: triggers from granular shear, dynamic pore pressure, ballistic impacts and shock waves. Solid Earth, 6, 1-20. doi:10.5194/se-6-1-2015*

This page was intentionally left blank.

Solid Earth, 6, 553–572, 2015
www.solid-earth.net/6/553/2015/
doi:10.5194/se-6-553-2015

Solid Earth Open Access

Syn-eruptive, soft-sediment deformation of deposits from dilute pyroclastic density current: triggers from granular shear, dynamic pore pressure, ballistic impacts and shock waves

G. A. Douillet[1], B. Taisne[2], È. Tsang-Hin-Sun[3], S. K. Müller[4], U. Kueppers[1], and D. B. Dingwell[1]

[1]Earth and Environmental Sciences, Ludwig-Maximilians-Universität, Munich, Germany
[2]Earth Observatory of Singapore, Nanyang Technological University, Singapore
[3]Université of Brest and CNRS, Laboratoire Domaines Océaniques, Plouzaré, France
[4]Meteorological Institute, Ludwig-Maximilians-Universität, Munich, Germany

Correspondence to: G. A. Douillet (g.douillet@min.uni-muenchen.de)

Received: 17 November 2014 – Published in Solid Earth Discuss.: 16 December 2014
Revised: 16 April 2015 – Accepted: 20 April 2015 – Published: 21 May 2015

Abstract. Soft-sediment deformation structures can provide valuable information about the conditions of parent flows, the sediment state and the surrounding environment. Here, examples of soft-sediment deformation in deposits of dilute pyroclastic density currents are documented and possible syn-eruptive triggers suggested. Outcrops from six different volcanoes have been compiled in order to provide a broad perspective on the variety of structures: Soufrière Hills (Montserrat), Tungurahua (Ecuador), Ubehebe craters (USA), Laacher See (Germany), and Tower Hill and Purrumbete lakes (both Australia).

The variety of features can be classified in four groups: (1) tubular features such as pipes; (2) isolated, laterally oriented deformation such as overturned or oversteepened laminations and vortex-shaped laminae; (3) folds-and-faults structures involving thick (> 30 cm) units; (4) dominantly vertical inter-penetration of two layers such as potatoids, dishes, or diapiric flame-like structures.

The occurrence of degassing pipes together with basal intrusions suggest fluidization during flow stages, and can facilitate the development of other soft-sediment deformation structures. Variations from injection dikes to suction-driven, local uplifts at the base of outcrops indicate the role of dynamic pore pressure. Isolated, centimeter-scale, overturned beds with vortex forms have been interpreted to be the signature of shear instabilities occurring at the boundary of two granular media. They may represent the frozen record of granular, pseudo Kelvin–Helmholtz instabilities. Their recognition can be a diagnostic for flows with a granular basal boundary layer. Vertical inter-penetration and those folds-and-faults features related to slumps are driven by their excess weight and occur after deposition but penecontemporaneous to the eruption. The passage of shock waves emanating from the vent may also produce trains of isolated, fine-grained overturned beds that disturb the surface bedding without occurrence of a sedimentation phase in the vicinity of explosion centers. Finally, ballistic impacts can trigger unconventional sags producing local displacement or liquefaction. Based on the deformation depth, these can yield precise insights into depositional unit boundaries. Such impact structures may also be at the origin of some of the steep truncation planes visible at the base of the so-called “chute and pool” structures.

Dilute pyroclastic density currents occur contemporaneously with seismogenic volcanic explosions. They can experience extremely high sedimentation rates and may flow at the border between traction, granular and fluid-escape boundary zones. They are often deposited on steep slopes and can incorporate large amounts of water and gas in the

sediment. These are just some of the many possible triggers acting in a single environment, and they reveal the potential for insights into the eruptive and flow mechanisms of dilute pyroclastic density currents.

1 Introduction

The dynamics of pyroclastic density currents (PDCs) remain poorly understood. This is despite the fact that they are one of the most efficient transport means on the flanks of volcanoes exhibiting explosive eruptions, thereby yielding a major risk potential for life, environment and infrastructures. Analogue and numerical modeling approaches are well-suited to investigate targeted hypothesized processes, but the question of which process to model can only be answered through real PDC data. Cross-bedded, dilute PDC deposits can contain intriguing overturned and deformed patterns attributed to soft-sediment deformation (SSD). The understanding of these structures can yield insight into the syn- and post-depositional processes surrounding the bed interface: i.e., the basal boundary layer (BBL), the bed state, and conditions extant in the emplacement environment. In particular, syn-depositional SSD structures provide constraint on the shearing and dynamic pore pressure at the BBL that controls the sedimentation of PDCs, whereas syn-eruptive SSD records information on the eruptive dynamics and depositional units. PDCs are largely emplaced subaerially under metastable deposition state favoring SSD. Thus a variety of specific SSD triggers may occur during an eruption and PDC deposits represent excellent targets for studies of SSD.

1.1 Soft-sediment deformation

Occasionally, stratified sediments exhibit anomalous patterns that cannot be explained by simple depositional schemes, and are understood as soft-sediment deformation (SSD) i.e., changes in the initial bed structure. This occurs during or shortly after deposition and prior to consequent diagenesis (Van Loon, 2009; Owen et al., 2011). SSD has been documented for subaqueous clastic sediments from the mud to coarse sand range (Van Loon, 2009; Owen and Moretti, 2011), including turbidites (Moretti et al., 2001), subglacial environments (Ghienne, 2003; Denis et al., 2010; Douillet et al., 2012; Pisarska-Jamroży and Weckwerth, 2013), carbonates (Ettensohn et al., 2011; Chen and Lee, 2013), and volcanic ash (Gibert et al., 2011). In subaerial environments, SSD is documented from earthquake-triggered liquefaction and can form sand blows and dykes.

A variety of triggers can be involved (Owen and Moretti, 2011), generally predominantly related to seismically induced liquefaction (Sediment. Geol. 235, Nichols et al., 1994; Mohindra and Bagati, 1996; Owen, 1996b; Owen and Moretti, 2011), but also to tsunami waves (Alsop and Marco, 2012), storms (Chen and Lee, 2013) or volcanic base surges (Crowe and Fisher, 1973).

1.1.1 Nomenclature

There is neither a single classification scheme nor agreement on the nomenclature of SSD patterns (e.g., Lowe, 1975; Owen, 1987; Van Loon, 2009; Owen et al., 2011). Here, a non-generic nomenclature based on descriptive characteristics is employed.

Pipes: masses of sediments having different characteristics compared to the surrounding unit and with a relatively tubular shape. Used here as a generic descriptive umbrella term for structures such as dikes or pillars (e.g., Mills, 1983; Nichols et al., 1994; Owen, 2003; Owen and Moretti, 2008; Douillet et al., 2012). Degassing (or de-watering) structures or injection dikes are interpretative terms of pipes.

Overturned laminae/beds and *vortex bedding*: a few laminations or layers that show a coherent recumbent overturning, generally aligned with the parent flow direction given by nearby sedimentary structures. They are laterally confined in otherwise undisturbed bedding. They can occur in sets of downstream repetitive but isolated patterns. They are distinct from *overturned stratification*, which is an overturning of a stratal package as a whole (Allen and Banks, 1972; Røe and Hermansen, 2006; Bridge and Demicco, 2008, p. 357–358). Vortex lamination/bedding is similar as overturned laminae/beds, but with a vortex shape (Rowley et al., 2011). "Vorticity" is preferred to "rotation" here and throughout since any simple shear deformation includes a rotational component.

Folds-and-faults structures: units involving several beds showing folding as well as discontinuities (microfaults) leading to concatenation (overlap). The general organization tends toward overturning with a coherent orientation (e.g., Odonne et al., 2011; Alsop and Marco, 2011). The term "slumped beds" is avoided because of its interpretative sense.

Potatoids, *dishes* and *diapiric flame-like structures*: result from the movement of two layers of significantly different characteristics (densities, grain size) that penetrate into each others. Potatoids result of dominantly vertical movement forming deformations with irregular rounded shapes. They are generally massive. Attached/detached potatoid is used to emphasize whether the intrusive body is still connected to the layer it initially belonged to or not (e.g., Owen, 1996a). Dishes are thin and tabular detached masses. Diapiric flame-like structures are laterally persistent deformation patches destroying the initial bedding. They have no coherent recumbence and dominantly vertical patterns (Crowe and Fisher, 1973; Owen, 1996b; Niebling et al., 2010). They are distinguished from convolute/contorted bedding, the latter preserving the original bed set succession (Owen et al., 2011). Terms such as load-casts or pseudo nodules are avoided here since they contain an interpretation on their formation.

The interpretation of the trigger mechanism(s) for SSD is not always straightforward and can include a combination of different effects. Here, distinction is made between the deformation, the agent of deformation, and the trigger. The deformation tensor in rock mechanics can be written as a sum of components of stretching, pure shear and simple shear (rotation). Identification of the relationships with the surroundings permits the interpretation of the physical agents responsible for the deformation as well as possible triggers.

Of interest here is the distinction between (1) syn-sedimentary BBL (flow) shearing and dynamic pore pressure effects, (2) intra-deposit movements, and (3) post depositional mass movements. Bioturbation and biochemical effects are not dealt with here. BBL shearing includes the effects of the flow drag during or directly after sedimentation. It can be enhanced by the sediment state and the nature of the BBL. Intra-deposit movements lead to sediment fabric rearrangement and deformation. These are often related to the expelling of trapped fluids during or after sedimentation, in situ releases, or compaction and loading. Mass movements are understood here as slumping, i.e., a short-scale, rather coherent sediment re-mobilization, the limit of which is taken to be debris flows. At the origin of the deformation, a trigger can occur – a phenomenon that is not directly described in terms of the forces producing the deformation, but is causally responsible for their generation (e.g., ground-shaking facilitating liquefaction of sediment, favoring fluid movements and producing ball-and-pillow structures).

1.2 PDCs and their possible SSD triggers

As particulate density currents, the depositional processes of PDCs are fundamental in their dynamics, since particles are both the agent of excess density driving momentum and the resulting sediment. Extreme and varied flow-substrate BBL processes may occur. The classification of Branney and Kokelaar (2002) emphasizes BBL processes and theorizes a classification into four end-member types: granular-, fluid-escape-, fallout-, and traction-dominated BBLs. Douillet et al. (2014) discussed different types of cross-bedding aggradation patterns as an upper or lower limit of the saltation threshold (the minimum shearing required to put grains in motion by wind), thus supposing a tractional BBL scheme. Alternatively, emplacement can be envisioned as a series of pulses with high basal concentration and no relationship to saltation, regardless of averaged concentration (Doronzo and Dellino, 2014), or stepwise en-masse deposition (Sulpizio and Dellino, 2008). The understanding of the nature and significance of BBL processes for PDCs may be further augmented by the study of syn-depositional SSD.

PDC deposits often display SSD (also “soft-state deformation”, Branney and Kokelaar, 1994, 2002). This may be associated with subaqueous eruptions (Fiske, 1963) or subaqueous deposition (Brand and White, 2007; Brand and Clarke, 2009; Jordan et al., 2013), but also importantly, subaerial emplacement (Vazquez and Ort, 2006). Hot-state, plastic deformation including partial deformation of the clasts themselves is referred to as rheomorphism (Branney et al., 2004; Andrews and Branney, 2011). Lava flows may also deform underlying soft-sediment beds (Rawcliffe and Brown, 2014). The high sedimentation rate characteristic of particulate density currents results in metastable deposits prone to further re-arrangement (Smith and Kokelaar, 2013). Moreover, the variations from very fine to very coarse beds typical of pyroclastic deposits as well as common inverse grading make them susceptible to SSD after deposition (Gibert et al., 2011).

In addition to their metastable nature, the eruptive environment itself is subject to a variety of triggers. Seismic activity associated with eruption further destabilizes freshly emplaced pyroclasts. Syn-PDC processes can be recorded in SSD (Crowe and Fisher, 1973), and the likely formation of traction carpets and granular BBL can produce granular shear instabilities (Rowley, 2010; Rowley et al., 2011; Smith and Kokelaar, 2013). “Flame-like” structures are often reported (McDonough et al., 1984; Valentine et al., 1989; Brand and White, 2007; Brand and Clarke, 2009) and when interpreted as sheared structures, can serve to reconstruct paleo-flow directions (Giannetti and Luongo, 1994; Brown et al., 2008). Fluid escape SSD (dikes, pipes, plumes, pillars) can occur by escape of water accompanying phreatomagmatic eruptions (Nocita, 1988, -later reinterpreted as water-escape in fluvial deposits by McPherson et al. (1989)), degassing of fresh pyroclasts (Gernon et al., 2008, 2009), burning underlying vegetation, or be due to thermal expansion (Branney and Kokelaar, 2002, p. 61–66, and references therein). Interestingly, the high deposition rates combined with possible fluidized state of the flow can trap gases in the deposits that subsequently escape as degassing pipes within seconds after deposition (Komorowski et al., 2013). These can occur as fines-depleted pipes, a few centimeters in length and diameter (Pistolesi et al., 2011; Smith and Kokelaar, 2013), or large decimeter–meter scale depressions at the surface of deposits (Charbonnier and Gertisser, 2008). The high deposition rates also trigger simple load casts (Mattsson and Tripoli, 2011). Blocks ejected ballistically during an eruptive event deform the fresh deposits by landing (Gençalioğlu-Kuşcu et al., 2007; Jordan et al., 2013). Post eruptive processes are also common on steep sided volcanic edifices, with freshly deposited material likely to be unstable and slump (Fiske and Tobisch, 1978; Voight et al., 1983; Branney and Kokelaar, 1994; Ward and Day, 2006) as well as inherent contraction and compaction fractures following emplacement (Whelley et al., 2012).

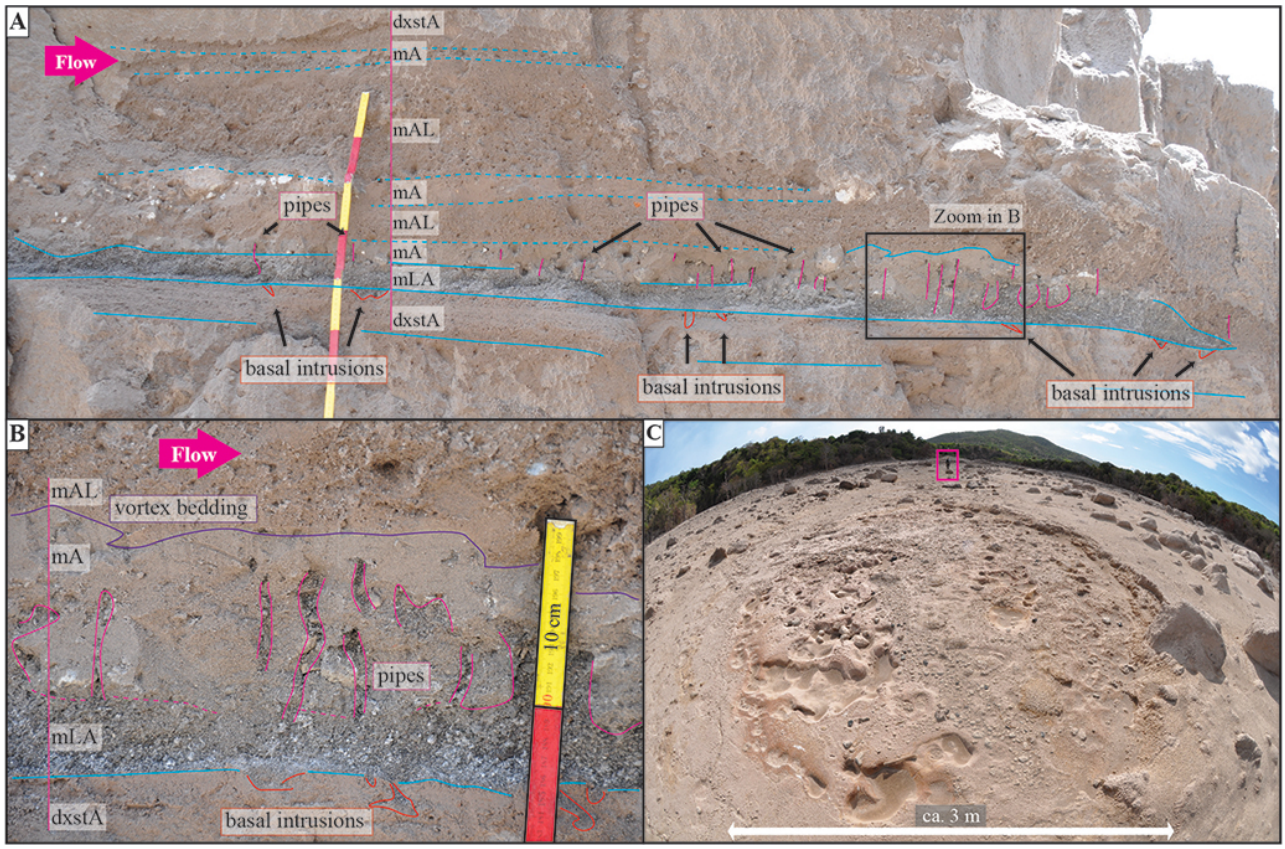

Figure 1. SSD from the 2010 dome collapse PDC deposits at Soufrière Hills in the Belham valley. **(a)** Degassing pipes occur in a massive ash (mA) layer, and seem to emanate from the underlying massive lapilli and ash layer (mLA). The base of the mLA layer also exhibits basal intrusions of small pipes, and attached potatoids in the underlying diffusely cross-stratified ash bed sets (dxstA). **(b)** Zoom in SSD structures. The upper contact is uneven with a vortex and undulating form. **(c)** Large-scale, circular depression, ca. 10 cm in throw. Note also smaller-scale structures within the main depression.

1.3 Granular shear instabilities

Observations of syn-flow shear structures bring further insights into the BBL processes of PDCs. Simple shear is often invoked for the formation of overturned stratification (e.g., Allen and Banks, 1972; Mills, 1983; Røe and Hermansen, 2006). For such structures, the flow transmits and imposes part of its shear stress to the ground and thus translates the uppermost beds. In the other hand, shear instabilities can be produced at the boundary between two fluids to form recurrent, vortex-shaped, Kelvin–Helmholtz instabilities. Valentine et al. (1989) suggested that flame-like SSD structures could be related to Kelvin–Helmholtz instabilities "between the bed load fluid and the overlying surge". Several analogue experimental studies with granular flows over grain beds have evidenced isolated but recurrent wave-like instabilities at the bed-flow interface (Goldfarb et al., 2002; Mangeney et al., 2010; Rowley, 2010; Roche et al., 2013; Farin et al., 2014). Goldfarb et al. (2002) have produced trains of wave instabilities with the shape of overturned laminae and noted that those were "likely produced by shearing differences" and "lacked any kind of vorticity". However, a rotational component must be present to produce the observed shark fin patterns. Rowley (2010) and Rowley et al. (2011) have imaged trains of shear instabilities with well-developed vortex bedding, convincingly interpreted as granular Kelvin–Helmholz instabilities. They further demonstrate the periodicity of these structures and document field examples. The wavy nature of those instabilities was further demonstrated in Farin et al. (2014), which also noted that the wavelength and amplitude are greatest for slopes close to the repose angle (highest speed). Roche et al. (2013) provided videos of the instabilities and an explanation for the fluid-like behavior of these instabilities. They suggested as a mechanism that negative dynamic pore pressures fluidize fine-grained beds and deform them as a whole rather than as individual grains. Other experimental work with granular flows has evidenced intriguing inter-penetration of beds over sinusoidal surfaces (Caicedo-Carvajal et al., 2006), longitudinal vortices in the

flow direction (Forterre and Pouliquen, 2001), or Taylor vortices (Conway et al., 2004).

2 Geological settings and occurrence of SSD structures

The SSD structures presented here belong to different volcanoes and both magmatic and phreatomagmatic eruptions of various intensities and depositional environments. As pointed by Mills (1983), SSD should be studied within their environment, and thus a brief context is introduced. Several types of SSD are identified with orders of magnitude between their dimensions as well as between the grain size of layers involved. Description of all discussed SSD structures is presented in Table 1.

2.1 Soufrière Hills (Montserrat)

The 11 February 2010 partial dome-collapse event of Soufrière Hills (Montserrat) produced a series of six block and ash flows, five of them occurring within 15 min, and was the largest event since the 1995 awakening (Wadge et al., 2014; Stinton et al., 2014). Numerous degassing pipes were observed in block and ash flow deposits as well as massive ash units (Stinton et al., 2014). Other post-depositional structures are described by Stinton et al. (2014) as "rootless phreatic explosion craters", i.e., structures related to hot blocks turning water into steam explosively. They can have diameters between 1 and 30 m, consist of "decimeter-sized blocks in a coarse ash-rich matrix derived from the underlying primary PDC deposits" and have a contact to underlying cross-bedded units or down to the pre-collapse surface. Here, SSD structures are documented from the Belham river valley less than 6 km from the vent (Fig. 1). According to Stinton et al. (2014), only three PDCs flowed in this drainage (stage 3-H, 4-K and 4–6), Wadge et al. (2014) also mentioning PDCs in this zone for the 11 February 2010 collapse. Basal, small-scale pipes and attached potatoids intrude underlying diffusely cross-stratified ash from a massive lapilli-and-ash lens, whereas fines-poor, small-scale pipes are found in the otherwise ash-rich, massive, overlying layer (Fig. 1a–b). The top of the latter has a contact with a series of three vortex and undulating forms (Fig. 1b). These deposits are found in the thalweg of the river valley, which may have contained some water. Another outcrop exhibits a large scale circular depression (ca. 3 m diam.) with ca. 10 cm deflation at the surface of the deposits (Fig. 1c).

2.2 Tungurahua (Ecuador)

The 17 August 2006 PDCs (Kelfoun et al., 2009; Douillet et al., 2013b; Hall et al., 2013; Bernard et al., 2014) are not linked to phreatomagmatic processes but rather to accumulation and subsequent destabilization of pyroclasts near the crater. The overbank sediments containing the SSD structures have been interpreted to have formed from dilute PDCs originating from dense PDCs by flow stripping (Douillet et al., 2013b). SSD was identified in a lacquer peel within well-developed millimeter-scale ash lamination (Fig. 2) located on the lee side (approx. 20 cm from the crest) of an aggrading, transverse dune bedform that indicated very high sedimentation rates (Douillet et al., 2013a) approx. 6 km from the vent. Two clusters of small-scale overturned and recumbent laminae occur at different height in the same horizons. The upper structure exhibits a single, well-developed overturned laminaset (Fig. 2b), whereas the lower one is a cluster of several recumbent overturned laminae forming a front followed by relatively massive material with diffuse oversteepened bedding in the upstream direction (Fig. 2c–d).

2.3 Ubehebe crater (California, USA)

Ubehebe tuff ring is part of the Holocene/Pleistocene Ubehebe Craters complex and may have erupted between 0.8 and 2.1 ka (Sasnett et al., 2012). They erupted onto ancient lake sediments, at least partially phreatomagmatically. The arid climate does not explain the phreatomagmatic activity and interaction with a shallow water table is preferred (Sasnett et al., 2012). Crowe and Fisher (1973) reported SSD structures such as contorted beds without preferred orientation, flame structures oriented with the flow direction and disrupted layers of thin tuff curled and pulled apart. They mapped the orientation of ballistic impact sags, mention post-eruption slumping on the northwestern and southeastern parts of the crater, and noted that SSD occurs within pre-existing channels filled with massive deposits but is absent in cross-bedded dominated overbanks. Here, a variety of SSD structures are documented from the southern flank: folds-and-faults, curled dishes, SSD from ballistic impact sags, a diapiric flame-like horizon and vortex features (Fig. 3).

2.4 Laacher See (Germany)

Laacher See was the location of a large eruption commonly attributed to phreatomagmatic explosions around 11 800 yrs B.P. (Schmincke et al., 1973). Dune bedforms cross-stratification made of coarse lapilli to fine ash intercalated with lapilli to volcanic dust fall horizons occur over tens of square kilometers. Three isolated SSD structures are found around the Wingertsbergwand area, several kilometers southward from the inferred vents (Fig. 4). A composite SSD structure several meters long and ca. 1 m thick occurs as a lateral series of tilted blocks that evolve into folds-and-faults beds in the (approximate) downstream direction, accommodating a local compression (Fig. 4a–f). It is abruptly confined in depth by the lower ash layer and underlying beds show no sign of deformation. A few tens of meters distant, a structure of similar dimensions characterized by very steep lamination and downward

Table 1. Main characteristics of SSD structures presented in figures and discussed in text. Abbreviations: F-F: folds-and-faults; P: potatoids; EP: elongate potatoids; PP: pipes; DFL: diapiric-flame-like; OtB/L: overturned bed/lamination; VB/L: vortex bed/lamination; OsB/L: oversteepened bed/lamination.

Location	Figure	SSD type	Description	Dimensions	SSD orientation	Involved beds	Underlying beds	Overlying beds	Water	Interpretation
Soufrière Hills	1a, b	P, EP, PP, VL	Dark lapilli ash layer concentrating SSD at its boarders	PP: 1 cm diam., < / 10 cm long, P: 3–8 cm, VL and EP: 2–4 cm	P unsheared VL with flow	Dark massive lapilli-ash layer and overlying massive ash layer	Diffusely stratified ash layer	Massive ash and lapilli layer	No	Basal D injections from over-pressured fluidized flow and degassing P from deflation after deposition
Soufrière Hills	1c	Depression	Circular depression at the surface	ca. 3 m diam., 10 cm depression	No orientation	Probably whole unit	/	/	Unlikely	Compaction structure by gas escape and grain re-arrangement
Tungurahua	2b	OtL/VL	Recumbent shark fin	1 cm amplitude, 3 and 5 cm length	Parallel to flow	six and seven laminae of ash	Similar ash lamination	Similar ash lamination	No	Granular Kelvin–Helmholtz instability
Tungurahua	2c	OtL	Recumbent tailing anticlines	0.8 cm amplitude, 3 cm	Parallel to flow	seven laminar of ash	Ripple cross-lamination	Similar ash lamination	No	Granular shear instability, possibly Kelvin–Helmholtz instability
Ubehebe	3a, c	F-F	Stack of angular folds imbricated by small thrust faults	Involved beds ca. 20 cm thick and 50 cm between faults	Toward a channel thalweg	ca. 20 cm-thick successions of massive fine ash, planar laminated fine ash, coarse ash, and planar laminated fine ash	Massive ash with deformed lenses of the remnants of a coarser horizon	Apparently massive fine ash and volcanic dust. Produce small scale SSD at the contact	Likely	Slump fold during channel reopening; wet sediment
Ubehebe	3b	Curled, isolated dishes	Curled and isolated layers of coarse ash	30–50 cm-long layers, few centimeters thick	No orientation	Layers of planar ash/coarse ash with local small scale DFL SSD	Massive ash	Massive ash	Likely	Detached clusters; granular Rayleigh–Taylor instabilities
Ubehebe	3d top	DFL	Chaotic vertical SSD, possible orientation recumbent with flow	ca. 15 cm amplitude; few centimeters-thick beds	Outcrop sub parallel to a channel	Diffuse planar bed set of ash and underlying massive fine ash	Massive fine ash	Sub-planar centimeters-thick fine ash overlain by planar, centimeters-thick coarse ash	Likely	Granular Rayleigh–Taylor instabilities
Ubehebe	3d mid right	OtB	Lonely, recumbent tailing anticline	ca. 5 cm thick and long	Outcrop sub parallel to a channel	Boarder between two layers of massive ash	Massive fine ash with clasts (dark)	Massive fine ash (gray)	Possible	Granular shear instability
Ubehebe	3d base	VB	Recumbent shark fin and vortices	5 cm thick and long	Outcrop sub parallel to a channel	Limit between two layers	Massive fine ash with clasts (dark)	Massive fine ash with less clasts (lighter)	Possible	Granular Kelvin Helmholtz instabilities
Ubehebe	3e	P, EP, sag	Impact sag underlain by P and small EP	0–5 cm amplitude P; 5–10 cm long EP	Unrelated to flow	Few centimeters-thick massive coarse ash	Massive to faintly planar-stratified ash	Roughly planar-stratified coarse ash laminations	Likely	Impact-induced liquefaction of the porous and water-saturated coarse ash
Laacher See	4a–f	Composite	Tilted blocks/concave beds with DFL/angular F-F concave beds/P/OsB	ca. 50–80 cm thick; ca. 5 m long	Roughly outward crater	sequence of faintly bedded ash and lapilli as well as ash beds	lapilli layer overlain by a thin (few cm) layer of ash	Cross-bedded lapilli and ash and two impact sags	Possible	Impact of bouncing block
Laacher See	4g–i	Composite	concave beds/P/OsB	ca. 50–80 cm thick / ca. 3 m long	Roughly outward crater	faintly bedded ash and lapilli	diffuse fore-front of massive ash	lens of large clasts	Possible	Impact of bouncing block with induced liquefaction
Laacher See	4g, h	Lonely anticline	Single upright convex bed (anticline)	15 cm amplitude and length	Sub-parallel to flow	5 cm of otherwise planar bedded ash	Faintly laminated coarse lapilli layer overlain by a massive layer of ash	Cross-bedded lapilli and ash with stoss-depositional dune bedform	Possible	Dynamic or pore pressure driven. Possibly triggered by the presence of overlying dune bedform
Tower Hill	5	In train OsB	Train of slightly OsB/OtB beds within ripple cross laminations	ca. 10 cm amplitude; ca. 50 cm wavelength, in train repetitions over 100 s m	Aligned with ripple bedding	ca. 40 cm-thick, fine ash bed set, with ripple cross-laminations.	Massive, coarse ash fining-up by increasing occurrence of thin sub-planar ash beds	Grading back into massive coarse-ash with reverse sequence	Probable	Shock wave destabilization
Purrumbete	6a, b, e	OtB; F-F	Trains of F-F showing VB. Evolution from gentle to ploughing SSD	Increase in amplitude and pseudo wavelength from 5 to 25 cm over 1.5 m	Outward crater	Planar laminated ash bed sets and underlying massive fine ash	Massive, clast rich, fine ash beds	Finely planar-laminated fallout ash	Possible	Shock wave destabilization
Purrumbete	6c, d	DFL	Chaotic DFL SSD	ca. 20 cm amplitude	Perpendicular to rim	Same outcrop	Same outcrop	Same outcrop	Possible	Possible fluid escape

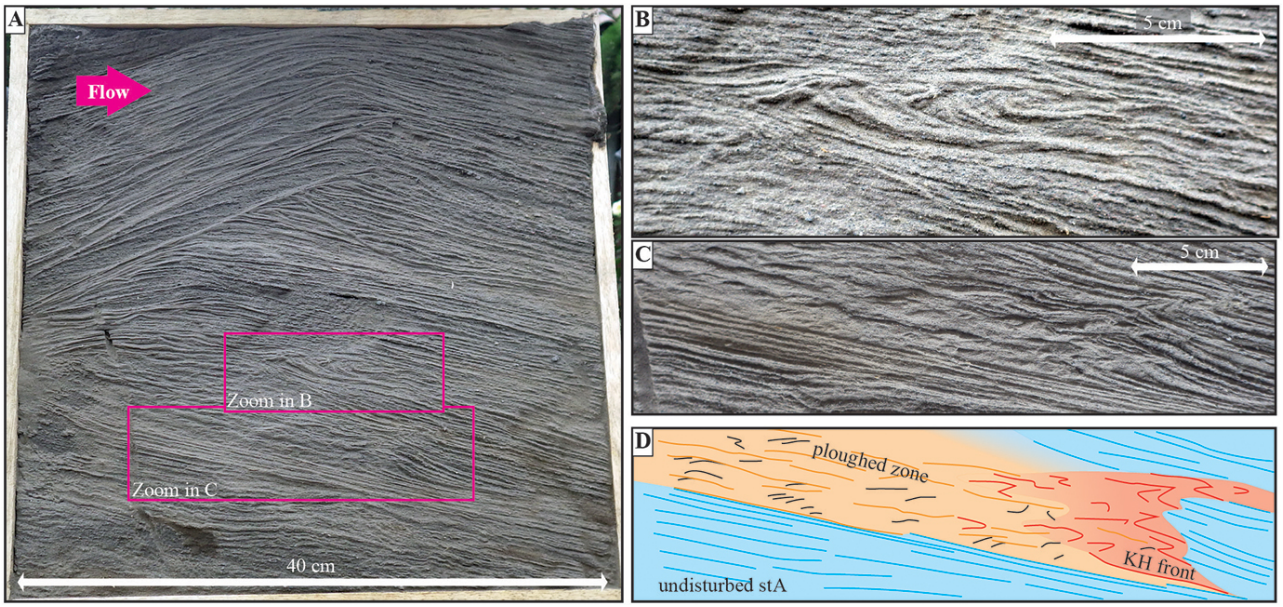

Figure 2. Overturned laminations from Tungurahua in the Achupashal valley (see Douillet et al., 2013a) illustrating shear in a granular BBL (imprint from lacquer peel). **(a)** Peel showing stoss-depositional ash bed sets, insets highlight the borders of **(b)** and **(c)**. **(b)** Imbricated, downflow-recumbent, vortex-shaped SSD structure. Panels **(c)** and **(d)** show recumbent and tailing overturned laminae form a front of deformation. The zone upstream the front contrasts with the downstream undisturbed bedding: it is comparatively massive, with thick beds and diffuse oversteepened stratification attributed to the ploughing effect of the downstream moving shear instabilities from the deformation front.

oriented, massive, lapilli potatoids resembles a "chute and pool" structure (Fig. 4g–i). A further structure, approx. 150 m away, has a convex symmetrical form (ca. 10 cm vertical displacement) in an initially planar fine-grained bed. It is intercalated above a massive ash bed and below coarse-ash to lapilli, sub-planar, diffuse bed sets (Fig. 4j–k). Flow direction inferred from overlying cross beds is roughly oriented from left to right but may be sub-parallel to the outcrop wall. The bed is partly missing on the right from the deformation. Similar ash layers pinch out above the convex shape and may represent an overlap of the same unit.

2.5 Tower Hill (Victoria, Australia)

Tower Hill maar (ca. 35 000 yrs B.P., Sherwood et al., 2004; Prata and Cas, 2012) exhibits intriguing trains of oversteepened laminations contained within a single bed set (Fig. 5). They outcrop in the upper part of the Southern rim (CRB quarry), parallel to the crater wall. Underlying beds fine up from massive coarse ash and lapilli by increasing occurrence of thin, sub-planar, ash beds forming a diffusely stratified lapilli-ash facies. This grades into the fine-grained ripple beds with topping SSD and the reverse sequence occurs above. This sequence suggests a fall phase progressively influenced by pseudo base surges (in the sense of Waters and Fisher, 1971) with increasingly efficient fragmentation related to phreatomagmatic explosions at the fine-grained SSD bed sets (optimally efficient water:magma ratio in Prata, 2012). The flow direction inferred from the underlying ripple bedding is oriented roughly parallel to the lateral extension of the outcrop (Prata, 2012). The SSD consists of isolated, oversteepened laminations with coherent orientation. They are recurrent with wavelength of ca. 50 cm and over hundreds of m.

2.6 Purrumbete Lake (Victoria, Australia)

The deposits forming the Purrumbete maar (ca. 20 000 yrs B.P.) are characterized by three temporally separated eruption phases and vent locations, with relatively dry as well as wet phreatomagmatic conditions (Jordan et al., 2013). Ballistic bombs with impact sags are widespread in these deposits, suggesting wet deposits (Jordan et al., 2013). The SSD documented here outcrops with two faces at right angles. Perpendicular to the crater, folds-and-faults structures increase in size, faulting and recumbence outward from the vent and seem to have a recurrence and increasing wavelength (Fig. 6a–b, e). Parallel to the rim, only chaotic flame-like structures are visible (Fig. 6c–d). The overlying deposits are planar laminated ash with individual laminae followed over several meters. They lie conformably on the SSD horizon and are related to fallout.

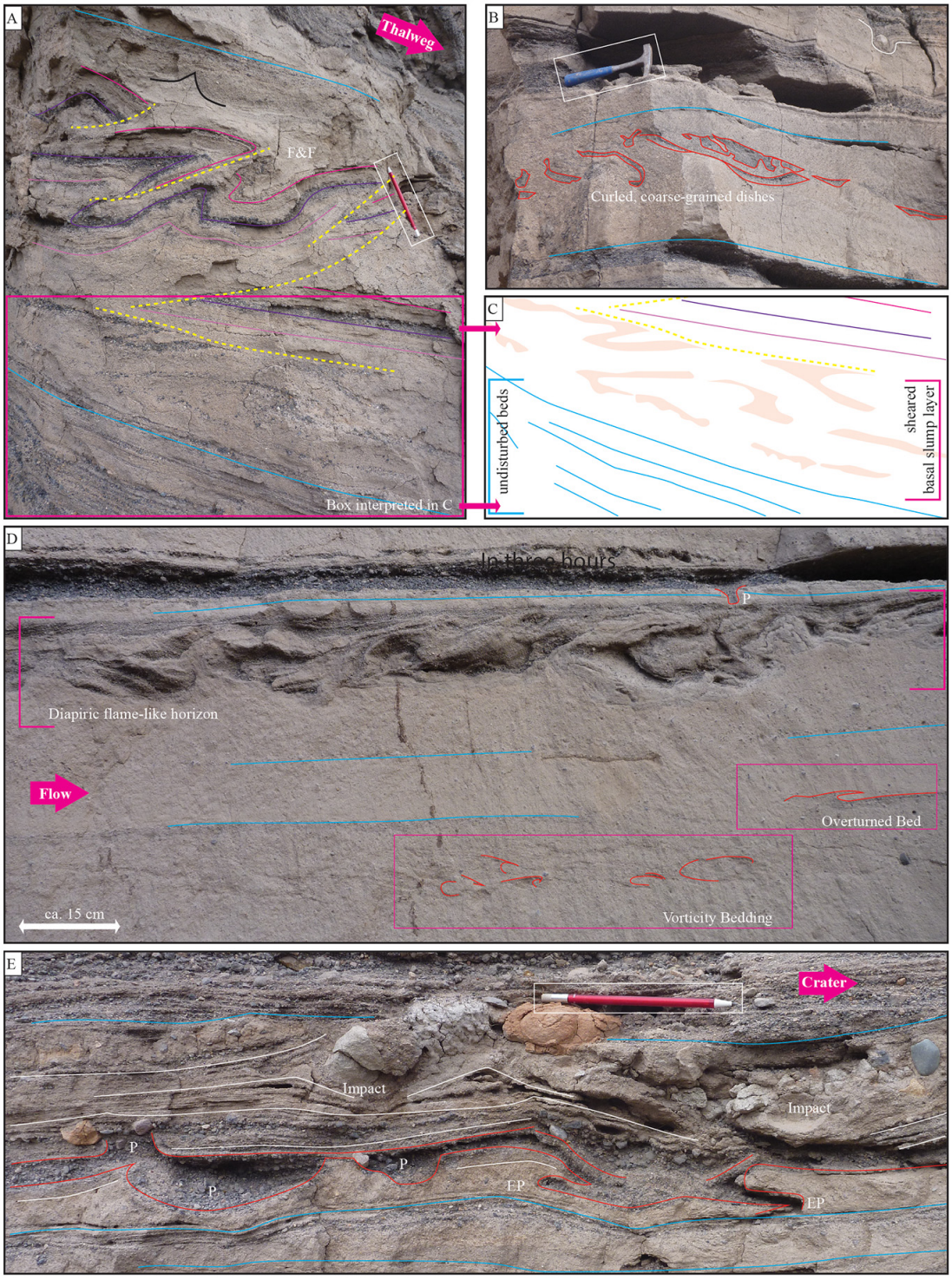

Figure 3. SSD structures from Ubehebe craters. **(a)** Folds-and-faults structure (F&F) related to slump, with interpretation of the outlined lower part in **(c)**. **(b)** Curled and pulled apart coarse-grained dishes interpreted as detached from the above. **(d)** Diapiric flame-like structures in upper part and a single downward-oriented, attached potatoid (P), recumbent overturned bed in the middle right, vortex beds in the lower part. **(e)** Interpenetrating coarse bed with potatoids and elongate potatoids (EP) at the base of ballistic impact sags.

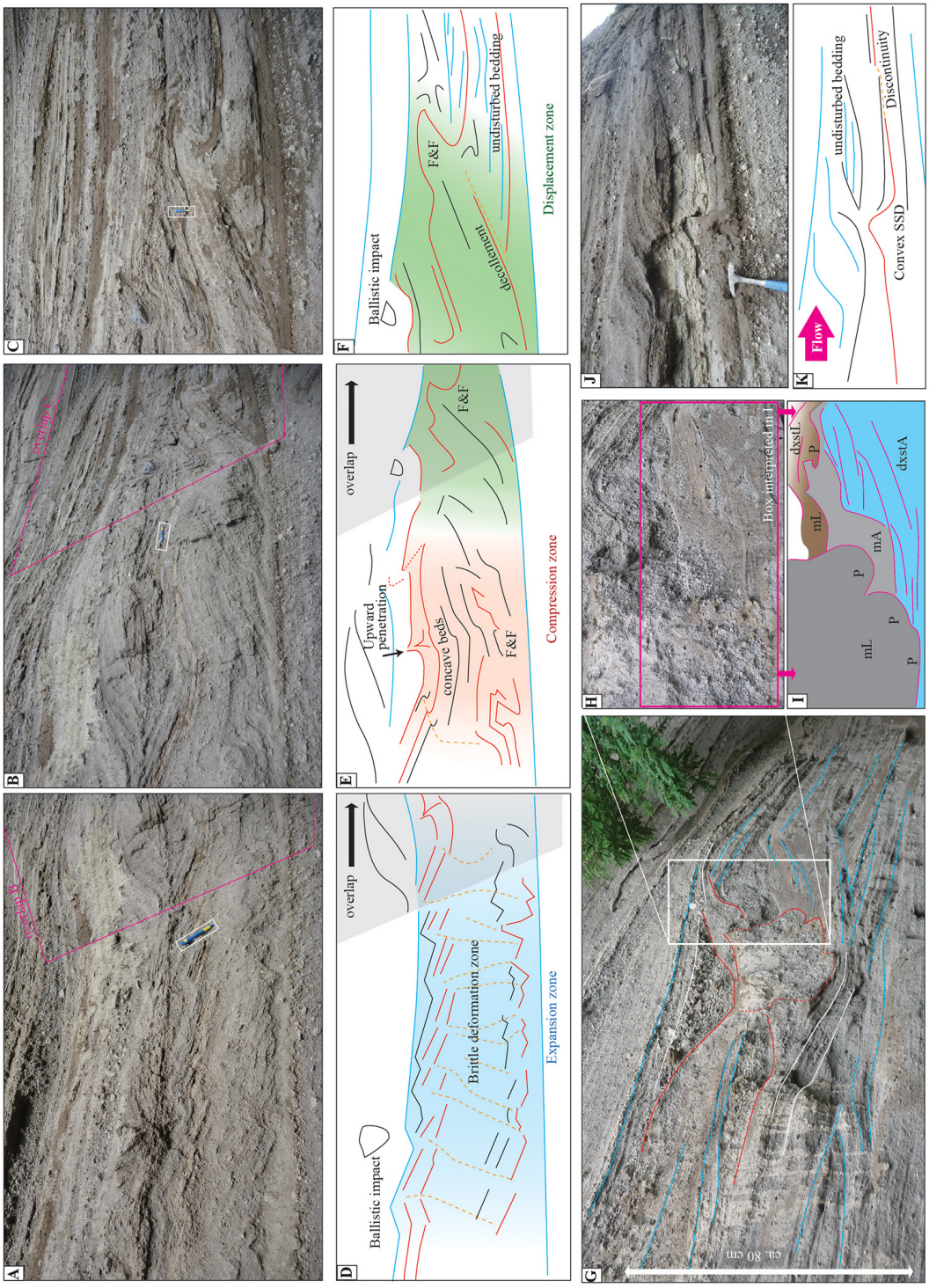

Figure 4. SSD structures from Laacher See. Panels **(a–c)** make a panorama of a composite structure due to impact interpreted in **(d–f)**. Extensional tilted block (thrust dominos) dipping to the right in **(a)**, compression due to impact in **(b)**, and compressional displacement towards the right with folds-and-faults (F&F) in **(c)** (image overlap dashed in gray). **(g–i)** Print of an impact resembling a pseudo "chute and pool" structure. Central compression is topped by lag breccia and rooted by massive lapilli (mL) potatoids (P), themselves contoured by massive ash (mA) in otherwise diffusely cross-stratified ash and lapilli (dxstA, dxstL). Zoom in **(h)**, with interpretation in **(i)**. In (**j** and **k**), a solitary symmetrical convex SSD resembling an anticline is contained in a fine grained fall layer and is related to dynamic pore pressure drop by subsequent flows.

3 Discussion and interpretation

As a general observation, many of the examples documented have a fine-grained underlying or basal layer (Purrumbete, Laacher See, Ubehebe, Merapi). Fine-grained layers are likely to have distinct rheological properties that account for initiation of deformation (Mills, 1983). Ash is no exemption, at both small (Gibert et al., 2011) and regional scales (Wiemer, 2014, and references therein). Fine deposits are likely to have low permeability, impacting either on the transfer and diffusion of dynamic pore pressure from subsequent flows (Roche et al., 2013), or on fluid escapes from enclosed layers (Peltier et al., 2012).

3.1 Influence of dynamic pore pressure

SSDs from Soufrière Hills seem to originate from the dark mLA lensoidal layer that connects to the small basal attached potatoids and intrusions to the overlying pipes (Fig. 1a–b). Komorowski et al. (2013) interpreted similar features in the deposits of the Merapi 2010 block and ash flows as small degassing pipes related to rapidly deposited and fluidized flows. Here, the dark mLA layer is interpreted as fluidized and overpressurized in dynamic pore pressure during flow in order to explain the basal potatoids and intrusions as injection features. Basal dikes in subglacial deposits are indeed usually interpreted as indicating overpressure of the flows and injections (e.g., Douillet et al., 2012). The associated mLA layer would have held part of the overpressure through rapid sedimentation, and subsequently released the gas during deflation and compaction after burial by the overlying layer, further producing degassing pipes. This could also have destabilized the overlying beds and eased the formation of shear instabilities found at the upper interface of the mA layer above the pipes. Alternatively, the influence of bed-water turned into steam cannot be ruled out in the river thalweg. The large scale depletion of the surface (Fig. 1c) may relate to similar deflation of liquefied pockets, although simple re-arrangement of the grains underneath or any depletion could lead to similar surface expressions. The surface mainly consists of coarse particles and small deflation cracks developed; thus, the structure may relate to elutriation of fines.

The convex deformation of the fine-grained planar strata at Laacher See (Fig. 4j–k) lacks any recumbent component, is isolated, and no impact is visible. A localized decrease of the dynamic pore pressure of subsequent flows may have been transferred to the ground and slightly deformed the fine bed by suction. The deformed layer would have acted as a comparatively impermeable seal, containing the underpressure above it and lifting up. Negative dynamic pore pressures are indeed recorded from experimental granular flows and PDCs and trigger remobilization (erosion) (Roche et al., 2013; Farin et al., 2014; Bernard et al., 2014). The influence of dynamic pore pressure in destabilizing the sediment bed may be of importance in all syn-flow SSD scenarios. Both over- or under- pressurization can occur, and may systematically relate to both flow unsteadiness and flow non-uniformity. In air-particles experiments, an underpressure is associated with dilation at a flow front, and is directly followed by overpressure (Roche et al., 2010). The dune bedform found just above the SSD may also have had some influence and produced a slight overweight. Aeolian dunes produce SSD on underlying beds, yet rather as load structures and in static settings (Chan and Bruhn, 2014).

3.2 Deformation driven by shearing of subsequent flows

3.2.1 Granular shear and pseudo Kelvin–Helmholz instabilities

At Tungurahua, the imbrication of overturned laminae with confinement within an otherwise undeformed bed set suggests syn-depositional processes (Fig. 2). SSD cannot be correlated with any impact sag. The orientation parallel to the direction of the flow suggests the influence of the latter. The vortex-shaped SSD structures are interpreted as granular shear instabilities related to Kelvin–Helmholtz vortices, based on reports and interpretations from analogue experiments (Rowley et al., 2011; Farin et al., 2014). If a pure wind BBL had moved the sediments, they would have begun to saltate as individual grains rather than deform as a whole (Douillet et al., 2014), and since the deposits were dry, no water can have caused cohesion. Roche et al. (2013) explains the formation of wave instabilities at the interface between a fine-grained erodible bed and granular flow as linked with movements as a whole related to fluidization. This suggests that the observed features are indicative of a granular BBL and possible occurrence of traction carpets on the lee of the dune bedform. Although cross-stratification is generally interpreted as indicative of low particle concentration at the BBL, experiments by Leclair and Arnott (2005) have shown that laminations can be produced at more than 35 % particle concentration, a concentration at which a granular BBL can occur. The scale of the structures being similar to experimental results, the granular BBL is interpreted to be of the same order of thickness and velocities (few centimeters thick and a few centimeters thick and a few meters per second velocity).

The downflow evolution of SSD at Tungurahua (Fig. 2c–d) brings further support to the discussion of Rowley et al. (2011). Indeed, they suggested that pseudo Kelvin–Helmholtz vortices may only be cryptic (hidden) in sedimentary records, since they intrinsically mix the deposits and create graded massive units. In the outcrop, well defined and thin lamination is visible downstream of the deformation front highlighted by vortices. In contrast, upstream from the front, stratification is comparatively thick and massive, with diffuse oversteepened laminations contained within

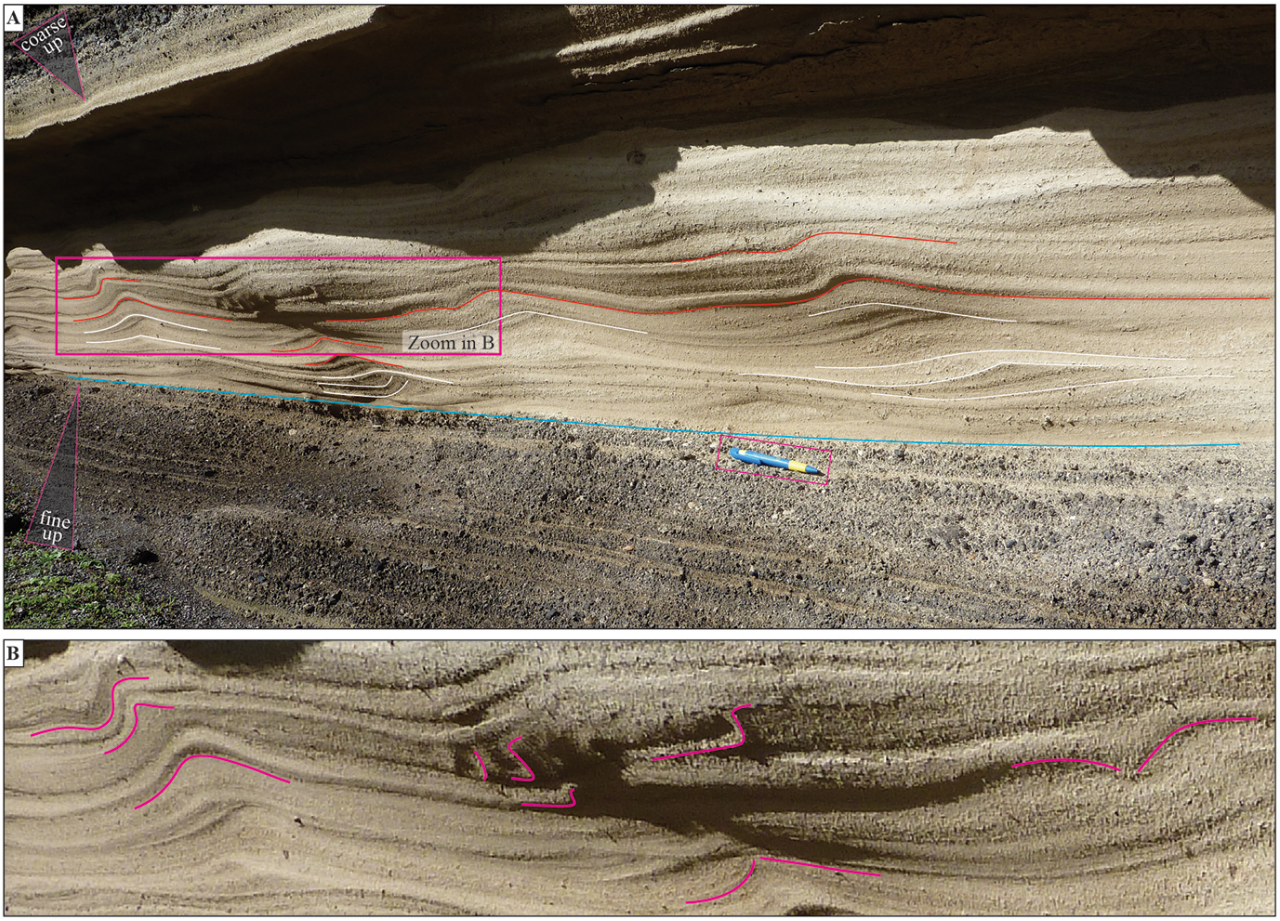

Figure 5. Tower Hill rim: **(a)** Train of slightly overturned and oversteepened laminations in fine ash bed sets with ripple cross-laminations related to shock waves at the vent. Triangles illustrate grading tendencies reflecting a transition from strombolian to phreatomagmatic explosions. **(b)** Zoom in oversteepened and slightly overturned beds.

the layers (Fig. 2d). This indicates the ploughing effect of the downstream migrating vortices that tend to mix and homogenize the initial bedding, as predicted by Rowley et al. (2011).

The recumbent and vortex structures at Ubehebe (Fig. 3d) have an overturning orientation with flow and a vortex shape. They only differ from Tungurahua by their occurrence in otherwise massive deposits. This may be an effect of successive ploughing by Kelvin–Helmholtz vortices or simply result from massive deposition. A vortex form is also observed at Soufrière Hills (Fig. 1b, top). In this case, the vortex is followed downstream by a gentle undulation and a steep step. Although the second and third structures have not a vortex shape, they are interpreted as proto, granular Kelvin–Helmholtz instabilities at different development stages. Moreover, the downstream repetition of deformation is taken as sign of the wavy nature of the instability.

Interestingly, sheared structure with a vortex-like structure are also present on the stoss and crest of dune bedforms covered by aggrading bed sets at Roccamonfina volcano (Italy, Figure 5 in Giannetti and Luongo, 1994). If all these structures represent granular Kelvin–Helmholtz instabilities, they could share similar dynamics to their fluid analogue and quantitative information could be derived (Rowley et al., 2011, developed in Appendix). From theoretical considerations, BBL velocities of more than $2.5\,\mathrm{m\,s^{-1}}$ for 1 % relative particle concentration are necessary for instabilities to develop (Appendix, Fig. A1). This number rapidly drops for higher flow concentrations, and shear instabilities thus plausibly develop for basal granular BBL a few centimeters in thickness.

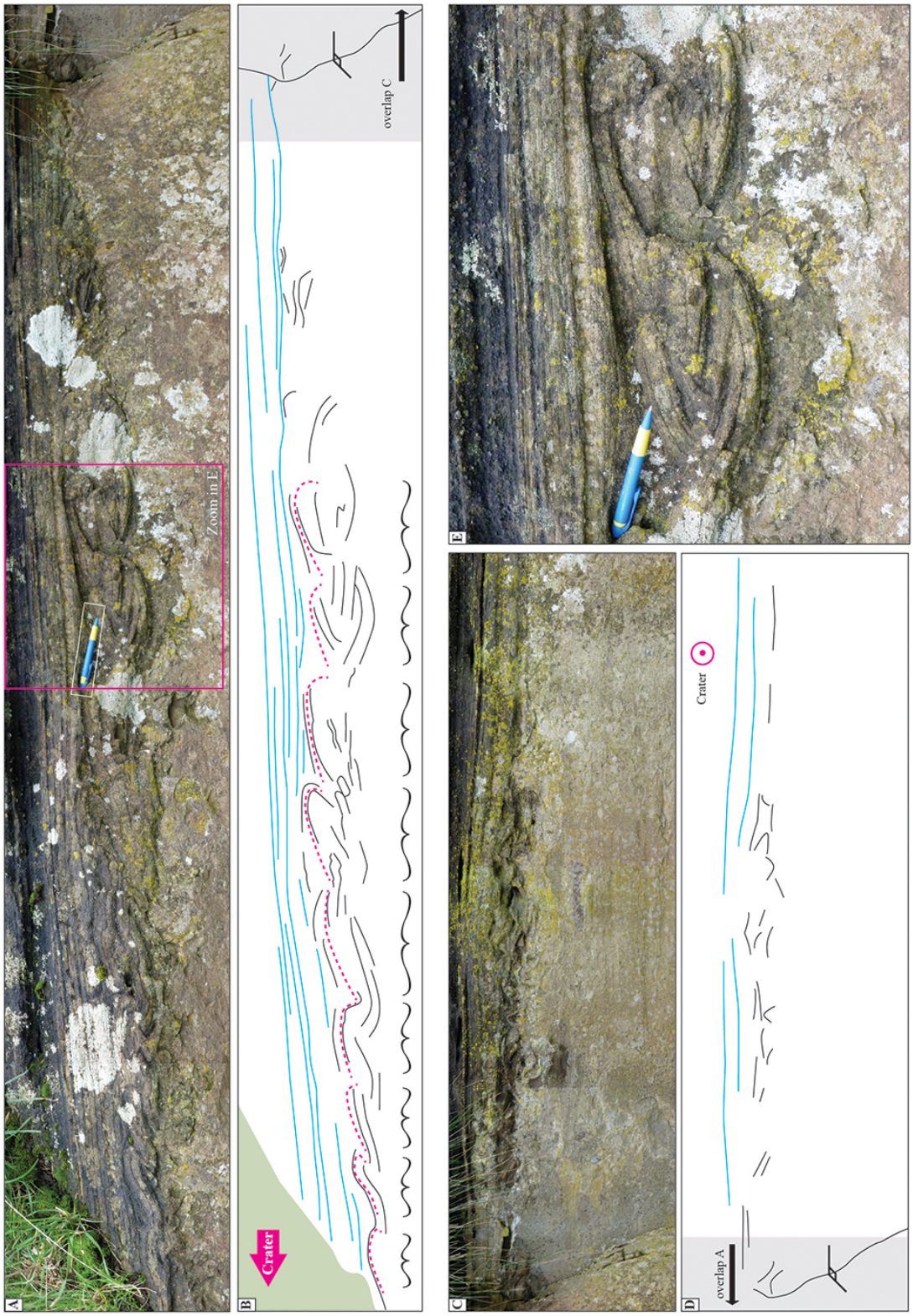

Figure 6. SSD at Purrumbete rim interpreted as related to shock waves. **(a)** Outcrop part oriented outward crater showing folds-and-faults with **(b)** interpretation; pink dashed lines highlight a pseudo recurrence and brackets a pseudo wavelength. Shaded zones indicates the overlap with **(c)**, the outcrop part oriented parallel to rim showing chaotic, diapiric flame-like structures with **(d)** interpretation. **(e)** Zoom into recumbent folds-and-faults structures with overlying planar lamination (location outlined in **a**).

3.3 Deformation driven by gravity

3.3.1 Slumps

For the Ubehebe thrusting folds-and-faults (Fig. 3a, top), observations point toward a gravitational slump: (1) deformed beds confined between undeformed strata; (2) large number of beds involved; (3) overturn orientation toward the thalweg of a channel; (4) axial planes of folds dipping upslope with folds' strike normal to microfaults; (5) imbrications and overlap (stacking) of deformed layers. The base of the folds-and-faults (Fig. 3a, base, and 3c) shows components of rotation, mixing and layer pull apart, indicating the floor thrust of slumping. Given the coherent state of the beds involved combined with their great variations in grain size and the thickness of SSD, a subaerial slump of wet sediment is favored. This would enhance cohesion on one hand, and the overweight due to water acting on freshly emplaced, unstable beds could also have triggered the sliding. The interpretation is further supported by the characteristics of the nearby ballistic impact sags. Overlying strata are not deformed and so the slump has occurred during or between eruptive phases.

3.3.2 Granular Rayleigh–Taylor instabilities

The diapiric flame-like structures at Ubehebe (Fig. 3d) are remarkably similar to structures produced by granular Rayleigh–Taylor instabilities between a granular medium and air (Niebling et al., 2010). Usual interpretations of such features point toward liquefaction, loading, or water escape structures (e.g., Owen, 1996b), a situation prone to occur during the eruption with high sedimentation rate and wet deposits. These explanations correspond to forms of granular Rayleigh–Taylor instabilities (Selker, 1993; Vinningland et al., 2007, 2010). Some of the flame-like structures are overturned toward the flow direction, which may indicate shearing and syn-PDC SSD. Asymmetrical features in turbidites were described by Moretti et al. (2001). They interpreted these as recording the paleo-slope and possibly paleo-flow direction, and made calculations to derive time-scales of deformations.

The curled and pulled apart, coarse-grained, isolated, flat dishes from Ubehebe (Fig. 3b) are interpreted as detached load casts. These form in the presence of an inverse density gradient resulting from changes of porosity driven by the grain size distribution of successive layers (Mills, 1983; Bridge and Demicco, 2008, p. 353–354), or when an underlying layer is fluidized (Nichols et al., 1994). In both cases, these also share the configuration for granular Rayleigh–Taylor instabilities (Nichols et al., 1994). A shock (seismicity or impact) may trigger detachment, but it is not necessary, and those structures may be post-eruptive. Their localized nature is taken to rule out remote triggers such as seismicity and no subsequent impact is visible above the structures. Further dynamic considerations coupled with the pseudo wavelength of the structures and interface characteristics may resolve the question of their similarity with Rayleigh–Taylor instabilities (see Selker, 1993, and Appendix).

3.4 Deformation driven by ballistic impacts

3.4.1 Impact records

At Laacher See, the tilted blocks (or domino/bookshelf structures) and thrust folds-and-faults packages locally share characteristics with slump folds (Fig. 4a–f). However, the very limited throw, absence of significant slope or possible slump trigger and the nested nature appear to exclude this interpretation. Given the great thickness of the disturbed beds, a surface instability, simple shearing or granular Kelvin–Helmholtz instability, also seems unlikely.

Yet, there is a preferential orientation directed roughly outward from the postulated vent. The lateral evolution of the SSD leads to another insight. (1) The upstream part dominated by tilted blocks indicates extension (Fig. 4a, 4d). (2) The central part with the concave shape of the upper beds together with upward-penetrating flame-like beds suggest vertical compression (Fig. 4b, 4e). (3) The folds-and-faults and local decollement in the downstream part record lateral displacement away from the central part ("escape zone", Fig. 4c, 4f). The source of the SSD can thus be localized above the central part, in the vertical compression zone, and with forced local displacement to the right. In light of this, the SSD is interpreted as the print of a large block bouncing on the bed and transmitting a deformation oriented with its trajectory. This is further supported by the presence of large blocks (> 3 m diam.) in nearby areas in deposits otherwise dominated by ash and lapilli. Noteworthy, the abrupt confinement of the deformation in depth indicates a higher state of compaction of the undeformed beds, and thus their belonging to an older event separated by sufficiently long time for compaction. The basal ash layer would represent an initial fall event belonging to the deformed unit. Thus impact sags may also be used to trace genetic units.

The diagnosis is easier at Ubehebe (Fig. 3e), where impacting blocks are nested in deformed beds and just above potatoids. Thorough observation indicates that the coarse and massive layer escaped into the enclosing fine-grained beds: it is the most disturbed and exhibits potatoids with lateral and vertical spreading with respect to both the over and underlying layers, which still contain stratification. The isotropic nature of the leakage with apparent absence of preferential escape directions supports a liquefaction mechanism. To account for the coarse-grained nature, water saturation is inferred, in agreement with the other Ubehebe SSD structures. A grain-flow triggered by an impact-induced liquefaction of the porous and water-saturated coarse-ash

enclosed in impermeable fine-grained layers has likely produced the nodules and dikes.

The pseudo "chute and pool" structure from Laacher See (Fig. 4g–i) shares similarities with both impact structures. The central part exhibits a depression with concave beds indicating compression. The right part is disturbed by massive lapilli material with downward-oriented potatoids (mL and P in Fig. 4h–i). These are related to a liquefied grain flow of porous and water-saturated lapilli beds (sensu Owen and Moretti, 2011). The potatoids are underlined on the right by a ca. 10 cm thick, massive, ash-dominated contour with a diffuse front to the undisturbed cross-stratified bed sets (mA and dxstA in Fig. 4i). The massive fore front is interpreted as representing the final escape of water that was less coupled with sediments. The liquefaction event is related to a large block impact that could have bounced and compacted the concave central depression. The extreme right of the structure containing stoss stratification dipping at more than the repose angle (upper part of Fig. 4h) may have been oversteepened by the rearrangement of the underlying sediment. Such a process was readily suggested by Nocita (1988), although the sediments of their study were later reinterpreted as fluvial rather than from PDCs (McPherson et al., 1989), without changing the accuracy of the process. The coarse lag breccia on top of the central depression may either indicate that the impacting block stayed in place and acted upon the depositional dynamics, resuspended fines during impact, or be a simple infill of the topography.

3.4.2 A trigger for "chute and pool" structures?

The two impact SSDs from Laacher See share remarkable similarities with the basal oversteepened truncations observed in structures generally interpreted as "chute and pool" structures (types I to IV of Schmincke et al., 1973). If the disturbed beds had been slightly more destabilized and permitted entrainment, the same configuration would be observed. Such impact SSDs would explain the oversteepened truncations and be at the origin of some of the "chute and pool" structures (see also Nocita, 1988). This would also explain the observation by Schmincke et al. (1973) that "chute and pool" structures occur in rather proximal parts, since ballistic blocks are likely to land closer to the crater than the total distance traveled by a PDC. This interpretation does not contradict the subsequent hydraulic jump dynamics of the structures, but the jump would be a consequence of the bed morphology rather than the other way round as usually suggested. A hydraulic jump would however not be necessary and simple morphological blocking of the bed load equally well explains the "chute and pool" depositional patterns (basal blocking and stop-and-go models in Douillet et al., 2013a; Martínez et al., 2007, resp.). The answer likely lies upstream from these structures, at the proximal truncation limit.

3.5 Deformation driven by shock waves

At Tower Hill (Fig. 5), the regularity of patterns, high degree of preservation and absence of slope appear to discredit slumping. The lateral persistence indicates a large-scale effect and discredit shear instabilities. Indeed, a flow with thin granular BBL forming pseudo Kelvin–Helmholtz instabilities is unlikely to stay in this state over several hundred meters. Moreover, either lateral flow velocities were slow enough for fine ash and volcanic dust with ripple lamination to deposit, or the ground was covered with a stretch of water. During the phreatomagmatic phase with efficient fragmentation associated with the fine beds, shock waves may have been produced by the explosions (e.g., Scolamacchia and Schouwenaars, 2009). These could propagate close to the rim, quaquaversal to the southern vent, and destabilize the fine-grained bed sets by transmitting their orientation to the ground. Valentine et al. (1989) suggested shock waves as a possible trigger for overturned flame-like structures. They noted that "when a shock passes over a granular deposit, bed particles experience a lift force due to the change in velocity across the shock" and "the bed immediately behind the shock has been observed in experiments to take on a wavelike configuration" citing the convincing experiments by Borisov et al. (1967). Recent shock experiments by Wayne et al. (2013) developed recumbent vortex-like shapes on dust beds and further support the interpretation (see also Fedorov, 2004).

The Purrumbete structure (Fig. 6) has a preferential direction away from crater: (1) all beds are overturned outside of the crater; (2) the deformation, vorticity degree and thickness of beds involved increase away from crater; whereas (3) the crater-parallel face is chaotic. Microfaults suggest cohesion, and there is neither evidence of traction nor of granular flow in the overlying planar deposits related to fallout; thus, granular shear is excluded. An envisaged interpretation is that these beds are involved in a small-scale slump. However, overlying beds lie conformably on top of the deformed strata, and are thus emplaced after deformation. This implies that a very small amount of material would be involved in a slump on an only gently sloping bed, unlikely to be sufficient to yield enough gravitational potential to initiate movement. The overturn, vorticity direction as well as the imbrication fabric at thrust faults would suggest an outward oriented slump, but no scar is visible at the deformation onset (left part). Rather, the evolution of intensity of deformation, absence of scar in the proximal side, and imbrication suggest that deformation could origin from the distal part, with some force pushing the sediment toward the crater. Similarly as for the Tower Hill maar, these structures can be the record of shock waves that destabilized the uppermost deposits and conferred them a tilt. Here again, the vortex-like entrainment evidenced in shock experiments supports the interpretation (Borisov et al., 1967; Wayne et al., 2013), and the proximity to the vent make shock wave influence probable. The

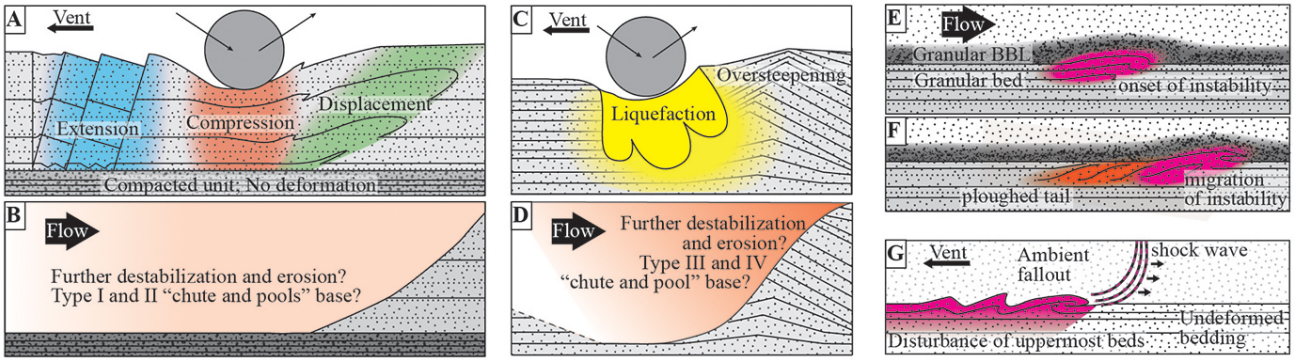

Figure 7. Interpretative sketch of syn-eruptive SSD. **(a)** and **(c)** SSD formed by ballistic impacts. Panels **(b)** and **(d)** show the envisaged scenario if destabilization of **a** and **c** permitted complete remobilization. These would form the base for types I and II "chute and pool" structures in Schmincke et al. (1973). **(e)** Formation of pseudo Kelvin Helmholtz instabilities between the bed and basal granular flow, and **(f)** the ploughing effect of a migrating instability. **(g)** Destabilization by shock waves.

passage of a shock wave would not be associated with direct sedimentation and here, the conformity of overlying fall beds supports a trigger mechanism without sedimentation. Indeed the signature is uniquely present as deformation. As SSD triggered by shock waves, these can share similarities with Richtmyer–Meshkov instabilities, the interaction of a shock wave with the interface between two fluids (Brouillette, 2002).

4 Conclusions

The exercise presented here has demonstrated the richness of information contained in SSD structures from the dilute PDC environment. SSD contains a record of syn-flow and syn-eruptive processes combined with post-depositional bed-state information.

Syn-flow processes were evidenced through granular, pseudo Kelvin–Helmholtz instabilities as well as evidences of suction and injection related to dynamic pore pressure of the flows. These observations feed the understanding of BBL processes of PDCs. Basal intrusions support the interpretation of fluidized flows with dynamic pore overpressure. Vortex-shaped laminae may be a valid indicator of granular-based flows or traction carpets. The suction vs. injection at the base of flows likely relate to changes in pore-pressure of the flow, and thus inform on its inhomogeneity.

Several syn-eruptive processes are recorded by SSD. Ballistic impacts may take more evolved forms than simple sags. They yield information on the bed state such as the compaction degree and water content, which helps to delimit eruptive units and environmental context. Some forms of impact may be at the origin of the so-called "chute and pool" bedforms. Slumps similarly inform on water content and eruptive units. The understanding of prevailing eruption type (wet vs. dry eruptions) may thus benefit from thorough analysis of SSD. Finally, we suggest that shock waves may leave a signature in the sediments by destabilization and overturning of the surface beds close to the vent without any direct deposits.

SSD from PDCs are of interest in the context of sedimentary research since they record subaerial, syn- and post-flow SSD structures, emphasizing that water is not a prerequisite for SSD. Moreover, PDC deposits can be unstable and have large permeability contrasts that facilitate SSD formation. Finally, the recognition of structures similar to instabilities occurring at fluid boundaries (Kelvin–Helmholz, Rayleigh–Tailor) further emphasizes the similarities between fluids and granular mixtures. SSD seems widespread in deposits of dilute PDCs, especially from phreatomagmatic eruptions, and should be addressed more attention. The variety of possible triggers, especially in the context of explosive volcanic eruptions, calls for further field and experimental work.

Appendix A: Instabilities between two fluids

A1 Granular Kelvin–Helmholtz instabilities at a bed-flow interface

Given structures interpreted as granular Kelvin–Helmholtz instabilities, a theoretical resolution similar to the fluid instability can be expressed (Rowley et al., 2011). Any fluid dynamics analysis is based on the integration of "infinitesimal fluid elements", a notion comparable to grains in a granular mixture. The fluid-dynamics analytical method just justify in itself its applicability to granular mediums.

The problem is taken in 2-D with reference frame ($\boldsymbol{e_x}$ -flow parallel direction-, $\boldsymbol{e_z}$ -upward direction parallel to $\boldsymbol{g}$, the gravity acceleration-). Consider two homogenous mediums F_1 and F_2, F_2 lying above F_1 and the interface an infinite horizontal plane. Suppose the fluids of densities ρ_1 and ρ_2 incompressible ($D\rho_{1,2}/Dt = 0$), inviscid ($\nu = 0$), with constant horizontal velocity $u_{1,2}(z) = U_{1,2}\boldsymbol{e_x}$, and irrotational. The surface disturbance (ξ) can be written in the form (see Drazin, 2002; Douillet, 2014, Chap. 2):

$$\xi = \widetilde{\xi}\exp(i(kx) - st) \tag{A1}$$

with k being the wave number. Linearization of the problem posed by the boundary conditions has the following solution (see Drazin, 2002; Douillet, 2014, Chap. II.2):

$$s = ik\frac{\rho_1 U_1 + \rho_2 U_2}{\rho_1 + \rho_2} \pm \left[\frac{k^2\rho_1\rho_2(U_1 - U_2)^2}{(\rho_1 + \rho_2)^2} - \frac{kg(\rho_1 - \rho_2)}{\rho_1 + \rho_2}\right]^{1/2}. \tag{A2}$$

Assumptions can be made for the case of an instability between a granular flow and deposit. The deposit does not move ($U_1 = 0$), and the flow density is a portion of the deposit density ($\rho_2 = x\rho_1$ with $0 \leq x \leq 1$). Thus Eq. (A2) simplifies into

$$s = ikU_2\frac{x}{1+x} \pm \left[k^2U_2^2\frac{x}{(1+x)^2} - kg\frac{(1-x)}{(1+x)}\right]^{1/2}. \tag{A3}$$

In order that a wave occurs, Eq. (A3) must have an imaginary component (the angular velocity $w = Im(s)$). The second term in s must be real for an exponential decay or increase to develop, and thus, be an instability. Thus the term under the square root must be positive and a condition for a bed-flow instability is (see also Rowley et al., 2011)

$$U_2^2 > \frac{g}{k}\frac{(1-x^2)}{x}. \tag{A4}$$

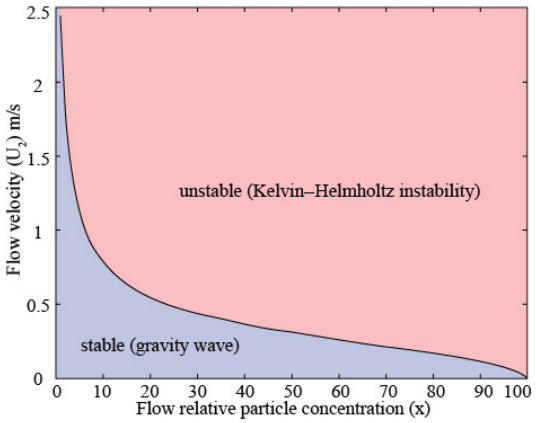

Figure A1. Threshold flow velocity (U_2) as a function of flow's particle concentration compared to bed's particle concentration (x) following Eq. (A4).

This condition is granted for large wave number (k), i.e., short waves, high particle concentrations (x), or large flow velocities (Fig. A1).

Further, the phase velocity of an instability ($c = w/k$) can be derived

$$c = \frac{x}{1+x}U_2. \tag{A5}$$

Under the assumptions, the wave velocity is thus entirely characterized by the concentration difference between the bed and flow (x) and the velocity of the latter (U_2), and the wavelength of the instability ($\lambda = 2\pi/k$) does not appear explicitly.

A2 Granular Rayleigh–Taylor instabilities

A Rayleigh–Taylor instability is a surface instability between two resting fluids of different densities. Thus Eq. (A2) can be equally used with $U_{1,2} = 0$. For the case of the curled and pulled-apart structures at Ubehebe (Fig. 3b), the upper coarse grained layer was sinking in the massive fine-grained layer underneath; thus $\rho_2 = x\rho_1$ with $x \geq 1$, and Eq. (A2) simplifies into

$$s = \pm\left[kg\frac{|1-x|}{1+x}\right]^{1/2}. \tag{A6}$$

The field observation is the length scale of the curled layers ($\lambda = 2\pi/k =$ ca. $15 - 30$ cm). The missing variables are a timescale for the growth of the instability and the density ratio. Estimating one permits to quantify the other.

Acknowledgements. We are grateful to M. Heap for editing the manuscript. Useful comments from an anonymous reviewer together with comments and discussion with Massimo Moretti greatly contributed to the improvement of the manuscript. We are indebted to the following (partial) funding sources: the Bavarian grant THESIS (GAD), the German Deutsche Forschungsgemeinschaft grant KU2689/2-1 (GAD and UK), a Research Professorship (LMUexcellent) of the Bundesexzellenzinitiative and an advanced grant from the European Research Council-EVOKES (DBD).

Edited by: M. Heap

References

Allen, J. and Banks, N.: An interpretation and analysis of recumbent-folded deformed cross-bedding, Sedimentology, 19, 257–283, 1972.

Alsop, G. and Marco, S.: Soft-sediment deformation within seismogenic slumps of the Dead Sea Basin, J. Struct. Geol., 33, 433–457, 2011.

Alsop, G. I. and Marco, S.: Tsunami and seiche-triggered deformation within offshore sediments, Sediment. Geol., 261, 90–107, 2012.

Andrews, G. D. and Branney, M. J.: Emplacement and rheomorphic deformation of a large, lava-like rhyolitic ignimbrite: Grey's Landing, southern Idaho, Geol. Soc. Am. Bull., 123, 725–743, 2011.

Bernard, J., Kelfoun, K., Le Pennec, J.-L., and Vargas, S. V.: Pyroclastic flow erosion and bulking processes: comparing field-based vs. modeling results at Tungurahua volcano, Ecuador, B. Volcanol., 76, 1–16, 2014.

Borisov, A., Lyubimov, A., Kogarko, S., and Kozenko, V.: Instability of the surface of a granular medium behind sliding shock and detonation waves, Combust. Explo. Shock+, 3, 95–97, 1967.

Brand, B. D. and Clarke, A. B.: The architecture, eruptive history, and evolution of the Table Rock Complex, Oregon: From a Surtseyan to an energetic maar eruption, J. Volcanol. Geoth. Res., 180, 203–224, 2009.

Brand, B. D. and White, C. M.: Origin and stratigraphy of phreatomagmatic deposits at the Pleistocene Sinker Butte volcano, western Snake River Plain, Idaho, J. Volcanol. Geoth. Res., 160, 319–339, 2007.

Branney, M., Barry, T., and Godchaux, M.: Sheathfolds in rheomorphic ignimbrites, B. Volcanol., 66, 485–491, 2004.

Branney, M. J. and Kokelaar, B. P.: Pyroclastic density currents and the sedimentation of ignimbrites, Geo. Soc. Mem., 27, 143 pp., 2002.

Branney, M. J. and Kokelaar, P.: Volcanotectonic faulting, soft-state deformation, and rheomorphism of tuffs during development of a piecemeal caldera, English Lake District, Geol. Soc. Am. Bull., 106, 507–530, 1994.

Bridge, J. and Demicco, R.: Earth surface processes, landforms and sediment deposits, Cambridge University Press, 2008.

Brouillette, M.: The richtmyer-meshkov instability, Annu. Rev. Fluid Mech., 34, 445–468, 2002.

Brown, R. J., Orsi, G., and de Vita, S.: New insights into Late Pleistocene explosive volcanic activity and caldera formation on Ischia (southern Italy), B. Volcanol., 70, 583–603, 2008.

Caicedo-Carvajal, C. E., Glasser, B. J., and Shinbrot, T.: Granular flow transitions on sinusoidal surfaces, J. Fluid Mech., 556, 253–269, 2006.

Chan, M. A. and Bruhn, R. L.: Dynamic liquefaction of Jurassic sand dunes: processes, Origins, and implications, Earth Surf. Proc. Land., 39, 1478–1491, 2014.

Charbonnier, S. J. and Gertisser, R.: Field observations and surface characteristics of pristine block-and-ash flow deposits from the 2006 eruption of Merapi Volcano, Java, Indonesia, J. Volcanol. Geoth. Res., 177, 971–982, 2008.

Chen, J. and Lee, H. S.: Soft-sediment deformation structures in Cambrian siliciclastic and carbonate storm deposits (Shandong Province, China): Differential liquefaction and fluidization triggered by storm-wave loading, Sediment. Geol., 288, 81–94, 2013.

Conway, S. L., Shinbrot, T., and Glasser, B. J.: A Taylor vortex analogy in granular flows, Nature, 431, 433–437, 2004.

Crowe, B. M. and Fisher, R. V.: Sedimentary structures in base-surge deposits with special reference to cross-bedding, Ubehebe Craters, Death Valley, California, Geol. Soc. Am. Bull., 84, 663–682, 1973.

Denis, M., Guiraud, M., Konaté, M., and Buoncristiani, J.-F.: Subglacial deformation and water-pressure cycles as a key for understanding ice stream dynamics: evidence from the Late Ordovician succession of the Djado Basin (Niger), Int. J. Earth Sci., 99, 1399–1425, 2010.

Doronzo, D. M. and Dellino, P.: Pyroclastic density currents and local topography as seen with the conveyer model, J. Volcanol. Geoth. Res., 278, 25–39, 2014.

Douillet, G., Ghienne, J.-F., Géraud, Y., Abueladas, A., Diraison, M., and Al-Zoubi, A.: Late Ordovician tunnel valleys in southern Jordan, Geol. Soc. Sp., 368, 275–292, 2012.

Douillet, G. A.: Flow and sedimentation from pyroclastic density currents. From large scale to boundary layer processes. PhD Dissertation, October 2014, Earth and Environmental Sciences, Ludwig Maximilian University, 2014.

Douillet, G. A., Pacheco, D. A., Kueppers, U., Letort, J., Tsang-Hin-Sun, È., Bustillos, J., Hall, M., Ramón, P., and Dingwell, D. B.: Dune bedforms produced by dilute pyroclastic density currents from the August 2006 eruption of Tungurahua volcano, Ecuador, B. Volcanol., 75, 1–20, 2013a.

Douillet, G. A., Tsang-Hin-Sun, È., Kueppers, U., Letort, J., Pacheco, D. A., Goldstein, F., Von Aulock, F., Lavallée, Y., Hanson, J. B., Bustillos, J., et al.: Sedimentology and geomorphology of the deposits from the August 2006 pyroclastic density currents at Tungurahua volcano, Ecuador, B. Volcanol., 75, 1–21, 2013b.

Douillet, G. A., Rasmussen, K. R., Kueppers, U., Lo Castro, D., Merrison, J. P., Iversen, J. J., and Dingwell, D. B.: Saltation threshold for pyroclasts at various bedslopes: Wind tunnel measurements, J. Volcanol. Geoth. Res., 278, 14–24, 2014.

Drazin, P. G.: Introduction to hydrodynamic stability, Cambridge university press, 2002.

Ettensohn, F., Zhang, C., Gao, L., and Lierman, R.: Soft-sediment deformation in epicontinental carbonates as evidence of paleoseismicity with evidence for a possible new seismogenic

indicator: Accordion folds, Sediment. Geol., 235, 222–233, 2011.

Farin, M., Mangeney, A., and Roche, O.: Fundamental changes of granular flow dynamics, deposition, and erosion processes at high slope angles: insights from laboratory experiments, J. Geophys. Res.-Earth, 119, 504–532, 2014.

Fedorov, A.: Mixing in wave processes propagating in gas mixtures (review), Combustion, Combust. Explo. Shock+, 40, 17–31, 2004.

Fiske, R. S.: Subaqueous pyroclastic flows in the Ohanapecosh Formation, Washington, Geol. Soc. Am. Bull., 74, 391–406, 1963.

Fiske, R. S. and Tobisch, O. T.: Paleogeographic significance of volcanic rocks of the Ritter Range pendant, central Sierra Nevada, California, Pacific Coast Paleogeography Symposium 2: Mesozoic Paleogeography of the Western United States, 391–406, 1978.

Forterre, Y. and Pouliquen, O.: Longitudinal vortices in granular flows, Phys. Rev. Lett., 86, 5886–5889, 2001.

Gençalioğlu-Kuşcu, G., Atilla, C., Cas, R. A., and Kuşcu, İ.: Base surge deposits, eruption history, and depositional processes of a wet phreatomagmatic volcano in Central Anatolia (Cora Maar), J. Volcanol. Geoth. Res., 159, 198–209, 2007.

Gernon, T., Fontana, G., Field, M., Sparks, R., Brown, R., and Mac Niocaill, C.: Pyroclastic flow deposits from a kimberlite eruption: the Orapa South Crater, Botswana, Lithos, 112, 566–578, 2009.

Gernon, T. M., Sparks, R. S. J., and Field, M.: Degassing structures in volcaniclastic kimberlite: examples from southern African kimberlite pipes, J. Volcanol. Geoth. Res., 174, 186–194, 2008.

Ghienne, J.-F.: Late Ordovician sedimentary environments, glacial cycles, and post-glacial transgression in the Taoudeni Basin, West Africa, Palaeogeogr. Palaeocl., 189, 117–145, 2003.

Giannetti, B. and Luongo, G.: Trachyandesite scoria-flow and associated trachyte pyroclastic flow and surge at Roccamonfina Volcano (Roman Region, Italy), J. Volcanol. Geoth. Res., 59, 313–334, 1994.

Gibert, L., Alfaro, P., García-Tortosa, F., and Scott, G.: Superposed deformed beds produced by single earthquakes (Tecopa Basin, California): Insights into paleoseismology, Sediment. Geol., 235, 148–159, 2011.

Goldfarb, D. J., Glasser, B. J., and Shinbrot, T.: Shear instabilities in granular flows, Nature, 415, 302–305, 2002.

Hall, M. L., Steele, A. L., Mothes, P. A., and Ruiz, M. C.: Pyroclastic density currents (PDC) of the 16–17 August 2006 eruptions of Tungurahua volcano, Ecuador: Geophysical registry and characteristics, J. Volcanol. Geoth. Res., 265, 78–93, 2013.

Jordan, S., Cas, R., and Hayman, P.: The origin of a large (>3 km) maar volcano by coalescence of multiple shallow craters: Lake Purrumbete maar, southeastern Australia, J. Volcanol. Geoth. Res., 254, 5–22, 2013.

Kelfoun, K., Samaniego, P., Palacios, P., and Barba, D.: Testing the suitability of frictional behaviour for pyroclastic flow simulation by comparison with a well-constrained eruption at Tungurahua volcano (Ecuador), B. Volcanol., 71, 1057–1075, 2009.

Komorowski, J.-C., Jenkins, S., Baxter, P. J., Picquout, A., Lavigne, F., Charbonnier, S., Gertisser, R., Preece, K., Cholik, N., Budi-Santoso, A., et al.: Paroxysmal dome explosion during the Merapi 2010 eruption: Processes and facies relationships of associated high-energy pyroclastic density currents, J. Volcanol. Geoth. Res., 261, 260–294, 2013.

Leclair, S. F. and Arnott, R. W. C.: Parallel lamination formed by high-density turbidity currents, J. Sediment. Res., 75, 1–5, 2005.

Lowe, D. R.: Water escape structures in coarse-grained sediments, Sedimentology, 22, 157–204, 1975.

Mangeney, A., Roche, O., Hungr, O., Mangold, N., Faccanoni, G., and Lucas, A.: Erosion and mobility in granular collapse over sloping beds, J. Geophys. Res.-Earth, 115, F03040, doi:10.1029/2009JF001462, 2010.

Martínez, E., Pérez-Penichet, C., Sotolongo-Costa, O., Ramos, O., Måløy, K., Douady, S., and Altshuler, E.: Uphill solitary waves in granular flows, Phys. Rev. E,, 75, 031303, doi:10.1103/PhysRevE.75.031303, 2007.

Mattsson, H. B. and Tripoli, B. A.: Depositional characteristics and volcanic landforms in the Lake Natron–Engaruka monogenetic field, northern Tanzania, J. Volcanol. Geoth. Res., 203, 23–34, 2011.

McDonough, W. F., Waibel, A. F., and Gannet, M. W.: The re-interpretation of the Leone Lake sediments as a pyroclastic surge deposit and its tectonic significance, J. Volcanol. Geoth. Res., 20, 101–115, 1984.

McPherson, J., Flannery, J. R., and Self, S.: Discussion of -Soft-sediment deformation (fluid escape) features in a coarse-grained pyroclasticsurge deposit, north-central New Mexico-, Sedimentology, 36, 943–947, 1989.

Mills, P. C.: Genesis and diagnostic value of soft-sediment deformation structures?a review, Sediment. Geol., 35, 83–104, 1983.

Mohindra, R. and Bagati, T.: Seismically induced soft-sediment deformation structures (seismites) around Sumdo in the lower Spiti valley (Tethys Himalaya), Sediment. Geol., 101, 69–83, 1996.

Moretti, M., Soria, J. M., Alfaro, P., and Walsh, N.: Asymmetrical soft-sediment deformation structures triggered by rapid sedimentation in turbiditic deposits (Late Miocene, Guadix Basin, southern Spain), Facies, 44, 283–294, 2001.

Nichols, R., Sparks, R., and Wilson, C.: Experimental studies of the fluidization of layered sediments and the formation of fluid escape structures, Sedimentology, 41, 233–253, 1994.

Niebling, M. J., Flekkøy, E. G., Måløy, K. J., and Toussaint, R.: Sedimentation instabilities: impact of the fluid compressibility and viscosity, Phys. Rev. E, 82, 051302, doi:10.1103/PhysRevE.82.051302, 2010.

Nocita, B. W.: Soft-sediment deformation (fluid escape) features in a coarse-grained pyroclastic-surge deposit, north-central New Mexico, Sedimentology, 35, 275–285, 1988.

Odonne, F., Callot, P., Debroas, E.-J., Sempere, T., Hoareau, G., and Maillard, A.: Soft-sediment deformation from submarine sliding: Favourable conditions and triggering mechanisms in examples from the Eocene Sobrarbe delta (Ainsa, Spanish Pyrenees) and the mid-Cretaceous Ayabacas Formation (Andes of Peru), Sediment. Geol., 235, 234–248, 2011.

Owen, G.: Deformation processes in unconsolidated sands, Geol. Soc. Sp., 29, 11–24, 1987.

Owen, G.: Anatomy of a water-escape cusp in Upper Proterozoic Torridon Group sandstones, Scotland, Sediment. Geol., 103, 117–128, 1996a.

Owen, G.: Experimental soft-sediment deformation: structures formed by the liquefaction of unconsolidated sands and some ancient examples, Sedimentology, 43, 279–293, 1996b.

Owen, G.: Load structures: gravity-driven sediment mobilization in the shallow subsurface, Geol. Soc. Sp., 216, 21–34, 2003.

Owen, G. and Moretti, M.: Determining the origin of soft-sediment deformation structures: a case study from Upper Carboniferous delta deposits in south-west Wales, UK, Terra Nova, 20, 237–245, 2008.

Owen, G. and Moretti, M.: Identifying triggers for liquefaction-induced soft-sediment deformation in sands, Sediment. Geol., 235, 141–147, 2011.

Owen, G., Moretti, M., and Alfaro, P.: Recognising triggers for soft-sediment deformation: current understanding and future directions, Sediment. Geol., 235, 133–140, 2011.

Peltier, A., Finizola, A., Douillet, G. A., Brothelande, E., and Garaebiti, E.: tructure of an active volcano associated with a resurgent block inferred from thermal mapping: The Yasur–Yenkahe volcanic complex (Vanuatu), J. Volcanol. Geoth. Res., 243, 59–68, 2012.

Pisarska-Jamroży, M. and Weckwerth, P.: Soft-sediment deformation structures in a Pleistocene glaciolacustrine delta and their implications for the recognition of subenvironments in delta deposits, Sedimentology, 60, 637–665, 2013.

Pistolesi, M., Delle Donne, D., Pioli, L., Rosi, M., and Ripepe, M.: The 15 March 2007 explosive crisis at Stromboli volcano, Italy: assessing physical parameters through a multidisciplinary approach, J. Geophys. Res.-Sol. Ea., 116, doi:10.1029/2011JB008527, 2011.

Prata, G.: Complex eruption style and deposit changes during the evolution of the late Pleistocene Tower Hill maar- scoria cone Volcanic Complex, Newer Volcanics Province, Victoria, Australia, Monash University Melbourne, 2012.

Prata, G. and Cas, R.: Cyclicity in Fluctuating Phreatomagmatic and Magmatic Eruptive Styles at the 35 ka Tower Hill Volcanic Complex, Southeast Australia, Geoscience Society of New Zealand Miscellaneous Publication 131A, p. 136, 2012.

Rawcliffe, H. J. and Brown, D. J.: Lithofacies architecture of basaltic andesite lavas and their interaction with wet-sediment: Part A – Chroinn, Kerrera, NW Scotland, Scot. J. Geol., 50, 49–55, 2014.

Roche, O., Montserrat, S., Niño, Y., and Tamburrino, A.: Pore fluid pressure and internal kinematics of gravitational laboratory air-particle flows: Insights into the emplacement dynamics of pyroclastic flows, Journal of Geophysical Research: Solid Earth (1978–2012), 115, 2010.

Roche, O., Niĩno, Y., Mangeney, A., Brand, B., Pollock, N., and Valentine, G. A.: Dynamic pore-pressure variations induce substrate erosion by pyroclastic flows, Geology, 41, 1170–1110, 2013.

Røe, S.-L. and Hermansen, M.: New aspects of deformed cross-strata in fluvial sandstones: examples from Neoproterozoic formations in northern Norway, Sediment. Geol., 186, 283–293, 2006.

Rowley, P. J.: Analogue modelling of pyroclastic density current deposition, Royal Holloway, University of London. Unpublished PhD thesis, 2010.

Rowley, P. J., Kokelaar, P., Menzies, M., and Waltham, D.: Shear-derived mixing in dense granular flows, J. Sediment. Res., 81, 874–884, 2011.

Sasnett, P., Goehring, B. M., Christie-Blick, N., and Schaefer, J. M.: Do phreatomagmatic eruptions at Ubehebe Crater (Death Valley, California) relate to a wetter than present hydro-climate?, Geophys. Res. Lett., 39, 2012.

Schmincke, H.-U., Fisher, R. V., and Waters, A. C.: Antidune and chute and pool structures in the base surge deposits of the Laacher See area, Germany, Sedimentology, 20, 553–574, 1973.

Scolamacchia, T. and Schouwenaars, R.: High-speed impacts by ash particles in the 1982 eruption of El Chichon, Mexico, J. Geophys. Res.-Sol. Ea., 114, doi:10.1029/2008JB005848, 2009.

Selker, J. S.: Expressions for the formation of load casts in soft sediment, J. Sediment. Res., 63, 1149–1151, 1993.

Sherwood, J., Oyston, B., and Kershaw, A.: The age and contemporary environments of Tower Volcano, Southwest Victoria, Australia, Proceedings of the Royal Society of Victoria, 116, 69–76, 2004.

Smith, N. J. and Kokelaar, B. P.: Proximal record of the 273 ka Poris caldera-forming eruption, Las Cañadas, Tenerife, B. Volcanol., 75, 1–21, 2013.

Stinton, A. J., Cole, P. D., Stewart, R. C., Odbert, H. M., and Smith, P.: The 11 February 2010 partial dome collapse at Soufrière Hills Volcano, Montserrat, Geological Society, London, Memoirs, 39, 133–152, 2014.

Sulpizio, R. and Dellino, P.: Sedimentology, depositional mechanisms and pulsating behaviour of pyroclastic density currents, Dev. Volcano., 10, 57–96, 2008.

Valentine, G. A., Buesch, D. C., and Fisher, R. V.: Basal layered deposits of the Peach Springs Tuff, northwestern Arizona, USA, B. Volcanol., 51, 395–414, 1989.

Van Loon, A.: Soft-sediment deformation structures in siliciclastic sediments: an overview, Geologos, 15, 3–55, 2009.

Vazquez, J. A. and Ort, M. H.: Facies variation of eruption units produced by the passage of single pyroclastic surge currents, Hopi Buttes volcanic field, USA, J. Volcanol. Geoth. Res., 154, 222–236, 2006.

Vinningland, J. L., Johnsen, Ø., Flekkøy, E. G., Toussaint, R., and Måløy, K. J.: Granular rayleigh-taylor instability: Experiments and simulations, Phys. Rev. Lett., 99, 1149–1151, 2007.

Vinningland, J. L., Johnsen, Ø., Flekkøy, E. G., Toussaint, R., and Måløy, K. J.: Size invariance of the granular Rayleigh-Taylor instability, Phys. Rev. E, 81, 041308, doi:10.1103/PhysRevE.81.041308, 2010.

Voight, B., Janda, R., Douglass, P., et al.: Nature and mechanics of the Mount St Helens rockslide-avalanche of 18 May 1980, Geotechnique, 33, 243–273, 1983.

Wadge, G., Robertson, R., and Voight, B.: The Eruption of Soufriere Hills Volcano, Montserrat from 2000 to 2010, Geological Society of London, 2014.

Ward, S. N. and Day, S.: Particulate kinematic simulations of debris avalanches: interpretation of deposits and landslide seismic signals of Mount Saint Helens, 1980 May 18, Geophys. J. Int., 167, 991–1004, 2006.

Waters, A. C. and Fisher, R. V.: Base surges and their deposits: Capelinhos and Taal volcanoes, J. Geophys. Res., 76, 5596–5614, 1971.

Wayne, P. J., Vorobieff, P., Smyth, H., Bernard, T., Corbin, C., Maloney, A., Conroy, J., White, R., Anderson, M., Kumar, S., et al.: Shock-Driven Particle Transport Off Smooth and Rough Surfaces, J. Fluid. Eng.-T. ASME, 135, 061302, doi:10.1115/1.4023786, 2013.

Whelley, P. L., Jay, J., Calder, E., Pritchard, M., Cassidy, N., Alcaraz, S., and Pavez, A.: Post-depositional fracturing and subsidence of pumice flow deposits: Lascar Volcano, Chile, B. Volcanol., 74, 511–531, 2012.

Wiemer, G.: On the Role of volcanic ash in submarine landslide initiation processes, PhD dissertation, Fachbereich Geowissenschaften der Universitaet Bremen, 2014.

Chapter 6

Sedimentary peels for fine-scale imaging of pyroclastic sediments

This chapter reports preliminary results from an ongoing campaign of impregnation of sedimentary peels at Tungurahua and other areas. The method, put in perspective with the wind tunnel measurements of Douillet et al. (2014), may bring new quantitative results on turbulence level in pyroclastic density currents as well as image unexpected fine-scale features.

This page was intentionally left blank.

Sedimentary peels image fine-scale laminations in pyroclastic deposits

Abstract

Sedimentary peels (also called lacquer peels) are thin peels of undisturbed sediment that have been consolidated with an interstitial artificial matrix, usually an epoxy resin (Fig. 1). Such peels are produced directly on an outcrop by impregnating the surface of the sediment with a low viscosity hardener (epoxy). That way, the peel can be transported and examined in the lab without disturbing the initial organization of the particles. Additionally, the difference in epoxy uptake as a function of grain size pronounces sedimentary structures in the resulting peel. In order to better document and investigate the genesis of dune bedforms formed by dilute pyroclastic density currents (PDCs), we used the sedimentary peels method on the cross-bedded deposits from the August 2006 eruption of Tungurahua (Ecuador) and from the Astroni U7 deposits in the Campi Flegrei volcanic district (Italy).

1 Background

Sedimentary peels are board-samples of particles, few particle-diameter in thickness and cm^2 to m^2 in area that have been consolidated in their initial sedimentary state. They have been widely produced in the fields of coastal sedimentology, archeology, palaeontology, and many examples of peels are used to decorate walls of universities or museums. The technique was developed in Germany in the 1930s (Voigt, 1933, 1936), and received lots of attention from the Utrecht university group (Bouma, 1969), up to modern time (Van den Berg and Nio, 2010). Sedimentary peels are often used in tidal settings, where an outcrop cannot be given the time to dry and mature enough to let sedimentary structures appear, but the wet and unconsolidated sediment is easy to dig and impregnate (Nio et al., 1980; Van den Berg et al., 2007). Impregnation methods have also been used in experimental flumes or granular flows to consolidate the deposits (Owen, 1996; Baas et al., 2004, Rowley et al., 2011), for calibration of ground penetrating radar profiles (Van Dam and Schlager, 2000), to sample pyroclastic deposits (Klapper et al., 2010), or cast ant nests (Tschinkel, 2010). PDC deposits are reacting well to the lacquer peel method and peels are exhibited in volcano museums around the world (e.g. Sakurajima -Japan, Merapi -Indonesia, Smithsonian Institution -USA).

The principle to produce peels is to impregnate the surface of an outcrop with a low viscosity resin. The viscosity and surface tension of the resin together with the capillary force of sediment pores will define the penetration depth. That way, the dry peel will enhance and underline the grain-size related stratification to a level of details that would not be accessible otherwise, and allow for transportation to the lab with full preservation of the deposition history.

Sedimentary peels have several advantages as an imaging method: 1) Peels permit sampling without disturbing the structure of the sediments, keeping the relative position of individual clasts in regards to their neighbors. They thereby preserve the organization of small-scale structures such as individual laminae that would otherwise not even be expected with traditional methods (Fig. 1). 2) Since the natural unconsolidated deposit has not been altered during impregnation, other high-resolution imaging techniques such as computer tomography (Fig. 5) or thin section analysis (Fig. 3) can be applied in the lab. 3) Producing and storing peels is an opportunity for future researchers, which will be able to access an undisturbed dataset long after erosion of the natural outcrop and for studies beyond the expectations of the initial investigator. 4) Peels wear a very aesthetic side, especially for geologists. The educational impact of showing a peel of real sediment to a class or to the public rather than a picture is great. Sedimentary peels may have a great impact in museums, as artwork and educational and public outreach tools.

The genesis of pyroclastic dune bedforms is largely under understood. However, those structures bear important information on the sedimentary dynamics of dilute PDCs, which might have implications for the dynamics of the whole flow. In that context, rather than any hasty interpretation, a thorough documentation of outcrop is necessary. The GPR and laser scanning studies presented in Dujardin (2014) are an attempt to document in a non-intrusive and unconventional form the deposits of the 2006 eruption of Tungurahua (Ecuador). They permit to have large investigation depths and a record of the deposit that will be re-usable by other researchers after erosion of the natural outcrops. The dataset of lacquer peels is thought to complement this and image the finest-scale structures. Bulk samples of loose particles do not preserve an accurate sedimentary signature. Sedimentary peels allow to sample the variability in grain size distribution within mm-scale laminae, which can in turn be measured non-intrusively by micro computer tomography. This precision can reveal the intensity of turbulence within dilute PDCs, since the variation in size distribution reflects the capacity and competence of a flow at time of deposition. Coupled with recent lab measurements that link the grain size of sediments to a wind's shear stress (Douillet et al. 2014), sedimentary peels could permit to give a speed variation near the ground during emplacement of the sediment.

2 Method

Several types of epoxy have been tested in the field. The final choice was given to a 2-component epoxy (Refs: RE6410 and DE6410) from M.A.CK (http://www.mack-kayak.com/) based on 1) cost effectiveness (less than 15 euros/kg in 2012), 2) the appropriate viscosity that permitted to underline the grain size variations, 3) the fact that this was a 2-component epoxy (and thus can be stored for several years without altering the quality of the resin or drying) and 4) for practical shipping reasons (M.A.CK is the only seller found able to export their product over-Atlantic).

Acetone has proven to be the best thinner and permits to reduce the viscosity of the resin without changing its final characteristics. However, acetone is not for sale legally in

Figure 1: Steep-sided, stoss-aggrading laminasets of ash in a transverse dune bedform from the 2006 eruption of Tungurahua (Ecuador). Flow is from left to right.

Figure 2: Outcrop from Fig. 1 prepared for impregnation. Note : The peel is a mirror of the field image, since the internal part of the outcrop serves for imaging.

Ecuador since it is a major component in the production of cocaine. Thus in Ecuador, conventional gasoline was used as a thinning agent. Although it produces an emulsion with the epoxi, it permitted to obtain a less viscous mixture and the final results are only slightly whiter than with acetone, possibly due to micro-bubbles of gasoline within the resin. In some cases, a soft rubbery texture can result. This is attributed to gasoline that remained after the epoxy set, since not all gasoline can evaporate in a casting mass. No solution was found and acetone can pose the same problem.

Many methods in many steps are described in many details in Bouma (1969), but do not need to be followed. The simplest method for application of the resin was by simple brushing. In order to transport, strengthen and achieve a more aesthetic final product, wooden frames (40*40 cm; 0.5 cm thick) were confectioned and inserted in the outcrop before application of the epoxy (Fig. 2). The outer surface was made even prior to the application of the epoxy with a straight piece of metal. If necessary, the outcrop was sprayed with water before brushing the epoxy in order to avoid mechanical erosion or peeling off. No cheesecloth was needed and the epoxy was simply brushed directly on the outcrop. Around 400 g of epoxy thinned with 80 g gasoline are necessary for a 40*40 cm^2 peel of ca. 0.5 cm penetration depth consisting of ash (considering loses during brushing). A much larger amount is needed for coarser peels, resulting in thicker and heavier peels. Epoxy application by spraying was also tested and found to produce similar results; however, this technique was abandoned because of the higher exposure to inhalable fumes. Upon hardening (minimum 40 hours), the peels could be transported by cargo without damage, provided adequate packaging. Samples could be sawed for thin sections (Fig. 3).

The peels from Astroni were used as preliminary tests, and are made from several types of epoxy thinned with acetone, mainly sprayed.

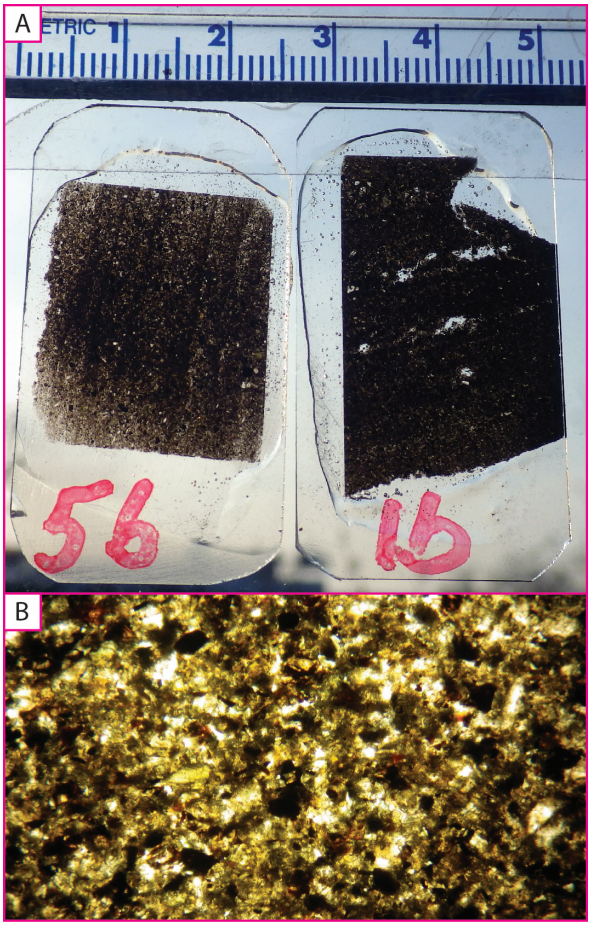

Figure 3: Thin section of impregnated sediments from Tungurahua.

3 Results

3.1 Tungurahua peels

Sedimentary peels permit to reveal fine-scale stratification that would otherwise not be visible. This is well expressed in the Tungurahua samples. Impressive is the occurrence of cm-scale structures within bedsets that were thought to be massive. Thin oblique prograding lamination bedsets are visible (Fig. 1a). Their containing bedsets are stoss-aggrading, which has often been interpreted as indicating super-critical flow conditions, but the laminae inside are prograding. This supports the suggestion of Douillet et al.

(2014) that stoss-aggradation is a result of blocking of the saltating load on steep stoss sides, rather than a flow free-boundary interaction with the bed.

Also very interesting is the occurrence of small-scale overturned beds (1 cm thick; 4 cm long, Fig. 1b) that might be field examples of shearing instabilities at the bed boundary, and possibly a granular equivalent of Kelvin-Helmholz instabilities (see Douillet et al., 2015, chapter 5 of this dissertation). This may reflect traction carpets occurring on the lee sides of bedforms.

Figure 4: Accretionary structures in peels from the Astroni outcrops.

3.2 Astroni peels

Within the Astroni peels, the most striking feature was the evidence of some massive layers containing numerous accretionary pellets (Fig. 4; Brown et al., 2012). They have a diameter of ca. 0.5 cm, an outer concentric structure made of volcanic dust, but no structure was recognized in the central part and grains seem accreted chaotically. Selected pellets were investigated at 1 μm-resolution by computer tomography (GE phoenix ®v/tome/x s micro-CT scanner). They are massive and poorly sorted in their central part, with some voids, the size of which being comparable to the coarsest particles in the sample (Fig. 5a). The central massive core has an oblate shape, possibly due to an erosive event. The core

is subsequently coated with a "layer" of darker color that adapts the form to a highly spherical shape by preferential filling of the "troughs". Note that this layer may previously have been uneven and of larger scale, and subsequently re-eroded into a spherical shape. The outer layer is finer grained and seems poorly laminated, with concentric aggradation at the outer surface. It is absent on one side, revealing the spherical shape of the underlying layer. This suggests that the coating was less competent than the central part, but is possibly due to post-impregnation reworking.

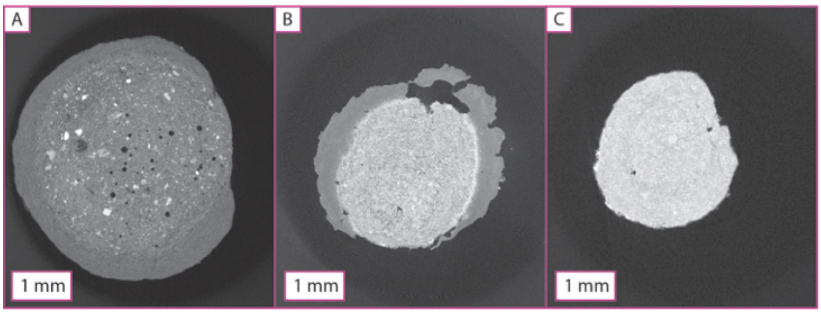

Figure 5: Computer tomography images through impregnated accretionary structures.

4 Preliminary conclusions

Sedimentary peels have proven to be a very good imaging technique as such, bringing new and unexpected data at fine scale. Moreover, they can be coupled with recent techniques such as computer tomography to reveal the undisturbed organization of sediments, and retrace the evolution of a bedform within minutes of intervals (mm laminae). Once the sediment is consolidated, it can be treated as a hard rock, and thin sections and other techniques can be applied. Once studied, the remaining sedimentary peels are an ideal present for colleagues, ornament for labs, and tool for classes. The artistic perspectives of sedimentary peels are also not negligible.

Acknoledgements

Kai-Uwe Hess is acknowledged for the computer tomography measurements. The M.A.CK Company is acknowledged for their help for importing epoxy in Ecuador. GAD acknowledges financial support by the Bavarian grant Thesis. GAD and UK are financially supported by the Deutsche Forschungsgemeinschaft grant KU2689/2-1 grant. GAD and UK thank Sandro di Vito for logistical help during the fieldwork in the Astroni crater.

References

-

Baas J.H., Van Kesteren W., Postma G. (2004) Deposits of depletive high-density turbidity currents: a flume analogue of bed geometry, structure and texture. Sedimentology 51:1053-1088

Bouma A.H. (1969) Methods for the Study of Sedimentary Structures.Wiley, New York; N.Y., 458 pp.

Brown R.J., Bonadonna C., Durant A.J. (2012) A review of volcanic ash aggregation. Physics and Chemistry of the Earth 45-46:65-78

Douillet G.A., Rasmussen K.R., Kueppers U., Lo Castro D., Merrison J., Iversen J., Dingwell D.B. (2014) Saltation threshold for pyroclasts at various bedslopes: Wind tunnel measurements. J. Volc. Geotherm. Res. 278-279:14-24

Douillet G.A., Taisne B., Tsang-Hin-Sun E., Mueller S.K., Kueppers U., Dingwell D.B. (2015) Syn-eruptive, soft-sediment deformation of dilute pyroclastic density current deposits: triggers from granular shear, dynamic pore pressure, ballistic impacts and shock waves. Solid Earth Discussion. http://www.solid-earth-discuss.net/6/3261/2014/sed-6-3261-2014.pdf

Klapper D., Kueppers U., Castro J.M., Pacheco J.M.R., Dingwell D.B. (2010) Impregnating unconsolidated pyroclastic sequences: A tool for detailed facies analysis. Geophysical Research Abstracts Vol. 12, EGU2010-11780

Owen G. (1996) Experimental soft-sediment deformation: structures formed by the liquefaction of unconsolidated sands and some ancient examples. Sedimentology, 43(2), 279-293.

Rowley P.J., Kokelaar P., Menzies M., Waltham D. (2011) Shear derived mixing in dense granular flows. Journal of Sedimentary Research, 2011, v. 81, 874-884. Research Article DOI: 10.2110/jsr.2011.72

Tschinkel W. R. (2010) Methods for casting subterranean ant nests. Journal of Insect Science, 10(88), 1-17.

Van Dam R.L., Schlager W. (2000) Identifying causes of ground-penetrating radar reflections using time-domain reflectometry and sedimentological analyses. Sedimentology 47:435-449

Van den Berg J.H., Nio S.W. (2010) Sedimentary structures and their relation to bedforms and flow conditions. EAGE publications, The Netherlands. ISBN 978-90-73781-76-4

Van den Berg J.H., Boersma J.R., Van Gelder A. (2007) Diagnostic sedimentary structures of the fluvial-tidal transition zone - Evidence from deposits of the Rhine and Meuse. Netherlands Journal of Geosciences - Geologie en Mijnbouw 86 - 3 287 - 306

Voigt E. (1933) Die Uebertragung fossiler Wirbeltierleichen auf Zellulose-Filme, eine Bergungsmethode fr Wirbeltiere aus der Braunkohle, Palaeont. Zeitschrift 15:72-78

Voigt E. (1936) Ein neues Verfahren zur Konservierung von Bodenprofilen. Z. Pflanzenern., Dngung und Bodenk. 45:111-115

Nio S.W., Van den Berg J.H., Goesten M., Smulders F. (1980) Dynamics and sequential analysis of a mesotidal shoal and intershoal channel complex in the eastern Scheldt (Sounthwestern netherlands). Sedimentary Geology, 26 263-279

Outlook

Suggestions for future studies are grouped in three major investigation themes related to this PhD. If I had the funding, time and knowledge for, this is what I would continue.

Large scale flow dynamics

Large scale processes are what eventually affects human activity, i.e. the directly useable output for risk.

In the lab:

Investigate the effects of topography in large scale experiments with highly polydisperse grain mixtures flowing through different geometries. The experimental facility available at Massey University is a perfect tool for that. Dilute PDCs are extremely sensitive to topography. This is not quantified yet.

In the field:

Monitor the evolution of topography in zones frequently affected by PDCs. This can be done rapidly with photogrammetry from drone data. Doing so, the pre-eruptive topography would be known and can be used by modelers. Moreover, deposited volumes would be known precisely and the post deposition reworking could be quantified in time (lahar monitoring).

Bedform dynamics

The question on antidunes and supercritical bedforms is far from resolved and there is a current regain of interest in the geomorphology/sedimentology communities on this theme.

In the lab:

Produce bedforms from sub-aqueous particulate density currents. PDCs, hyperpicnal particulate flows and turbidity currents share the same characteristics, apart the ambient fluid, and their deposits have similar sedimentary signatures. The answer is to be searched in the common link: the particulate density current nature.

In the field:

Full 3D and digital acquisition schemes, by any means. A digital set of data is preserved for later investigators and unbiased. Subsurface geophysical methods such as micro seismic or ground penetrating radar are great tools combined with direct detailed observations (e.g. sedimentary peels). Photogrammetry combined with drones leads accurate and fast topography results.

Boundary processes

The concepts of threshold and end-members are not natural. The thresholds for motion are only time-averaged, macroscopic concepts, but research on boundary processes needs to go beyond these artificial limits for a better understanding of transport and deposition.

In the lab:

Wind tunnel modeling with constant feeding by fallout of particles. Boundary layer processes with high sedimentation conditions and the saturation flux are still poorly understood. The transition from stratified to massive deposits needs to be investigated in terms of turbulence levels (both in shearing and particle concentration) in the lab, based on field data.

The dynamic saltation threshold for pyroclasts has not been measured yet. It may lead unexpected results compared to the static threshold investigated here (although it's an artificial threshold).

In the field:

Soft sediment deformation is under exploited for PDCs, both in the lab and in the field. Deformed strata may contain way more information than expected.

Sedimentary peels could become common for sampling.

Acknowledgements

Figure 6.6: Explosive eruption and geologist. Left handed watercolor painting. Pingu (2012)

So, I first need to thank Don and Ulli. I think it's rare that PhD students are happy about their PhD for the whole time of the project (even this last day is a lot of fun!). It's really great to have freedom, be considered, and trusted like they both did. On top of that, Don has been a generous producer and Ulli an attentive and helpful friend. It could not

have been better. I am really happy to have had them, and to thank them very honestly.

My interest for learning, what drove me to academic research first begun with kayak trainers and college teachers: Marie-Antoinette Grosskopf, Stephane Jeannot, Olivier Jamain, Alice trainard, Alain Houille. I have also used all of them as parent substitutes.

But first I was born, thanks to Aziz Mesbah and next to Guillaume Herbertz and Michele.

Comes university time, where I randomly changed cursus, until Max Wehrlurier convinced me for EOST. Without knowing what he launched, he became coupable for my geophysics cursus.

There, I found again a bunch of great professors: Yves Rogister, Valerie Ansel, Alain Cochard, Jean Paul Boy, Daniele Grosheny. There were also very good friends: Lolo Bouzeran, Thiebault Schoffi, Adriano Bronelli, Basile Crocodile, Alexandra Groland, Marie, Gauvain Wiemer, Jean Letord, Gabi, Fanny, Francine, Lucas Pimenté.

The one that gave me the interest to look at sediments was Philippe Duringer, and JF Ghienne brought me to the nicest outcrop ever and hammered it in.

The first time I climbed on an active volcano was recruited by Sneph Cabusson, and had fun with Svetlana Byrdina, Anthony Finizola, Aline Peltier on Yasur, where I also met Kilema and Yetica. Claude Robin then brought me to Tungurahua, and he showed me the pyroclastic bedforms with Julie. Other volcano friends are Jean Battaglia always around, and Tullio Ricci, Matteo Lupi, Anna, Andrea Miranda, Melanie Froude, Grace, Zack.

Going in Ecuador, I met very nice people, the ones from IG that helped during my internship and then PhD, Pathy Mothes, Jorge Bustillos, Silvana Hidalgo, Silvia Vallejo, Daniel Andrade, Julie and Andrea, Ben Bernard, Diego, JC, Mario Ruiz, Patricio Ramn and outside IG, Teresa, Karla, Edwin, Evelyn, Kathi, Ramiro, Ketu, Anne, Ligia, and the Padilla Arias family that welcome me and took care of me.

And then I came to Munich, thinking of Eve. I met very nice people, Frantz, Regina, Romain, Nora und Bass, Ina, Mira, Domi mck, Ceni, Juliette, Vanessa, Zamirha, Nina, the flatmates Jenny Domi Basti, and here in the lab, Célinette and Klaus, Teresa la mama, Mike, and many that helped me a lot; Renate, Rosa, Andre, Marina, Friederike, Margot und Sandra, David, Fabian, Jeremie, Paul, Wenja, Woschtl, Kai, Laura, Betty, Valeria, the ones that left, Fabian, Felix, Stephan, Charlotte, Jon, Jackie, Yan, Oryaelle, Daniele. I think absolutely all my data have been rescued at least once by Andre, sometimes much more!

People that helped in the field, in the lab, or shared field work, Lina, Aaron, Markus, Célia, Facundo, Joann, Eve, JR Dujardin, Amir Abolghasem, Jon Hall, Daniel Pacheco,

Benoit Cordonnier (mmm). Ramiro Guevara is the craziest Taxi around Tungurahua and uses the machete like no one. I spent nice time with Pepe the carpintero, who makes the boxes for samples. Isabel Arias saved a shipping.

Someone that saved my college years, my university inscription, my master thesis, my engineer degree, well, my whole scholar life was Marie Anselm, Christelle also helped in early life.

There are plenty of people from conferences that I really like, Mathieu Schuster, Laure Guerit, Lewis, Julien, Elodie, Patric, Matthieu, Stephen, Lucie Mayjonnade, and others that I forget here about!

Celinette Gideon and Manon helped for LaTeX a lot even on the last hours before the deadline.

There are nice volcano drawings in between this lot of cartesian chapters from the artists Almut Winkler, Guillaume Herbertz, Jérome Huss and Pingu !

People I don't know where to put in that story but want to mention are: Aspirine Gadoue, Moritz et Pascal Buck, Flo Baloo, Lena, Bastien and Teuw, Now Bass, les Labarelles, Ysori, Floflo, Vincent, les Fixs, Sarah Richardier, Dudule, Jo Bauer, Georgie et encore une fois Lolo boubou.

Anyway, it's time to print, and if you're not in the list, it may be on purpose, but most of you I probably just forget because I'm late again and very tired. Oh and I think I really need to acknowledge Franckie Vincent for singing with me and the petit Guilhem these last few nights. Cyrin, shtügu for you.

I add a post-defence sentence here for the referees and Frau Roeske from the deans office that have done a very fast job, and permitted the defence to happen in the best conditions! This was really really great, thanks a lot!

Thanks to everybody

Oh and as well: Money money money, makes it funny... Without these grants, there wouldn't have been data: ESA grant TNA2-Europlanet (wind tunnel measurements) THESIS Elite Network of Bavaria (from March 2010 to August 2012); Deutsche Forschungsgemeinschaft grant KU2689/2-1 (from August 2012 to December 2014), and support from Don Dingwell. They also sponsored a great field campaign on Tungurahua that kept me busy in the last 2.5 years, yet the result couldn't be presented here, they were already published in the PhD thesis of Jean Remi Dujardin (EOST, Strasbourg).